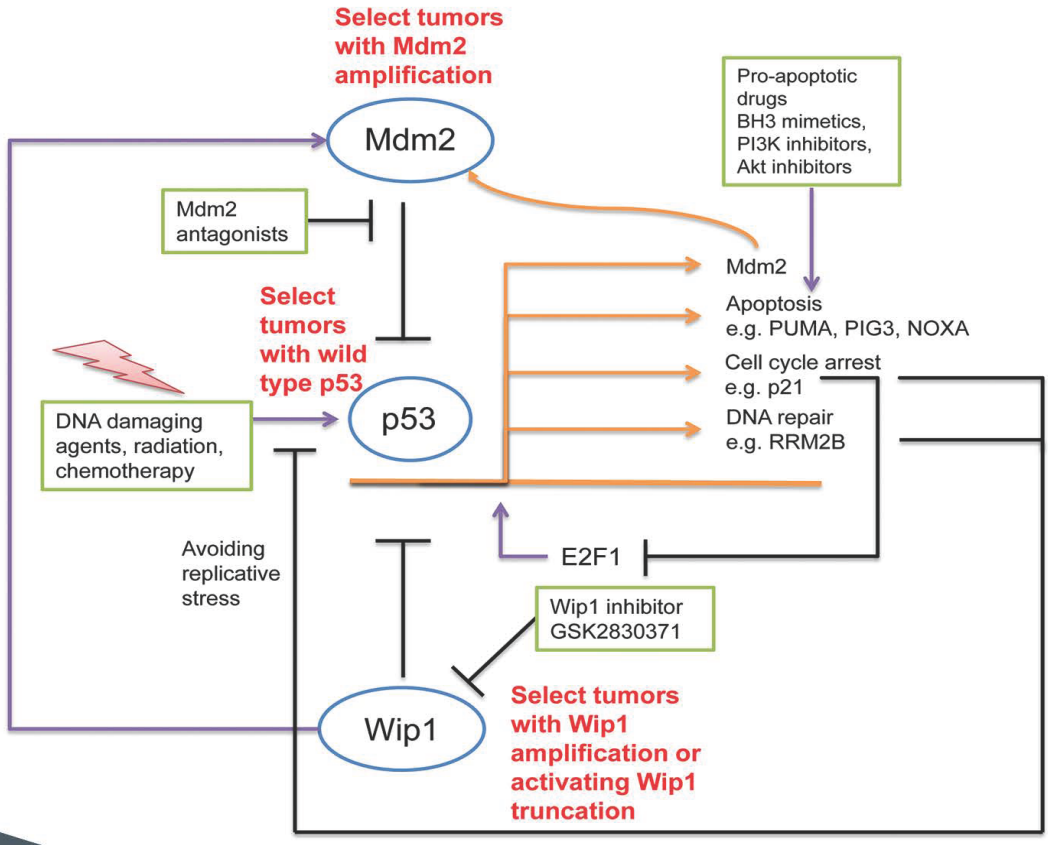

Special Collection on p53

Strategies to fortify p53 in cancer therapy, see Sriraman et al. - "Fortifying p53 – beyond Mdm2 inhibitors

p53

AGING

ONLINE ISSN: 1945-4589

AGING

www.aging-us.com

EDITORIAL BOARD

EDITORS-IN-CHIEF

Jan Vijg - Albert Einstein College of Medicine, Bronx, NY, USA

David A. Sinclair - Harvard Medical School, Boston, MA, USA

Vera Gorbunova - University of Rochester, Rochester, NY, USA

Judith Campisi - The Buck Institute for Research on Aging, Novato, CA, USA

Mikhail V. Blagosklonny - Roswell Park Cancer Institute, Buffalo, NY, USA

EDITORIAL BOARD

Frederick Alt - Harvard Medical School, Boston, MA, USA

Vladimir Anisimov - Petrov Institute of Oncology, St.Petersburg, Russia

Johan Auwerx - Ecole Polytechnique Federale de Lausanne, Switzerland

Andrzej Bartke - Southern Illinois University, Springfield, IL, USA

Nir Barzilai - Albert Einstein College of Medicine, Bronx, NY, USA

Elizabeth H. Blackburn - University of California, San Francisco, CA, USA

Maria Blasco - Spanish National Cancer Center, Madrid, Spain

Vilhelm A. Bohr - National Institute on Aging, NIH, Baltimore, MD, USA

William M. Bonner - National Cancer Institute, NIH, Bethesda, MD, USA

Robert M. Brosh, Jr. - National Institute on Aging, NIH, Baltimore, MD, USA

Anne Brunet - Stanford University, Stanford, CA, USA

Rafael de Caba - NIA, NIH, Baltimore, MD, USA

Ronald A. DePinho - Dana-Farber Cancer Institute, Boston, MA, USA

Jan van Deursen - Mayo Clinic, Rochester, MN, USA

Lawrence A. Donehower - Baylor College of Medicine, Houston, TX, USA

Caleb E. Finch - University of Southern California, Los Angeles, CA, USA

Toren Finkel - National Institutes of Health, Bethesda, MD, USA

Luigi Fontana - Washington University, St. Louis, MO, USA

Claudio Franceschi - University of Bologna, Bologna, Italy

David Gems - Inst. of Healthy Ageing, Univ. College London, UK

Myriam Gorospe - National Institute on Aging, NIH, Baltimore, MD, USA

Leonard Guarente - MIT, Cambridge, MA, USA

Andrei Gudkov - Roswell Park Cancer Institute, Buffalo, NY, USA

Michael Hall - University of Basel, Basel, Switzerland

Philip Hanawalt - Stanford University, CA, USA

Nissim Hay - University of Illinois at Chicago, Chicago, IL, USA

Siegfried Hekimi - McGill University, Montreal, Canada

Stephen L. Helfand - Brown University, Providence, RI, USA

Jan H.J. Hoeijmakers - Erasmus MC, Rotterdam, The Netherlands

John 0. Holloszy - Washington University, St. Louis, MO, USA

Stephen P. Jackson - University of Cambridge, Cambridge, UK

Heinrich Jasper - The Buck Institute for Research on Aging, Novato, CA, USA

Pankaj Kapahi - The Buck Institute for Research on Aging, Novato, CA, USA

Jan Karlseder - The Salk Institute, La Jolla, CA, USA

Cynthia Kenyon - University of California San Francisco, San Francisco, CA, USA

James L. Kirkland - Mayo Clinic, Rochester, MN, USA

Guido Kroemer - INSERM, Paris, France

Titia de Lange - Rockefeller University, New York, NY, USA

Arnold Levine - The Institute for Advanced Study, Princeton, NJ, USA

Michael P. Lisanti - University of Salford, Salford, UK

Lawrence A. Loeb - University of Washington, Seattle, WA, USA

Valter Longo - University of Southern California, Los Angeles, CA, USA

Gerry Melino - University of Rome, Rome, Italy

Simon Melov - The Buck Institute for Research on Aging, Novato, CA, USA

Alexey Moskalev - Komi Science Center of RAS, Syktyvkar, Russia

Masashi Narita - University of Cambridge, Cambridge, UK

Andre Nussenzweig - National Cancer Institute, NIH, Bethesda, MD, USA

William C. Orr - Southern Methodist University, Dallas, TX, USA

Daniel S. Peeper - The Netherlands Cancer Institute, Amsterdam, The Netherlands

Thomas Rando - Stanford University School of Medicine, Stanford, CA, USA

Michael Ristow - Swiss Federal Institute of Technology, Zurich, Switzerland

Igor B. Roninson - Ordway Research Institute, Albany, NY, USA

Michael R. Rose - University of California, Irvine, CA, USA

K Lenhard Rudolph - Hannover Medical School, Hannover, Germany

Paolo Sassone-Corsi - University of California, Irvine, CA, USA

John Sedivy - Brown University, Providence, RI, USA

Manuel Serrano - Spanish National Cancer Research Center, Madrid, Spain

Gerald S. Shadel - Yale University School of Medicine, New Haven, CT, USA

Norman E. Sharpless - University of North Carolina, Chapel Hill, NC, USA

Vladimir P. Skulachev - Moscow State University, Moscow, Russia

Sally Temple - NY Neural Stem Cell Institute, Albany, NY, USA

George Thomas - University of Cincinnati, Cincinnati, OH, USA

Jonathan L. Tilly - Massachusetts General Hospital, Boston, MA, USA

John Tower - University of Southern California, LA, CA, USA

Eric Verdin - University of California, San Francisco, CA, USA

Thomas von Zglinicki - Newcastle University, Newcastle, UK

Alex Zhavoronkov - Insilico Medicine, Baltimore, MD, USA

Aging (ISSN: 1945 - 4589) is published monthly by Impact Journals, LLC.
6666 East Quaker St., Suite 1B, Orchard Park, NY 14127

Abstracted and/or indexed in: PubMed/Medline (abbreviated as "Aging (Albany NY)"), PubMed Central (abbreviated as "Aging (Albany NY)"), Web of Science/Science Citation Index Expanded (abbreviated as Aging-US) & listed in the Cell Biology-SCIE and Geriatrics & Gerontology category, Scopus /Rank Q1(the highest rank) (abbreviated as Aging)- Aging and Cell Biology category, Biological Abstracts, BIOSIS Previews, EMBASE, META (Chan Zuckerberg Initiative), Dimensions (Digital Science's).

This publication and all its content, unless otherwise noted, is licensed under CC-BY 3.0 Creative Commons Attribution License.
Impact Journals, LLC meets Wellcome Trust Publisher requirements.
IMPACT JOURNALS is a registered trademark of Impact Journals, LLC.

IMPACT JOURNALS

Editorial and Publishing Office Aging
6666 E. Quaker St., Suite 1,
Orchard Park, NY 14127
Phone: 1-800-922-0957
Fax: 1-716-508-8254
e-Fax: 1-716-608-1380

Submission
Please submit your manuscript on-line at http://aging.msubmit.net

Editorial
For editorial inquiries, please call us or email editors@impactaging.com

Production
For questions related to preparation of your article for publication, please call us or email krasnova@impactaging.com

Indexing
If you have questions about the indexing status of your paper, please email kurenova@impactaging.com

Billing/Payments
If you have questions about billing/invoicing or would like to make a payment, please call us or email payment@impactaging.com

Media
If you have questions about post publication promotion, Altmetric, video interviews or social media, please email media@impactjournals.com

Printing
Each issue or paper can be printed on demand. To make a printing request, please call us or email printing@impactjournals.com

Publisher's Office
Aging is published by Impact Journals, LLC
To contact the Publisher's Office, please email: publisher@impactjournals.com, visit www.impactjournals.com, or call 1-800-922-0957

Aging (ISSN: 1945 - 4589) is published twice a month by Impact Journals, LLC.
6666 East Quaker St., Suite 1B, Orchard Park, NY 14127

Abstracted and/or indexed in: PubMed/Medline (abbreviated as "Aging (Albany NY)"), PubMed Central (abbreviated as "Aging (Albany NY)"), Web of Science/Science Citation Index Expanded (abbreviated as Aging-US) & listed in the Cell Biology-SCIE and Geriatrics & Gerontology category, Scopus /Rank Q1(the highest rank) (abbreviated as Aging) - Aging and Cell Biology category, Biological Abstracts, BIOSIS Previews, EMBASE, META (Chan Zuckerberg Initiative), Dimensions (Digital Science's).

This publication and all its content, unless otherwise noted, is licensed under CC-BY 3.0 Creative Commons Attribution License.
Impact Journals, LLC meets Wellcome Trust Publisher requirements.
IMPACT JOURNALS is a registered trademark of Impact Journals, LLC.

IMPACT JOURNALS

Table of Contents

Originally published in Volume 2, Issue 7 pp 445-452

The choice between p53-induced senescence and quiescence is determined in part by the mTOR pathway

Originally published in Volume 2, Issue 6 pp 344-352

Drosophila melanogaster p53 has developmental stage-specific and sex-specific effects on adult life span indicative of sexual antagonistic pleiotropy

Originally published in Volume 1, Issue 11 pp 903-936

The relative contributions of the p53 and pRb pathways in oncogene-induced melanocyte senescence

Originally published in Volume 1, Issue 6 pp 542-556

Alterations in gene expression and sensitivity to genotoxic stress following HdmX or Hdm2 knockdown in human tumor cells harboring wild-type p53

Originally published in Volume 1, Issue 1 pp 89-108

Research Paper

Altered S-nitrosylation of p53 is responsible for impaired antioxidant response in skeletal muscle during aging

Sara Baldelli[1,3] and Maria Rosa Ciriolo[2,3]

[1]Università Telematica San Raffaele Roma, Rome, Italy
[2]Department of Biology, University of Rome 'Tor Vergata', Rome, Italy
[3]IRCCS San Raffaele 'La Pisana', Rome, Italy

Correspondence to: Maria Rosa Ciriolo **email:** ciriolo@bio.uniroma2.it
Keywords: S-nitrosylation, antioxidant, sarcopenia, aging, atrophy
Received: November 03, 2016 **Accepted:** November 29, 2016 **Published:** December 20, 2016

ABSTRACT

p53 transcriptional activity has been proposed to regulate both homeostasis and sarcopenia of skeletal muscle during aging. However, the exact molecular function of p53 remains to be clearly defined. We demonstrated a requirement of nuclear p53 S-nitrosylation in inducing a nitric oxide/PGC-1α-mediated antioxidant pathway in skeletal muscle. Importantly, mutant form of p53-DNA binding domain (C124S) did not undergo nuclear S-nitrosylation and failed in inducing the expression of antioxidant genes (i.e. SOD2 and GCLC). Moreover, we found that during aging the nuclear S-nitrosylation of p53 significantly declines in gastrocnemius/soleus leading to an impairment of redox homeostasis of skeletal muscle. We suggested that decreased level of nuclear neuronal nitric oxide synthase (nNOS)/Syntrophin complex, which we observed during aging, could be responsible for impaired nuclear S-nitrosylation. Taken together, our data indicate that altered S-nitrosylation of p53 during aging could be a contributing factor of sarcopenia condition and of other skeletal muscle pathologies associated with oxidative/nitrosative stress.

INTRODUCTION

Sarcopenia is defined as the degenerative loss of skeletal muscle size and function that occurs during aging. This condition may be exacerbated by a decrease in physical activity, metabolic changes and oxidative stress [1, 2]. In fact, at the molecular level, increase of oxidative/nitrosative stress has been implicated in muscle wasting of aged skeletal muscle [3, 4].

Next to this, it is known in literature that p53 (transformation related protein 53, Trp53) transcription factor plays important roles during both myogenesis and sarcopenia of skeletal muscle [5-7]. Under unstressed conditions p53 cooperates with the myogenic regulatory factor MyoD (myogenic differentiation 1) to promote myogenesis by binding p53-response elements (p53-RE) on retinoblastoma (pRb) gene promoter, indicating that this transcriptional control may play an important role during myogenesis [6, 8, 9]. On the contrary, p53 has also been shown to induce atrophy/sarcopenia. In particular, upon genotoxic stress p53 binds to a highly conserved p53-RE on the Myogenin gene and transcriptionally represses its transcription, favoring muscle degeneration [10]. Despite such evidence, the molecular mechanisms responsible for the induction of p53 in myogenesis or muscle atrophy/sarcopenia remain to be clearly determined.

We previously highlighted a key role of p53 in regulating an antioxidant response essential for skeletal muscle homeostasis. Hence, under mild oxidative stress, p53 binds to the peroxisome proliferator-activated receptor gamma coactivator 1-alpha (PGC-1α) promoter, inducing the activation of a nitric oxide (NO)-dependent antioxidant signaling pathway [11]. Through this axis, p53 was able to buffer oxidative/nitrosative stress that otherwise would lead to premature sarcopenia and skeletal muscle atrophy. Moreover, we have recently demonstrated an

impairment in the NO/PGC-1α-mediated signaling process in skeletal muscle of old mice, which resulted in increased oxidative/nitrosative stress [12].

In this work, we questioned whether the decline of the antioxidant response could be due to an alteration of p53 transcriptional activity on the *ppargc1a* promoter, resulting in increased oxidative/nitrosative stress and premature aging of skeletal muscle. We demonstrated that p53 S-nitrosylation at a specific cysteine residue (C124) is essential to assure efficient p53-mediated antioxidant response. Moreover, an altered shuttle of neuronal nitric oxide synthase (nNOS) to nuclear membrane during muscle aging is responsible for a decrement in nuclear S-nitrosylated p53. These findings clarify the role of NO in signaling transduction and provide evidence of its function in assuring a beneficial antioxidant signaling pathway in muscle tissue upon mild oxidative stress.

RESULTS

C124S mutation in p53-DBD causes inhibition of NO/PGC-1α-mediated antioxidant response

We have previously demonstrated that p53 was able to orchestrate a PGC-1α-mediated antioxidant response upon mild oxidative stress. Moreover, the inhibition of this signaling pathway results in increased levels of atrophy-related molecular factors in C2C12 myoblasts [11, 13]. Here, we deeply dissect the mechanism(s) through which p53 imposes pro-survival or pro-death pathway upon NO-mediated post-translational modifications of its DBD.

First, we transfected C2C12 myoblasts with either wild type p53 (Wt-p53) or single point mutation of DBD Cys277, 275 and 124 to Ser (p53C277S, p53C275S and p53C124S) (Fig.1A). As shown in Fig.1B an increase of PGC-1α protein level and its downstream antioxidant genes was observed in Wt-p53, p53C277S and p53C275S overexpressing myoblasts, upon 1mM BSO treatment. Contrarily, p53C124S mutant was completely unresponsive. A corresponding increase in the transcription levels of PGC-1α, NFE2L2 (Nuclear factor erythroid-derived 2-like 2), SOD2 (superoxide dismutase 2) and CGCL (Glutamate-cysteine ligase catalytic subunit) was also observed (Fig.1B and C).

To confirm the previously assessed involvement of NO in the induction of p53 we treated C2C12 myoblasts with a NOSs inhibitor, L-NAME, at the concentration of 100 μM. Fig.1C shows that L-NAME is able to prevent the increase of PGC-1α mRNA and its downstream target genes only in BSO-treated Mock, Wt-p53, p53C277S and p53C275S myoblasts.

It is known in literature that p53 is able to bind the -2317 p53RE on the mouse *ppargc1a* promoter, assuring the expression of PGC-1α [11]. Therefore, we evaluated whether the binding capacity of the mutant p53C124S could be affected. A 10-fold increase in the occupancy of -2317 p53RE in BSO-treated Wt-p53, -p53C277S and -p53C275S myoblasts was observed (Fig.1D). On the contrary, *ppargc1a* promoter was not bound by the mutant p53C124S (Fig.1D). Consistent with the role of NO in mediating PGC-1α expression, the binding of Wt-p53, p53C277S and p53C275S was efficiently reduced by L-NAME treatment (Fig.1D). These data suggest that only specific sequences of p53-DBD are capable to induce the *ppargc1a* gene transcription in a NO-dependent manner, contributing to the antioxidant response necessary for muscle homeostasis.

S-nitrosylation of C124 promotes p53 binding on *ppargc1a* promoter

NO-mediated effects were primarily executed by protein S-nitrosylation, a reversible post-translational modification that produces NO-cysteine-thiol engagement [14]. S-nitrosylation represents an important post-translational modification that affects the functionality of p53, activating or inhibiting its binding on gene promoters [15, 16]. Thus, on the basis of results obtained, p53 S-nitrosylation status could be responsible for the ability to repress/activate *ppargc1a* gene transcription in skeletal muscle cells. Using the biotin-switch technique, we found that Wt-p53 myoblasts have increased level of S-nitrosylated p53 in nuclei (p53-SNO) than p53C124S myoblasts upon BSO treatment (Fig.2A). These results suggest that the increment of endogenous flux of NO due to GSH depletion [13], raises p53 transcriptional activity on *ppargc1a* promoter, through S-nitrosylation of a specific cysteine of its DBD. To clarify whether the low levels of nuclear p53C124S S-nitrosylation could affect the total transcriptional activity of p53 we analyzed the mRNA and protein levels of p21 (cyclin-dependent kinase inhibitor 1), a well-known p53-target gene. Fig.2B shows that mRNA (*upper*) and protein (*bottom*) levels of p21 were significantly higher in p53C124S myoblasts, demonstrating that the mutated form is transcriptionally active. The absence of S-nitrosylation on the specific C124 of p53-DBD mainly prevents the transcription of *ppargc1a* gene and the concomitant activation of antioxidant response in skeletal muscle.

The same set of experiments was performed using a triple p53-DBD mutant with the same three mutations Cys277, 275 and 124 to Ser (3Cys-p53) (Fig.2C). Western blot and RT-qPCR analysis of PGC-1α, NFE2L2, SOD2 and GCLC show that GSH deficiency increased their expression both in terms of protein

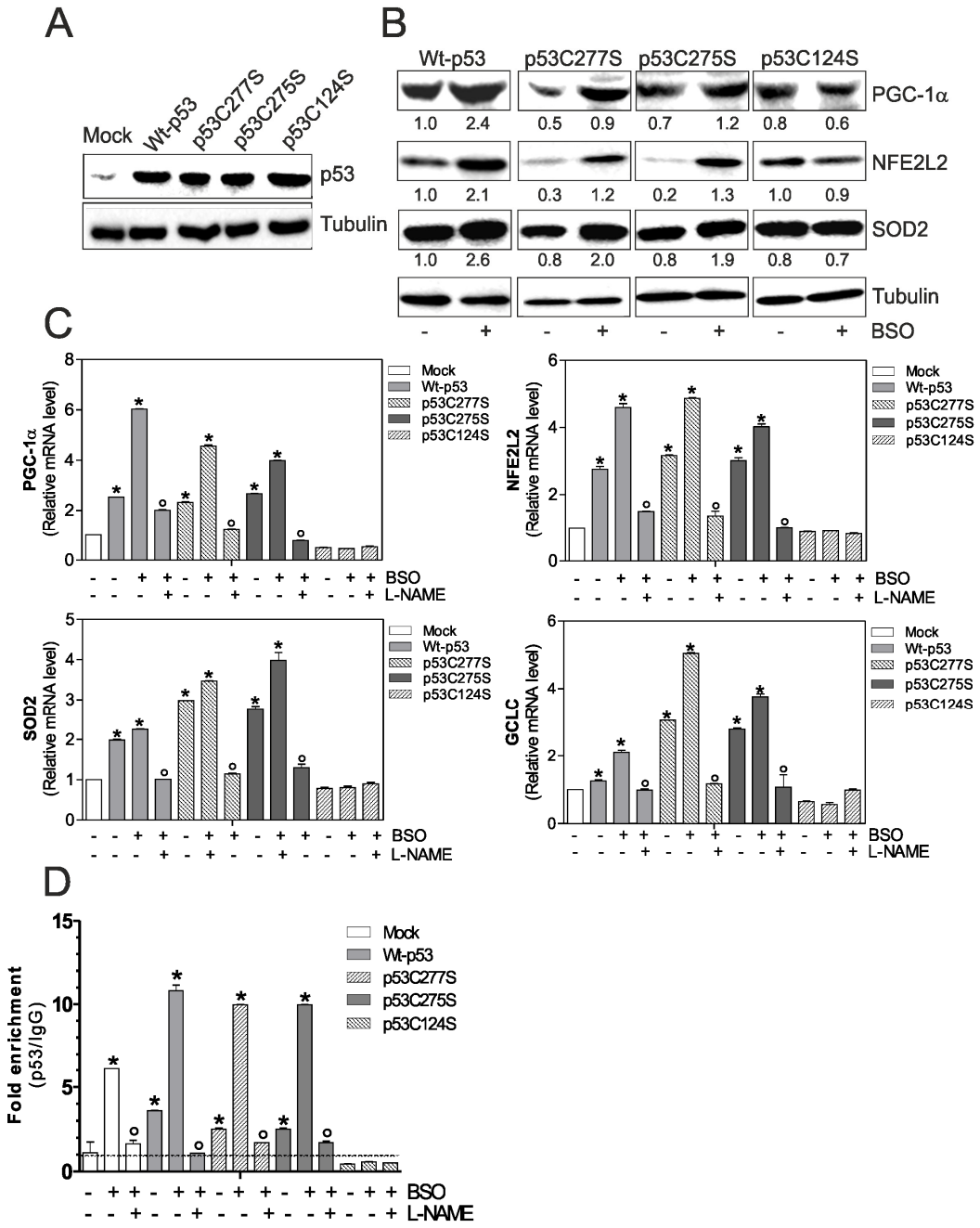

Figure 1. p53C124S mutant fails to induce NO/PGC-1α-mediated antioxidant pathway in C2C12 myoblasts. (**A, B**) C2C12 myoblasts were transfected with pcDNA3.1 vector containing cDNA for wild type p53 (Wt-p53), three single p53 mutants in DBD (p53C277S, p53C275S, p53C124S) or with empty vector (Mock). After 15 h from transfection, myoblasts were treated with 1 mM BSO for 24 h. Cells were lysed and 20 μg of proteins were loaded for Western blot analysis of p53, PGC-1α, NFE2L2 and SOD2. Tubulin was used as loading control. Numbers indicate the density of immunoreactive bands calculated using the Software Quantity one (Bio-Rad) and reported as the ratio of PGC-1α, NFE2L2 and SOD2/Tubulin. (**C**) L-NAME (100 μM) was added 1 h before BSO treatment (15 h) and maintained throughout the experiment. Total RNA was isolated and relative mRNA levels of PGC-1α, NFE2L2, SOD2 and GCLC were analyzed by RT-qPCR. Data are expressed as means ± S.D. (n=4; *p<0.001 *vs* Mock; °p<0.001 *vs* BSO-treated cells). (**D**) ChIP assay was carried out on cross-linked nuclei from Mock, Wt-p53, p53C277S, p53C275S and p53C124S cells using p53 antibody followed by qPCR analysis of p53RE. Dashed line indicates the value of IgG control. Data are expressed as means ± S.D. (n=3; *p<0.001 *vs* Mock; °p<0.05 *vs* BSO-treated cells). All the immunoblots reported are from one experiment representative of four that gave similar results.

(Fig.2D) and mRNA (Suppl.Fig.S1A) levels in Mock and Wt-p53 myoblasts. Contrarily, the transfection of 3Cys-p53 mutant failed to induce PGC-1α-mediated antioxidant pathway (Fig.2D and Suppl.Fig.S1A). Also, in this case, the inhibition of NOSs activity significantly reduced NO-mediated antioxidant pathway only in Mock and Wt-p53 cells (Suppl.Fig.S1A).

To investigate whether the binding capacity of 3Cys-p53 mutant on *ppargc1a* gene was affected, C2C12 nuclear extracts were incubated with biotinylated oligonucleotides representing -2317 p53RE and Western blot analysis of p53 was carried out after oligo pull-down. As reported in Suppl.Fig.S1B the p53 DNA-binding activity was significantly enhanced in BSO-treated Wt-p53 cells. Through quantitative ChIP analysis we also observed p53 enrichment at -2317 p53RE only in Wt-p53 myoblasts (Suppl.Fig.S1C) with respect to 3Cys-p53 mutant. In line with previous results, the concomitant administration of L-NAME completely abrogated the binding of p53 on *ppargc1a* promoter (Suppl.Fig.S1B and C). Moreover, using the biotin switch technique, we did not found any modulation of p53-SNO in nuclei of 3Cys-p53 myoblasts with respect Wt-p53 cells (Suppl.Fig.S2A). These results were also confirmed by evaluating Wt-p53 and 3Cys-p53 binding activity on *ppargc1a* promoter after treatment with a NO donor, S-nitrosoglutathione (GSNO). For this purpose we treated isolated nuclei from Wt-p53 and 3Cys-p53 myoblasts with GSNO and we performed an oligo-pull-down assay by using biotinylated oligonucleotides corresponding to -2317 p53RE. Suppl.Fig.S2B shows that the amount of Wt-p53 able to bind the -2317 p53RE was markedly higher only in GSNO-Wt-p53 treated nuclei and L-NAME treatment was able to

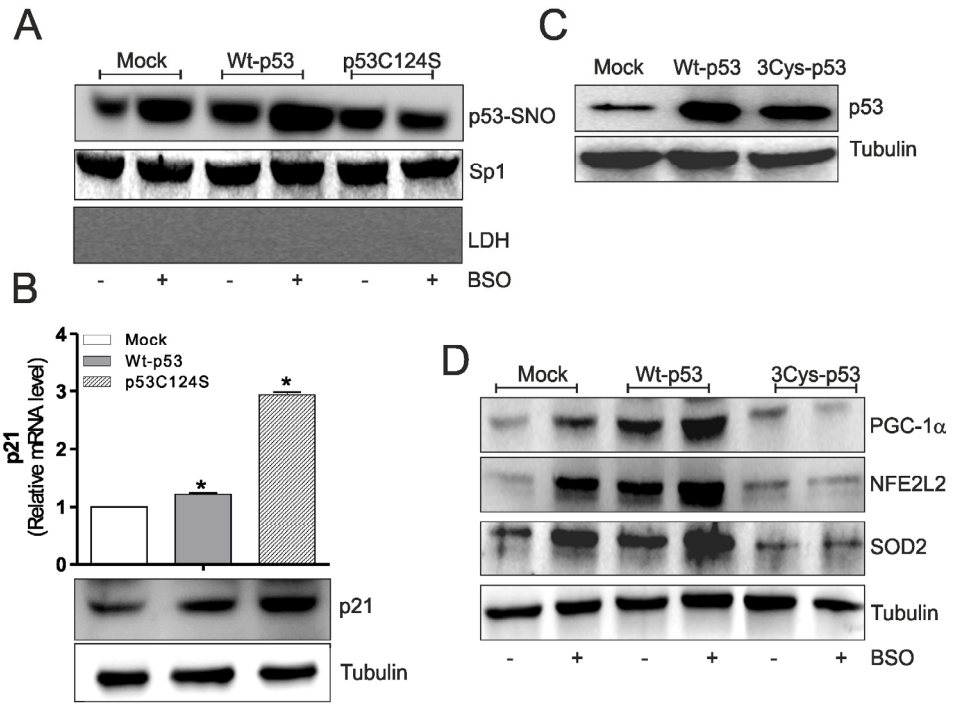

Figure 2. p53C124S mutant does not undergo S-nitrosylation after BSO treatment in C2C12 myoblasts. (**A**) C2C12 myoblasts were transfected with pcDNA3.1 vector containing cDNA for wild type p53 (Wt-p53), single p53 mutant in DBD (p53C124S) or with empty vector (Mock). After 15 h from transfection myoblasts were treated with 1 mM BSO for 24 h. Nuclear proteins (500 μg) were subject to S-NO derivatization with biotin. After Western blot the nitrocellulose was incubated with p53 antibody for detection of p53-SNO. Sp1 was used as loading control. The possible presence of cytoplasmic contaminants was tested by incubating nitrocellulose with rabbit anti-LDH. (**B**) *Upper*: Total RNA was isolated and relative mRNA level of p21 was analyzed by RT-qPCR . Data are expressed as means ± S.D. (n=3; *p<0.05). *Bottom*: Cells were lysed and 20 μg of proteins were loaded for Western blot analysis of p21. Tubulin was used as loading control. (**C, D**) C2C12 myoblasts were transfected with pcDNA3.1 vector containing cDNA for wild type p53 (Wt-p53), triple p53 mutant in DBD (C277S, C275S and C124S) (3Cys-p53) or with empty vector (Mock). After 15 h from transfection myoblasts were treated with 1 mM BSO for 24 h. Cells were lysed and 20 μg of proteins were loaded for Western blot analysis of p53, PGC-1α, NFE2L2 and SOD2. Tubulin was used as loading control. All the immunoblots reported are from one experiment representative of five that gave similar results.

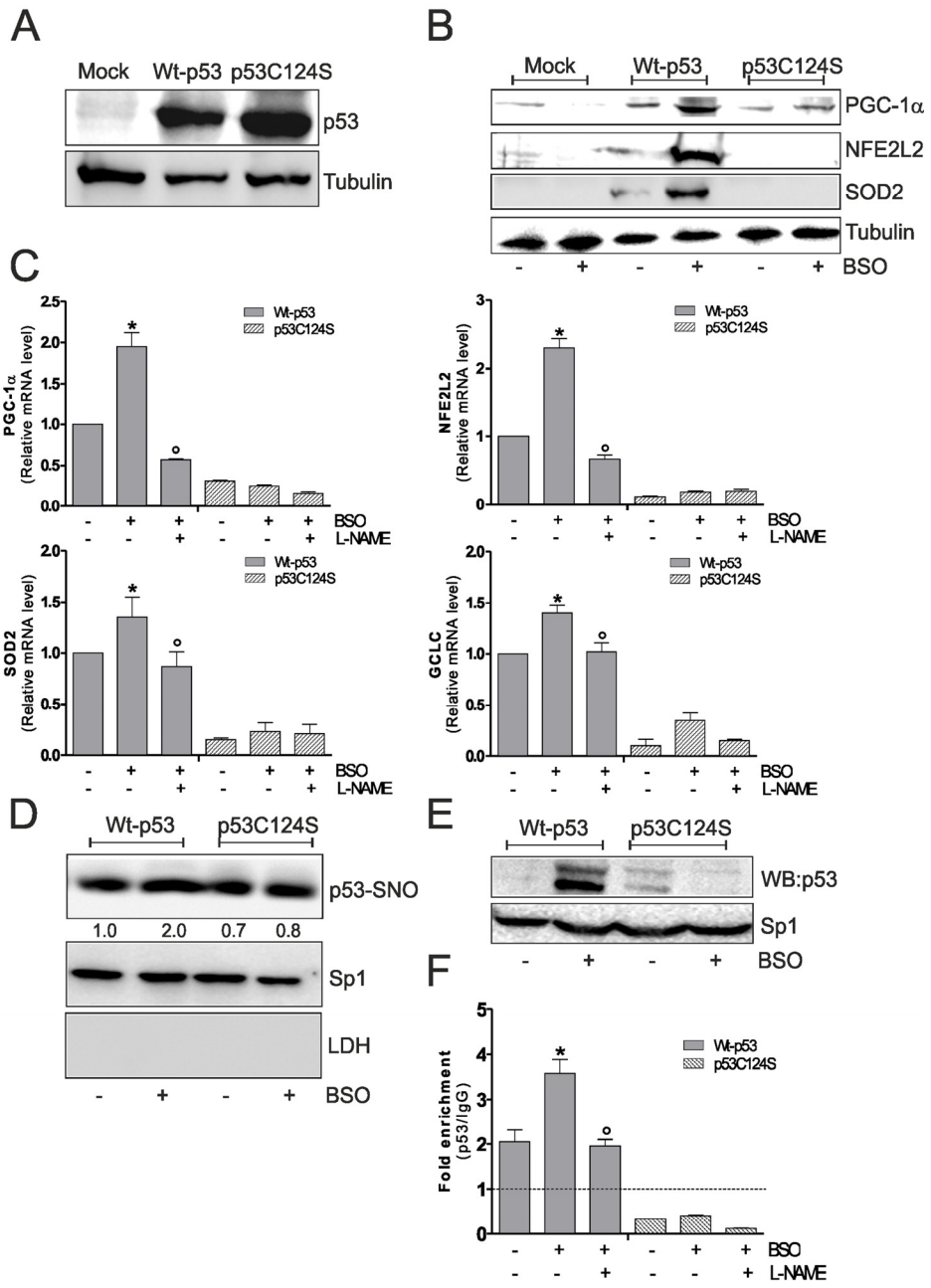

Figure 3. NO/PGC-1α-mediated antioxidant pathway is inhibited after p53C124S overexpression in p53-null NCI-H1299 cells. (**A, B**) NCI-H1299 cells were transfected with pcDNA3.1 vector containing cDNA for wild type p53 (Wt-p53), single p53 mutant in DBD (p53C124S) or with empty vector (Mock). Cells were lysed and 20 μg of proteins were loaded for Western blot analysis of p53, PGC-1α, NFE2L2 and SOD2. Tubulin was used as loading control. (**C**) L-NAME (100 μM) was added 1 h before BSO treatment (15 h) and maintained throughout the experiment. Total RNA was isolated and relative mRNA levels of PGC-1α, NFE2L2, SOD2 and GCLC were analyzed by RT-qPCR. Data are expressed as means ± S.D. (n=3; *p<0.05 *vs* untreated Wt-p53; °p<0.001 *vs* BSO-treated Wt-p53 cells). (**D**) Nuclear proteins (500 μg) were subject to S-NO derivatization with biotin. After Western blot the nitrocellulose was incubated with p53 antibody for detection of p53-SNO. Sp1 was used as loading control. The possible presence of cytoplasmic contaminants was tested by incubating nitrocellulose with rabbit anti-LDH. Numbers indicate the density of immunoreactive bands calculated using the Software Quantity one (Bio-Rad) and reported as the ratio of p53-SNO/Sp1. (**E**) Nuclear protein extracts (500 μg) were subjected to oligo-pull-down by using the biotinylated oligonucleotide representing the p53RE on the PPARGC1A promoter and bound p53 was detected by Western blot. Twenty μg of nuclear proteins (input) were used for Western blot analysis of Sp1. (**F**) ChIP assay was carried out on cross-linked nuclei from Wt-p53 and p53C124S NCI-H1299 cells using p53 antibody followed by qPCR analysis of p53RE. Dashed line indicates the value of IgG control. Data are expressed as means ± S.D. (n=4; *p<0.05 *vs* untreated Wt-p53; °p<0.05 *vs* BSO-treated Wt-p53 cells). All the immunoblots reported are from one experiment representative of four that gave similar results.

restore this event. Contrarily, the use of NO scavenger carboxy-PTIO was not able to reduce the Wt-p53-binding on *ppargc1a* promoter after GSNO treatment (Suppl.Fig.S2B).

In summary, these data suggest that S-nitrosylation of p53 increases its transcriptional activity on *ppargc1a* gene after GSH depletion activating the antioxidants and ensuring the skeletal muscle homeostasis.

S-nitrosylation of C124 is involved in p53 binding on PPARGC1A promoter also in p53-null-NCI-H1299 cell

Overall these results were confirmed in human lung cancer NCI-H1299 cells, which are null for p53. BSO treatment in these cells was able to induce PGC-1α, NFE2L2, SOD2 and GCLC up-regulation only after Wt-p53 transfection and L-NAME is able to inhibit the activation of this antioxidant pathway (Fig.3A, B and C). In accordance with previous results, Wt-p53 NCI-H1299 cells showed a significant increment of nuclear p53-SNO after BSO administration (Fig.3D). The capacity of Wt-p53 to bind the human PPARGC1A promoter at -1237 position was also investigated in NCI-H1299 cells. Fig.3E and F show the inability of p53C124S mutant to bind the PPARGC1A promoter upon GSH depletion. Conversely, an increase of PPARGC1A promoter occupancy in Wt-p53 cells was observed after BSO treatment, confirming the importance of a preserved p53-DBD and of p53 S-nitrosylation status in the signaling pathway that leads to NO/PGC-1α-mediated antioxidant response.

C124S mutation induces atrophy in C2C12 myoblasts

As mentioned above, p53C124S mutant interferes with antioxidant pathways in C2C12 myoblasts, probably altering the homeostasis of skeletal muscle. For this reason, we explored the effect of p53 single mutants on myoblasts differentiation program. We induced differentiation of C2C12 cells after transfection of Wt-p53, p53C277S p53C275S and p53C124S plasmids. Consistent with our previous results, cells transfected with Wt-p53, p53C277S, p53C275S and treated with differentiation medium exhibited increased mRNA levels of differentiation markers MyoD, Pax7 (Paired box 7) and Myogenin. On the contrary, p53C124S cells failed to increase such markers, suggesting a defective myogenesis (Fig.4A).

The effect of p53C124S overexpression on cell growth and viability was analyzed by direct counting by Trypan Blue staining. We found that the C124S mutation profoundly affected cell proliferation (Fig.4B) with an increase in dead cells (Fig.4C), indicating that both proliferation arrest and death occur. This is in line with the p21 protein increase observed in Fig.2B. Next, we have analyzed the mRNA levels of two atrophy markers Atrogin-1 (F-box protein 32) and MuRF-1 (tripartite motif-containing 63), which are two muscle-specific E3 ubiquitin ligases that are increased transcriptionally in skeletal muscle under atrophy-inducing conditions. Fig.4D highlights a significant raise of their expression only in undifferentiated and differentiated p53C124S cells, suggesting that this mutation not only inhibits antioxidant pathway but also blocks myoblasts cell differentiation inducing a degenerative process. To support the hypothesis that p53C124S mutant promotes the transcription of atrophy genes, we analyzed mouse MuRF-1 and Atrogin-1 promoters using Genomatix Software Suite database to identify p53RE. We have found five and one p53RE in mouse Atrogin-1 and MuRF-1 promoters, located at -519, -319, -82, -40, +31 and -351 respectively (Suppl.Fig.S2D, Suppl. Table S1). ChIP analyses of all p53RE were carried out to confirm the regulatory role of p53C124 mutant on the murine Atrogin-1 and MuRF-1 promoters. The qPCR analysis shows a significant increase only in p53C124S occupancy of -351 region on MuRF-1 promoter (Fig.4E), while -519, -319, -82, -40 and +31 regions on Atrogin-1 promoter did not show p53C124S binding at day 0 and 4 of differentiation (data not shown).

Nuclear p53-S-nitrosylation diminished in aged skeletal muscle inhibiting antioxidant response

We have recently demonstrated that during aging of skeletal muscle a significant increase of oxidative/nitrosative stress occurs. In particular, we observed a decrease of GSH levels and a diminished induction of NO/PGC-1α-mediated redox signaling pathway accompanied by an accumulation of total S-nitrosylated proteins [12]. Since S-nitrosylation of C124 on p53-DBD seems to play a key role in the induction of NO/PGC-1α-mediated antioxidant pathway, we investigated the involvement of such mechanism in PGC-1α-mediated antioxidant response decrement during aging. Firstly, we confirmed the increase of total S-nitrosylated protein in skeletal muscle of old mice (Fig.5A). This result was also confirmed by the analysis of NADH-dependent *S*-nitrosoglutathione (GSNO) reductase (GSNOR), a denitrosylating enzyme that indirectly buffers the concentration of protein SNOs, by reducing the low-molecular-weight nitrosothiol GSNO. Fig.5B clearly indicates diminished protein levels of GSNOR in aged skeletal muscle, which could be in part responsible for S-nitrosylation protein increase. Moreover, total protein levels of p53 were slightly decreased in old with respect to young mice (Fig.5B). Subsequently, we analyzed the levels of nuclear S-

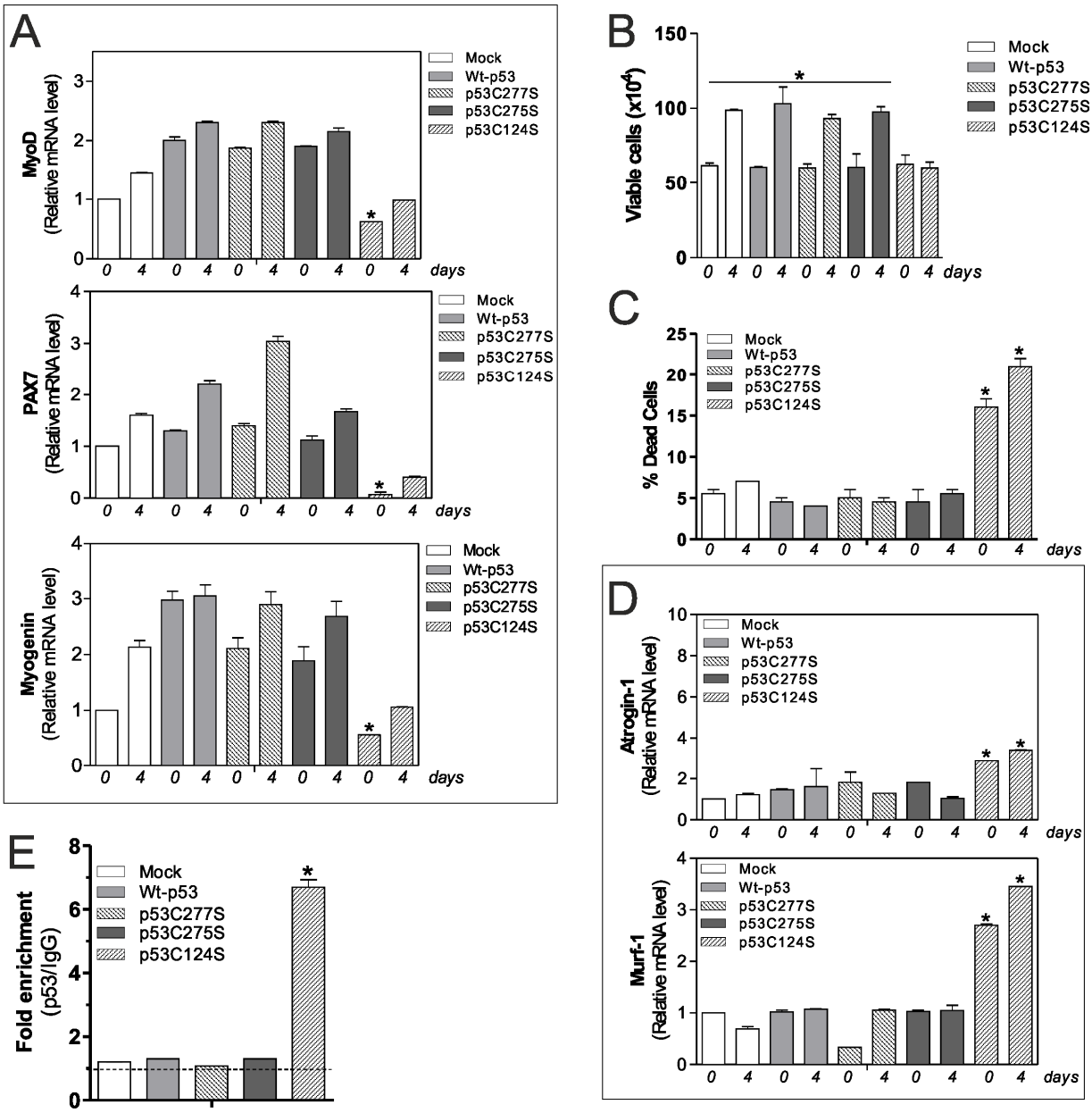

Figure 4. p53C124S mutant induces atrophy of C2C12 myoblasts. (**A**) C2C12 myoblasts were transfected with pcDNA3.1 vector containing cDNA for wild type p53 (Wt-p53), three single p53 mutants in DBD (p53C277S, p53C275S, p53C124S) or with empty vector (Mock). After 24 h from transfection C2C12 cells were differentiated for 4 days. Total RNA was isolated and relative mRNA levels of MyoD, PAX7 and Myogenin were analyzed by RT-qPCR. Data are expressed as means ± S.D. All the values were significantly different with respect to Mock day 0/4 (n=3, $p<0.05$; *$p<0.05$ was significantly decreased with respect Mock day 0). (**B**) Cells were counted by Trypan Blue exclusion. Data are expressed as means ± S.D. All the values were significantly different with respect to day 0 (n=4 *$p<0.05$). (**C**) Dead cells were counted by Trypan blue exclusion. Data are expressed as means ± SD (n=4, *$p<0.001$ *vs* Mock-, Wt-p53-, p53C277S- and p53C275S-day 0/4 cells). (**D**) Total RNA was isolated and relative mRNA levels of MuRF-1 and Atrogin-1 were analyzed by RT-qPCR. Data are expressed as means ± S.D. (n=3; *$p<0.05$ *vs* Mock-, Wt-p53-, p53C277S- and p53C275S-day 0/4 cells). (**E**) ChIP assay was carried out on cross-linked nuclei from Mock, Wt-p53, p53C277S, p53C275S and p53C124S cells at day 4 of myogenesis using p53 antibody followed by qPCR analysis of p53RE. Dashed line indicates the value of IgG control. Data are expressed as means ± S.D. (n=3; *$p<0.001$ *vs* Mock-, Wt-p53-, p53C277S- and p53C275S-day 4 cells).

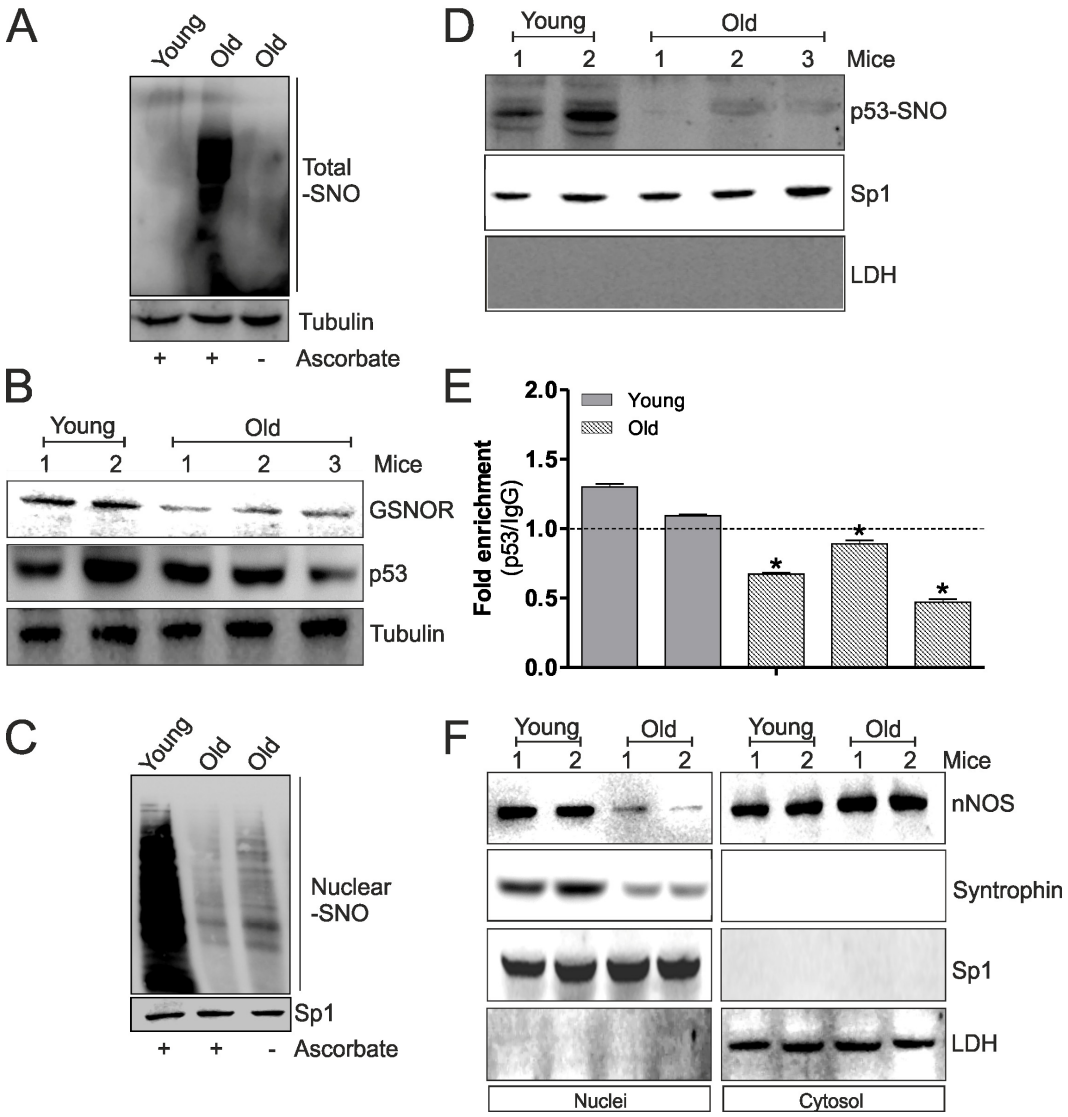

Figure 5. The decrement of nNOS nuclear localization inhibits p53 S-nitrosylation and its binding on *ppargc1a* promoter during aging. (**A**) Skeletal muscle of young (12 weeks) and old (80 weeks) mice was homogenized and total proteins (500 μg) were subjected to S-NO derivatization with biotin. After Western blot, biotin adducts were identified by incubating nitrocellulose membrane with HRP-conjugate streptavidin. Proteins incubated in labeling buffer without ascorbate were used as negative control (-Ascorbate). Tubulin was used as loading control. (**B**) Skeletal muscle of two young (12 weeks) and three old (80 weeks) mice was homogenized and total proteins (20 μg) were loaded for Western blot analysis of GSNOR and p53. Tubulin was used as loading control. (**C**) Skeletal muscle of young (12 weeks) and old (80 weeks) mice was homogenized and nuclear proteins (500 μg) were subjected to S-NO derivatization with biotin. After Western blot, biotin adducts were identified by incubating nitrocellulose membrane with HRP-conjugate streptavidin. Proteins incubated in labeling buffer without ascorbate were used as negative control (-Ascorbate). Sp1 was used as loading control. (**D**) Skeletal muscle of two young (12 weeks) and three old (80 weeks) mice was homogenized and nuclear proteins (500 μg) were subjected to S-NO derivatization with biotin. After Western blot the nitrocellulose was incubated with p53 antibody for detection of p53-SNO. Sp1 was used as loading control. The possible presence of cytoplasmic contaminants was tested by incubating nitrocellulose with rabbit anti-LDH. (**E**) ChIP assay was carried out on cross-linked nuclei from two young (12 weeks) and three old (80 weeks) mice using p53 antibody followed by qPCR analysis of p53RE. Dashed line indicates the value of IgG control. Data are expressed as means ± S.D. (n=3; *p<0.05). (**F**) Skeletal muscle of two young (12 weeks) and two old (80 weeks) mice was homogenized and 20 μg of nuclear and cytoplasmic extracts were loaded for detection of nNOS and Syntrophin by Western blot. Sp1 was used as loading control. The possible presence of cytoplasmic contaminants was tested by incubating nitrocellulose with rabbit anti-LDH. All the immunoblots reported are from one experiment representative of four that gave similar results.

nitrosylated proteins in aged skeletal muscle. As shown in Fig.5C, a decrease of nuclear S-nitrosylation is observed in skeletal muscle of aged mice. These results were confirmed by a decrease of p53-SNO levels in nuclei and a diminished binding of p53 on *ppargc1a* promoter (Fig.5D and E). These events probably elicited decreased PGC-1α-mediated antioxidant response observed during aging. Next to this, we have previously demonstrated that nNOS, interacting with Syntrophin, locates on nuclear membrane favoring local NO production, nuclear S-nitrosylation and induction of mitochondrial biogenesis during myogenesis [17]. These results strongly suggest the importance of nuclear nNOS activity in transcriptional regulation of NO/PGC-1α-mediated antioxidant target genes also during aging. For this reason, we analyzed nNOS and Syntrophin nuclear and cytoplasmic localization in young and old skeletal muscle. Western blot analysis of nNOS and Syntrophin carried out on nuclear fraction showed that these proteins were able to localize in nuclei only in young mice (Fig.5F), which exhibited a higher extent of S-nitrosylated proteins in nuclei with respect to aged mice (Fig.5C). Contrarily, nuclear associated nNOS was significantly diminished in aged mice, whereas its content is likely increased in cytoplasmic extracts (Fig.5F). Taken together, these results indicate that p53 binding on *ppargc1a* promoter requires the nuclear NO flux, which permits the transcription of *ppargc1a* gene and consequently the induction of antioxidant response, through the nitrosylation of p53-DBDC124. The decrement of nuclear nNOS localization during aging determines a loss of nuclear S-nitrosylated p53 and a failure in inducing PGC-1α-mediated pathway.

DISCUSSION

Among the multifactorial aspects characterizing aging, sarcopenia, a continuous and progressive loss of muscle mass, represents an important public health problem related to frailty and disability [2]. Sarcopenia is characterized by alteration of a multitude of pathways largely ascribed to endocrine system and molecular processes that lead to the tight-related alterations in grip strength, physical performance and muscle mass homeostasis. Moreover, age-related changes in skeletal muscle are attributed also to activation and/or repression of specific molecules, such as atrogenes and PGC-1α [18, 19].

At molecular level a well-established hallmark of aged muscle is the increase in oxidative/nitrosative damage, which is recognized to contribute to skeletal muscle degeneration [20, 21]. Moreover, we found that, upon mild oxidative stress, nNOS is recruited to nuclei where it increases local NO production, S-nitrosylation of nuclear proteins and the induction of mitochondrial biogenesis in C2C12 cells [17]. In this context, p53 was capable to restrain oxidative stress, by orchestrating an antioxidant response through induction of antioxidant genes [11]. Overall data uncover an additional role for p53 in transcriptional regulation of genes involved in skeletal muscle homeostasis and functionality.

Here, we deeply dissected the p53-mediated signaling process under mild oxidative stress and we were able to identify a cysteine residue in the p53 DBD essential for the antioxidant response activation. Indeed, the data obtained with p53 mutants clearly indicated that the cysteine 124 was the sole and pivotal for induction of p53-mediated antioxidant response. Actually, the p53 C124S mutant failed to bind the p53RE on *ppargc1a* promoter abolishing the activation of antioxidant response.

Cysteine-S-nitrosylation represents one of the post-translational modifications through which redox signaling pathways can be tuned. Therefore, being aware that NO is the most suited molecule for constraining such modification and that upon mild redox unbalance its concentration raises at nuclear level, the data obtained with the C124S mutant undoubtedly indicated that this cysteine residue was prone to S-nitrosylation and this process was necessary for activating p53-downstream target genes. Even other cysteine residues characterized the p53 DBD domain, but only the C124S mutant did not undergo S-nitrosylation abolishing the binding to the *ppagc1a* promoter, highlighting, at the molecular level, the specificity of this residue in the redox signaling process.

We recently showed that during aging the increase of oxidative damage to proteins was paralleled by a decrement in glutathione, the main low molecular weight antioxidant, and complemented by the alteration of a PPAR-α/PGC-1α-mediated antioxidant signaling axis in gastrocnemius/soleus of old mice [4]. In this report, we demonstrated that although an increase in total protein S-nitrosylation occurred during muscle aging, a decrease of such process at nuclear level was observed. This evidence nicely associated with a concomitant decrement in p53 S-nitrosylation and with the observed diminished recruitment of nNOS/Syntrophin complex on nuclear membrane. We speculated that this failure by preventing nuclear sited NO flux inhibited local S-nitrosylation of p53 and might be responsible for the loss of efficient p53-SNO-dependent antioxidant response during aging. On the contrary, the increased total protein S-nitrosylation, in aged muscle, found a rationale in the observed glutathione decrement [4] as well as on the present data indicating a significant diminution of the expression levels of GSNOR. In fact, GSNOR is the primary

system of the cell for degrading the main non-protein S-nitrosothiol GSNO, which by being in equilibrium with protein S-NOs, indirectly controls cellular concentrations of protein S-NOs [22]. The decrement in both glutathione and GSNOR makes the physiological NO flux more detrimental for proteins at cytosolic and other compartments, unless nucleus; another oxidative risk damage for aged muscle. Overall this evidence confirmed that NO is the principal mediator of p53 transcriptional activity on *ppargc1a* promoter. Accordingly, in-batch treatment of isolated nuclei with NO donor significantly increases the binding capacity of WT-p53 on its *consensus* sequence.

p53 plays important roles during differentiation and sarcopenia of skeletal muscle, though the exact mechanism(s) that regulate its transcriptional activity are still unclear. Some evidence demonstrated that the protein levels of p53 as well of p21 and GADD45a, two established transcriptional targets of p53, are higher in older muscle tissue, suggesting a requirement of p53 in promoting and regulating sarcopenia of skeletal muscle [23]. Schwarzkopf and colleagues suggested that chronic activation of p53 leads to premature aging associated with a significant atrophy [7, 24]. Contrarily, Feng *et al.* demonstrated a progressive decline of p53 protein level and p53-dependent pathways in various tissues of older mice, leading to premature aging [25]. Here, we give the proof that the inhibition of p53-SNO/PGC-1α-mediated antioxidant pathway is associated with increased markers of myotube degeneration. In particular, our data showed that failure of C124 S-nitrosylation switched the binding of p53 on MuRF-1 gene promoter inducing premature atrophy and cell death of skeletal muscle cells. Similarly, other studies reported that p53 knockout mice showed an alteration of mitochondrial activity in mixed muscle and lowered PGC-1α protein levels in gastrocnemius. Intermyofibrillar mitochondria of these animals were characterized by reduced respiration and elevated reactive oxygen species production. In addition, these animals displayed greater fatigability and less locomotor endurance [26].

It is possible to postulate that C124-S-nitrosilatyion of p53 by inducing myogenesis and antioxidant response is implicated in maintaining skeletal muscle homeostasis and functions. Thus, our findings could be helpful for the comprehension of molecular mechanism underlying muscular pathologies or myopathies characterized by alteration in antioxidant response.

In conclusion, our results show that under mild oxidative stress nuclear NO is the primary mediator of p53 post-translational modification in skeletal muscle. S-nitrosylation of C124 is the mandatory event for NO/p53/PGC-1α-mediated antioxidant response. Thus, during aging the loss of nuclear nNOS/Syntrophin complex located on nuclear membrane may contribute to both an increase of total protein S-nitrosylation and myopathy. Therefore, maintaining/restoring p53 S-nitrosylation status could represent a new tool to prevent or treat myopathies and atrophy condition.

METHODS

Animals

We conducted all mouse experimentations in accordance with accepted standard of humane animal care and with the approval by relevant national (Ministry of Welfare) and local (Institutional Animal Care and Use Committee, Tor Vergata University, Rome, Italy) committees. C57BL/6 mice were purchased from Harlan Laboratories Srl (Urbino, Italy). 12- and 80-weeks-old mice were considered as young and old mice, respectively. Mice were fed ad libitum with standard pellet diet and free access to water. Before sacrifice mice were subjected to fasting for seven hours. Mice were killed by cervical dislocation, gastrocnemius/soleus muscle was explanted immediately, frozen on dry ice and stored -80 °C.

Cell cultures and treatments

The murine skeletal muscle C2C12 cells and human lung cancer NCI-H1299 cells were obtained from the European Collection of Cell Cultures (Salisbury, UK). NCI-H1299 cells lacking of p53 were a kind gift of Prof. Gianni Cesareni (Department Biology, University of Rome Tor Vergata). C2C12 myoblasts and NCI-H1299 cells were cultured in growth medium composed of Dulbecco's Modified Eagle's Medium (DMEM) and RPMI-1640 medium respectively, supplemented with 10% fetal bovine serum, 100 U/ml penicillin/streptomycin and 2mM glutamine (Lonza Sales, Basel, Switzerland) and maintained at 37°C in an atmosphere of 5% CO_2 in air. C2C12 myoblasts were plated at 80% of confluence and cultured in growth medium for 24 h. To induce differentiation, cells were washed in PBS and growth medium was replaced with differentiation medium (DM), which contained 2% heat inactivated horse serum (Lonza, ECS0090D) [4].

BSO, a highly selective and potent inhibitor of the enzyme GCLC, was added in the culture medium at a concentration of 1 mM after 15 h from transfection. The NOS inhibitor L-NAME was used at a concentration of 100 μM (1 h before BSO treatment) and maintained throughout the experiment. The NO scavenger carboxy-PTIO was added at a concentration of 2 μM and maintained throughout the experiment as previously

described [11, 27]. GSNO was added to purified nuclei at a concentration of 5 mM at 4°C for 30 min in nucleus lysis buffer (NLB) containing 50 mM Tris-HCl pH 8.1, 10 mM EDTA, 1% SDS, 10 mM sodium butyrate, protease inhibitors and incubated 1 h at 4°C.

Transfection

C2C12 myoblasts and NCI-H1299 cells were stably transfected with the following plasmids: pcDNA3.1-p53 (Wt-p53), four mutants (single mutants: p53C124S, p53C277S, p53C275S and triple mutant C124-277-275S) or pcDNA3.1 empty vector (kindly donated by Dr. Yvonne Sun, The Cancer Institute of New Jersey, NJ and Dr. Marikki Laiho, Marikki Laiho, Haartman Institute, Department of Virology, University of Helsinki, Hensinky) by electroporation using Nucleofector 4D® (Lonza, Sales) according to the manufacturer's instructions, and were immediately seeded into fresh medium. Transfection efficiency was estimated by co-transfecting the cells with pMAX-FP-GreenC vector (Lonza Sales). Only experiments that gave transfection efficiency of 80% were considered. Twenty-four hours after transfection (day 0), differentiation was induced.

RT-qPCR analysis

Total RNA was extracted using TRI Reagent (Sigma-Aldrich) and used for retro-transcription. qPCR was performed in triplicate by using validated qPCR primers (BLAST), Ex TAq qPCR Premix (Lonza Sales) and the Roche Real Time PCR LightCycler II (Roche Applied Science, Monza, Italy). mRNA levels were normalized to RPL, and the relative mRNA levels were determined by using the $2^{-\Delta\Delta Ct}$ method [28]. The primer sequences are listed in Supplementary Table S2.

Preparation of cell lysates and Western blot analyses

Cell pellets were resuspended in RIPA buffer (50 mM Tris-HCl, pH 8.0, 150 mM NaCl, 12 mM deoxycholic acid, 0.5% Nonidet P-40 and protease inhibitors). Protein samples were used for SDS-PAGE followed by Western blotting as previously described [12]. Nitrocellulose membranes were stained with primary antibodies against Tubulin (1:1000), PGC-1α (1:500), SOD2 (1:2000), NFE2L2 (1:1000), p53 (1:1000), p21 (1:1000), Sp1 (1:500), GSNOR (1:500), nNOS (C-terminal 1:500), Syntrophin (1:1000) and LDH (1:1000). Afterward, the membranes were incubated with the appropriate horseradish peroxidase conjugated secondary antibody, and immunoreactive bands were detected by a Fluorchem Imaging System upon staining with ECL Select Western Blotting Detection Reagent (GE Healthcare, Pittsburgh, PA, USA; RPN2235). Immunoblots reported in the figures are representative of at least four experiments that gave similar results. Tubulin and Sp1 were used as loading controls.

Proteins were assayed by the method of Lowry [29].

Preparation of nuclear extracts

Cell pellets were resuspended in NLB. Nuclei were collected by centrifugation at 600 x g for 5 min at 4°C and pellets were resuspended in 1 ml of NLB. Subsequently, nuclei were purified on NLB containing 30% sucrose (w/v) and centrifuged at 700 x g for 10 min. The pellets were resuspended in NLB to remove nuclear debris and finally used for Western blot, oligo-pull-down or ChIP assays.

Oligo-pull-down

The assay was performed essentially as previously described [30] by using the p53RE at –2317 and -1237 on the mouse and human PGC-1α gene promoter (*ppargc1a* and PPARGC1A), respectively (Suppl. Table S1). Briefly, nuclear protein extracts were incubated with 1 μg of promoter biotinylated at 5' and proteins were allowed to bind the oligonucleotide for 30 min at room temperature. The oligonucleotides were precipitated with UltraLink streptavidin beads (Pierce) for 1 h at 4°C. Bound fractions were washed three times with wash buffer (20 mM Tris-HCl, pH 7.5, 1 mM EDTA, 10% glycerol, 0.1% Triton X-100), eluted with denaturing buffer, and analyzed by Western Blotting using anti-p53 antibody. Oligo-pull-down specificity was demonstrated with mutant oligonucleotides used as negative controls (data not shown).

Chromatin immunoprecipitation assay

ChIP was carried out according to the protocol of Im et al. [31] with some modifications. Briefly, after cross-linking the nuclei extracted from C2C12 and NCI-H1299 cells were fragmented by ultrasonication using 4x15 pulse (output 10%, duty 30%). Samples were pre-cleared with pre-adsorbed salmon sperm Protein G agarose beads (1 h, 4°C), and overnight immunoprecipitation using anti-p53 or control IgG antibody was carried out. After de-cross-linking (1% SDS at 65°C for 3 h), qPCR was used to quantify the promoter binding with 30 cycles total (95°C, 1 s; 60°C, 30 s; 72°C, 60 s). Results are expressed as fold enrichment with respect to IgG control. The primers used are reported in Supplementary Table S1.

Biotin switch assay

Biotin switch assay was performed as previously described [17]. Briefly, proteins were subjected to S-NO derivatization by incubation in the presence of ascorbate, which reduces S-NO groups. The same sample incubated in the presence of biotin without ascorbate was used as negative control. After protein separation by non-reducing SDS-PAGE and Western blot, biotinylated proteins were detected by incubation of nitrocellulose membrane with HRP-conjugated streptavidin (1:1000).

Analysis of cell viability

Adherent (after trypsinization) and detached cells were combined, washed with PBS and directly counted by optical microscope on hemocytometer, after Trypan Blue staining.

Statistical analysis

The results are presented as means ± S.D. Statistical evaluation was conducted by ANOVA, followed by the post Student-Newman-Keuls test. Differences were considered to be significant at $p<0.05$.

CONFLICTS OF INTEREST

The authors have no conflict of interests to declare.

FUNDING

This work was partially supported by grants from Ministero dell'Istruzione, dell'Università e della Ricerca (MIUR) and Italian Association for Cancer Research (AIRC-IG 15403).

REFERENCES

1. Wall BT, Dirks ML, van Loon LJ. Skeletal muscle atrophy during short-term disuse: implications for age-related sarcopenia. Ageing Res Rev. 2013; 12:898–906. doi: 10.1016/j.arr.2013.07.003

2. Bell KE, von Allmen MT, Devries MC, Phillips SM. Muscle disuse as a pivotal problem in sarcopenia-related muscle loss and dysfunction. J Frailty Aging. 2016; 5:33–41. doi: 10.14283/jfa.2016.78

3. Doria E, Buonocore D, Focarelli A, Marzatico F. Relationship between human aging muscle and oxidative system pathway. Oxid Med Cell Longev. 2012; 2012:830257. doi: 10.1155/2012/830257

4. Aquilano K, Baldelli S, La Barbera L, Lettieri Barbato D, Tatulli G, Ciriolo MR. Adipose triglyceride lipase decrement affects skeletal muscle homeostasis during aging through FAs-PPARα-PGC-1α antioxidant response. Oncotarget. 2016; 7:23019–32. doi: 10.18632/oncotarget.8552

5. Molchadsky A, Rivlin N, Brosh R, Rotter V, Sarig R. p53 is balancing development, differentiation and de-differentiation to assure cancer prevention. Carcinogenesis. 2010; 31:1501–08. doi: 10.1093/carcin/bgq101

6. White JD, Rachel C, Vermeulen R, Davies M, Grounds MD. The role of p53 in vivo during skeletal muscle post-natal development and regeneration: studies in p53 knockout mice. Int J Dev Biol. 2002; 46:577–82.

7. Schwarzkopf M, Coletti D, Sassoon D, Marazzi G. Muscle cachexia is regulated by a p53-PW1/Peg3-dependent pathway. Genes Dev. 2006; 20:3440–52. doi: 10.1101/gad.412606

8. P orrello A, Cerone MA, Coen S, Gurtner A, Fontemaggi G, Cimino L, Piaggio G, Sacchi A, Soddu S. p53 regulates myogenesis by triggering the differentiation activity of pRb. J Cell Biol. 2000; 151:1295–304. doi: 10.1083/jcb.151.6.1295

9. Cam H, Griesmann H, Beitzinger M, Hofmann L, Beinoraviciute-Kellner R, Sauer M, Hüttinger-Kirchhof N, Oswald C, Friedl P, Gattenlöhner S, Burek C, Rosenwald A, Stiewe T. p53 family members in myogenic differentiation and rhabdomyosarcoma development. Cancer Cell. 2006; 10:281–93. doi: 10.1016/j.ccr.2006.08.024

10. Yang ZJ, Broz DK, Noderer WL, Ferreira JP, Overton KW, Spencer SL, Meyer T, Tapscott SJ, Attardi LD, Wang CL. p53 suppresses muscle differentiation at the myogenin step in response to genotoxic stress. Cell Death Differ. 2015; 22:560–73. doi: 10.1038/cdd.2014.189

11. Aquilano K, Baldelli S, Pagliei B, Cannata SM, Rotilio G, Ciriolo MR. p53 orchestrates the PGC-1α-mediated antioxidant response upon mild redox and metabolic imbalance. Antioxid Redox Signal. 2013; 18:386–99. doi: 10.1089/ars.2012.4615

12. Aquilano K, Baldelli S, La Barbera L, Lettieri Barbato D, Tatulli G, Ciriolo MR. Adipose triglyceride lipase decrement affects skeletal muscle homeostasis during aging through FAs-PPARα-PGC-1α antioxidant response. Oncotarget. 2016; 7:23019–32. doi: 10.18632/oncotarget.8552.

13. Aquilano K, Baldelli S, Cardaci S, Rotilio G, Ciriolo MR. Nitric oxide is the primary mediator of

cytotoxicity induced by GSH depletion in neuronal cells. J Cell Sci. 2011; 124:1043–54. doi: 10.1242/jcs.077149

14. Gould N, Doulias PT, Tenopoulou M, Raju K, Ischiropoulos H. Regulation of protein function and signaling by reversible cysteine S-nitrosylation. J Biol Chem. 2013; 288:26473–79. doi: 10.1074/jbc.R113.460261

15. Schonhoff CM, Daou MC, Jones SN, Schiffer CA, Ross AH. Nitric oxide-mediated inhibition of Hdm2-p53 binding. Biochemistry. 2002; 41:13570–74. doi: 10.1021/bi026262q

16. Rainwater R, Parks D, Anderson ME, Tegtmeyer P, Mann K. Role of cysteine residues in regulation of p53 function. Mol Cell Biol. 1995; 15:3892–903. doi: 10.1128/MCB.15.7.3892

17. Aquilano K, Baldelli S, Ciriolo MR. Nuclear recruitment of neuronal nitric-oxide synthase by α-syntrophin is crucial for the induction of mitochondrial biogenesis. J Biol Chem. 2014; 289:365–78. doi: 10.1074/jbc.M113.506733

18. Sakuma K, Aoi W, Yamaguchi A. The intriguing regulators of muscle mass in sarcopenia and muscular dystrophy. Front Aging Neurosci. 2014; 6:230. doi: 10.3389/fnagi.2014.00230

19. Baldelli S, Lettieri Barbato D, Tatulli G, Aquilano K, Ciriolo MR. The role of nNOS and PGC-1α in skeletal muscle cells. J Cell Sci. 2014; 127:4813–20. doi: 10.1242/jcs.154229

20. Brioche T, Lemoine-Morel S. Oxidative stress, sarcopenia, antioxidant strategies and exercise: molecular aspects. Curr Pharm Des. 2016; 22:2664–78. doi: 10.2174/1381612822666160219120531

21. Jackson MJ. Reactive oxygen species in sarcopenia: should we focus on excess oxidative damage or defective redox signalling? Mol Aspects Med. 2016; 50:33–40. doi: 10.1016/j.mam.2016.05.002

22. Hogg N. The biochemistry and physiology of S-nitrosothiols. Annu Rev Pharmacol Toxicol. 2002; 42:585–600. doi: 10.1146/annurev.pharmtox.42.092501.104328

23. Edwards MG, Anderson RM, Yuan M, Kendziorski CM, Weindruch R, Prolla TA. Gene expression profiling of aging reveals activation of a p53-mediated transcriptional program. BMC Genomics. 2007; 8:80. doi: 10.1186/1471-2164-8-80

24. Rodier F, Campisi J, Bhaumik D. Two faces of p53: aging and tumor suppression. Nucleic Acids Res. 2007; 35:7475–84. doi: 10.1093/nar/gkm744

25. Feng Z, Hu W, Teresky AK, Hernando E, Cordon-Cardo C, Levine AJ. Declining p53 function in the aging process: a possible mechanism for the increased tumor incidence in older populations. Proc Natl Acad Sci USA. 2007; 104:16633–38. doi: 10.1073/pnas.0708043104

26. Saleem A, Adhihetty PJ, Hood DA. Role of p53 in mitochondrial biogenesis and apoptosis in skeletal muscle. Physiol Genomics. 2009; 37:58–66. doi: 10.1152/physiolgenomics.90346.2008

27. Baldelli S, Aquilano K, Rotilio G, Ciriolo MR. Glutathione and copper, zinc superoxide dismutase are modulated by overexpression of neuronal nitric oxide synthase. Int J Biochem Cell Biol. 2008; 40:2660–70. doi: 10.1016/j.biocel.2008.05.013

28. Pagliei B, Aquilano K, Baldelli S, Ciriolo MR. Garlic-derived diallyl disulfide modulates peroxisome proliferator activated receptor gamma co-activator 1 alpha in neuroblastoma cells. Biochem Pharmacol. 2013; 85:335–44. doi: 10.1016/j.bcp.2012.11.007

29. Lowry OH, Rosebrough NJ, Farr AL, Randall RJ. Protein measurement with the Folin phenol reagent. J Biol Chem. 1951; 193:265–75.

30. Baldelli S, Aquilano K, Rotilio G, Ciriolo MR. Neuronal nitric oxide synthase interacts with Sp1 through the PDZ domain inhibiting Sp1-mediated copper-zinc superoxide dismutase expression. Int J Biochem Cell Biol. 2011; 43:163–69. doi: 10.1016/j.biocel.2010.10.016

31. Im H, Grass JA, Johnson KD, Boyer ME, Wu J, Bresnick EH. Measurement of protein-DNA interactions in vivo by chromatin immunoprecipitation. Methods Mol Biol. 2004; 284:129–46. doi: 10.1385/1-59259-816-1:129

SUPPLEMENTARY MATERIALS

Supplementary Table S1: List of primers used for ChIP analysis and Oligo-pull-down assay.

Genes	Sequence
mppargc1a	FW 5'-GCGAGGTTTCTGCTTAGTCA-3'
(-2317)	RV 5'-ACAATGACTAAGCAGAAACCTCG-3'
hPPARGC1A	FW 5'-TGTCTGTGAACTGAGGGAAAAA-3'
(-1237)	RV 5'-AGGGCTAATGCAGGTAGGTG-3'
mMuRF-1	FW 5'-GAGCCGCGGGCGCCTCGGAAAAC-3'
(-351)	RV 5'-AGAGCAGGCTGAGGACATGTGAAAG-3'
mAtrogin-1	Atrogin-1 agccgCATGgccaggccagatgtcc -319
	Atrogin-1 gatcgtggcctttcaCATGtcctca +31
	Atrogin-1 agagCAGGctgaggacatgtgaaag -40
	Atrogin-1 acccCAAGgtccctacaagttccca -82
	Atrogin-1 atatgaggctctggcCATGacctaa -519
hPPARGC1A	5'-(btn)AACATGTTTATTCACACAGA-3'
(-1237)	5'-(btn)TCTGTGTGAATAAACATGTT-3'
mppargc1a	5'-(btn)CTCTAAATAAAAAATGTTATAC-3'
(-2317)	5'-(btn)GTATAACATTTTTTATTTAGAG-3'

Supplementary Table S2: List of primers used for RT-qPCR analysis.

Genes	Sequences
mAtrogin-1 FW	5'-GCGACCTTCCCCAACGCCTG-3'
mAtrogin-1 RV	5'-GGCGACCGGGACAAGAGTGG-3'
mCGLC FW	5'-CGCACAGCGAGGAGCTTCGG-3'
mCGLC RV	5'-CTCCACTGCATGGGACATGGTGC-3'
hCGLC FW	5'-AGGAGCGAGGACTGGAGCCAT-3'
hCGLC RV	5'-GCAACATGCTGGGCCAGGAGA-3'
mMuRF-1 FW	5'-AGGGGCTACCTTCCTCTAAGTG-3'
mMuRF-1 RV	5'-TCTTCCCCAGCTGGCAGCCC-3'
mMyoD FW	5'-GGGGCCGCTGTAATCCATCATGC-3'
mMyoD RV	5'-GGAGATCCTGCGCAACGCCA-3'
mNFE2L2 FW	5'-TCCGCCAGCTACTCCCAGGTTG-3'
mNFE2L2 RV	5'-TGGGCCTGATGAGGGGCAGTG-3'
hNFE2L2 FW	5'-ACAGGAGGAGGAAGTGGAGGGACT-3'
hNFE2L2 RV	5'-TCAGCTGGCGCGTAGGTTTGT-3'
mPAX-7 FW	5'-TTCGATTAGCCGAGTGCTCA-3'
mPAX-7 RV	5'-ATCCAGACGGTTCCCTTTG-3'
mPGC-1α FW	5'-ACTGCAGGCCTAACTCCTCCCAC-3'
mPGC-1α RV	5'-CCCTCTTGGTTGGCGGTGGC-3'

hPGC-1α FW	5’-ACTGCAGGCCTAACTCCACCCA-3’
hPGC-1α RV	5’-ACTCGGATTGCTCCGGCCCT-3’
mRPL FW	5’-GTACGACCACCACCTTCCGGC-3’
mRPL RV	5’-ATGGCGGAGGGGCAGGTTCTG-3’
hRPL FW	5’-GGCGGACCGTGCGAGGTATG-3’
hRPL RV	5’-GGCGGTGGGATGCCGTCAAA-3’
mSOD2 FW	5’-GTGTCTGTGGGAGTCCAAGG-3’
mSOD2 RV	5’-AGCGGAATAAGGCCTGTTGT-3’
hSOD2 FW	5’-GCAAGGAACAACAGGCCTTA-3’
hSOD2 RV	5’-AAGAGCTTAACATACTCAGCATAAC-3’
mp21 FW	5’- CAGAATAAAAGGTGCCACAGGC-3’
mp21 RV	5’- CGTCTCCGTGACGAAGTCAA-3’

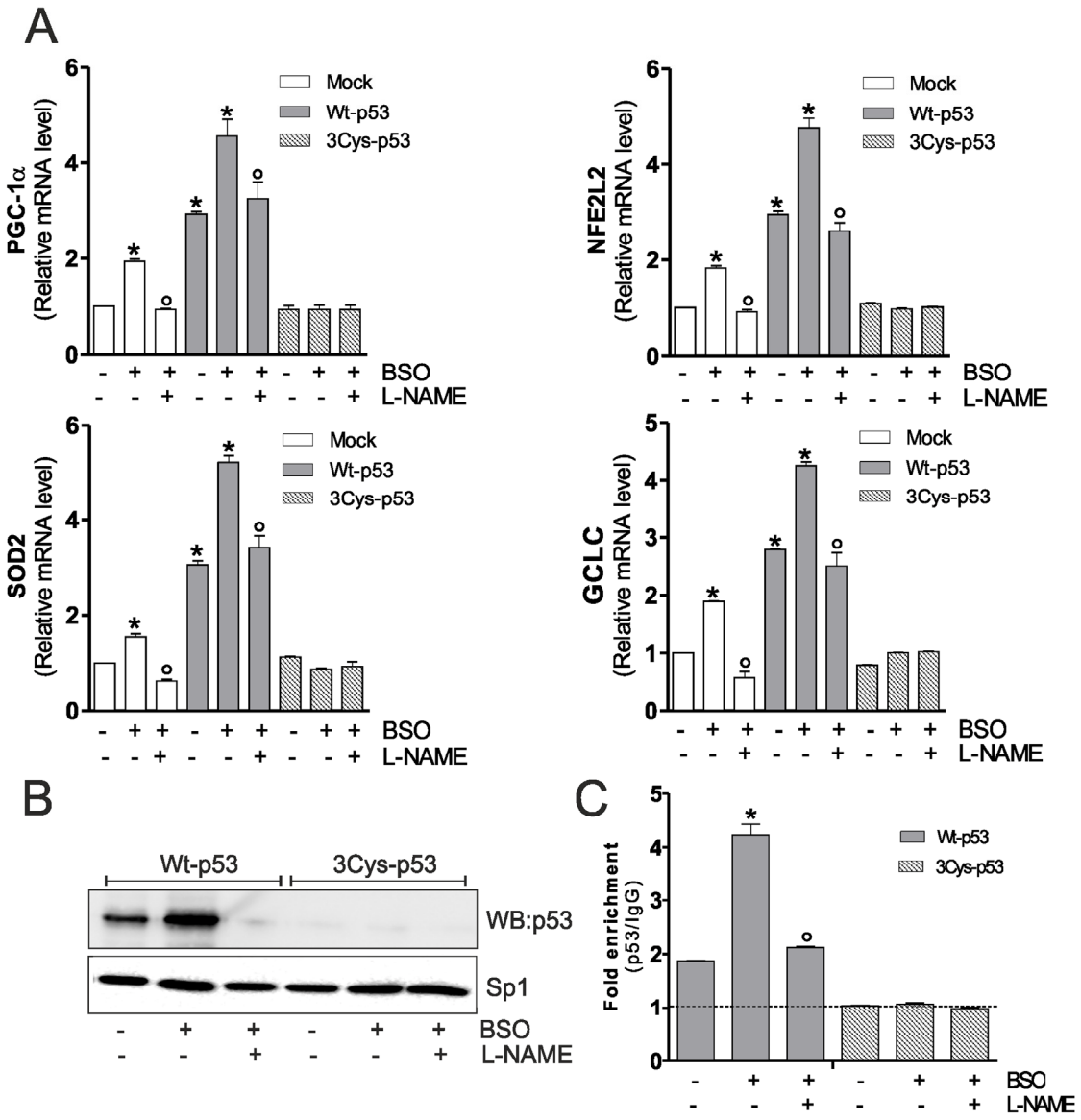

Supplementary Figure S1. 3Cys-p53 mutant impairs NO/PGC-1α-mediated antioxidant response in C2C12 myoblasts. (**A**) C2C12 myoblasts were transfected with pcDNA3.1 vector containing cDNA for wild type p53 (Wt-p53), triple p53 mutant in DBD (C277S, C275S and C124S) (3Cys-p53) or with empty vector (Mock). After 15 h from transfection myoblasts were treated with 1 mM BSO for 24 h. L-NAME (100 μM) was added 1 h before BSO treatment (15 h) and maintained throughout the experiment. Total RNA was isolated and relative mRNA levels of PGC-1α, NFE2L2, SOD2 and GCLC were analyzed by RT-qPCR. Data are expressed as means ± S.D. (n=5; *p<0.001 *vs* Mock; °p<0.01 *vs* BSO-treated cells). (**B**) Nuclear protein extracts (500 μg) were subjected to oligo-pull-down by using the biotinylated oligonucleotide representing the p53RE on the *ppargc1a* promoter and bound p53 was detected by Western blot. Twenty μg of nuclear proteins (input) were used for Western blot analysis of Sp1. (**C**) ChIP assay was carried out on cross-linked nuclei from Wt-p53 and 3Cys-p53 cells, using p53 antibody followed by qPCR analysis of p53RE. Dashed line indicates the value of IgG control. Data are expressed as means ± S.D. (n=4; *p<0.001 *vs* Mock; °p<0.001 *vs* BSO-treated cells). All the immunoblots reported are from one experiment representative of four that gave similar results.

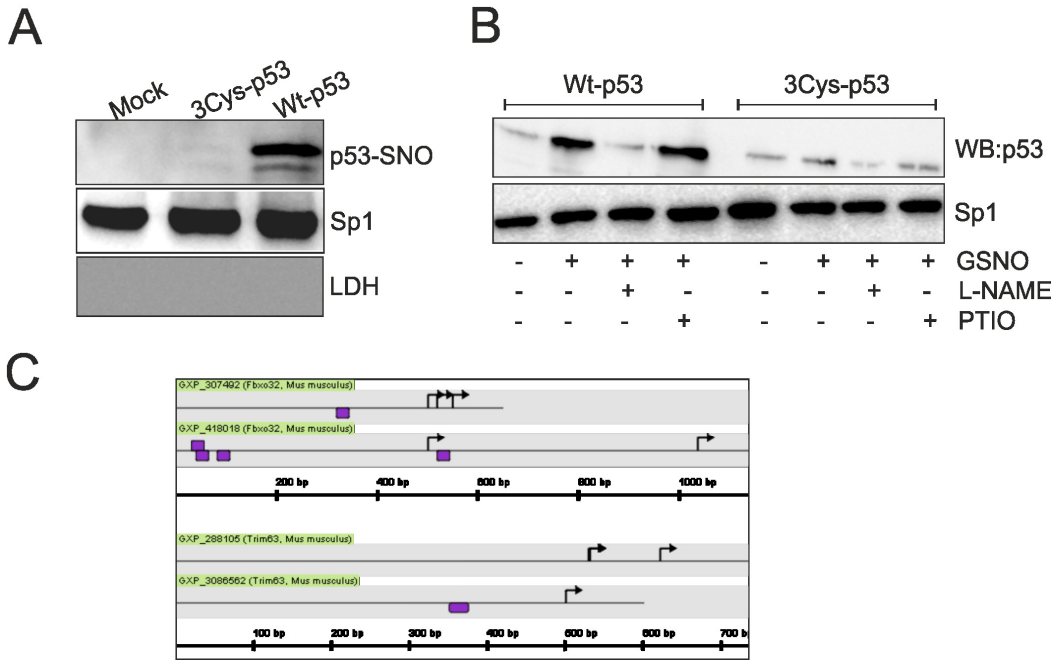

Supplementary Figure S2. 3Cys-p53 mutant not bind the p53RE on *ppargc1a* promoter. (**A**) C2C12 myoblasts were transfected with pcDNA3.1 vector containing cDNA for wild type p53 (Wt-p53), triple p53 mutant in DBD (C277S, C275S and C124S) (3Cys-p53) or with empty vector (Mock). After 15 h from transfection myoblasts were treated with 1 mM BSO for 24 h. Nuclear proteins (500 µg) were subjected to S-NO derivatization with biotin. After Western blot the nitrocellulose was incubated with p53 antibody for detection of p53-SNO. Sp1 was used as loading control. The possible presence of cytoplasmic contaminants was tested by incubating nitrocellulose with rabbit anti-LDH. (**B**) L-NAME (100 µM) was added 1 h before BSO treatment (15 h) and maintained throughout the experiment. Intact nuclei of C2C12 cells were pre-treated with 100 µM L-NAME or with 2 µM carboxy PTIO (PTIO) for 10 minute and subsequently incubated with 5 mM GSNO at 4°C for 30 minute. Nuclear protein extracts (500 µg) were subjected to oligo-pull-down by using the biotinylated oligonucleotide representing the p53RE on the *ppargc1a* promoter and bound p53 was detected by Western blot. Twenty µg of nuclear proteins (input) were used for Western blot analysis of Sp1. (**C**) Schematic representation of murine Atrogin-1 (Fbox32, *upper*) and MuRF-1 (Trim63, *bottom*) promoters. The black arrows indicate the p53RE identified on Atrogin-1 and MuRF-1 promoters. All the immunoblots reported are from one experiment representative of four that gave similar results.

Editorial

Fortifying p53 – beyond Mdm2 inhibitors

Anusha Sriraman, Yizhu Li, Matthias Dobbelstein

The tumor suppressor p53 is mutated in roughly 50% of all human malignancies. However, in the other 50% of tumors which retain wildtype p53, it appears insufficiently active to confer tumor suppression, through cell cycle arrest or apoptosis. Much of this p53-inactivation occurs through the Mdm2 oncoprotein, the product of a p53-inducible gene. Mdm2 is an E3 ubiquitin-ligase that targets p53 for proteasomal degradation. In 2004, a small-molecule antagonist of Mdm2 was identified, known as Nutlin-3a or Nutlin. It binds to Mdm2 at the p53 binding pocket, thereby leading to activation of p53 and its target genes [2]. Recently, similar Mdm2 antagonists were taken to clinical trials, such as RG7388 (NCT02633059, NCT02407080, NCT02828930, NCT02670044, NCT02545283, NCT02624986), HDM201 (NCT02780128, NCT02143635), and MI-773 (NCT01636479), but the results regarding their efficacy have not been reported so far. Thus, delivering a wake-up call to dormant p53 in tumors remains a tempting but currently not proven option for cancer therapy.

While Nutlin readily induces cell cycle arrest, it was found ineffective in causing apoptosis in most tumor cells tested, even when p53 was wild type [3]. This raises the need to fortify the ability of Mdm2 antagonists to induce the pro-apoptotic functions of p53. In analogy to Mdm2, Wip1 (Wild-type p53 induced phosphatase, also known as PPM1D) is another p53-inducible antagonist to p53, often overexpressed in p53-wildtype cancer cells. Wip1 belongs to the PP2C family of Mg^{2+}/Mn^{2+}-dependent serine/threonine phosphatases and causes the dephosphorylation of p53 at Ser 15, thereby reducing p53 activity. It also dephosphorylates Mdm2, resulting in even more efficient p53 inhibition [4]. In 2014, an allosteric inhibitor of Wip1 known as GSK 2830371 was identified. It binds to the structural flap domain of Wip1 and reduces tumor cell growth in lymphoma xenograft models, the breast cancer cell line MCF-7, and neuroblastoma cells [5].

In our study [1], we tested whether the simultaneous inhibition of both p53-antagonists, Mdm2 and Wip1, might induce p53 more potently than single inhibitors. And indeed, the combination of Nutlin and Wip1 inhibitor led to increased activity and stability of p53 that resulted in a major proportion of cells arresting at the G2/M phase of the cell cycle and/or undergoing senescence. Similar results were independently obtained by others [6, 7]. Thus, p53 activity can be fortified by the combined inhibition of factors that otherwise provide negative feedback on p53. This raises the perspective of interfering with p53-regulation at multiple levels (Fig. 1) to further boost p53 for cancer cell elimination.

The most traditional way of enhancing p53 activity in tumor cells consists in the initiation of a DNA damage response (DDR) by chemotherapy or irradiation. This activates DDR kinases – ATM, ATR, Chk1 and Chk2 – that target p53, resulting in p53 stabilization and activation. Future experiments might reveal whether genotoxic treatment will act synergistically when combined with inhibitors of Mdm2 and Wip1.

At present, even the combination of Nutlin and Wip1 inhibitor did not strongly induce apoptosis in the cells we analyzed. This setback may be caused, at least in part, by anti-apoptotic mechanisms frequently found in tumor cells. Future efforts might therefore include pro-apoptotic drugs such as BH3 mimetics or inhibitors of PI3 Kinase-Akt-signaling. Such strategies could complement p53 activation to induce cell death.

For successful application of Mdm2- or Wip1-inhibitors, the selection of responsive tumors might be essential. A wild type p53 status is an obvious requirement. Furthermore, tumors harboring amplified Wip1, or otherwise an activating truncation of Wip1, seem most promising regarding the successful use of a Wip1 inhibitor. These include breast cancer, neuroblastoma, medulloblastoma, and melanoma. Furthermore, Mdm2 antagonists appear most effective in tumors that contain amplifications of Mdm2, such as liposarcoma and osteosarcoma.

Of note, Nutlin can also confer protective effects on cells against chemotherapy. We and others have shown that Nutlin protects p53-proficient cells from the harmful effects of gemcitabine, taxanes, or Wee1 inhibition, at least in part by temporarily preventing the cells from entry into S phase or mitosis. The induction of DNA repair genes, such as Ribonucleotide reductase RRM2B, might further protect cells against genotoxic stress. Thus, care must be taken while combining Mdm2- and Wip1-inhibitors with conventional chemotherapeutics, e. g. by choosing a scheme where genotoxic drugs are applied before the inhibitors of Mdm2 or Wip1.

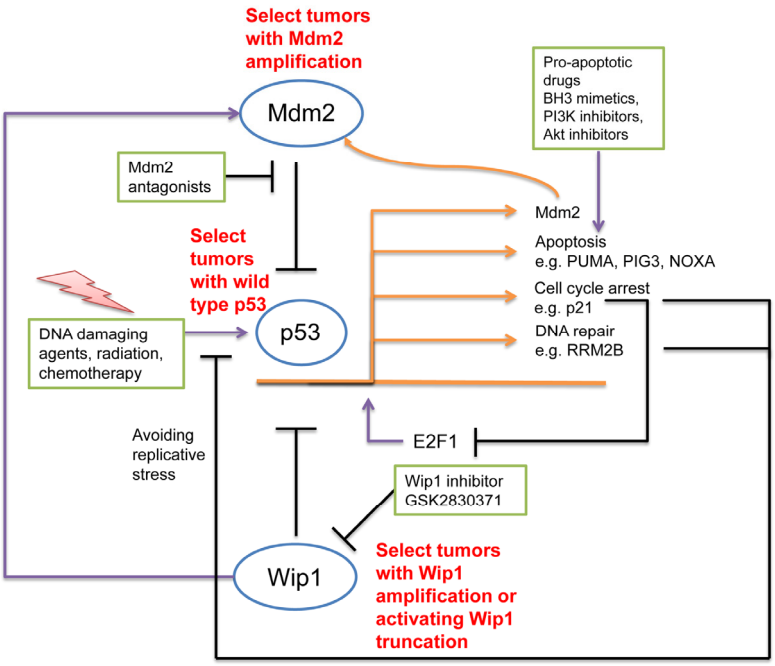

Figure 1. Strategies to fortify p53 in cancer therapy. p53 activation occurs through most conventional chemo-therapeutics and irradiation, by DNA damage signaling. However, p53 activation is also achieved by inhibitors of the p53-antagonists Mdm2 and Wip1. p53, when active, promotes apoptosis or cell cycle arrest. On the other hand, a number of negative feedback loops attenuate p53. p53 activates the expression of Mdm2 and Wip1, and Wip1 further increases Mdm2 activity. Both Mdm2 and Wip1 antagonize p53. Moreover, p53 induces the CDK inhibitor p21, which impairs the activity of E2F1. Since E2F1 induces the Mdm2-antagonist p14/ARF and also some of the pro-apoptotic p53 target genes (e. g. NOXA), negative regulation of E2F1 attenuates some of p53's activities. Moreover, p21-induced cell cycle arrest prevents DNA replication and thus reduces DNA damage. Finally, p53 can promote DNA repair, consequently diminishing the efficacy of conventional chemotherapy. The fortification of p53 in this situation can be achieved by antagonists to Mdm2 and Wip1, but also through pro-apoptotic drugs. Such strategies are particularly promising in tumors that not only have wild type p53, but also amplifications of the Mdm2 gene and/or amplifications or activating truncations of Wip1.

Enhancing p53 activity still appears like an attractive strategy to eliminate tumor cells that retain wild type p53 status. However, interfering with the Mdm2-p53-interaction often appears insufficient to eliminate tumors. Targeting additional antagonists of p53, in combination with genotoxic stress and pro-apoptotic strategies, might fortify p53 to the point where it induces cancer cell death.

REFERENCES

1. Sriraman A, et al. Oncotarget. 2016; 7:31623–38. doi: 10.18632/oncotarget.9302.
2. Vassilev LT, et al. Science. 2004; 303:844–48. doi: 10.1126/science.1092472
3. Tovar C, et al. Proc Natl Acad Sci USA. 2006; 103:1888–93. doi: 10.1073/pnas.0507493103
4. Lu X, et al. Cancer Cell. 2007; 12:342–54. doi: 10.1016/j.ccr.2007.08.033
5. Gilmartin AG, et al. Nat Chem Biol. 2014; 10:181–87. doi: 10.1038/nchembio.1427
6. Esfandiari A, et al. Mol Cancer Ther. 2016; 15:379–91. doi: 10.1158/1535-7163.MCT-15-0651
7. Pechackova S, et al. Oncotarget. 2016; 7:14458–75. doi: 10.18632/oncotarget.7363.

Matthias Dobbelstein: Institute of Molecular Oncology, Göttingen Center of Molecular Biosciences (GZMB), University Medical Center Göttingen, D-37077 Göttingen, Germany

Correspondence: *Matthias Dobbelstein*
Email: *mdobbel@uni-goettingen.de*

Keywords: *p53, Mdm2, PPM1D, Wip1, cancer treatment*

Received: September 20, 2016
Published: September 29, 2016

Editorial

Targeting mutant p53 for cancer therapy

Moshe Oren, Perry Tal, and Varda Rotter

The p53 tumor suppressor protein serves as a major barrier against cancer; consequently, mutations in the TP53 gene, encoding p53, are the most frequent single genetic alteration in human cancer, occurring in about half of all individual cancer cases [1]. Besides abrogating the tumor suppressive effects of the wild type (WT) p53 protein, many of the TP53 mutations endow the mutant p53 protein with new oncogenic gain-of-function activities, which actively promote a variety of features characteristic of aggressive tumors, such as increased migratory and invasive capacities and increased resistance to many types of anti-cancer therapy agents [1]. This pertains particularly to tumors that carry single amino acid substitutions (missense mutations) within p53's DNA binding domain (DBD), and display abundant accumulation of the mutant p53 protein within the tumor cells [1].

In tumors that retain non-mutated TP53 genes, the tumor suppressive effects of the remaining WTp53 are also often compromised, owing to genetic and epigenetic alterations that occur during cancer progression [1]. Altogether, the normal functionality of p53 is thus abrogated in the vast majority of human tumors. This realization has led to extensive attempts to restore full p53 functionality in cancer cells, as a novel cancer therapy strategy [1, 2]. However, these attempts have been seriously hampered by the fact that p53 has no known enzymatic activities, and rather operates primarily as a sequence-specific transcription factor. Furthermore, restoring the activity of a defective tumor suppressor protein is vastly more difficult than abrogating the activity of a hyperactive oncoprotein.

Nevertheless, significant advances have been achieved in recent years, and hopes for the introduction of p53-based novel cancer therapies into the clinic are becoming increasingly supported by evidence. In principle, attempts to develop such therapies have taken 3 main approaches: (1) Introduction of WTp53, mainly via viral transduction ("gene therapy"), into tumors that have sustained TP53 mutations; (2) enhancement of the functionality of the endogenous WTp53 in tumors that have retained a non-mutated TP53 gene, mainly be disrupting the interaction of the WTp53 protein with its major negative regulator MDM2; and (3) "correction" of the mutant p53 protein in tumors that have sustained TP53 missense mutations, thereby restoring its ability to perform the tumor suppressive activities of WTp53 [1, 2].

The latter approach, namely the "re-education" of mutant p53, is particularly appealing. First of all, it can simultaneously reinstate WTp53 tumor suppressive activity together with abrogating the gain-of-function oncogenic effects of the mutant p53 protein. Additionally, since cancer cells bearing TP53 missense mutations often accumulate massive amounts of the mutant p53, its conversion into a WT-like state will potentially flood the cancer cell with excessive amounts of tumor suppressive p53, far beyond what one finds in normal cells. This may provide a large therapeutic window and may potentially circumvent the severe limiting toxicity observed with compounds that augment the activity of non-mutated p53 in cancer cells (approach #2 above).

Indeed, attempts to "re-educate" mutant p53 in cancer cells have seen substantial progress in the last several years. The most advanced effort has been spearheaded by Wiman and coworkers, who identified a small molecule named PRIMA-1, which can reactivate mutant p53 (reviewed in [3]). PRIMA-1 was subsequently further modified, and its derivative, PRIMA-1-met, has recently entered a Phase 2 clinical trial under the commercial name APR-246 [3]. An additional strategy, developed by Carpizo, Levine and co-workers (reviewed in [4]), is based on the facts that Zn(2+) ions are crucial for stabilizing the correct folding of the DBD of WTp53, and that many (but not all) cancer-associated mutant p53 proteins bind Zn(2+) less avidly that WTp53 and therefore tend to misfold. Specifically, these investigators have identified small molecules (zinc metallochaperones) that deliver Zn(2+) to the DBD of mutant p53 and facilitate its correct refolding, thereby restoring WTp53-like function [4]. However, such molecules work only on a subset of p53 mutants, which have a conformational defect due to reduced Zn(2+) binding. Moreover, like PRIMA-1/APR-246, they possess a rather generic chemical activity are not specific for p53 only; this may result in undesirable side effects that are presently hard to predict. Recently, El-Deiry and coworkers have described 2 additional mutant p53-targeing small molecules: prodigiosin,

which disrupts the interaction of mutant p53 with the p53 family member p73, and thereby unleashes the cytotoxic and cytostatic activities of p73 [5], and NSC59984, which augments p53 degradation and also unleashes p73 activity [6].

We have opted for a different approach, based on identification of small peptides that specifically stabilize mutant p53 proteins in a functional state [7]. Combining phage display screening with several alternating functional readouts, which minimize the frequency of false-positives, we were able to obtain a series of such bioactive peptides. These peptides can stabilize the WT conformation of mutant p53, and restore its ability to engage in sequence-specific DNA binding and activate canonical WTp53 target genes. Moreover, they promote selective apoptotic death of cancer cells harboring mutant p53, and very effectively reduce, and even completely block, the growth of human cell line-derived mouse xenograft tumors representing several types of highly aggressive cancer [7]. Importantly, all common p53 mutants tested in our study were found to be amenable to functional stabilization by these peptides. Remarkably, our lead peptide, pCAP-250, shares perfect homology with the RAD9 protein, a validated p53 interactor. This attests to the high specificity of the interaction.

Of note, Eisenberg and coworkers have recently described another type of mutant p53-targeting peptide, which acts by disrupting the aggregation of particular aggregation-prone p53 mutants [8]. The spectrum of mutants targeted by such peptide still remains to be determined.

Bringing small peptides into the clinic remains challenging, mainly owing to the need to deliver the peptides efficiently into the tumor cells. Nevertheless, their greater specificity, relative to small molecules of the types described above, bears the hope for minimal non-specific toxicity, rendering such approach potentially highly promising in the long run.

REFERENCES

1. Rivlin N, et al. Genes Cancer. 2011; 2:466-74. doi: 10.1177/1947601911408889.

2. Khoo KH, et al. Nat Rev Drug Discov. 2014; 13:217-36.

3. Bykov VJ, et al. Front Oncol, 2016; 6:21.

4. Blanden AR, et al. Drug Discov Today. 2015. 20: 1391-97.

5. Hong B, et al. Cancer Res. 2014; 74:1153-65.

6. Zhang S, et al. Cancer Res. 2015; 75:3842-52.

7. Tal P, et al. Oncotarget, 2016; 7: 11817-37. doi: 10.18632/oncotarget.7857

8. Soragni A, et al. Cancer Cell. 2016; 29: 90-103.

Moshe Oren and Varda Rotter: Department of Molecular Cell Biology, The Weizmann Institute, Rehovot 76100, Israel

Correspondence: *Moshe Oren and Varda Rotter*

Email: *moshe.oren@weizmann.ac.i;l varda.rotter@weizmann.ac.il*

Keywords: *TP53; mutant p53 gain-of-function; peptide therapy; tumor suppressor; MDM2*

Received: June 16, 2016

Published: June 26, 2016

Research Paper

The p53/miR-17/Smurf1 pathway mediates skeletal deformities in an age-related model via inhibiting the function of mesenchymal stem cells

Wenjia Liu [1,2*], Meng Qi [1,2*], Anna Konermann [3*], Liqiang Zhang [1], Fang Jin [4], and Yan Jin [1,2]

[1] *State Key Laboratory of Military Stomatology, Center for Tissue Engineering, School of Stomatology, The Fourth Military Medical University, Xi'an, Shaanxi 710032, People's Republic of China;*
[2] *Research and Development Center for Tissue Engineering, Fourth Military Medical University, Xi'an, Shaanxi 710032, People's Republic of China;*
[3] *Department of Orthodontics, Medical Faculty, University of Bonn, Bonn, Germany;*
[4] *State Key Laboratory of Military Stomatology, Department of Orthodontic, School of Stomatology, The Fourth Military Medical University, Xi'an, Shaanxi 710032, People's Republic of China.*
[*] *These authors contributed equally to this work.*

Key words: *Aging, mesenchymal stem cells, osteogenesis, p53, miR-17*
Abbreviations: *ALP, Alkaline phosphatase; BCA, Bicinchoninic acid; BMMSCs, Bone marrow mesenchymal stem cells; BMD, Bone mineral density; BMP, Bone morphogenetic protein; CFU-F/-Ob, Colony forming unit-fibroblast/-osteoblast; EDTA, Ethylenediaminetetraacetic acid; FBS, Fetal bovine serum; GAPDH, Glyceraldehyde-3-phosphate dehydrogenase; HE, Hematoxylin and eosin; HA/TCP, Hydroxyapatite/tricalcium phosphate; IFN-γ, Interferon gamma; MSC, Mesenchymal stem cell; miRNA, MicroRNA; α-MEM, Minimum Essential Medium α; PDLSC, Periodontal ligament stem cell; PBS, Phosphate buffered saline; PVDF, Polyvinylidene difluoride; Runx2, Runt-related transcription factor 2; Smurf1, Smad ubiquitin regulatory factor one; siRNA, Small interfering RNA; BV/TV, Trabecular bone volume fraction relative to tissue volume; TCF3, Transcription factor 3; MiRNA, microRNA; MTT, 3-(4,5-dimethylthiazol-2yl)-2,5-diphenyltetrazolium bromide; TNF-α, Tumor necrosis factor alpha.*
Received: *12/21/14; Accepted: 03/05/15; Published: 03/07/15*
Correspondence to: *Yan Jin, PhD; Fang Jin, PhD;* ***E-mail:*** *yanjin@fmmu.edu.cn; fangjin@fmmu.edu.cn*

Copyright: *Liu et al. This is an open-access article distributed under the terms of the Creative Commons Attribution License, which permits unrestricted use, distribution, and reproduction in any medium, provided the original author and source are credited*

Abstract: Osteoporosis is an age-related progressive bone disease. Trp53 (p53) is not only a famous senescence marker but also a transcription regulator which played a critical role in osteogenesis. However, how p53 contributes to the bone mass loss in age-related osteoporosis is still unclear. Here, we found that bone mass and osteogenic differentiation capacity of mesenchymal stem cells (MSCs) is significantly reduced with advancing age. Serum levels of TNF-α and INF-γ and senescence-associated ß-galactosidase, p16, p21 and p53 are significantly increased in elder mice, but antipodally, osteogenic marker expression of Runx2, ALP and osterix are reduced. Overexpression p53 by lentivirus inhibits osteogenesis in young MSCs in culture and upon implantation in NOD/SCID mice through inhibiting the transcription of miR-17-92 cluster, which is decreased in old mice. In addition, miR-17 mimics could partially rescue the osteogenesis of old MSCs both *in vitro* an *in vivo*. More importantly, Smurf1 as a direct target gene of miR-17, plays an important role in the p53/miR-17 cascade acting on osteogenesis. Our findings reveal that p53 inhibits osteogenesis via affecting the function of MSCs through miRNA signaling pathways and provide a new potential target for treatment in future.

INTRODUCTION

Age-related diseases include cancer, cardiovascular disease, diabetes, various neurodegenerative diseases [1], and especially osteoporosis. A reduction in these age-related diseases will not only enhance the quality of life but also reduce the overall burden to society and families. Bone marrow mesenchymal stem cells

(BMMSCs) are pluripotent cells with the potential for self-renewal and multiple differentiations into other cell types, dedicating them for regenerative medicine and tissue engineering, as they provide tissue maintenance and repair after damaging insults [2, 3]. In addition, bone homeostasis is supposed to fundamentally depend on the transformation potential of BMMSCs, particularly in this case different into osteoblastic cells [4]. However, the qualification of BMMSCs for recovery of multiple tissue systems is contingently compromised with age [3, 5]. As senescent cells can remain and agglomerate in tissues in contrast to apoptotic cells that are immediately removed by host-defensively processes, their existence can profoundly affect homeostatic mechanisms of the whole body [6-8].

The age-related restrictions of BMMSCs take special effect on their osteogenic and adipogenic potential and imply expression changes of associated marker genes and of senescence-related molecules [2, 9, 10]. Osteogenesis and adipogenesis appear to decline with age and passage of the cultivated cells [11-14], and the loss of osteogenic potential is presumably connected with an inhibited upregulation of key osteogenic transcription factors due to an altered p53 level [4, 15], which commonly recognized as tumor suppressing gene, is also one of the most widely studied genes in aging. A mutant p53 heterozygote mouse model developed by Donehower et al. ($p53^{+/m}$ mice) demonstrated increased osteoporosis, organ atrophy, diminished stress tolerance and shortened life span in the $p53^{+/m}$ mice as compared to wild type littermates [16]. In addition, researches revealed that p53 occupies a dual role in its mode of operation, as it manifests both sequence-specific DNA-binding mechanisms and transcription-independent capacities and can operate as transcriptional activator as well as repressor on certain genes [17-19].

MiRNAs consisting of 21-23 nucleotide RNA molecules not only provide stability and translational efficiency of target mRNAs, but also involved in cellular differentiation, proliferation and apoptosis [20-22]. Stem cell lineage commitment into osteoblasts is likewise governed by diverse miRNAs, either in terms of inhibition or enhancement of osteogenesis, by miR-204/211 suppressing Runx2 or by miR-20a activating BMP signaling for example [23, 24]. Our previous research revealed that miR-17 acted as a negative regulator of osteogenesis in a physiological microenvironment, but contrarily as promoter for osteoblastic commitment of tissue-specific MSCs under inflammatory pathological conditions due to targeting different genes [25, 26]. Recent investigations show that p53 can repress miR-17-92, a cluster of 7 microRNA (miRNAs), on transcriptional level via action on p53-binding site located on the proximal part of the miR-17-92 promoter region [27, 28]. However, the detailed mechisnam of how p53 contributes to bone mass loss in age-related osteoporosis is still unclear. In this study, we choose natural aging mice as our study model and demonstrate that BMMSCs from 16-month old (old) mice express decreased osteogenic differentiation capacity and increased senescence markers, expecially p53. Overexpression p53 in 4-month-old (young) BMMSCs could inhibit the osteogensis of them both *in vitro* and *in vivo*. In addition, miR-17 mimics particular rescue the osteogenesis of old BMMSCs both *in vitro* and *in vivo*. We also elucidated the underlying mechanism that p53 restained the osteogenesis via modulating the trancription of pri-miR-17 and then affecting the expression of Smurf1, a direct target of miR-17. Our study aims to reveal a novel mechanism of age-related osteoporosis and provide a new potential target for treatment in future.

RESULTS

Bone formation and osteogenic differentiation capacity are significantly reduced with advancing age

In order to assess bone formation ability with advancing age *in vivo*, bone mass was analyzed in 4 (young) and 16-month-old (old) mice via micro-CT analysis as much as via histological staining of femur tissue sections. Both methods and the corresponding analyses comprising BMD and BV/TV measurements as much as determination of the number of bone trabeculae revealed that bone mineral density was decreased in old mice relative to young mice with significant loss in trabecular bone volume and in the number of trabeculae (Fig. 1A-B). In BMMSCs derived from young and old mice, the CFU assay showed that the number of CFU-F and CFU-Ob of old mice was significantly less compared to young mice (Fig. 1C-D), especially the CFU-Ob number, thus confirming the *in vivo* data. In addition, analyses on serum levels of TNF-α and IFN-γ both in young and old mice revealed significantly higher values of these cytokines in elder mice (Fig. 1E), suggesting more inflammation with advancing age.

In old mice, senescence-associated ß-galactosidase was detectable to a significantly greater amount compared to cells from young mice, and the senescence-associated markers p16, p21 and p53 were also significantly increased both in bone tissues and in BMMSCs on gene protein level (Fig. 2A-D). Additionally, the osteogenic differentiation capacity of BMMSCs derived from old mice was significantly reduced compared to the ones obtained from young mice, which was evident from the

results of the alizarin red staining as much as the gene and protein expression analyses of osteogenic marker expression, namely Runx2, ALP and osterix (Fig. 2E-G). In addition, the proliferation capacity of BMMSCs from old mice was also lower than BMMSCs from young mice, as indicated by MTT and flow cytometric cell cycle analysis (Supplementary Fig. 1).

p53 is causative for inhibited osteogenesis in BMMSCs

As we observed that old BMMSCs express significantly higher gene and protein levels of the senescence-related markers p21, p16 and most substantially p53, we further investigated the relationship between p53 and osteogenic differentiation capacity of BMMSCs. We constructed the lentiviral vector to induce a stable up-regulation of p53 in BMMSCs. The lentiviral construct (pLenti-p53) increased the p53 expression level more than 5-fold compared with the control (Supplementary Fig. 2). Then we cultured the cells in osteogenic differentiation medium for an additional 14 days. Alizarin red staining and the expression of ALP, Runx2 and osterix showed that the osteogenic differentiation of BMMSCs from young mice was suppressed after transducing pLenti-p53 *in vitro* (Fig. 3A-C). Then, we expended this study for ectopic bone formation *in vivo*. The BMMSCs transduced with pLenti-p53 or control vector were loaded onto HA/TCP powder scaffolds and implanted in NOD/SCID mice for 8 weeks. The control group was found to form a considerable amount of bone tissue around the HA/TCP powder. The new bone tissue was stained red using HE staining. The pLenti-p53-transduced BMMSCs only formed some threadlike collagen fibers around the surface of the HA/TCP powders. Osteoid formation was decreased 45% in the implants treated with the pLenti-p53 compared with those treated with the vector control (Fig. 3D-E).

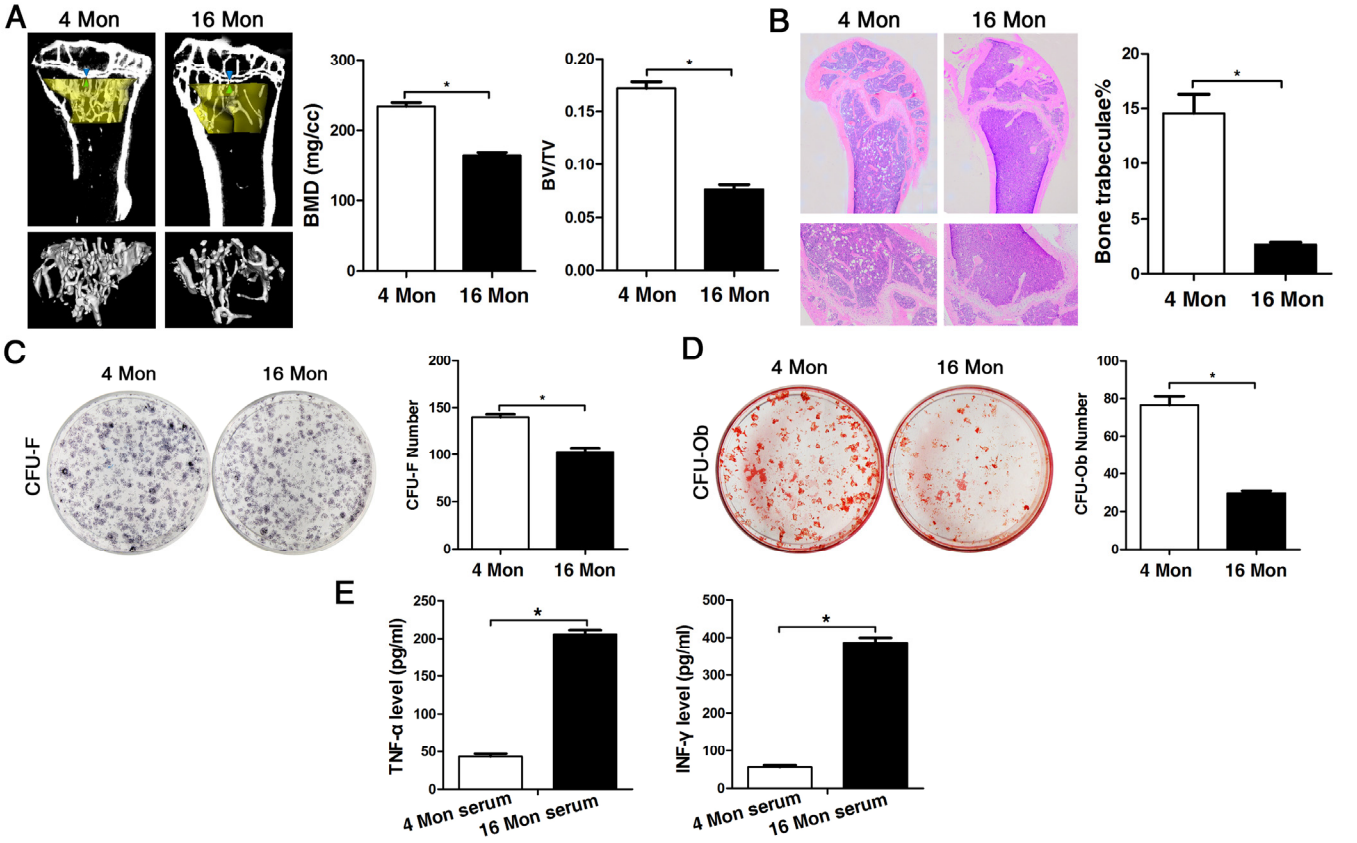

Figure 1. The osteogenic capacity of old mice is significantly reduced both *in vivo* and *in vitro*. Statistically analyzed values show the mean ± SD (n=10). * $p < 0.05$. **(A)** Micro-CT analysis of trabecular bone mass in the tibiae of 4 (young) and 16 month-old (old) mice. Quantitative analyses were performed via volumetric bone mineral density (BMD) and trabecular bone volume fraction (BV/TV) measurements. **(B)** HE stainings of histological sections from femur derived from young and old mice for detection of the number of bone trabeculae. **(C-D)** Representative images of the CFU-F assay for determination of proliferation capacity and of the CFU-Ob assay for osteogenic differentiation ability of BMMSCs obtained from young and old mice and stained with crystal violet and alizarin red, respectively. CFU efficiency was determined by the number of colonies relative to the total number of seeded cells in each plate. **(E)** Serum levels of TNF-α and INF-γ in young and old mice determined via ELISA. Results are expressed as pg/ml.

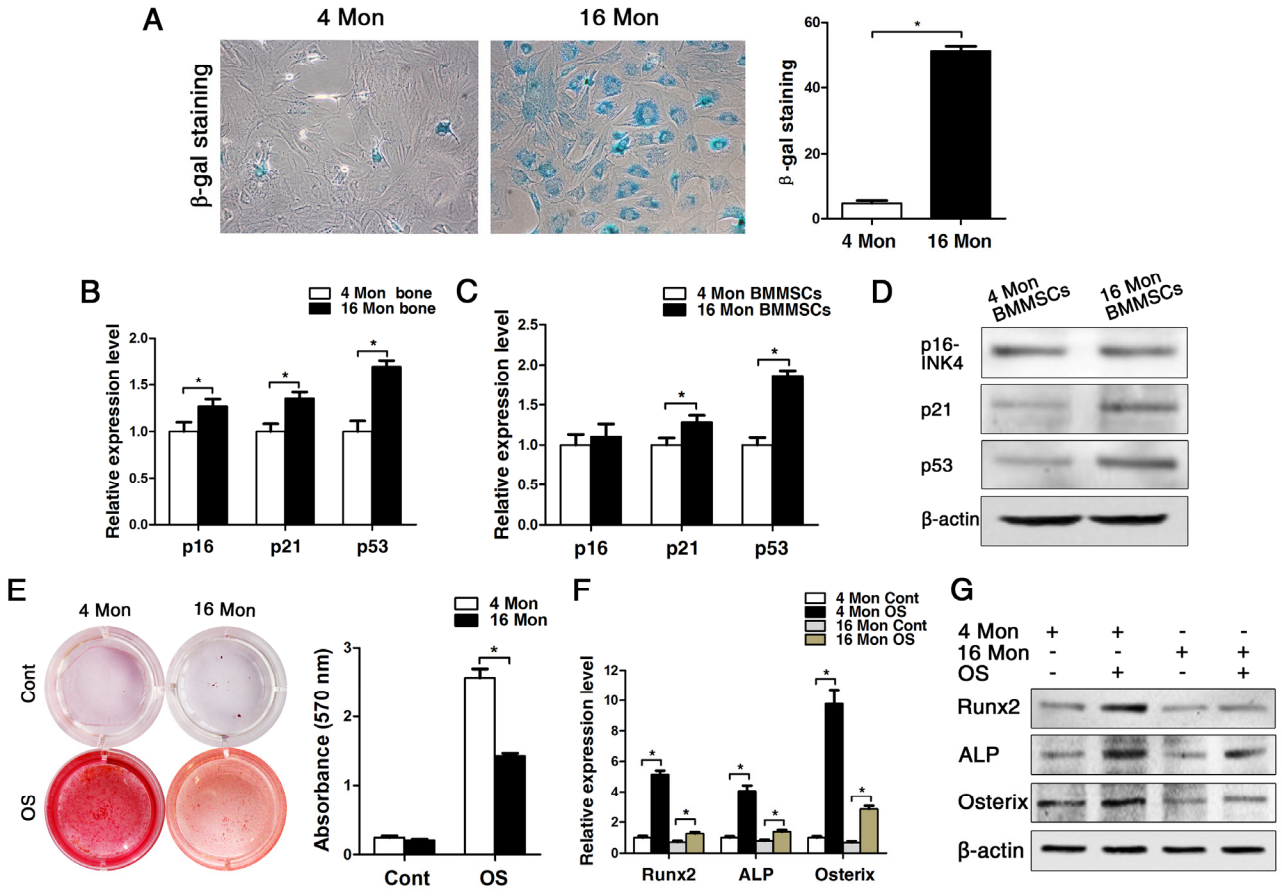

Figure 2. BMMSCs from old mice express higher levels of senescence markers and lower osteoblast markers compared to young ones. Statistically analyzed values show the mean ± SD (n=10). * $p < 0.05$. **(A)** In vitro staining of the senescence-related marker ß-galactosidase in BMMSCs cultures derived from young and old mice. Quantitative analysis of the total number of positively stained cells. **(B-C)** Real-time PCR analyses on whole bone tissue extracts (**B**) and on BMMSCs (**C**) for the senescence-related genes p16, p21 and p53. Normalization to ß-actin. **(D)** The western blot showed that the protein level changed as the mRNA. **(E)** Alizarin red staining of BMMSCs from young and old mice osteogenically induced for 14 d. Cont = Control, OS = osteogenically induced. **(F-G)** Real-time PCR and western blot analyses on BMMSCs for the osteogenic markers Runx2, ALP, osterix. Normalization to ß-actin.

p53 regulates the osteogenesis of BMMSCs through inhibiting the transcription of miR-17-92 cluster

Considering that senescence can be correlated to a chronic inflammatory microenvironment (Fig.1E) and as our previous research revealed that miR-17 acts as positive regulator of osteogenesis in an inflammatory microenvironment [25], we investigated the expression pattern of miR-17-92 cluster in BMMSCs from young and old mice. Real-time PCR analyses showed a significant decrease of miR-17, miR-18a, miR-20a and miR-92a in bone tissues, reduction of all family members in bone marrow and reduced expression of miR-17, miR-18a, miR-19a, miR-20a and miR-92a could be observed in BMMSCs (Fig. 4A-C). Importantly, the expression pattern of p53 and miR-17 were exactly opposite in BMMSCs from both 4 and 16-month-old mice during osteogenic differentiation (Fig. 4D-F). Furthermore, the expression of pri-miR-17 and mature miR-17-92 family members significantly decreased upon overexpression of p53, suggesting that p53 can potently block the transcription of miR-17-92 (Fig. 4G, H).

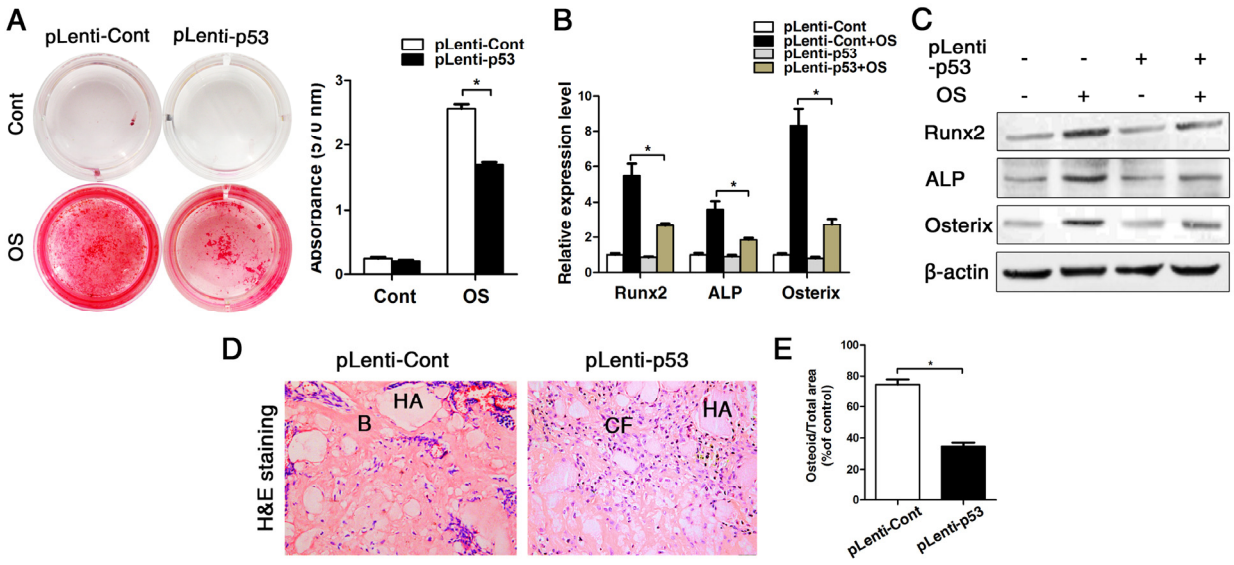

Figure 3. Overexpression of p53 changed the phenotype of young BMMSCs into old BMMSCs. BMMSCs from young mice were lentivirally transduced to upregulate the expression level of p53 (= pLenti-p53) or were transduced as lentiviral control (= pLenti-Cont). Statistically analyzed values show the mean ± SD (n=10). * $p < 0.05$. **(A)** Alizarin red staining of pLenti-p53 and of pLenti-Cont after osteogenic inducing for 14 days. Cont = Control, OS = osteogenically induced. The values show the mean ± SD (n=10). * $p < 0.05$. (**B-C)** Real-time PCR and western blot analyses on BMMSCs with lentiviral transduction (pLenti-p53 and pLenti-Cont) and with/without osteogenic induction for the osteogenic markers Runx2, ALP, osterix. Normalization to ß-actin. (**D-E)** Histological analyses and corresponding statistical analysis of tissue sections from subcutaneous pockets on the backs of 6-week-old NOD/SCID mice with implanted HA/TCP ceramic particles mixed with BMMSCs from young mice with lentiviral transduction of p53 and control.

Since miR-17 were decreased obvious in old mice (bone, bone marrow and BMMSCs), we next used miR-17 mimics to up-regulated expression of miR-17 in old BMMSCs. Our data showed that the transfection efficiencies of miR-17 mimics and inhibitor persisted at least for 14 d (Supplementary Fig. 3). After osteogenic induction of old BMMSCs for 14 d *in vitro*, alizarin red staining suggested that the osteogenic differentiation of BMMSCs was obviously enhanced after upregulating miR-17 expression (Fig. 5A). These data of the staining results were supported by the transcriptional and protein analyses of the osteoblast-related genes Runx2, ALP and Osterix, which is illustrated in Fig. 5B-C. The *in vitro* results could be substantiated *in vivo* by the HA/TCP transplantation experiments earlier described, as after a transplantation perio d for 8 weeks, BMMSCs from old mice formed plenty of new bony structures around the HA/TCP granules when miR-17 was upregulated in the transplanted cells (Fig. 5D-E).

Smurf1 plays an important role in the p53/miR-17 cascade acting on osteogenesis of BMMSCs

As microRNA has to bind to its target gene for regulating cellular characteristics, we subsequently tested the expression of two direct target genes of miR-17, namely TCF3 and Smurf1. Both real-time PCR and western blot data showed that the expression of Smurf1 was increased after upregulating p53, and here especially on protein level, as miRNA acts on post-transcriptional level and mostly affects protein expression. However, the other target gene TCF3 was not changed after upregulating p53 (Fig. 6A). Next, we transfected cells which were stably upregulated p53 with miR-17 mimics for following investigation of Smurf1 expression. The western blot data showed that the Smurf1 level was almost unchanged (Fig. 6B), suggesting that p53 affects the expression level of Smurf1 mainly through miR-17, which is illustrated as an overview model in Fig. 7.

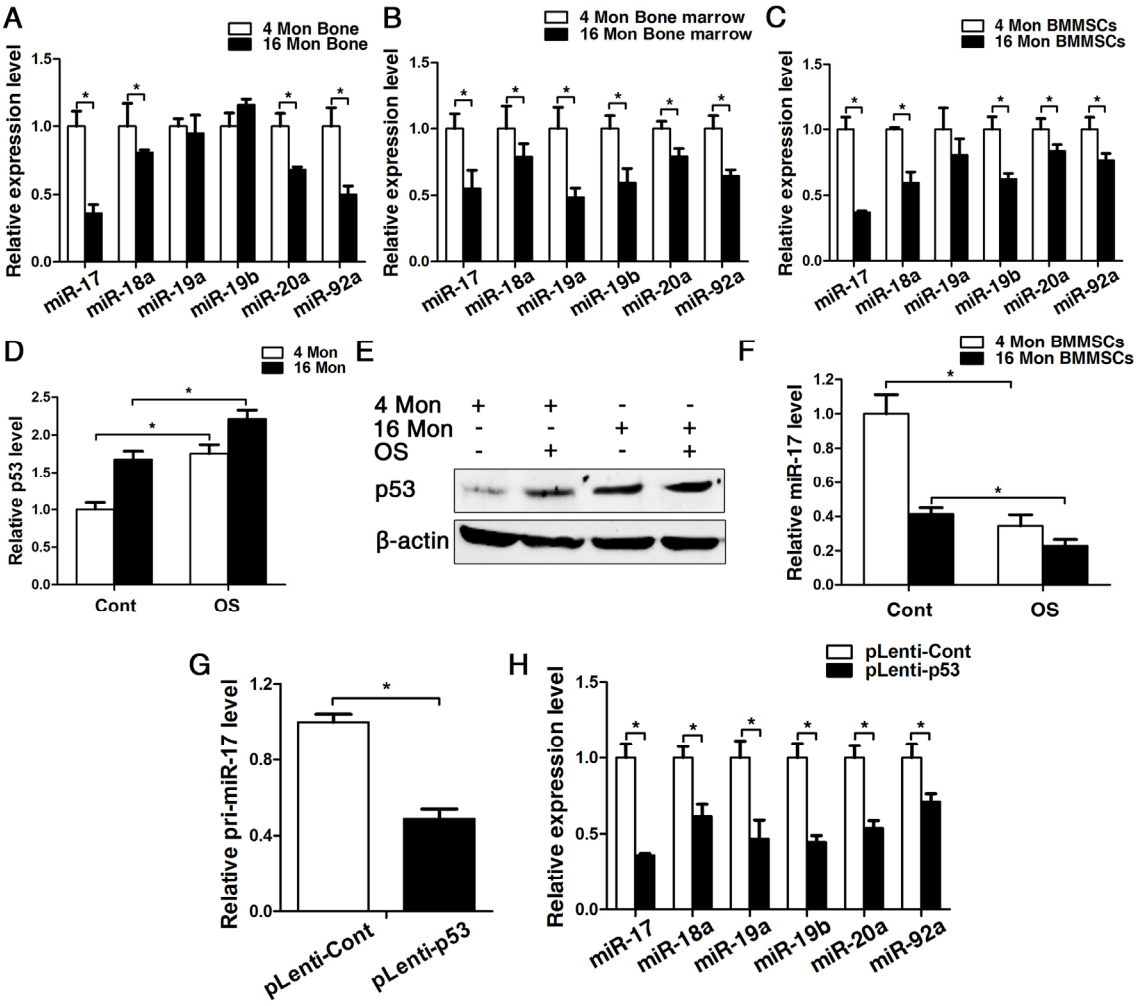

Figure 4. p53 contribute to impaired osteogenesis of BMMSCs via inhibiting the transcription of miR-17-92 cluster. BMMSCs were lentivirally transduced to upregulate the expression level of p53 (= pLenti-p53) or were transduced as lentiviral control (= pLenti-Cont). Statistically analyzed values show the mean ± SD (n=10). * $p < 0.05$. **(A-C)** Real-time PCR analyses for the expression of miR-17, miR-18a, miR-19a, miR-19b, miR-20a and miR-92a in bone (**A**), bone marrow (**B**) and BMMSCs (**C**) of young and old mice. Normalization to ß-actin. **(D-F)** Real-time PCR and western blot analysis of p53 (**D**, **E**) and real-time PCR of miR-17 (F) expression in BMMSCs derived from young and old mice after osteogenic differentiation for 7 d. Normalization to ß-actin and U6. **(G)** Pri-miR-17 transcript analysis by Taqman-based qPCR. Normalization to GAPDH. **(H)** Real-time PCR analysis of the mature miR-17-92 cluster after upregulating P53 for 48 h. Normalization to U6.

Then, we examined the expression pattern of Smurf1 during osteogenic differentiation of young and old BMMSCs and could surprisingly found that the expression of Smurf1 was increased in both groups upon osteogenic differentiation, although Smurf1 is announced as negative regulator of osteogenesis (Fig. 6C-D). In both the control and the osteogenically induced group, Smurf1 expression was higher in old compared to young BMMSCs. Therefore, we used siRNA to down-regulate the level of Smurf1 in BMMSCs from old mice in a next step (Supplementary Fig. 4). After a 14 d period of osteogenic induction, the alizarin red staining displayed that osteogenic differentiation of old BMMSCs could partially be rescued after downregulating Smurf1 expression. However, this effect disappeared after decrease of miR-17 expression by miR-17 inhibitor, which could be substantiated by gene expression analysis of osteoblast-related genes (Fig. 6E-F).

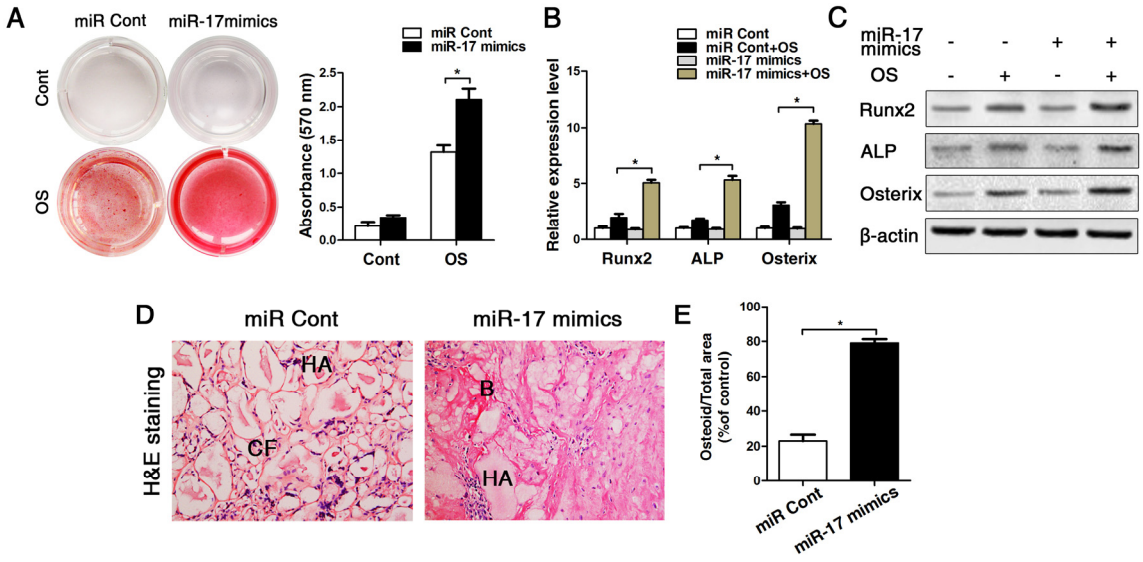

Figure 5. Up-regulation of miR-17 by miR-17 mimics reversed the effect of p53 on inhibiting osteogenic differentiation in old BMMSCs. miR-17 was stable upregulated in BMMSCs by miR-17 mimics (= miR-17 mimics). miRNA control (= miR Cont). Statistically analyzed values show the mean ± SD (n=10). * $p < 0.05$. **(A)** Osteogenic induction for 14 d of BMMSCs derived from old mice and subsequent alizarin red staining resulted in a heightened osteogenic differentiation of BMMSCs with previously upregulated miR-17 expression. **(B-C)** Real-time PCR and western blot analyses on old BMMSCs with miR-17 mimic treatment or miRNA control and with/without osteogenic induction for the osteogenic markers Runx2, ALP, osterix. Normalization to ß-actin. **(D-E)** Histological analysis (D) and corresponding statistical analysis (E) on osteoid formation of tissue sections from subcutaneous pockets on the backs of 6-week-old NOD/SCID mice with implanted HA/TCP ceramic particles mixed with BMMSCs from 16-month-old mice with/without miR-17 upregulation.

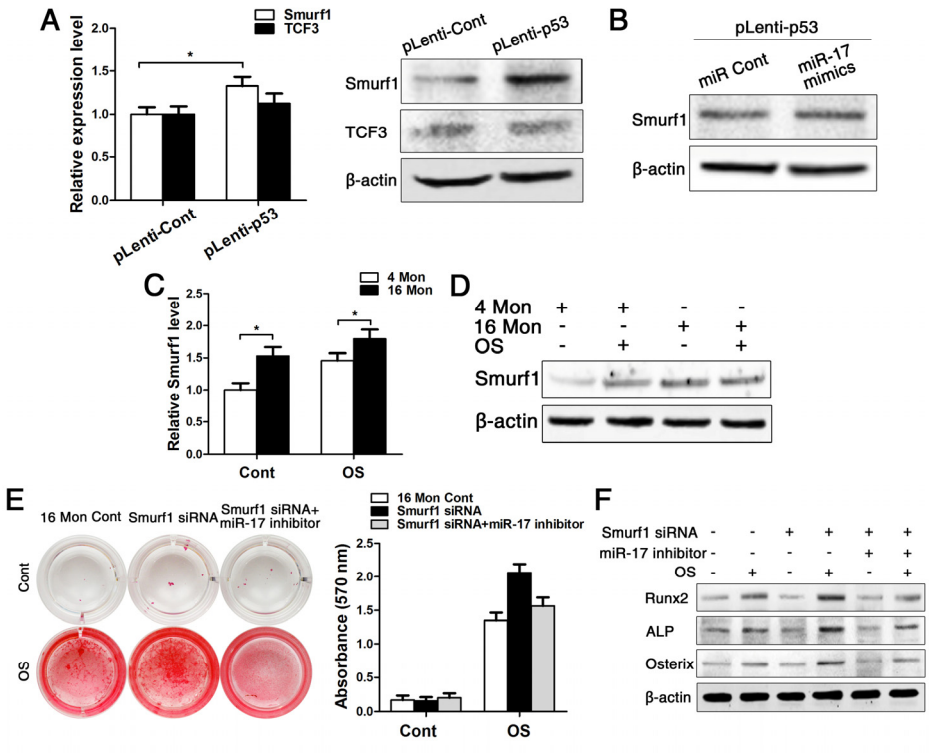

Figure 6. Smurf1 plays an important role in miR-17-mediated osteogenic differentiation of BMMSCs. BMMSCs were lentivirally transduced to upregulate the expression level of P53 (= pLenti-P53) or were transduced as lentiviral control (= pLenti-Cont). miR-17 was stable upregulated in BMMSCs by miR-17 mimics (= miR-17 mimics). miRNA control (= miR Cont). 16 Mon Cont = control BMMSCs, Smurf1 siRNA = downregulated Smurf1 level via si-RNA, miR-17 inhibitor = transfection with anti-miR-17. Statistically analyzed values show the mean ± SD (n=10). * $p < 0.05$. **(A)** Real-time PCR and western blot analysis on the expression of Smurf1 and TCF3 after upregulation of p53 (pLenti-p53) in BMMSCs derived from young mice. Normalization to ß-actin. **(B)** Western blot analysis on the expression of Smurf1. Transfection of miR-17 mimics in stable upregulated p53 BMMSCs derived from young mice. Normalization to ß-actin. **(C-D)** Real-time PCR and western blot analysis of Smurf1 expression in osteogenically differentiated BMMSCs from young and old mice. Normalization to ß-actin. **(E)** Alizarin red staining after osteogenic induction for 14 d of BMMSCs derived from old mice with/without siRNA-downregulated Smurf1 level and with/without transfection with miR-17 inhibitor. **(F)** Western blot analysis on old BMMSCs with/without siRNA-down-regulated Smurf1 level and with/without transfection with anti-miR-17 for the osteogenic markers Runx2, ALP, osterix. Normalization to ß-actin.

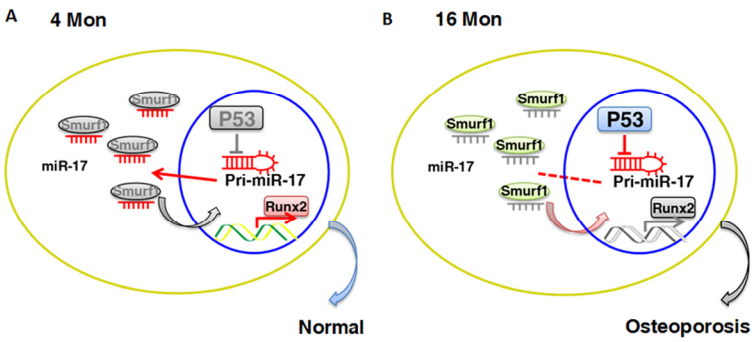

Figure 7. Schematic diagram of p53/miR-17/Smurf1 cascade. **(A, B)** p53 regulates the osteogenic differentiation of BMMSCs through inhibiting transcription of miR-17-92 cluster and subsequent modulating Smurf1, a direct target gene of miR-17, aslo acts as a negative regulator for osteogenic differentiation of mesenchymal stem cells.

DISCUSSION

Senescence of cells and especially of stem cells is an ongoing matter of debate, and its potential impact on tissue homeostasis is up to date still largely obscure. Aggravating this concern is the fact that there is no clear evidence whether the age-related cellular changes observed *in vitro* such as growth stagnation and diminished differentiation capacity also impact tissue homeostasis *in vivo* [3]. Additionally, the molecular mechanisms involved in and activated by occurrence of senescence are widely unknown, thus making a disclosure of possible consequences for cellular signaling pathways and the corres ponding effects in tissues almost impossible. Therefore, our study was meant to investigate the cellular characteristics of aging BMMSCs and the resulting changes in their osteogenic potential both *in vivo* and *in vitro*.

Our analyses revealed that *in vivo* bone formation in terms of volumetric bone mineral density and trabecular bone volume fraction in femur tissue sections and *in vitro* correspondingly osteogenic differentiation of murine BMMSCs are reduced with advancing age. BMMSCs from elder mice exhibit an increase in senescence-associated ß-galactosidase, p16, p21, p53 and concurrently a decrease in proliferation and occurrence of osteogenic markers alizarin red, Runx2, ALP and osterix. Interestingly, inflammatory molecules TNF-α and IFN-γ both revealed significantly higher values of these cytokines in elder mice, suggesting more inherent inflammation with advancing age. Previous studies detected a dependence between heightened levels of inflammatory molecules and impaired bone formation capacity in inflammatory bone diseases, and due to our results evidence suggests an intrinsic predisposition for inflammatory priming in senescent cells [29, 30]. In consideration that inflammatory cytokines are qualified to induce inflammatory settings by modulation of miRNAs, our findings are concordant with these results [31, 32]. We could show that p53 inhibits osteogenic differentiation of BMMSCs *in vivo* and that these effects impair osteoid formation about 45% *in vitro* when p53-transfected BMMSCs are loaded on implanted HA/TCP.

Analyses on the molecular pathways involved in this repressive influence of p53 uncovered a reversion of the inhibitory effects of p53 on osteogenesis upon miR-17 overexpression with rescue of osteogenic differentiation of old BMMSCs and vice versa a restraint of miR-17 by p53 overexpression. MiR-17-92 cluster plays an important role in senescence and has a close relationship with p53, as p53 can bind to the promoter region of miR-17-92 for repression of its function, which plays a key role in hypoxia-induced apoptosis [20]. MiR-17 is closely related to TCF3 and Smurf1, two direct target genes in the cells that miR-17 can bind and thus block these negative regulators of osteogenesis [25, 26]. In both our control and osteogenically induced group, Smurf1 expression was higher in old compared to young BMMSCs, and upregulation of p53 increased Smurf1 expression as well. Rising of both p53 and miR-17 at the same time did not alter the level of Smurf1, demonstrate-ing that p53 regulates Smurf1 indirectly by inhibition of miR-17. Contrarily, TCF3 remained unaffected by any of the treatments, providing an indication that the target gene miR-17 binds to is dependent on the microenvironment and the cellular components involved. On the basis of our previous results, miR-17 tends to target TCF3 in the normal microenvironment, while it aims to target Smurf1 under inflammatory conditions [25, 26]. As senescent cells have been shown to display elevated expression profiles of inflammatory molecules, the trend that miR-17 has an affinity for binding Smurf1 can be interpreted in this manner.

In summary, our results illustrate that cellular senescence involves inhibiting effects on osteogenesis *in vitro* as well as *in vivo* with major impact of regulatory mechanisms engaging in miRNA signaling pathways. This knowledge provides the basis for the development of new treatment strategies in age-related changes of bone homeostasis both under physiological and pathological conditions.

METHODS

Mice. Twenty 4-month and 16-month old C57/BL6 mice, female, respectively (n=10 specimens per group for histology, n=10 for cell culture) and 6-week old immunocompromised nude mice (CAnN.Cg-Foxn1nu/CrlVr) (n=10 specimens per group), female, were purchased from Vital River Laboratory Animal Technology Co. Ltd. (Beijing, China). All procedures involving animals were approved by the Animal use and Care Committee of the Fourth Military Medical University (license number: SCXK 2007-007).

Micro-CT analysis. The mice (n=5) from each experimental group were scanned with the Inveon micro-CT system (Siemens Healthcare Diagnostics GmbH, Eschborn, Germany). Cross-sectional volumetric BMD was measured at right tibia mid-diaphysis. Using two-dimensional images, a region of interest in secondary spongiosa was manually drawn near the endocortical surface, and cancellous bone morphometric parameters including BV/TV in % were assessed. Experiments were performed in triplicate.

Bone histological analysis. The femurs derived from the mice of each experimental group were fixed with 4% paraformaldehyde, decalcified with 10% EDTA (pH 7.0) and embedded in paraffin. For histological analysis, tissue sections were deparaffinized and stained with HE followed by trabecular percentage calculation using Image J software. Experiments were performed in triplicate.

Isolation of murine BMMSCs. Bone marrow cells (3×10^7) were flushed out from long bones of each experimental group of mice (n=5) with 2% FBS in PBS. A single-cell suspension of all nucleated cells was obtained by passing bone marrow cells through a 70 μm cell strainer (BD Biosciences, New Jersey, USA). Then, 5×10^6 cells were seeded into 5 cm culture dishes and initially incubated at 37 °C and 5% CO_2. After 24 h, cultures were washed with PBS to eliminate non-adherent cells. The attached cells were cultured for 10 to 15 d with a-MEM supplemented with 20% FBS, 2mM L-glutamine, 100 U/ml penicillin and 100 mg/ml streptomycin (Invitrogen, Carlsbad, CA, USA). Passage 1 and 2 were used in all experiments.

CFU assay. To assess the CFU efficiency of BMMSCs, 1×10^3 primary cultured BMMSCs derived from each experimental group of mice (n=5) were seeded in 5 cm culture dishes (Corning, Lowell, MA, USA) and cultured in proliferation or osteogenic differentiation medium for 14 days. Then, the newly formed colonies were visualized with 0.1% toluidine blue or Alizarin Red/ALP staining following 4% paraformaldehyde fixation for CFU-F and CFU-Ob assay. Aggregates of 50 or more cells were scored as colonies under the microscope (Leica Microsystems, Heerbrugg, Switzerland). CFU efficiency was determined by the number of colonies relative to the total number of seeded cells in each plate. Experiments were performed in triplicate.

β-galactosidase staining assays. To assess the senescence of the cultured BMMSCs after 48 h (both 4 mon and 16 mon), β-galactosidase staining was determined via a staining Kit (Beyotime Institute of Biotechnology, Jiangsu China) according to the manufacturer's protocol. Experiments were performed in triplicate.

Real-time PCR analysis. Total RNA was isolated from cultured BMMSCs and from femur bone tissues using Trizol (Invitrogen) according to the manufacturer's instructions. MiRNA was extracted with the mirVana miRNA Isolation Kit (Ambion, Austin, *TX,* USA). The conversion of miRNA and mRNA into cDNA and the detection of miRNAs were carried out according to the manufacturer's instructions using the miScript Reverse Transcription Kit and the miScript SYBR Green PCR Kit (Takara Bio Inc., Shiga, Japan), respectively. Sequences were determined with the CFX96 Real-Time System (Bio-Rad, CA, USA). The optimized miRNA-specific primers for has-miR-17 and the endogenous control U6 were commercially obtained (RiboBio Co., Guangzhou, China). Primary-miR-17 and GAPDH as endogenous control were commercially purchased (Invitrogen). The expression levels of p16, p21, p53, Runx2, ALP, Osterix, TCF3 and Smurf1 (Takara Bio Inc.) were examined. The primers were listed in Table 1. Experiments were performed in triplicate.

Western blot analysis. BMMSCs were harvested in RIPA lysis buffer (Beyotime Institute of Biotechnology) and whole-cell protein extracts were quantified by a BCA assay, separated on SDS-PAGE 8%-12%, and then transferred to PVDF membranes (Millipore, Billerica, MA, USA). Antibodies included p16ink4 (1:800, Abbiotec, San Diego, USA), p21 (1:500, Abcam, Cambridge, England), p53 (1:500, Cell Signaling

Technology, Boston, MA, USA), Runx2 (1:500, Abcam), ALP (1:800, Abcam), OSX (1:500, Santa Cruz Biotechnology, Santa Cruz, CA, USA), TCF3 (1:500, Abcam), Smurf1 (1:500, Abcam). In addition, stripped membranes were reprobed with β-actin (1:5000, Abcam) as loading control. Signal detection was performed using the ECL Kit after incubation with an anti-rabbit or anti-mouse IgG secondary antibody (1:5000, CoWin Bioscience Co., Beijing, China). The relative band intensities in the scanned images were analyzed with Image J software (National Institutes of Health, Maryland, USA). Experiments were performed in triplicate.

Osteogenic differentiation assays. BMMSCs were incubated with osteogenic medium containing 100 nM dexamethasone, 50 mg/ml ascorbic acid and 1 mM b-glycerophosphate for 1 to 2 weeks according to the manufacturer´s instructions. To assess osteogenic differentiation, cells were fixed with 60 % isopropanol after 14 d in culture, stained with 1 % alizarin red (Sigma-Aldrich, St. Louis, MO, USA) and lysed in hexadecylpyridinium chloride. Then, the quantification of alizarin red staining intensity was determined with a microplate reader (Bio-TEK Instruments, Winooski, VT, USA) by absorbance at 570 nm. Experiments were performed in triplicate.

Table 1. Primers for Real-time PCR.

Primer name	Sequence (5' to 3')	Temperature (℃)	Length (bp)
U6	F:5'GCTTCGGCAGCACATATACTAAAAT3' R:5'CGCTTCACGAATTTGCGTGTCAT3'	60	89
β-actin	F:5' TGGCACCCAGCACAATGAA3' R:5' CTAAGTCATAGTCCGCCTAGAAGCA 3'	62	186
p53	F:5' GCTTTGAGGTGCGTGTTTGTG3' R:5' TTGGGCAGTGCTCGCTTAG 3'	60	126
p16	F:5' GCTTCCTGGACACGCTGGT 3' R:5' CATCTATGCGGGCATGGTTA3'	60	174
p21	F:5' GGGAGCAGGCTGAAGGGT3' R:5' CGGCGTTTGGAGTGGTAGAA 3'	60	97
Runx2	F:5' CACTGGCGCTGCAACAAGA 3' R:5' CATTCCGGAGCTCAGCAGAATAA 3'	60	127
ALP	F:5' CCTTGTAGCCAGGCCCATTG3' R:5' GGACCATTCCCACGTCTTCAC 3'	60	137
Osterix	F:5' TGGCGTCCTCCCTGCTTG 3' R:5' TGCTTTGCCCAGAGTTGTTG3'	60	125
Smurf1	F:5' CGTGGGGAAGAAGGTTTGG 3' R:5' TGGTCGGGGTTGATTGAAGA 3'	60	158
TCF3	F:5' AATAACTTCTCGTCCAGCCCTT 3' R:5' CTCGTCCAGGTGGTCTTCTATCT 3'	60	159

Lentiviral vector construction and transduction. To construct a lentiviral vector for mouse transformation-related protein 53 (p53), p53 was amplified from mouse cDNA via PCR. Primers for lentiviral construct transduction were as follows:
m-tp53-SalI acgGTCGACggATGACTGCCATGGAG GAGTC
m-tp53-NotI ATAAGAATGCGGCCGCcagTCAGTC TGAGTCAGG
The PCR product was digested with Sal I and Not I and inserted into the pLenti 6.3/v5-DEST vector (Invitrogen). The inserted fragments were verified by Sanger sequencing. A lentiviral construct containing the scrambled p53 sequence was used as negative control. The lentivirus was produced by co-transfecting 293T cells with the transfer vector and two packaging vectors (psPAX2, pMD2.G). The virus was subsequently purified by ultracentrifugation. 1×10^5 BMMSCs were plated in 6-well plates and transduced with lentiviral constructs and 5 μg/ml polybrene (Sigma). Experiments were performed in triplicate.

Transfection assay. MiR-17 mimics and inhibitor (Ribobio, Guangdong, China) were transfected into BMMSCs at a concentration of 50 nM with the siPORT NeoFX Transfection Agent (Ambion). The medium was replaced 8 h later and the cells were harvested for mRNA analysis after 24 h of transfection and for protein analysis after 48 h of transfection.

SiRNA duplex oligonucleotides against mouse Smurf1 and the negative control (Gene-Pharma Co., Shanghai, China) were chemically modified (2'-O-Methyl) and transfected into the cells at a final concentration of 100 nM using the siPORT NeoFX (Ambion). Experiments were performed in triplicate.

ELISA assay. TNF-α and IFN-γ serum levels were measured by ELISA using murine TNF-α and IFN-γ assay kits (Neobioscience technology, Shenzhen, China). Experiments were performed in triplicate according to the manufacturer's protocol.

In vivo bone formation assay. For a single transplant complex, BMMSCs were transduced with a pLenti-p53 lentiviral construct as described above and then cultured for 3 d. 2×10^6 cells were mixed with 15 mg HA/TCP ceramic particles (Sigma-Aldrich) and implanted into subcutaneous pockets on the backs of the 8-weeks NOD/SCID mice (Fourth Military Medical University). As control, BMMSCs from the same sources treated with the lentivirus control were implanted into the other side of the same host's back. The implants were taken out 8 weeks after transplantation, fixed with 4% paraformaldehyde and decalcified with buffered 10% EDTA (pH 6.0). For histological analyses, the sections were stained with HE or Masson's Trichrome (BaSO Diagnostic Inc, Guangdong, China) according to the manufacturer's instructions. Experiments were performed in triplicate.

Statistics. Statistical evaluation was performed using a t-test and one-way ANOVA for experiments comprising more than three groups, respectively. The data are presented as mean ± SD. $P< 0.05$ was considered statistically significant. The *p*-values were adjusted using the Bonferroni method. Each experiment was repeated three times. Analytic tests were performed using SPSS17.0 Software.

ACKNOWLEDGEMENTS

This work was supported by grants from the National Basic Research Program (973 Program) (2011CB964700) and the Nature Science Foundation of China (31200972, 81171001).

Authors' contributions

Wenjia Liu designed the experiments and analyzed the data. Meng Qi did part of the experiments and collected data. Anna Konermann wrote the whole manuscript. Liqiang Zhang participated in the experiments of western blotting. Fang Jin and Yan Jin made critical intellectual contributions that formed the central concept of this study and were involved in the writing process of the manuscript.

Conflict of interest statement

The authors declare no conflict of interest.

REFERENCES

1. Anton B, Vitetta L, Cortizo F, Sali A. Can we delay aging? The biology and science of aging. Ann N Y Acad Sci. 2005; 1057: 525-535.

2. Wilson A, Shehadeh LA, Yu H, Webster KA. Age-related molecular genetic changes of murine bone marrow mesenchymal stem cells. BMC Genomics. 2010; 11: 229.

3. Cheng H, Qiu L, Ma J, Zhang H, Cheng M, Li W, Zhao X, Liu KY. Replicative senescence of human bone marrow and umbilical cord derived mesenchymal stem cells and their differentiation to adipocytes and osteoblasts. Mol Biol Rep. 2011; 38: 5161-5168.

4. Despars G, Carbonneau CL, Bardeau P, Coutu DL, Beauséjour CM. Loss of the osteogenic differentiation potential during senescence is limited to bone progenitor cells and is dependent on p53. PLoS One. 2013; 8: e73206.

5. Picinich SC, Mishra PJ, Mishra PJ, Glod J, Banerjee D. The therapeutic potential of mesenchymal stem cells. Cell- & tissue-based therapy. Expert Opin Biol Ther. 2007; 7: 965-973.

6. Michaloglou C, Vredeveld LC, Soengas MS, Denoyelle C, Kuilman T, van der Horst CM, Majoor DM, Shay JW, Mooi WJ, Peeper DS. BRAFE600-associated senescence-like cell cycle arrest of human naevi. Nature. 2005; 436: 720-724.

7. Collado M, Serrano M. Senescence in tumours: evidence from mice and humans. Nat Rev Cancer. 2010; 10: 51-57.

8. Tchkonia T, Zhu Y, van Deursen J, Campisi J, Kirkland JL. Cellular senescence and the senescent secretory phenotype: therapeutic opportunities. J Clin Invest. 2013; 123: 966-972.

9. Park JS, Kim HY, Kim HW, Chae GN, Oh HT, Park JY, Shim H, Seo M, Shin EY, Kim EG, Park SC, Kwak SJ. Increased caveolin-1, a cause for the declined adipogenic potential of senescent human mesenchymal stem cells. Mech Ageing Dev. 2005; 126: 551-559.

10. Terai M, Uyama T, Sugiki T, Li XK, Umezawa A, Kiyono T. Immortalization of human fetal cells: the life span of umbilical cord blood-derived cells can be prolonged without manipulating p16INK4a/RB braking pathway. Mol Biol Cell. 2005; 16: 1491-1499.

11. Moerman EJ, Teng K, Lipschitz DA, Lecka-Czernik B. Aging activates adipogenic and suppresses osteogenic programs in mesenchymal marrow stroma/stem cells: the role of PPAR-gamma2 transcription factor and TGF-beta/BMP signaling pathways. Aging Cell. 2004; 3: 379-389.

12. Wall ME, Bernacki SH, Loboa EG. Effects of serial passaging on the adipogenic and osteogenic differentiation potential of adipose-derived human mesenchymal stem cells. Tissue Eng. 2007; 13: 1291-1298.

13. Tokalov SV, Grüner S, Schindler S, Wolf G, Baumann M, Abolmaali N. Age-related changes in the frequency of mesenchymal stem cells in the bone marrow of rats. Stem Cells Dev. 2007; 16: 439-446.

14. Zhou S, Greenberger JS, Epperly MW, Goff JP, Adler C, Leboff MS, Glowacki J. Age-related intrinsic changes in human bone-marrow-derived mesenchymal stem cells and their differentiation to osteoblasts. Aging Cell. 2008; 7: 335-343.

15. Pan Z, Yang J, Guo C, Shi D, Shen D, Zheng Q, Chen R, Xu Y, Xi Y, Wang J. Effects of hindlimb unloading on ex vivo growth and osteogenic/adipogenic potentials of bone marrow-derived mesenchymal stem cells in rats. Stem Cells Dev. 2008; 17: 795-804.

16. Tyner SD, Venkatachalam S, Choi J, Jones S, Ghebranious N, Igelmann H, Lu X, Soron G, Cooper B, Brayton C, Park SH, Thompson T, Karsenty G, et al.p53 mutant mice that display early ageing-associated phenotypes. Nature. 2002; 415: 45-53.

17. Vousden KH, Lu X. Live or let die: the cell's response to p53. Nat Rev Cancer. 2002; 2: 594-604.

18. Levine AJ. p53, the cellular gatekeeper for growth and division. Cell. 1997; 88: 323-331.

19. Sharpless NE, DePinho RA. p53: good cop/bad cop. Cell. 2002; 110: 9-12.

20. Bartel DP. MicroRNAs: genomics, biogenesis, mechanism, and function. Cell. 2004; 116: 281-97.

21. Croce CM, Calin GA. miRNAs, cancer, and stem cell division. Cell. 2005; 122: 6-7.

22. Cheng AM, Byrom MW, Shelton J, Ford LP. Antisense inhibition of human miRNAs and indications for an involvement of miRNA in cell growth and apoptosis. Nucleic Acids Res. 2005; 33: 1290-1297.

23. Huang J, Zhao L, Xing L, Chen D. MicroRNA-204 regulates Runx2 protein expression and mesenchymal progenitor cell differentiation. Stem Cells. 2010; 28: 357-364.

24. Zhang JF, Fu WM, He ML, Xie WD, Lv Q, Wan G, Li G, Wang H, Lu G, Hu X, Jiang S, Li JN, Lin MC, et al. MiRNA-20a promotes osteogenic differentiation of human mesenchymal stem cells by co-regulating BMP signaling. RNA Biol. 2011; 8: 829-838.

25. Liu Y, Liu W, Hu C, Xue Z, Wang G, Ding B, Luo H, Tang L, Kong X, Chen X, Liu N, Ding Y, Jin Y. MiR-17 modulates osteogenic differentiation through a coherent feed-forward loop in mesenchymal stem cells isolated from periodontal ligaments of patients with periodontitis. Stem Cells. 2011; 29: 1804-1816.

26. Liu W, Liu Y, Guo T, Hu C, Luo H, Zhang L, Shi S, Cai T, Ding Y, Jin Y. TCF3, a novel positive regulator of osteogenesis, plays a crucial role in miR-17 modulating the diverse effect of canonical Wnt signaling in different microenvironments. Cell Death Dis. 2013; 4: e539.

27. Yan HL, Xue G, Mei Q, Wang YZ, Ding FX, Liu MF, Lu MH, Tang Y, Yu HY, Sun SH. Repression of the miR-17-92 cluster by p53 has an important function in hypoxia-induced apoptosis. EMBO J. 2009; 28: 2719-2732.

28. Tanzer A, Stadler PF. Molecular evolution of a microRNA cluster. J Mol Biol. 2004; 339: 327-335.

29. Khosla S, Riggs BL. Pathophysiology of age-related bone loss and osteoporosis. Endocrinol Metab Clin North Am. 2005; 34: 1015-1030.

30. Raisz LG. Pathogenesis of osteoporosis: concepts, conflicts, and prospects. J Clin Invest. 2005; 115: 3318-25.

31. Kurowska-Stolarska M, Alivernini S, Ballantine LE, Asquith DL, Millar NL, Gilchrist DS, Reilly J, Ierna M, Fraser AR, Stolarski B, McSharry C, Hueber AJ, Baxter D, et al. MicroRNA-155 as a proinflammatory regulator in clinical and experimental arthritis. Proc Natl Acad Sci U S A. 2011; 108: 11193-11198.

32. Tili E, Michaille JJ, Wernicke D, Alder H, Costinean S, Volinia S, Croce CM. Mutator activity induced by microRNA-155 (miR-155) links inflammation and cancer. Proc Natl Acad Sci U S A. 2011; 108: 4908-4913.

Research Paper

Rapamycin extends lifespan and delays tumorigenesis in heterozygous p53+/- mice

Elena A. Komarova[1], Marina P. Antoch[2], Liliya R. Novototskaya[1], Olga B. Chernova[3], Geraldine Paszkiewicz[1], Olga V. Leontieva[1], Mikhail V. Blagosklonny[1], and Andrei V. Gudkov[1]

[1] *Department of Cell Stress Biology, Roswell Park Cancer Institute, BLSC, L3-312, Buffalo, NY 14263, USA;*
[2] *Department of Molecular & Cellular Biology, Roswell Park Cancer Institute, BLSC, L3-312, Buffalo, NY 14263, USA*
[3] *Tartis Aging, Inc., Buffalo, NY 14203, USA*

Key words: *cancer, mutations, DNA damage, aging, mTOR*
Received: *8/30/12; Accepted: 10/27/12; Published: 10/29/12*
Correspondence to: *Andrei V. Gudkov, PhD;* ***E-mail:*** *andrei.gudkov@roswellpark.org and Mikhail V. Blagosklonny, MD/PhD;*
E-mail: *blagosklonny@oncotarget.com*

Copyright: *© Komarova et al. This is an open-access article distributed under the terms of the Creative Commons Attribution License, which permits unrestricted use, distribution, and reproduction in any medium, provided the original author and source are credited*

Abstract: The TOR (Target of Rapamycin) pathway accelerates cellular and organismal aging. Similar to rapamycin, p53 can inhibit the mTOR pathway in some mammalian cells. Mice lacking one copy of p53 (p53+/- mice) have an increased cancer incidence and a shorter lifespan. We hypothesize that rapamycin can delay cancer in heterozygous p53+/- mice. Here we show that rapamycin (given in a drinking water) extended the mean lifespan of p53+/- mice by 10% and when treatment started early in life (at the age less than 5 months) by 28%. In addition, rapamycin decreased the incidence of spontaneous tumors. This observation may have applications in management of Li-Fraumeni syndrome patients characterized by heterozygous mutations in the *p53* gene.

INTRODUCTION

The mTOR (mammalian Target of Rapamycin) pathway plays a crucial role in the geroconversion from cell cycle arrest to senescence (geroconversion) [1]. Rapamycin suppresses or decelerates geroconversion, maintaining quiescence instead [2-8]. Furthemore, inhibition of the TOR pathway prolongs lifespan in model organisms, including mice [9-13]. In an organism, nutrients activate mTOR [14-16], whereas fasting or calorie restriction deactivates mTOR [17-19]. Calorie restriction slows down aging [20] and postpones tumorigenesis in several animal models [21, 22], including p53-deficient mice [23-25].

Similar to other tumor suppressors, p53 can inhibit mTOR in mammalian cells [26-31]. While causing cell cycle arrest, p53 can suppress geroconversion, thus preventing a senescent phenotype in the arrested cells [30, 31]. Therefore, it is not suprising that p53 inhibits hyper-secretory phenotype, a hallmark of senescence [32] whereas p53-deficiency resulted in pro-inflammatory phenotype [33, 34]. Noteworthy, the activity of p53 is decreased with aging [35]. Lack of one p53-allele (p53+/-) accelerates carcinogenesis and shortens lifespan [36-41]. We propose that rapamycin can decelerate cancer development in p53+/- mice. Here we show experimental evidence supporting this hypothesis.

RESULTS

Rapamycin (approximate dose, 1.5 mg/kg/day) was given in drinking water. 75 mice were divided into two groups: control (n=38) and rapamycin-treated (n=37). The mean lifespan of animals in control group was 373 days and the last 10% of survivals lived as long as 520 days (Fig. 1 A). In rapamycin-treated mice, the mean lifespan was 410 days and lifespan of the last 10% of survivals could not be determined (Fig. 1 A). Mice in both groups were also monitored for tumor development. The data presented in Fig. 1B

demonstrate that carcinogenesis was significantly delayed in rapamycin-treated mice compared to control mice.

Since in our experiments animals started to receive rapamycin at different age, we sought to test whether this affected the outcome of the treatment.

For this, we further subdivided all mice used into two groups: "young" (receiving rapamycin from the age of 5 months or earlier) and "old" (receiving rapamycin starting at 5 months of age or older). Results of the data analysis for the "young" group are shown in Figure 1C and D. The mean lifespan in control group was 373 days, whereas in rapamycin-treated "young" mice the mean lifespan reached 480 days, 3.5 months increase over the control group. Furthermore, 40% of rapamycin-treated "young" mice survived 550 days (Fig. 1C) and by this age developed 2 times less tumors than control mice (Fig. 1D). In the "old" group the difference between control and treated group was blunted (data not shown).

Thus, the life-extending effect of rapamycin is more pronounced when treatment starts earlier in life. In order to confirm that rapamycin administered with drinking water has biological activity in vivo, we measured levels of phosphorylated ribosomal protein S6 (pS6), a marker of the mTOR activity in tissues of control and rapamycin-treated mice. After receiving rapamycin in drinking water for 2 days, mice were sacrificed and the levels of total S6 and pS6 were estimated by Western blot analysis and immuno-cytochemistry (Fig. 2).

As shown in Fig. 2A, levels of pS6 were reduced in the heart, kidney and liver of rapamycin-treated mice. Also, pS6/S6 ratios were lower in rapamycin-treated mice (Fig. S1).

These results were confirmed by immunohistochemical staining showing lower levels of pS6 in tissues of rapamycin-treated mice (Fig. 2B). The variability of pS6 levels among mice may explain the variability of biological effects of rapamycin.

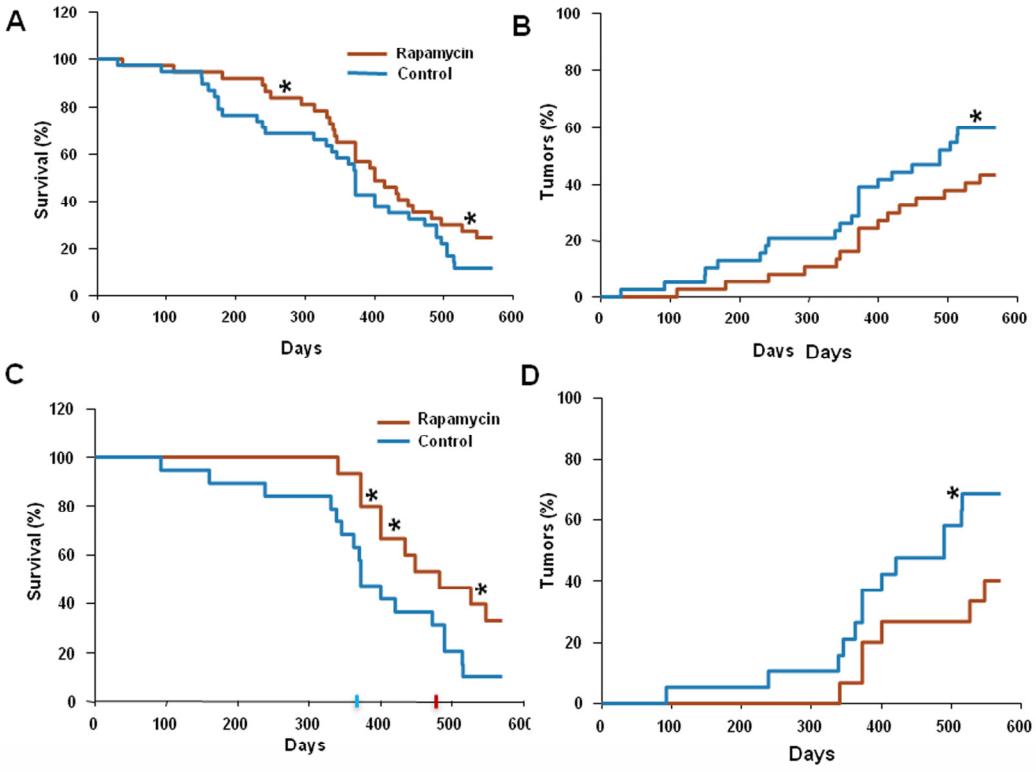

Figure 1. Administration of rapamycin extends lifespan and delays carcinogenesis in p53+/- male mice. (**A**) Kaplan Meier survival curve of rapamycin-treated (red line) and control (blue line) mice. (**B**) Incidence of tumors in rapamycin-treated (red) and control (blue) mice. Animals received rapamycin starting at various ages at 1.5 mg/kg per day in drinking water throughout entire life. * $p<0.05$. (**C**) Kaplan Meier survival curve of rapamycin-treated (red line) and control (blue line) mice that start receiving rapamycin early in life (<5 months). (**D**) Incidence of tumors in rapamycin-treated (red) and control (blue) mice that start receiving rapamycin early in life (<5 months). * $p<0.05$ toph

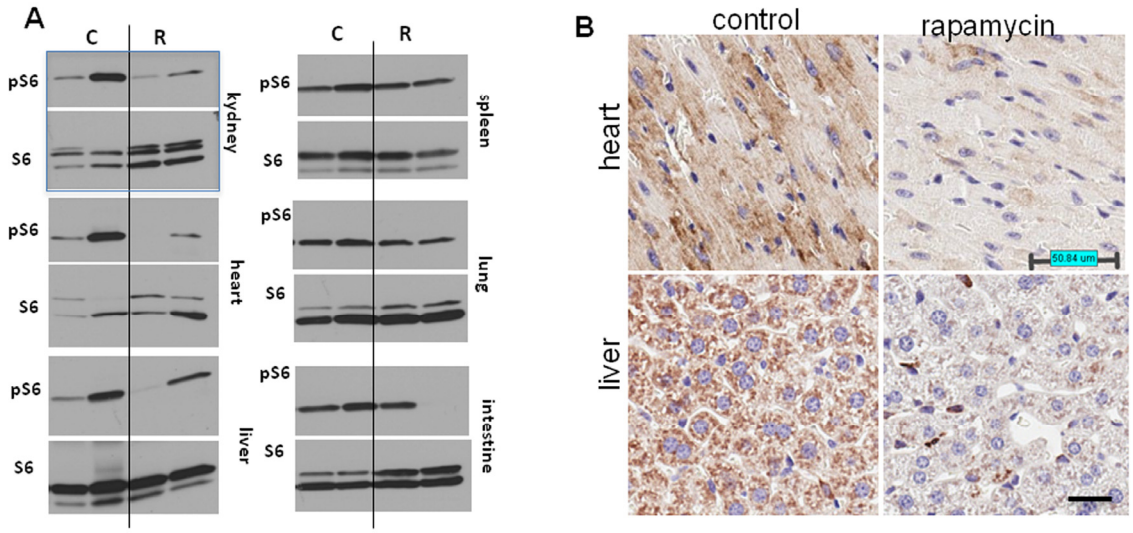

Figure 2. Administration of rapamycin in drinking water inhibits the mTOR pathway in p53+/- male mice. (**A**) Western blot analysis of whole cell lysates of 6 organs of rapamycin-treated and control mice probed with antibodies specific to S6 and phospho-S6 (Ser240/244). Mice received rapamycin in drinking water for 2 days. (**B**) Immunohistochemistry. pS6 in the heart and the liver. Mice received rapamycin in drinking water for 2 days.

DISCUSSION

Previously it was shown that rapamycin prolongs lifespan in genetically heterogeneous mice [11], [12], inbred mice [42] and Her2-expressing mice [13]. In normal genetically heterogeneous mice, rapamycin extended life span even when its administration was started later in life [11]. Our data in p53+/- mice show that the effect of rapamycin was blunted when treatment started at the age of 5 months or older.

This indicates that the anti-cancer effect of rapamycin is likely to be indirect and is imposed via its systemic effect at the level of an organism rather than through direct inhibition of tumor growth. To further address this question we plan to test the effect of rapamycin on animals with established tumors (by measuring tumor growth) along with evaluating the functional status of mTOR and the ability of rapamycin to suppress it in tumors and normal tissues. As we report here, administration of rapamycin starting early in life increased mean lifespan in p53+/- male mice by 28%. Previous work has demonstrated that the life-extending effects of rapamycin [11, 12] as well as metformin [43, 44], calorie restriction [45] and genetic inhibition of the IGF-I/mTOR/S6K pathway [46, 47] were less pronounced in male mice compared with female mice. Moreover, in some cases, life span extension was achieved in female mice only [43, 47]. Therefore, the observed increase in the median lifespan is dramatic, taking into account that it was achieved in male mice. However, because of low bioavailability of rapamycin, it was given constantly (in drinking water) without interruptions, whereas intermittent schedules may be more appropriate for future clinical developments as cancer-preventive interventions. In fact, a novel formulation of rapamycin (Rapatar) may be given intermittently, which still reveal even more pronounced extension of life span in p53-deficient mice (Comas et al, Aging 2012; this issue).

Our study suggests that rapamycin can be considered for cancer prevention in patients with Li-Fraumeni syndrome. Li-Fraumeni syndrome is an autosomal dominant disorder with a germline p53 mutation [48]. The incidence of cancer in carriers of mutation reaches 50% at the age of 40 and 90% at the age 60. Children of affected parents have an approximate 50% risk of inheriting the familial mutation [48]. Although functional assays have been established allowing for easy genetic testing for TP53 mutation, no effective chemopreventive therapy is currently available. The p53 rescue compounds may hold some promise in the future [48-50]; however these are not clinically approved drugs. In contrast, rapamycin has been used in the clinic for over a decade mostly in renal transplant patients. It was reported that rapamycin significantly decreased cancer incidence in renal transplant patients [51-53].

Our data suggest that rapamycin or its analogs can be considered for cancer prevention in Li-Fraumeni syndrome.

METHODS

Mice. All animal studies were conducted in accordance with the regulations of the Committee of Animal Care and Use at Roswell Park Cancer Institute. The colony of p53-knockout mice on a C57B1/6 background (originally obtained from Jackson Laboratories, Bar Habor, ME) was maintained by crossing p53+/- females with p53-/- males followed by genotyping of the progeny (PCR) as described previously [54]. Heterozygous p53+/- mice were generated by crossing p53-/- males with wild type p53 females. Male mice were kept in polypropelene cages (30x21x10 cm) under standard light/dark regimen (12 hours light : 12 hours darkness) at 22 ± 2 °C, And received standard laboratory chow and water ad libitum.

Rapamycin treatment. Rapamycin (LC Laboratories, USA) was diluted in ethanol at concentration 15 mg/ml. Then the stock was diluted 1:1000 in drinking water. Drinking water was changed every week. Male mice were randomly divided into two groups. Mice of the first group (n=37) were given rapamycin in drinking water (approximately 1.5 mg/kg per day), whereas mice of the second group (n=38) were given tap water without rapamycin and served as control. Once a week all mice were palpated for detection of tumor mass appearance.

Pathomorphological examination. All animals were autopsied. Site, number and size of tumors were checked. All tumors, as well as the tissues and organs with suspected tumor development were excised and fixed in 10% neutral formalin. After the routine histological processing the tissues were embedded into paraffin. 5-7 μm thin histological sections were stained with haematoxylin and eosine and were microscopically examined. Tumors were classified according to International Agency for Research on Cancer recommendations.

Western blot analysis. Tissues were homogenized in Bullet blender using stainless steel 0.5 mm diameter beads (Next Advantage, Inc. NY, USA) and RIPA lysis buffer supplemented with protease and phosphatase inhibitors tablets (Roche Diagnostics, Indianopolis, IN, USA). Lysates were cleared by centrifugation at 4°C at 13000 rpm. Equal amounts of protein were separated on gradient Criterion gels (BioRad) and immunoblotting was performed with rabbit anti-phospho S6 (Ser 240/244) and mouse anti-S6 antibodies from Cell Signaling Biotechnology as described previously [55], [56].

Immunochemistry. Dissected tissue samples were fixed in 10% buffered formalin, embedded into paraffin. 5-7 μm thin histological sections were stained with anti-phospho S6 (Ser240/244) antibody (Cell Signaling) and counterstained with Hematoxylin.

Statistical analyses. The SigmaStat software package was used for analysis. The P values were calculated using Fisher's Exact Test (2-tail). $P<0.05$ was considered as statistically significant.

Conflict of Interest Statement

The authors of this manuscript have no conflict of interests to declare.

REFERENCES

1. Blagosklonny MV. Cell cycle arrest is not yet senescence, which is not just cell cycle arrest: terminology for TOR-driven aging. Aging (Albany NY). 2012; 4: 159-165.

2. Demidenko ZN, Zubova SG, Bukreeva EI, Pospelov VA, Pospelova TV, Blagosklonny MV. Rapamycin decelerates cellular senescence. Cell Cycle. 2009; 8: 1888-1895.

3. Gan B, Sahin E, Jiang S, Sanchez-Aguilera A, Scott KL, Chin L, Williams DA, Kwiatkowski DJ, DePinho RA. mTORC1-dependent and -independent regulation of stem cell renewal, differentiation, and mobilization. Proc Natl Acad Sci U S A. 2008; 105: 19384-19389.

4. Gan B, DePinho RA. mTORC1 signaling governs hematopoietic stem cell quiescence. Cell Cycle. 2009; 8: 1003-1006.

5. Chen C, Liu Y, Liu R, Ikenoue T, Guan KL, Zheng P. TSC-mTOR maintains quiescence and function of hematopoietic stem cells by repressing mitochondrial biogenesis and reactive oxygen species. J Exp Med. 2008; 205: 2397-2408.

6. Chen C, Liu Y, Zheng P. mTOR regulation and therapeutic rejuvenation of aging hematopoietic stem cells. Sci Signal. 2009; 2: ra75.

7. Adhikari D, Zheng W, Shen Y, Gorre N, Hamalainen T, Cooney AJ, Huhtaniemi I, Lan ZJ, Liu K. Tsc/mTORC1 signaling in oocytes governs the quiescence and activation of primordial follicles. Human Molecular Genet. 2010; 19:397-410.

8. Kolesnichenko M, Hong L, Liao R, Vogt PK, Sun P. Attenuation of TORC1 signaling delays replicative and oncogenic RAS-induced senescence. Cell Cycle. 2012; 11: 2391-2401.

9. Kapahi P, Zid BM, Harper T, Koslover D, Sapin V, Benzer S. Regulation of lifespan in Drosophila by modulation of genes in the TOR signaling pathway. Curr Biol. 2004; 14: 885-890.

10. Bjedov I, Toivonen JM, Kerr F, Slack C, Jacobson J, Foley A, Partridge L. Mechanisms of life span extension by rapamycin in the fruit fly Drosophila melanogaster. Cell Metab. 2010; 11: 35-46.

11. Harrison DE, Strong R, Sharp ZD, Nelson JF, Astle CM, Flurkey K, Nadon NL, Wilkinson JE, Frenkel K, Carter CS, Pahor M, Javors MA, Fernandezr E, Miller RA. Rapamycin fed late in life extends

lifespan in genetically heterogenous mice. Nature. 2009; 460: 392-396.

12. Miller RA, Harrison DE, Astle CM, Baur JA, Boyd AR, de Cabo R, Fernandez E, Flurkey K, Javors MA, Nelson JF, Orihuela CJ, Pletcher S, Sharp ZD, Sinclair D, Starnes JW, Wilkinson JE et al. Rapamycin, but not resveratrol or simvastatin, extends life span of genetically heterogeneous mice. J Gerontol A Biol Sci Med Sci. 2011; 66: 191-201.

13. Anisimov VN, al. e, Antoch M, Blagosklonny MV. Am J Pathol. 2010: in press.

14. Khamzina L, Veilleux A, Bergeron S, Marette A. Increased activation of the mammalian target of rapamycin pathway in liver and skeletal muscle of obese rats: possible involvement in obesity-linked insulin resistance. Endocrinology. 2005; 146: 1473-1481.

15. Tremblay F, Krebs M, Dombrowski L, Brehm A, Bernroider E, Roth E, Nowotny P, WaldhŠusl W, Marette A, Roden M. Overactivation of S6 kinase 1 as a cause of human insulin resistance during increased amino acid availability. Diabetes. 2005; 54: 2674-2684.

16. Krebs M, Brunmair B, Brehm A, Artwohl M, Szendroedi J, Nowotny P, Roth E, FŸrnsinn C, Promintzer M, Anderwald C, Bischof M, Roden M. The Mammalian target of rapamycin pathway regulates nutrient-sensitive glucose uptake in man. Diabetes. 2007; 56: 1600-1607.

17. Jiang W, Zhu Z, Thompson HJ. Dietary energy restriction modulates the activity of AMP-activated protein kinase, Akt, and mammalian target of rapamycin in mammary carcinomas, mammary gland, and liver. Cancer Res. 2008; 68: 5492-5499.

18. Estep PWr, Warner JB, Bulyk ML. Short-term calorie restriction in male mice feminizes gene expression and alters key regulators of conserved aging regulatory pathways. PLoS One. 2009; 4: e5242.

19. Masternak MM, Panici JA, Bonkowski MS, Hughes LF, Bartke A. Insulin sensitivity as a key mediator of growth hormone actions on longevity. J Gerontol A Biol Sci Med Sci. 2009; 64: 516-521.

20. Wang C, Maddick M, Miwa S, Jurk D, Czapiewski R, Saretzki G, Langie SA, Godschalk RW, Cameron K, von Zglinicki T. Adult-onset, short-term dietary restriction reduces cell senescence in mice. Aging (Albany NY). 2010; 2: 555-566.

21. Dirx MJ, Zeegers MP, Dagnelie PC, van den Bogaard T, van den Brandt PA. Energy restriction and the risk of spontaneous mammary tumors in mice: a meta-analysis. Int J Cancer. 2003; 106: 766-770.

22. Sarkar NH, Fernandes G, Telang NT, Kourides IA, Good RA. Low-calorie diet prevents the development of mammary tumors in C3H mice and reduces circulating prolactin level, murine mammary tumor virus expression, and proliferation of mammary alveolar cells. Proc Natl Acad Sci U S A. 1982; 79: 7758-7762.

23. Berrigan D, Perkins SN, Haines DC, Hursting SD. Adult-onset calorie restriction and fasting delay spontaneous tumorigenesis in p53-deficient mice. Carcinogenesis. 2002; 23: 817-822.

24. Hursting SD, Perkins SN, Phang JM. Calorie restriction delays spontaneous tumorigenesis in p53-knockout transgenic mice. Proc Natl Acad Sci U S A. 1994; 91: 7036-7040.

25. Hursting SD, Perkins SN, Brown CC, Haines DC, Phang JM. Calorie restriction induces a p53-independent delay of spontaneous carcinogenesis in p53-deficient and wild-type mice. Cancer Res. 1997; 57: 2843-2846.

26. Feng Z, Hu W, de Stanchina E, Teresky AK, Jin S, Lowe S, Levine AJ. The regulation of AMPK beta1, TSC2, and PTEN expression by p53: stress, cell and tissue specificity, and the role of these gene products in modulating the IGF-1-AKT-mTOR pathways. Cancer Res. 2007; 67: 3043-3053.

27. Feng Z, Zhang H, Levine AJ, Jin S. The coordinate regulation of the p53 and mTOR pathways in cells. Proc Natl Acad Sci U S A. 2005; 102: 8204-8209.

28. Levine AJ, Feng Z, Mak TW, You H, Jin S. Coordination and communication between the p53 and IGF-1-AKT-TOR signal transduction pathways. Genes Dev. 2006; 20: 267-275.

29. Budanov AV, Karin M. p53 target genes sestrin1 and sestrin2 connect genotoxic stress and mTOR signaling. Cell. 2008; 134: 451-460.

30. Demidenko ZN, Korotchkina LG, Gudkov AV, Blagosklonny MV. Paradoxical suppression of cellular senescence by p53. Proc Natl Acad Sci U S A. 2010; 9660-4: 9660-9664.

31. Korotchkina LG, Leontieva OV, Bukreeva EI, Demidenko ZN, Gudkov AV, Blagosklonny MV. The choice between p53-induced senescence and quiescence is determined in part by the mTOR pathway. Aging (Albany NY). 2010; 2: 344-352.

32. CoppŽ JP, Patil CK, Rodier F, Sun Y, Mu–oz DP, Goldstein J, Nelson PS, Desprez PY, Campisi J. Senescence-associated secretory phenotypes reveal cell-nonautonomous functions of oncogenic RAS and the p53 tumor suppressor. PLoS Biol. 2008; 6: 2853-2868.

33. Komarova EA, Krivokrysenko V, Wang K, Neznanov N, Chernov MV, Komarov PG, Brennan ML, Golovkina TV, Rokhlin OW, Kuprash DV, Nedospasov SA, Hazen SL, Feinstein E, Gudkov AV. p53 is a suppressor of inflammatory response in mice. FASEB J. 2005; 19: 1030-1032.

34. Gudkov AV, Gurova KV, Komarova EA. Inflammation and p53: A Tale of Two Stresses. Genes Cancer. 2011; 2: 503-516.

35. Feng Z, Hu W, Teresky AK, Hernando E, Cordon-Cardo C, Levine AJ. Declining p53 function in the aging process: a possible mechanism for the increased tumor incidence in older populations. Proc Natl Acad Sci U S A. 2007; 104: 16633-16638.

36. Donehower LA, Harvey M, Slagle BL, McArthur MJ, Montgomery CA, Jr., Butel JS, Bradley A. Mice deficient for p53 are developmentally normal but susceptible to spontaneous tumours. Nature. 1992; 356: 215-221.

37. Harvey M, McArthur MJ, Montgomery CA, Jr., Butel JS, Bradley A, Donehower LA. Spontaneous and carcinogen-induced tumorigenesis in p53-deficient mice. Nat Genet. 1993; 5: 225-229.

38. Jacks T, Remington L, Williams BO, Schmitt EM, Halachmi S, Bronson RT, Weinberg RA. Tumor spectrum analysis in p53-mutant mice. Curr Biol. 1994; 4: 1-7.

39. Donehower LA, Harvey M, Vogel H, McArthur MJ, Montgomery CA, Jr., Park SH, Thompson T, Ford RJ, Bradley A. Effects of genetic background on tumorigenesis in p53-deficient mice. Mol Carcinog. 1995; 14: 16-22.

40. Venkatachalam S, Shi YP, Jones SN, Vogel H, Bradley A, Pinkel D, Donehower LA. Retention of wild-type p53 in tumors from p53 heterozygous mice: reduction of p53 dosage can promote cancer formation. Embo J. 1998; 17: 4657-4667.

41. Hinkal G, Parikh N, Donehower LA. Timed somatic deletion of p53 in mice reveals age-associated differences in tumor progression. PLoS One. 2009; 4: e6654.

42. Anisimov VN, Zabezhinski MA, Popovich IG, Piskunova TS, Semenchenko AV, Tyndyk ML, Yurova MN, Rosenfeld SV,

Blagosklonny MV. Rapamycin increases lifespan and inhibits spontaneous tumorigenesis in inbred female mice. Cell Cycle. 2011; 10: 4230-4236.

43. Anisimov VN, Piskunova TS, Popovich IG, Zabezhinski MA, Tyndyk ML, Egormin PA, Yurova MV, Rosenfeld SV, Semenchenko AV, Kovalenko IG, Poroshina TE, Berstein LM. Gender differences in metformin effect on aging, life span and spontaneous tumorigenesis in 129/Sv mice. Aging (Albany NY). 2010; 2: 945-958.

44. Blagosklonny MV. Metformin and sex: Why suppression of aging may be harmful to young male mice. Aging (Albany NY). 2010; 2: 897-899.

45. Turturro A, Duffy P, Hass B, Kodell R, Hart R. Survival characteristics and age-adjusted disease incidences in C57BL/6 mice fed a commonly used cereal-based diet modulated by dietary restriction. J Gerontol A Biol Sci Med Sci. 2002; 57: B379-389.

46. Holzenberger M, Dupont J, Ducos B, Leneuve P, Geloen A, Even PC, Cervera P, Le Bouc Y. IGF-1 receptor regulates lifespan and resistance to oxidative stress in mice. Nature. 2003; 421: 182-187.

47. Selman C, Tullet JM, Wieser D, Irvine E, Lingard SJ, Choudhury AI, Claret M, Al-Qassab H, Carmignac D, Ramadani F, Woods A, Robinson IC, Schuster E, Batterham RL, Kozma SC, Thomas G et al. Ribosomal protein S6 kinase 1 signaling regulates mammalian life span. Science. 2009; 326: 140-144.

48. Upton B, Chu Q, Li BD. Li-Fraumeni syndrome: the genetics and treatment considerations for the sarcoma and associated neoplasms. Surg Oncol Clin N Am. 2009; 18: 145-156, ix.

49. Glazer RI. A new therapeutic basis for treating Li-Fraumeni Syndrome breast tumors expressing mutated TP53. Oncotarget. 2010; 1: 470-471.

50. Herbert BS, Chanoux RA, Liu Y, Baenziger PH, Goswami CP, McClintick JN, Edenberg HJ, Pennington RE, Lipkin SM, Kopelovich L. A molecular signature of normal breast epithelial and stromal cells from Li-Fraumeni syndrome mutation carriers. Oncotarget. 2010; 1: 405-422.

51. Mathew T, Kreis H, Friend P. Two-year incidence of malignancy in sirolimus-treated renal transplant recipients: results from five multicenter studies. Clin Transplant. 2004; 18: 446-449.

52. Campistol JM, Eris J, Oberbauer R, Friend P, Hutchison B, Morales JM, Claesson K, Stallone G, Russ G, Rostaing L, Kreis H, Burke JT, Brault Y, Scarola JA, Neylan JF. Sirolimus Therapy after Early Cyclosporine Withdrawal Reduces the Risk for Cancer in Adult Renal Transplantation. J Am Soc Nephrol. 2006; 17: 581-589.

53. Blagosklonny MV. Prevention of cancer by inhibiting aging. Cancer Biol Ther. 2008; 7: 1520-1524.

54. Leonova KI, Shneyder J, Antoch MP, Toshkov IA, Novototskaya LR, Komarov PG, Komarova EA, Gudkov AV. A small molecule inhibitor of p53 stimulates amplification of hematopoietic stem cells but does not promote tumor development in mice. Cell Cycle. 2010; 9: 1434-1443.

55. Leontieva O, Gudkov A, Blagosklonny M. Weak p53 permits senescence during cell cycle arrest. Cell Cycle. 2010; 9: 4323-4327.

56. Leontieva OV, Blagosklonny MV. DNA damaging agents and p53 do not cause senescence in quiescent cells, while consecutive re-activation of mTOR is associated with conversion to senescence. Aging (Albany NY). 2010; 2: 924-935.

SUPPLEMENTAL FIGURE

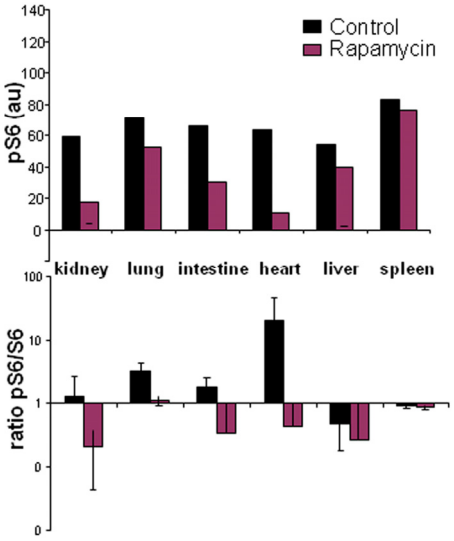

Supplemental Figure S1. Quantitative analysis of data shown in Figure 2A. Top panel - Intensity of phosphorylated S6 (pS6) signal was quantified using ImageJ program (intensity units, IU). Bottom panel – Intensity of pS6 and S6 signals were quantified and the ratio pS6/S6 was calculated.

Research Paper

New nanoformulation of rapamycin Rapatar extends lifespan in homozygous *p53*$^{-/-}$ mice by delaying carcinogenesis

Maria Comas[1,5], Ilia Toshkov[2], Karen K. Kuropatwinski[1], Olga B.Chernova[3], Alexander Polinsky[3], Mikhail V. Blagosklonny[4], Andrei V. Gudkov[4], and Marina P. Antoch[1]

[1] *Departments of Molecular and Cellular Biology, Roswell Park Cancer Institute, Buffalo, NY, USA*
[2] *Cleveland Biolabs, Buffalo, NY 14203, USA*
[3] *Tartis Aging, Inc, Buffalo, NY14203, USA*
[4] *Cell Stress Biology, Roswell Park Cancer Institute, Buffalo, NY USA;*
[5] *Cancer Research Program, Garvan Institute of Medical Research, Darlinghurst, New South Wales, Australia*

Key words: *mTOR pathway, p53-/-, lifespan, rapamycin, oral formulation, cancer prevention*
Received: *8/30/12; Accepted: 10/27/12; Published: 10/29/12*
Correspondence to: *Marina P. Antoch, PhD;* ***E-mail:*** *marina.antoch@roswellpark.org*

Copyright: *© Comas et al. This is an open-access article distributed under the terms of the Creative Commons Attribution License, which permits unrestricted use, distribution, and reproduction in any medium, provided the original author and source are credited*

Abstract: The nutrient-sensing mTOR (mammalian Target of Rapamycin) pathway regulates cellular metabolism, growth functions, and proliferation and is involved in age-related diseases including cancer, type 2 diabetes, neurodegeneration and cardiovascular disease. The inhibition of mTOR by rapamycin, or calorie restriction, has been shown to extend lifespan and delays tumorigenesis in several experimental models suggesting that rapamycin may be used for cancer prevention. This requires continuous long-term treatment making oral formulations the preferred choice of administration route. However, rapamycin by itself has very poor water solubility and low absorption rate. Here we describe pharmacokinetic and biological properties of novel nanoformulated micelles of rapamycin, Rapatar. Micelles of Rapatar were rationally designed to increase water solubility of rapamycin to facilitate oral administration and to enhance its absorption. As a result, bioavailability of Rapatar was significantly increased (up to 12%) compared to unformulated rapamycin, which concentration in the blood following oral administration remained below level of detection. We also demonstrated that the new formulation does not induce toxicity during lifetime administration. Most importantly, Rapatar extended the mean lifespan by 30% and delayed tumor development in highly tumor-prone *p53*$^{-/-}$ mice. Our data demonstrate that water soluble Rapatar micelles represent safe, convenient and efficient form of rapamycin suitable for a long-term treatment and that Rapatar may be considered for tumor prevention.

INTRODUCTION

Rapamycin (or Sirolimus) is a macrolide antibiotic that was first isolated from *Streptomyces hydroscopicus* and was initially utilized as an antifungal agent [1, 2]. Under the name of Rapamune, it is now used as an immunosuppressant to prevent organ rejection after transplantation. Rapamycin inhibits the nutrient-sensing mTOR (mammalian Target of Rapamycin), a conserved protein kinase that controls cellular growth and metabolism. The mTOR signaling pathway is activated by nutrients, growth factors, hormones, cytokines, and cellular energy status. When nutrients and growth factors are abundant, mTOR promotes protein synthesis, ribosome biogenesis, angiogenesis, cell cycle progression and cytoskeleton re-organization (reviewed in [3]-5]).

Recent data demonstrated that rapamycin extends life span in various model organisms including mammals [4-6]. The life-long administration of rapamycin inhibits age-related weight gain, decreases aging rate and increases lifespan of inbred [7] and genetically heterogeneous [6] mice. Previous data has

demonstrated that rapamycin significantly delayed the onset of spontaneous carcinogenesis both in normal (129/Sv [7]) and cancer-prone (HER-2/neu transgenic [8] and $p53^{+/-}$ [9]) mice. Importantly, the anti-cancer effect of rapamycin in $p53^{+/-}$ mice was blunted when treatment started at the age of 5 months [9] suggesting that rapamycin does not directly inhibit tumor growth but rather has an indirect effect.

Since rapamycin exhibits poor water solubility and instability in aqueous solutions, its clinical use through oral administration requires development of special drug design such as complex nanoparticle formulation to facilitate increased bioavailability and efficacy. Therefore, various oral formulations, such as inclusion complexes [10, 11], liposomes [12], nanocrystals [13], and solid dispersion [14] have been developed and tested in pre-clinical and clinical studies. In this study, we tested the biological activity of a novel formulation of rapamycin, Rapatar. This formulation is based on Pluronic block copolymers as nanocarriers, which serves to improve water solubility of the drug, and to enhance various biological responses favorable for therapeutics, such as activity of drug efflux transporters (reviewed in [15]). We show that Rapatar has significantly higher bioavailability after oral administration when compared to unformulated rapamycin. We also show that Rapatar effectively blocks mTOR in mouse tissues. Moreover, life-long administration of Rapatar increases lifespan and delays carcinogenesis in highly tumor-prone $p53^{-/-}$ mice.

RESULTS

Rapatar is efficiently absorbed and systemically distributed and effectively inhibits mTOR *in vivo*

To compare the absolute and relative bioavailability and other pharmacokinetic properties of Rapatar with those of an unformulated rapamycin, we administered both compounds as a single dose to female ICR mice. Rapatar was administered intravenously (IV) or orally (PO) at a dose of 0.4 mg/kg and 4 mg/kg respectively, while rapamycin was administered PO at 4 mg/kg. Blood samples were collected at different times after administration and analyzed for rapamycin by mass spectrometry **(**LC/MS/MS). Pharmacokinetic values of the area under the curve (AUC), the maximum drug concentration (C_{max}), the time of peak concentration (T_{max}), and the absolute bioavailability (F) were calculated from whole blood drug concentration-time data (Fig. 1A). Importantly, following oral administration, rapamycin could only be detected in whole blood samples of mice that received Rapatar whereas its concentration in blood of rapamycin-treated mice was beyond the level of detection. As shown in Table 1, when compared to unformulated rapamycin, Rapatar demonstrated very fast absorption (T_{max} 15 min) and significant increase in AUC value with mean $T_{1/2}$ extending to 6.4 hours. Consequently, a single oral administration of Rapatar resulted in 12% bioavailability, which is comparable with commercially available formulations used in clinical practice (14% when administered orally in combination with cyclosporine A).

Ribosomal protein S6 is a substrate of mTOR, and therefore phospho-ribosomal protein S6 is a marker of mTOR activity [16-19]. To test whether Rapatar inhibits mTOR activity in vivo, we compared levels of phosphorylated S6 (pS6) in livers of wild type C57Bl/6J mice, in which mTOR was suppressed by a period of food deprivation. Rapatar (0.5mg/kg or PBS were given by gavage at a time when animals were allowed access to food. Fig. 1B shows that S6 is highly phosphorylated in livers of control animals indicating mTOR activation in response to food. In contrast, in animals that received Rapatar, S6 phosphorylation was reduced ~10-fold. Thus, Rapatar successfully inhibits mTOR activity in the liver in vivo.

Table 1. Pharmacokinetic parameters of unformulated rapamycin and Rapatar in C57Bl/6J mice. Abbreviations: C_{max} – the peak concentration; T_{max} – time taken to reach peak concentration; AUC – area under the curve; F – absolute bioavailability.

	Units	Rapamycin, IV 0.4mg/kg	Rapatar, PO 4mg/kg
Dose amount	ng	10.4	104
Dosage	ng/kg	400	4000
Cmax	ng/ml	958	656
Tmax	hr	0.04	0.25
AUC	ng-hr/ml	2634.6	3161.5
Half-life	hr	6.4	N/A
F	%	100	12

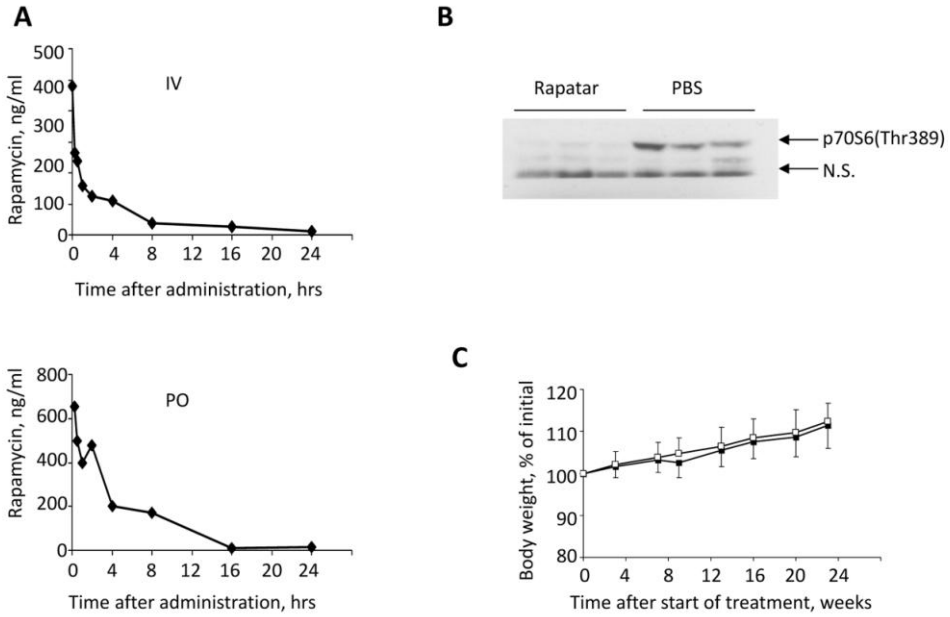

Figure 1. Pharmacokinetic and biological characteristics of Rapatar. (**A**) Rapamycin concentration–time profile in blood after intravenous (IV, top) and oral (PO, bottom) administration of Rapatar to mice (mean values, n = 3). A single dose of Rapatar was administered either IV (0.4mg/kg) or PO (4mg/kg). Blood samples were collected at designated times and analyzed for rapamycin by **LC/MS/MS.** (**B**) Rapatar blocks mTOR activation in vivo. Six C57/Bl/6J mice were food-deprived for 18 hrs. At the end of fasting period animals received either Rapatar (0.5mg/kg) or PBS via gavage and were allowed access to food. One hour later animals were sacrificed, livers were dissected and protein lysates were analyzed for mTOR activity by probing with p70S6(Thr389) antibody. (**C**) No acute or long-term toxicity are associated with PO administration of Rapatar. C57Bl/6J male mice received either Rapatar or PBS starting 8 weeks of age (10 mice/group) for 24 weeks according to the protocol described above. No loss in body weight was detected in experimental group throughout the treatment period. Both experimental and control groups showed similar gain in body weight with age.

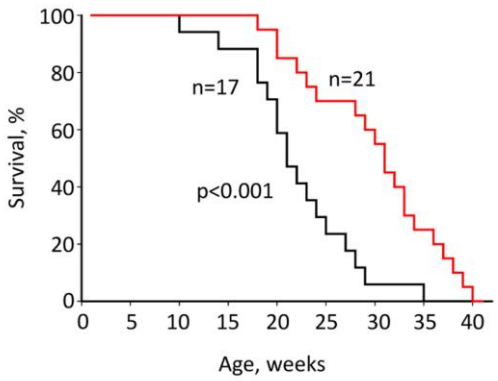

Figure 2. Rapatar increases lifespan in *p53*$^{-/-}$ mice. Mice received Rapatar at 0.5 mg/kg via gavage according to the schedule described in Materials and Methods. Rapatar increased lifespan from 23 to 31 weeks (p<0.001, Mantel-Cox log-rank test).

To test whether life-long administration of Rapatar causes in vivo toxicity, we administered it to wild type C57Bl/6J mice at 0.5 mg/kg via gavage according to protocol described in Materials and Methods section. Rapatar- and PBS-treated animals were monitored for any signs of toxicity by visual inspection and body weight measurements. Mice receiving Rapatar maintained a healthy appearance with physical activities and body weights comparable to the control mice (Fig. 1C).

Rapatar increases lifespan of *p53*$^{-/-}$ mice

Our data showed that Rapatar effectively inhibits mTOR *in vivo*. Suppression of mTOR by rapamycin has been shown to increase lifespan in various model organisms including mice [6-8, 20-25]. To test whether Rapatar can extend lifespan, we administered it to mice with targeted disruption of tumor suppressor p53. *p53*$^{-/-}$

mice are characterized by increased carcinogenesis and reduced lifespan (reviewed in [26]. Twenty $p53^{-/-}$ mice received Rapatar starting 8 weeks of age at a dose of 0.5mg/kg according to the schedule described in Material and Methods. Another group of 17 $p53^{-/-}$ mice received PBS as control. Throughout the experiment, animals were monitored for tumor development by visual inspection and total body weight measurements. Both Rapatar- and PBS-treated $p53^{-/-}$ mice die early in life due to a high rate of spontaneous carcinogenesis, which is characteristic for this mouse model. However, treatment with Rapatar resulted in an overall significant increase in median survival of $p53^{-/-}$ mice from 23 (±10) weeks in the control group to 31 (±1.5) weeks in the experimental group (Fig. 2A).

To gain insight into the potential mechanism of increase in survival of Rapatar-treated animals, we performed a detailed histological analysis of all tissues collected from each individual animal in the course of the experiment (summarized in Table 2). Based on this analysis, 82% of mice in the control group (14 out of 17) developed lymphomas whereas 12% (2 out of 17) developed sarcomas. One animal showed the presence of both sarcoma and lymphoma and one animal developed myeloid leukemia. This spectrum of tumors is characteristic to $p53^{-/-}$ mice and comparable to previous reports [27]. The mice developed these spontaneous neoplasms from 2 to over 8 months of age with an average latency time of 161 days. When compared to the control group, Rapatar-treated mice showed later appearance and delayed progression of spontaneous tumors. They arose from 4.5 to over 9.5 months, with average latency of 261 days; one animal remained tumor-free until the end of the experiment. Interestingly, the incidence of sarcomas in Rapatar-treated mice was increased to 30% compared to 17% in control group (Table 2); however the number of animals used in the experiment was not enough to obtain a statistically significant difference.

Table 2. Summary of histological analysis. Tissues of 17 control and 20 Rapatar-treated $p53^{-/-}$ mice were evaluated for the presence of tumor cells. The type of tumors and the stage of their development were determined as described in Materials and Methods. The incidence of sarcomas in Rapatar-treated $p53^{-/-}$ mice was higher than in control group (30% and 17% respectively); however, due to a relatively small group size, statistical significance was not achieved (p=0.2; Fisher's exact test).

	Initial Lymphoma	Advanced Lymphoma	Sarcoma	Leukemia	Tumor□free
Rapatar	7 (35%)	6 (30%)	6 (30%)	1 (5%)	1 (5%)
PBS	4 (23%)	10 (58%)	3 (17%)	1 (6%)	0

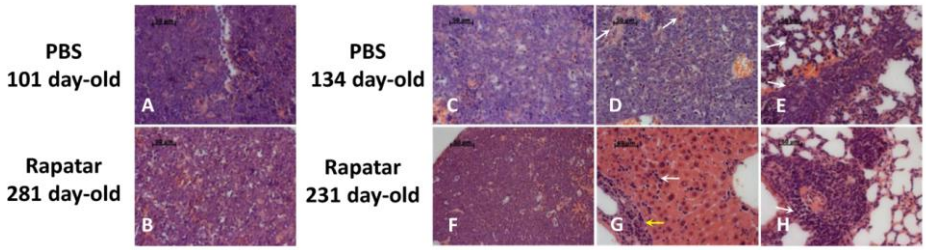

Figure 3. Rapatar delays development of lymphomas in $p53^{-/-}$ mice. (**A)** Representative initial lymphoma developed in control mouse at the age of 101 days. (**B**) Similar appearance of lymphoma in Rapatar-treated mouse at 281 days of age. Both **A** and **B** show monotonous infiltrate of medium-sized neoplastic cells with round nuclei, fine chromatin, indistinct nucleoli, and numerous mitotic figures and apoptotic cells. (**C**) Advanced lymphoma in 134-day old control mouse with metastases in liver (**D**) and lung (**E**). (**D**) Metastasis in liver showing the extensive spread of neoplastic cells effaces the normal structure and only minimal remnants of hepatocytes (marked by arrows). (**E**) Metastasis in the lung showing neoplastic infiltrates in perivascular area and in the alveolar walls (arrows) (**F**) Advanced lymphoma with pathological changes similar to shown in C in the thymus of 241day-old Rapatar-treated animal with metastasis in liver (**G**) and lung (**H**). (**G**) Metastasis in liver showing neoplastic infiltrates in portal tract (yellow arrow) and sinusoids (white arrow). (**H**) Metastasis in the lung showing perivascular neoplastic infiltrate (arrow).

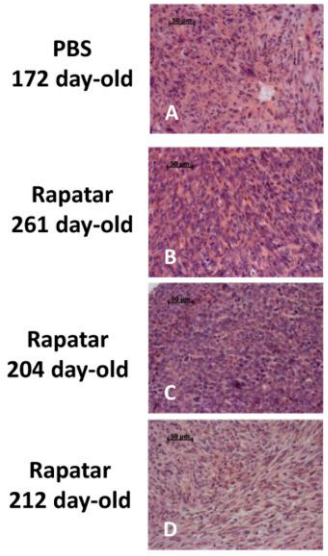

Figure 4. Rapatar delays development of sarcomas in *p53*$^{-/-}$ mice. (**A**) Liver sarcoma in 172-old control mouse. (**B,C**) Sarcoma developed in 261 day- and 204 day-old Rapatar-treated mice. No metastases are detected. D. Sarcoma in 212-day old Rapatar-treated mouse with metastases in the lung.

Since lymphomas represented the major type of tumor in both groups, we performed a detailed pathological evaluation of individual tumors. Based on the severity of pathological changes, the developmental stage, and involvement of non-lymphoid tissues, all lymphomas were graded as initial or advanced. Initial lymphomas mainly involved thymus and were presented macroscopically as enlarged masses. Under the microscope they were seen to be composed of broad sheets of densely packed rather uniform large lymphoblastic cells, with little or sparse cytoplasm that completely obliterated the normal thymus structure and cortical and medullary zones. In most cases, neoplastic lymphoid cells expanded through the thymic capsule and spread through the mediastinal fat, lymph nodes, along peritracheal and periaortal spaces, even infiltrating lungs and pericardium with limited penetration of the myocardium. Such lymphomas with predominantly local involvement were designated provisionally as initial. Tumors were graded as advanced when the rise of the malignancy and aggressiveness of the lymphoma cells resulted in metastases and infiltration into spleen, liver, lung, kidney, mesentery lymph nodes, testis, and bone marrow. Based on this designation, the proportion of the initial lymphomas in Rapatar-treated group was larger compared to controls (35% and 23% for experimental and control groups respectively) suggesting that Rapatar slows down tumorigenesis. Consistently, the proportion of the advanced disseminated lymphomas, spreading to other organs in Rapatar-treated group was smaller than in control (30% and 58% respectively). Although histopathological appearance of lymphomas and sarcomas were very similar in control and experimental groups, Rapatar-treated mice develop tumors significantly later in life (Fig. 3 and 4). Based on these data we concluded that Rapatar increased lifespan of *p53*$^{-/-}$ mice by delaying tumorigenesis.

DISCUSSION

The mTOR signaling pathway is a key coordinator of cell growth and cell proliferation in response to a variety of environmental conditions. Its deregulation has been implicated in many pathological conditions, including those that are associated with aging, such as cancer, type 2 diabetes, neurological and cardiovascular disorders (reviewed in [28, 29]). Furthermore, the activation of the mTOR pathway is the most universal alteration in cancer [30]. Several analogs of rapamycin (rapalogs) have been approved for cancer therapy [31-35] and numerous clinical trials are underway. However, as anti-cancer drugs rapamycin and other rapalogs showed modest efficacy. There are several reasons that can explain relatively low therapeutic effect. First, rapamycin itself is not cytotoxic. Additionally, mTOR inhibition activates several feedback loops that drive mitogenic signaling (reviewed in [28, 36]). Therefore, it is still not quite clear whether rapamycin exhibits direct antitumor activity or whether it acts in a more indirect systemic way. Our previous data [9] and data presented here show that rapamycin delays carcinogenesis in tumor-prone *p53*$^{+/-}$ and *p53*$^{-/-}$ mice, most likely by slowing down the process of aging. If this is the case, than rapamycin can be considered as a tumor-preventive agent (i.e. administration is required before tumor initiation). This necessitates the development of efficacious nontoxic rapamycin-formulations that could be taken orally for extended periods of time. Here we show that oral administration of Rapatar results in high systemic bioavailability and does not induce toxicity during life-long administration. Importantly, biological effects of Rapatar were prominent at low doses (0.5 mg/kg) and intermittent schedules. Taken together, our data suggest that Rapatar is a promising candidate for clinical use as an effective cancer prevention drug.

MATERIALS AND METHODS

Materials. Rapamycin was purchased from LC Laboratories (Woburn, MA). Polymeric formulation of

rapamycin (Rapatar) was developed by Tartis Aging, Inc. using Pluronic block co-polymers [15] according to the following protocol. One gram of rapamycin was dissolved in 25 ml of ethanol. The resulting solution was mixed with 5 grams of Pluronic L-92 (BASF) and 2 grams of citric acid dissolved in 200 ml of 20% Pluronic F-127 (BASF) solution in ethanol and water mixture (97:3 v:v). The solution was then incubated at 20-25ºC for 30 minutes with constant stirring. The ethanol was removed using Speedvac and the formulation was further dried using high vacuum.

Animals. ICR female mice were obtained from Charles River. C57Bl/6J mice were obtained from Jackson Laboratory. p53-/- mice on C57Bl/6J background originally obtained from Jackson Laboratory, were housed and bred at the Department of Experimental Animal Resources of Roswell Park Cancer Institute. For pharmacokinetic analysis, three groups of 8 weeks old ICR female mice received a single dose of either Rapatar (2 groups) or rapamycin. Rapatar was administered via gavage at 4mg/kg in 0.5% methyl cellulose or IV at 0.4mg/kg in PBS. Rapamycin was administered via gavage at 4mg/kg in 0.5% methyl cellulose.

For estimating potential long-term toxic effects of Rapatar, two groups of C57BL/6J mice received the drug at a dose of 0.5 mg/kg via gavage once a day for 5 consecutive days, followed by 9-day interval without treatment. Mice were maintained on this treatment schedule for 24 weeks and were weighed weekly. Control mice receive PBS according to the same schedule.

For longevity studies, 38 *p53*$^{-/-}$ male mice were randomly divided into two groups. Twenty one experimental animals received 0.5 mg/kg Rapatar and 17 animals received PBS according to the above described schedule. Treatment started at 8 weeks of age and continued until tumor appearance was visually observed or dramatic loss of weight, indicative of tumor appearance, was detected. At this point, mice were sacrificed and examined for gross pathological changes. Tumors, heart, kidney, liver, lungs, thymus and spleen were collected for histological evaluation. All procedures were approved by the Institutional Animal Care and Use Committee of Roswell Park Cancer Institute.

Pharmacokinetic study. Whole blood was collected into EDTA-blood tubes 0.5, 1, 2, 4, 8, 16 and 24 hours after administration of either Rapatar or unformulated rapamycin. Tubes were inverted a few times, and stored on ice in dark container during the experiment. At the end of the experiment, all samples were placed for storage at -70^{0}C in a light-protected container. Frozen blood samples were submitted to the Rocky Mountain Instrumental Laboratory (Fort Collins, Co) for LC/MS/MS analysis of rapamycin. Pharmacokinetic analysis was performed using data from individual mice for which the mean and standard error of the mean (SEM) were calculated for each group using PK Solutions software (Version 2.0).

Western blot analysis**.** In order to maximize and be able to detect p70S6 phosphorylation [37, 38], six C57Bl/6J mice were food-deprived for 18 hrs. At the end of the fasting period, animals received either Rapatar (0.5 mg/kg) or PBS via gavage and 15 minutes later were allowed access to food. One hour later animals were sacrificed; livers were dissected, lysed in RIPA buffer and loaded on a 8% SDS-PAGE gel. After separation and transfer to a PVDF membrane, protein lysates were analyzed for mTOR activation by probing with an antibody against phospho-*p70 S6* Kinase (*Thr389*) (1:1000; Cell Signaling) and Actin (1:10000 Cell Signaling). After incubation with HRP conjugated secondary antibodies (Santa Cruz Biotechnologies), transferred proteins were visualized with the ECL detection kit (Jackson Research Laboratories).

Histopathology. The mice were visually inspected for tumor development and weighed weekly. Animals showing deteriorating clinical status manifested by constant weight loss or visual tumor appearance were sacrificed and evaluated for gross pathological changes by complete necropsy. For histological evaluation, all tissues were fixed in 10% neutral formalin for 24 hours, and then transferred to 70% ethanol. Samples were embedded in paraffin, sectioned and stained with hema-toxylin and eosin. Histopathological examination was performed on tumors, gross lesions and target tissues using Zeiss AxioImager A1 with Axiocam MRc digital camera. The guidelines of Bethesda classification was used in determining the diagnosis [39].

Statistical Analyses. Differences in survival and tumor incidence were evaluated by the Mantel-Cox log-rank test.

ACKNOWLEDGEMENTS

We thank Mary Spengler for critical reading of the manuscript. This work was supported in part by NIH grant GM095874 and by Roswell Park Alliance Foundation (to M.P.A.) and Tartis, Inc. (to A.V.G.)

Conflict of Interest Statement

The authors of this manuscript have no conflict of interests to declare.

REFERENCES

1. Vézina C, Kudelski A and Sehgal S. Rapamycin (AY-22,989), a new antifungal antibiotic I. Taxonomy of the producing streptomycete and isolation of the active principle. Journal of antibiotics. 1975; 28:721-726.

2. Sehgal SN, Baker H and Vezina C. Rapamycin (AY-22,989), a new antifungal antibiotic. II. Fermentation, isolation and characterization. Journal of antibiotics. 1975; 28:727–732.

3. Wullschleger S, Loewith R and Hall MN. TOR Signaling in Growth and Metabolism. Cell. 2006; 124:471-484.

4. Kaeberlein M, Powers RW, 3rd, Steffen KK, Westman EA, Hu D, Dang N, Kerr EO, Kirkland KT, Fields S and Kennedy BK. Regulation of yeast replicative life span by TOR and Sch9 in response to nutrients. Science. 2005; 310:1193-1196.

5. Wilkinson JE, Burmeister L, Brooks SV, Chan CC, Friedline S, Harrison DE, Hejtmancik JF, Nadon N, Strong R, Wood LK, Woodward MA and Miller RA. Rapamycin slows aging in mice. Aging Cell.

6. Harrison DE, Strong R, Sharp ZD, Nelson JF, Astle CM, Flurkey K, Nadon NL, Wilkinson JE, Frenkel K, Carter CS, Pahor M, Javors MA, Fernandez E, et al. Rapamycin fed late in life extends lifespan in genetically heterogeneous mice. Nature. 2009; 460:392-395.

7. Spong A and Bartke A. Rapamycin slows aging in mice. Cell Cycle. 2012; 11:845.

8. Anisimov VN, Zabezhinski MA, Popovich IG, Piskunova TS, Semenchenko AV, Tyndyk ML, Yurova MN, Antoch MP and Blagosklonny MV. Rapamycin extends maximal lifespan in cancer-prone mice. Am J Pathol. 2010; 176:2092-2097.

9. Komarova E, Antoch M, Novototskaya L, Chernova O, Paszkiewicz G, Leontieva O, Blagosklonny M and Gudkov A. Rapamycin extends lifespan and delays tumorigenesis in heterozygous p53+/- mice. Aging (Albany NY). 2012.

10. Baspinar Y, Bertelmann E, Pleyer U, Buech G, Siebenbrodt I and Borchert HH. Corneal permeation studies of everolimus microemulsion. J Ocul Pharmacol Ther. 2008; 24:399-402.

11. Buech G, Bertelmann E, Pleyer U, Siebenbrodt I and Borchert HH. Formulation of sirolimus eye drops and corneal permeation studies. J Ocul Pharmacol Ther. 2007; 23:292-303.

12. Alemdar AY, Sadi D, McAlister V and Mendez I. Intracerebral co-transplantation of liposomal tacrolimus improves xenograft survival and reduces graft rejection in the hemiparkinsonian rat. Neuroscience. 2007; 146:213-224.

13. Junghanns JU and Muller RH. Nanocrystal technology, drug delivery and clinical applications. International journal of nanomedicine. 2008; 3:295-309.

14. Kim MS, Kim JS, Park HJ, Cho WK, Cha KH and Hwang SJ. Enhanced bioavailability of sirolimus via preparation of solid dispersion nanoparticles using a supercritical antisolvent process. International journal of nanomedicine. 2011; 6:2997-3009.

15. Batrakova EV and Kabanov AV. Pluronic block copolymers: evolution of drug delivery concept from inert nanocarriers to biological response modifiers. J Control Release. 2008; 130:98-106.

16. Brown EJ, Beal PA, Keith CT, Chen J, Bum Shin T and Schreiber SL. Control of p70 S6 kinase by kinase activity of FRAP in vivo. Nature. 1995; 377:441-446.

17. Brunn GJ, Fadden P, Haystead TAJ and Lawrence JC. The Mammalian Target of Rapamycin Phosphorylates Sites Having a (Ser/Thr)-Pro Motif and Is Activated by Antibodies to a Region near Its COOH Terminus. Journal of Biological Chemistry. 1997; 272:32547-32550.

18. Brunn GJ, Hudson CC, SekuliÄ‡ A, Williams JM, Hosoi H, Houghton PJ, Lawrence JC and Abraham RT. Phosphorylation of the Translational Repressor PHAS-I by the Mammalian Target of Rapamycin. Science. 1997; 277:99-101.

19. Burnett PE, Barrow RK, Cohen NA, Snyder SH and Sabatini DM. RAFT1 phosphorylation of the translational regulators p70 S6 kinase and 4E-BP1. Proceedings of the National Academy of Sciences. 1998; 95:1432-1437.

20. Miller RA, Harrison DE, Astle CM, Baur JA, Boyd AR, de Cabo R, Fernandez E, Flurkey K, Javors MA, Nelson JF, Orihuela CJ, Pletcher S, Sharp ZD, et al. Rapamycin, but not resveratrol or simvastatin, extends life span of genetically heterogeneous mice. J Gerontol A Biol Sci Med Sci. 2011; 66:191-201.

21. Moskalev AA and Shaposhnikov MV. Pharmacological inhibition of phosphoinositide 3 and TOR kinases improves survival of Drosophila melanogaster. Rejuvenation Res. 13:246-247.

22. Bjedov I, Toivonen JM, Kerr F, Slack C, Jacobson J, Foley A and Partridge L. Mechanisms of life span extension by rapamycin in the fruit fly Drosophila melanogaster. Cell Metab. 11:35-46.

23. Kapahi P, Chen D, Rogers AN, Katewa SD, Li PW, Thomas EL and Kockel L. With TOR, less is more: a key role for the conserved nutrient-sensing TOR pathway in aging. Cell Metab. 2010; 11:453-465.

24. Khanna A and Kapahi P. Rapamycin: killing two birds with one stone. Aging (Albany NY). 2011; 3:1043-1044.

25. Ramos FJ, Chen SC, Garelick MG, Dai DF, Liao CY, Schreiber KH, Mackay VL, An EH, Strong R, Ladiges WC, Rabinovitch PS, Kaeberlein M and Kennedy BK. Rapamycin Reverses Elevated mTORC1 Signaling in Lamin A/C-Deficient Mice, Rescues Cardiac and Skeletal Muscle Function, and Extends Survival. Sci Transl Med. 2012; 4:144ra103.

26. Donehower LA. Using mice to examine p53 functions in cancer, aging, and longevity. Cold Spring Harb Perspect Biol. 2009; 1:a001081.

27. Donehower LA, Harvey M, Slagle BL, McArthur MJ, Montgomery CA, Jr., Butel JS and Bradley A. Mice deficient for p53 are developmentally normal but susceptible to spontaneous tumours. Nature. 1992; 356:215-221.

28. Laplante M and Sabatini DM. mTOR signaling in growth control and disease. Cell. 2012; 149:274-293.

29. Dazert E and Hall MN. mTOR signaling in disease. Curr Opin Cell Biol. 2011; 23:744-755.

30. Guertin DA and Sabatini DM. Defining the role of mTOR in cancer. Cancer cell. 2007; 12:9-22.

31. Hudes G, Carducci M, Tomczak P, Dutcher J, Figlin R, Kapoor A, Staroslawska E, Sosman J, McDermott D, Bodrogi I, Kovacevic Z, Lesovoy V, Schmidt-Wolf IG, et al. Temsirolimus, interferon alfa, or both for advanced renal-cell carcinoma. The New England journal of medicine. 2007; 356:2271-2281.

32. Motzer RJ, Hudes GR, Curti BD, McDermott DF, Escudier BJ, Negrier S, Duclos B, Moore L, O'Toole T, Boni JP and Dutcher JP. Phase I/II trial of temsirolimus combined with interferon alfa for advanced renal cell carcinoma. J Clin Oncol. 2007; 25:3958-3964.

33. Wander SA, Hennessy BT and Slingerland JM. Next-generation mTOR inhibitors in clinical oncology: how pathway complexity informs therapeutic strategy. The Journal of clinical investigation. 121:1231-1241.

34. Chappell WH, Steelman LS, Long JM, Kempf RC, Abrams SL, Franklin RA, Basecke J, Stivala F, Donia M, Fagone P, Malaponte G, Mazzarino MC, Nicoletti F, et al. Ras/Raf/MEK/ERK and PI3K/PTEN/Akt/mTOR inhibitors: rationale and importance to inhibiting these pathways in human health. Oncotarget. 2011; 2:135-164.

35. Markman B, Dienstmann R and Tabernero J. Targeting the PI3K/Akt/mTOR pathway--beyond rapalogs. Oncotarget. 2010; 1:530-543.

36. Garrett JT, Chakrabarty A and Arteaga CL. Will PI3K pathway inhibitors be effective as single agents in patients with cancer? Oncotarget. 2011; 2:1314-1321.

37. Anand P and Gruppuso PA. The Regulation of Hepatic Protein Synthesis during Fasting in the Rat. Journal of Biological Chemistry. 2005; 280:16427-16436.

38. Demirkan G, Yu K, Boylan JM, Salomon AR and Gruppuso PA. Phosphoproteomic Profiling of <italic>In Vivo</italic> Signaling in Liver by the Mammalian Target of Rapamycin Complex 1 (mTORC1). PLoS ONE. 6:e21729.

39. Morse HC, 3rd, Anver MR, Fredrickson TN, Haines DC, Harris AW, Harris NL, Jaffe ES, Kogan SC, MacLennan IC, Pattengale PK and Ward JM. Bethesda proposals for classification of lymphoid neoplasms in mice. Blood. 2002; 100:246-258.

Research perspective

Tumor suppression by p53 without apoptosis and senescence: conundrum or rapalog-like gerosuppression?

Mikhail V. Blagosklonny

Department of Cell Stress Biology, Roswell Park Cancer Institute, Buffalo, NY 14263, USA

Key words: *tumor suppressors, aging, apoptosis, geroconversion*
Received: *7/15/12; Accepted: 7/30/12; Published: 7/31/12*
Correspondence to: *Mikhail V. Blagosklonny, MD/PhD;* ***E-mail:*** *blagosklonny@oncotarget.com*

Copyright: *© Blagosklonny . This is an open-access article distributed under the terms of the Creative Commons Attribution License, which permits unrestricted use, distribution, and reproduction in any medium, provided the original author and source are credited*

Abstract: I discuss a very obscure activity of p53, namely suppression of senescence (gerosuppression), which is also manifested as anti-hypertrophic, anti-hypermetabolic, anti-inflammatory and anti-secretory effects of p53. But can gerossuppression suppress tumors?

INTRODUCTION

Wt p53 can induce apoptosis, cell cycle arrest and senescence, which are sufficient to explain tumor suppression by p53 [1]. A recent paper in *Cell* described that these activities are dispensable for tumor suppression [2]. Mutant p53 ($p53^{3KR}$) that cannot cause arrest, senescence and apoptosis still suppressed tumors in mice [2, 3]. Why do then wt p53 induce apoptosis, cell cycle arrest and senescence? Before entertaining this intriguing question, I will focus on suppression of senescence (gerosuppression) by p53, overlapping with its anti-hypertrophic, anti-hypermetabolic, anti-inflammatory and anti-secretory effects.

P53 suppresses the conversion from arrest to senescence (geroconversion)

How can p53 suppress senescence, if it also can cause senescence? As recently suggested, induction of senescence is not an independent activity of p53 but a consequence of cell-cycle arrest [4-8]. This predicts that any mutant p53 that cannot cause arrest will not cause senescence too. In agreement, $p53^{3KR}$ did not cause senescence [2]. This is not trivial. To create $p53^{3KR}$, wt p53 was altered to abolish apoptosis and cell-cycle arrest only [2]. Li et al did not modify p53 to abolish senescence as an independent activity. It was not needed, simply because p53 does not induce senescence as an independent effect. (Note: Seemingly in contrast, it was reported that mutant p53, which cannot induce arrest in response to DNA damage, can cause senescence [9]. Although this mutant p53 did not cause instant arrest, it still arrested proliferation later and then senescence developed [9]. So there is no exception). p53 cannot induce senescence without inducing arrest. But p53 can induce quiescence, a reversible condition characterized by low protein synthesis and metabolism (see detailed definitions in ref. [7, 8]). It was assumed that when p53 causes quiescence, it simply fails to induce senescence. But another possibility is that in such cases p53 suppresses the conversion from cell-cycle arrest to senescence (geroconversion). How can that be tested? In some cell lines, induction of ectopic p21 causes irreversible senescence, whereas induction of p53 causes quiescence [4]. Does p53 suppresses a senescent program? This question can be answered by simultaneously inducing both p53 and ectopic p21. When both p21 and p53 were induced, then cells become quiescent not senescent [4]. p53 was dominant, actively suppressing senescence caused by p21... or by something else? In fact, p21 merely causes cell cycle arrest and does not inhibit mitogen-activated, nutrient-sensing and growth-promoting pathways such as Target of Rapamycin (mTOR) [4]. During several days, these pathways (gerogenic pathways, for brevity) convert p21-induced arrest into senescence. Rapamycin can decelerate geroconversion [10-13]. Also, p53 can inhibit the mTOR pathway [4-6, 14-17]. In some conditions, p53 can suppress senescence during arrest [4-6]. Wt p53 induces arrest and then if it fails to suppress senescence, then senescence prevails. Rather than p53, gerogenic

pathways drive senescence during cell-cycle arrest [18].

In summary, wt p53 seems to have three independent effects: apoptosis, cell-cycle arrest and gerosuppression. By inducing arrest, wt p53 primes cells for senescence, unless p53 is able or "willing" to suppress geroconversion. At high levels, gerosuppression by p53 is limited by apoptosis [6]. This predicts that $p53^{3KR}$ would potently suppress senescence because gero-suppression by $p53^{3KR}$ will not be limited by apoptosis.

Hyper-metabolic senescent phenotype

Senescent cells are hyper-functional: hypertrophic, hypermetabolic, hyper-secretory and hyper-inflammatory [8]. Also, senescent cells may accumulate lipids, becoming not only large but also "fat" (Figure1). Induction of p53 decreased both cellular hypertrophy and fat accumulation (Figure 1). This is in line with numerous metabolic effects of p53 including inhibition of glycolysis and stimulation of fatty acids oxidation [19-32]. Importantly, $p53^{3KR}$ retained the ability to inhibit glycolysis and reactive oxygen species (ROS) [2]. (Noteworthy, ROS and mTOR co-activate each other [33] and N-Acetyl Cysteine (NAC), which decreases ROS, also inhibits mTOR [34]). Also, p53 decreases hyper-secretory phenotype also known as SASP [35] and suppresses a pro-inflammatory phenotype [36, 37]. How might gerosuppression contribute to tumor suppression? There are several overlapping explanations, from different points of view of the same process.

Gerogenic conversion and oncogenic transformation

In proliferating epithelial cells, pro-gerogenic conversion may contribute to carcinogenesis directly. The PI3K/mTOR pathway is universally activated in cancer [38-49]. p53 can inhibit the PI3K/mTOR pathway [4-6, 14-17, 50]. Like p53, many other tumor suppressors such as PTEN, AMPK, TSC2, LKB1, NF1 inhibit the PI3K/mTOR pathway [51].

Geroconversion of stromal cells creates carcinogenic microenvironment

First, senescence creates a selective disadvantage for normal cells, thus selecting for cancer [52-54]. Also, senescent stromal cells secrete factors that favors pre-cancer and cancer growth [37, 54-62]. Third, the senescent stroma is hyper-metabolic and thus promotes cancer by fueling cancer growth [59, 60, 63-71]. In a model of accelerated host aging, mTOR activity was increased in normal tissues [72]. This pro-senescent microenvironment accelerated growth of implanted tumors. The tumor-promoting effects of pro-senescent microenvironment were abrogated by rapamycin [72].

Cancer is an age-related disease

The incidence of cancer is increased exponentially in aging mammals. Manipulations that slow down aging delay cancer [73]. For example, calorie restriction delays cancer [74-76] including cancer in p53-deficient mice [77, 78]. Rapamycin, which decelerates aging, also postpones cancer in animals [73, 79-81] and in patients after renal transplantation [82-86].

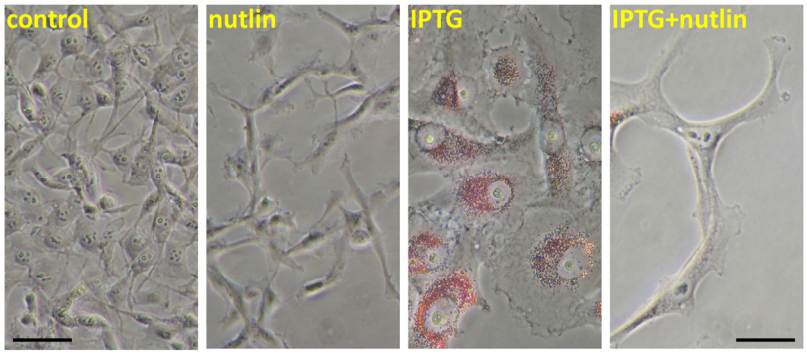

Figure 1. Nutlin-3a decreased lipid accumulation during IPTG-induced senescence. HT-p21 cells were treated with IPTG, nutlin-3a and IPTG+nutlin-3a (as indicated) for 3 days as described previously [4-6] and cells were stained with "oil red O" for lipids. In HT-p21 cells, IPTG induces ectopic p21 and senescence. As described previously, nutlin-3a induces endogenous p53 and suppresses IPTG-induced senescence [4-6].

Is aging accelerated in p53-deficient mice?

Inactivation of tumor suppressors accelerates both aging and cancer [87]. It was thought that p53 is an exception. Yet, given that p53 can suppress geroconversion, it may not be the exception after all. A complex role of p53 in cellular senescence and organismal aging was discussed [88-91]. Mice with increased, but normally regulated, p53 lives longer [92]. p53 knockout mice have both accelerated carcinogenesis and decreased longevity [93-98]. p53-/- mice have a pro-inflammatory phenotype characteristic of accelerated aging [36,37]. Also, atherosclerosis is accelerated in p53-/- animals [99-102]. While loss of p53 by itself makes cells prone to become tumorigenic, an increased rate of organismal aging in the absence of p53 may further accelerate carcinogenesis.

Rapalogs and p53

Rapamycin (sirolimus) and other rapalogs (everolimus and temsirolimus) are pharmacological tumor suppressors. Noteworthy, like p53, rapamycin decreases glycolysis [103] and lactate production [34] and stimulates oxidation of fatty acids [104, 105]. Furthermore, rapamycin slows cellular proliferation, and so, not surprisingly, $p53^{3KR}$ inhibits clonogenicity too [2]. Yet, p53 affects metabolism and aging not only via mTOR but also via direct transactivation of metabolic enzymes, rendering it a more potent tumor suppressor.

Puzzles remain

Still, even if gerosuppression and anti-hypermetabolic effects can in part explain tumor suppression, puzzles remain. Why does wt p53 cause "unneeded" apoptosis and "instant" (p21-dependent) arrest? Why is p53 needed at all? In the wild, most mice die from external/accidental causes and only a few would live long enough to die from cancer, regardless of p53 status. In the wild, starvation (natural calorie restriction) would delay cancer further. Yet, p53 is also needed very early in life, or technically speaking, even before life has begun, because p53 plays role in fertility and reproduction [106-113]. And is tumor suppression a late life function?

Alternatively, tumor suppression is a primary function of p53. And each of the three activities (apoptosis, arrest, gerosuppression) is partially sufficient for cancer prevention. In their combination, these activities are the most effective tumor suppressor. And each activity may be partially dispensable in some mice strains and in some conditions. For example, the gerosuppressive activity of p53 may be preferentially important in peculiar strains of laboratory mice, or mice fed *ad libitum*, which constantly activates mTOR and accelerates aging. In fact, calorie restriction, which deactivates mTOR and decelerates aging, partially substitutes for the loss of p53 in mice.

ACKNOWLEDGEMENTS

I thank Wei Gu, Arnold Levine and Bert Vogelstein for critical reading of the manuscript and excellent suggestions.

CONFLICT OF INTERESTS STATEMENT

The author of this manuscript has no conflict of interest to declare.

REFERENCES

1. Vogelstein B, Lane DP, Levine AJ. Surfing the p53 network. Nature. 2000; 408: 307-310.

2. Li T, Kon N, Jiang L, Tan M, Ludwig T, Zhao Y, Baer R, Gu W. Tumor Suppression in the Absence of p53-Mediated Cell-Cycle Arrest, Apoptosis, and Senescence. Cell. 2012; 149: 1269-1283.

3. Hock AK, Vousden KH. Tumor Suppression by p53: Fall of the Triumvirate? Cell. 2012; 149: 1183-1185.

4. Demidenko ZN, Korotchkina LG, Gudkov AV, Blagosklonny MV. Paradoxical suppression of cellular senescence by p53. Proc Natl Acad Sci U S A. 2010; 107: 9660-9664.

5. Korotchkina LG, Leontieva OV, Bukreeva EI, Demidenko ZN, Gudkov AV, Blagosklonny MV. The choice between p53-induced senescence and quiescence is determined in part by the mTOR pathway. Aging. 2010; 2: 344-352.

6. Leontieva O, Gudkov A, Blagosklonny M. Weak p53 permits senescence during cell cycle arrest. Cell Cycle. 2010; 9: 4323-4327.

7. Blagosklonny MV. Cell cycle arrest is not senescence. Aging. 2011; 3: 94-101.

8. Blagosklonny MV. Cell cycle arrest is not yet senescence, which is not just cell cycle arrest: terminology for TOR-driven aging. Aging. 2012; 4: 159-165.

9. Brady CA, Jiang D, Mello SS, Johnson TM, Jarvis LA, Kozak MM, Kenzelmann Broz D, Basak S, Park EJ, McLaughlin ME, Karnezis AN, Attardi LD. Distinct p53 transcriptional programs dictate acute DNA-damage responses and tumor suppression. Cell. 2011; 145: 571-583.

10. Demidenko ZN, Blagosklonny MV. Growth stimulation leads to cellular senescence when the cell cycle is blocked. Cell Cycle. 2008; 7: 3355-3361.

11. Demidenko ZN, Zubova SG, Bukreeva EI, Pospelov VA, Pospelova TV, Blagosklonny MV. Rapamycin decelerates cellular senescence. Cell Cycle. 2009; 8: 1888-1895.

12. Demidenko ZN, Blagosklonny MV. Quantifying pharmacologic suppression of cellular senescence: prevention of cellular hypertrophy versus preservation of proliferative potential. Aging. 2009; 1: 1008-1016.

13. Pospelova TV, Demidenko ZN, Bukreeva EI, Pospelov VA, Gudkov AV, Blagosklonny MV. Pseudo-DNA damage response in senescent cells. Cell Cycle. 2009; 8: 4112-4118.

14. Feng Z, Levine AJ. The regulation of energy metabolism and the IGF-1/mTOR pathways by the p53 protein. Trends Cell Biol. 2010; 20: 427-434.

15. Feng Z, Hu W, de Stanchina E, Teresky AK, Jin S, Lowe S, Levine AJ. The regulation of AMPK beta1, TSC2, and PTEN expression by p53: stress, cell and tissue specificity, and the role of these gene products in modulating the IGF-1-AKT-mTOR pathways. Cancer Res. 2007; 67: 3043-3053.

16. Levine AJ, Feng Z, Mak TW, You H, Jin S. Coordination and communication between the p53 and IGF-1-AKT-TOR signal transduction pathways. Genes Dev. 2006; 20: 267-275.

17. Budanov AV, Karin M. p53 target genes sestrin1 and sestrin2 connect genotoxic stress and mTOR signaling. Cell. 2008; 134: 451-460.

18. Leontieva OV, Blagosklonny MV. DNA damaging agents and p53 do not cause senescence in quiescent cells, while consecutive re-activation of mTOR is associated with conversion to senescence. Aging. 2010; 2: 924-935.

19. Bensaad K, Tsuruta A, Selak MA, Vidal MN, Nakano K, Bartrons R, Gottlieb E, Vousden KH. TIGAR, a p53-inducible regulator of glycolysis and apoptosis. Cell. 2006; 126: 107-120.

20. Bensaad K, Vousden KH. p53: new roles in metabolism. Trends Cell Biol. 2007; 17: 286-291.

21. Kawauchi K, Araki K, Tobiume K, Tanaka N. p53 regulates glucose metabolism through an IKK-NF-kappaB pathway and inhibits cell transformation. Nat Cell Biol. 2008; 10: 611-618.

22. Vousden KH, Ryan KM. p53 and metabolism. Nat Rev Cancer. 2009; 9: 691-700.

23. Vigneron A, Vousden KH. p53, ROS and senescence in the control of aging. Aging. 2010; 2: 471-474.

24. Cheung EC, Vousden KH. The role of p53 in glucose metabolism. Curr Opin Cell Biol. 2010; 22: 186-191.

25. Suzuki S, Tanaka T, Poyurovsky MV, Nagano H, Mayama T, Ohkubo S, Lokshin M, Hosokawa H, Nakayama T, Suzuki Y, Sugano S, Sato E, Nagao T, Yokote K, Tatsuno I, Prives C. Phosphate-activated glutaminase (GLS2), a p53-inducible regulator of glutamine metabolism and reactive oxygen species. Proc Natl Acad Sci U S A. 2010; 107: 7461-7466.

26. Jiang P, Du W, Wang X, Mancuso A, Gao X, Wu M, Yang X. p53 regulates biosynthesis through direct inactivation of glucose-6-phosphate dehydrogenase. Nat Cell Biol. 2011; 13: 310-316.

27. Zhu Y, Prives C. p53 and Metabolism: The GAMT Connection. Mol Cell. 2009; 36: 351-352.

28. Bensaad K, Cheung EC, Vousden KH. Modulation of intracellular ROS levels by TIGAR controls autophagy. Embo J. 2009; 28: 3015-3026.

29. Hu W, Zhang C, Wu R, Sun Y, Levine A, Feng Z. Glutaminase 2, a novel p53 target gene regulating energy metabolism and antioxidant function. Proc Natl Acad Sci U S A. 2010; 107: 7455-7460.

30. Ide T, Brown-Endres L, Chu K, Ongusaha PP, Ohtsuka T, El-Deiry WS, Aaronson SA, Lee SW. GAMT, a p53-inducible modulator of apoptosis, is critical for the adaptive response to nutrient stress. Mol Cell. 2009; 36: 379-392.

31. Park JY, Wang PY, Matsumoto T, Sung HJ, Ma W, Choi JW, Anderson SA, Leary SC, Balaban RS, Kang JG, Hwang PM. p53 improves aerobic exercise capacity and augments skeletal muscle mitochondrial DNA content. Circ Res. 2009; 105: 705-712.

32. Madan E, Gogna R, Bhatt M, Pati U, Kuppusamy P, Mahdi AA. Regulation of glucose metabolism by p53: emerging new roles for the tumor suppressor. Oncotarget. 2011; 2: 948-957.

33. Blagosklonny MV. Aging: ROS or TOR. Cell Cycle. 2008; 7: 3344-3354.

34. Leontieva OV, Blagosklonny MV. Yeast-like chronological senescence in mammalian cells: phenomenon, mechanism and pharmacological suppression. Aging. 2011; 3: 1078-1091.

35. CoppŽ JP, Patil CK, Rodier F, Sun Y, Mu–oz DP, Goldstein J, Nelson PS, Desprez PY, Campisi J. Senescence-associated secretory phenotypes reveal cell-nonautonomous functions of oncogenic RAS and the p53 tumor suppressor. PLoS Biol. 2008; 6: 2853-2868.

36. Komarova EA, Krivokrysenko V, Wang K, Neznanov N, Chernov MV, Komarov PG, Brennan ML, Golovkina TV, Rokhlin OW, Kuprash DV, Nedospasov SA, Hazen SL, Feinstein E, Gudkov AV. p53 is a suppressor of inflammatory response in mice. Faseb J. 2005; 19: 1030-1032.

37. Gudkov AV, Gurova KV, Komarova EA. Inflammation and p53: A Tale of Two Stresses. Genes Cancer. 2011; 2: 503-516.

38. Vogelstein B, Kinzler KW. Cancer genes and the pathways they control. Nat Med. 2004; 10: 789-799.

39. Shaw RJ, Cantley LC. Ras, PI(3)K and mTOR signalling controls tumour cell growth. Nature. 2006; 441: 424-430.

40. Janes MR, Fruman DA. Targeting TOR dependence in cancer. Oncotarget. 2010; 1: 69-76.

41. Guertin DA, Sabatini DM. Defining the role of mTOR in cancer. Cancer Cell. 2007; 12: 9-22.

42. Schmidt-Kittler O, Zhu J, Yang J, Liu G, Hendricks W, Lengauer C, Gabelli SB, Kinzler KW, Vogelstein B, Huso DL, Zhou S. PI3Kalpha inhibitors that inhibit metastasis. Oncotarget. 2010; 1: 339-348.

43. Martelli AM, Evangelisti C, Chiarini F, McCubrey JA. The phosphatidylinositol 3-kinase/Akt/mTOR signaling network as a therapeutic target in acute myelogenous leukemia patients. Oncotarget. 2010; 1: 89-103.

44. Zawel L. P3Kalpha: a driver of tumor metastasis? Oncotarget. 2010; 1: 315-316.

45. Zhang Z, Stiegler AL, Boggon TJ, Kobayashi S, Halmos B. EGFR-mutated lung cancer: a paradigm of molecular oncology. Oncotarget. 2010; 1: 497-514.

46. Shahbazian D, Parsyan A, Petroulakis E, Hershey J, Sonenberg N. eIF4B controls survival and proliferation and is regulated by proto-oncogenic signaling pathways. Cell Cycle. 2010; 9: 4106-4109.

47. Zhao L, Vogt PK. Hot-spot mutations in p110alpha of phosphatidylinositol 3-kinase (pI3K): differential interactions with the regulatory subunit p85 and with RAS. Cell Cycle. 2010; 9: 596-600.

48. Bhatia B, Nahle Z, Kenney AM. Double trouble: when sonic hedgehog signaling meets TSC inactivation. Cell Cycle. 2010; 9: 456-459.

49. Fujishita T, Aoki M, Taketo MM. The role of mTORC1 pathway in intestinal tumorigenesis. Cell Cycle. 2009; 8: 3684-3687.

50. Galluzzi L, Kepp O, Kroemer G. TP53 and MTOR crosstalk to regulate cellular senescence. Aging. 2010; 2: 535-537.

51. Blagosklonny MV. Molecular damage in cancer: an argument for mTOR-driven aging. Aging. 2011; 3: 1130-1141.

52. Blagosklonny MV. NCI's provocative questions on cancer: some answers to ignite discussion. Oncotarget. 2011; 2: 1352-1367.

53. Henry CJ, Marusyk A, Zaberezhnyy V, Adane B, DeGregori J. Declining lymphoid progenitor fitness promotes aging-

associated leukemogenesis. Proc Natl Acad Sci U S A. 2010; 107: 21713-21718.

54. Henry CJ, Marusyk A, DeGregori J. Aging-associated changes in hematopoiesis and leukemogenesis: what's the connection? Aging. 2011; 3: 643-656.

55. Parrinello S, Coppe JP, Krtolica A, Campisi J. Stromal-epithelial interactions in aging and cancer: senescent fibroblasts alter epithelial cell differentiation. J Cell Sci. 2005; 118: 485-496.

56. Coppe JP, Patil CK, Rodier F, Sun Y, Munoz DP, Goldstein J, Nelson PS, Desprez PY, Campisi J. Senescence-associated secretory phenotypes reveal cell-nonautonomous functions of oncogenic RAS and the p53 tumor suppressor. PLoS Biol. 2008; 6: 2853-2868.

57. Davalos AR, Coppe JP, Campisi J, Desprez PY. Senescent cells as a source of inflammatory factors for tumor progression. Cancer Metastasis Rev. 2011; 29: 273-283.

58. Coussens LM, Werb Z. Inflammation and cancer. Nature. 2002; 420: 860-867.

59. Lisanti MP, Martinez-Outschoorn UE, Pavlides S, Whitaker-Menezes D, Pestell RG, Howell A, Sotgia F. Accelerated aging in the tumor microenvironment: connecting aging, inflammation and cancer metabolism with personalized medicine. Cell Cycle. 2011; 10: 2059-2063.

60. Balliet RM, Capparelli C, Guido C, Pestell TG, Martinez-Outschoorn UE, Lin Z, Whitaker-Menezes D, Chiavarina B, Pestell RG, Howell A, Sotgia F, Lisanti MP. Mitochondrial oxidative stress in cancer-associated fibroblasts drives lactate production, promoting breast cancer tumor growth: understanding the aging and cancer connection. Cell Cycle. 2011; 10: 4065-4073.

61. Campisi J. Senescent cells, tumor suppression, and organismal aging: good citizens, bad neighbors. Cell. 2005; 120: 513-522.

62. Vicente-Duenas C, Abollo-Jimenez F, Ruiz-Roca L, Alonso-Escudero E, Jimenez R, Cenador MB, Criado FJ, Cobaleda C, Sanchez-Garcia I. The age of the target cell affects B-cell leukaemia malignancy. Aging. 2010; 2: 908-913.

63. Bonuccelli G, Whitaker-Menezes D, Castello-Cros R, Pavlides S, Pestell RG, Fatatis A, Witkiewicz AK, Vander Heiden MG, Migneco G, Chiavarina B, Frank PG, Capozza F, Flomenberg N, Martinez-Outschoorn UE, Sotgia F, Lisanti MP. The reverse Warburg effect: glycolysis inhibitors prevent the tumor promoting effects of caveolin-1 deficient cancer associated fibroblasts. Cell Cycle. 2010; 9: 1960-1971.

64. Castello-Cros R, Bonuccelli G, Molchansky A, Capozza F, Witkiewicz AK, Birbe RC, Howell A, Pestell RG, Whitaker-Menezes D, Sotgia F, Lisanti MP. Matrix remodeling stimulates stromal autophagy, "fueling" cancer cell mitochondrial metabolism and metastasis. Cell Cycle. 2011; 10: 2021-2034.

65. Chiavarina B, Whitaker-Menezes D, Martinez-Outschoorn UE, Witkiewicz AK, Birbe RC, Howell A, Pestell RG, Smith J, Daniel R, Sotgia F, Lisanti MP. Pyruvate kinase expression (PKM1 and PKM2) in cancer-associated fibroblasts drives stromal nutrient production and tumor growth. Cancer Biol Ther. 2011; 12.

66. Bonuccelli G, Tsirigos A, Whitaker-Menezes D, Pavlides S, Pestell RG, Chiavarina B, Frank PG, Flomenberg N, Howell A, Martinez-Outschoorn UE, Sotgia F, Lisanti MP. Ketones and lactate "fuel" tumor growth and metastasis: Evidence that epithelial cancer cells use oxidative mitochondrial metabolism. Cell Cycle. 2010; 9: 3506-3514.

67. Migneco G, Whitaker-Menezes D, Chiavarina B, Castello-Cros R, Pavlides S, Pestell RG, Fatatis A, Flomenberg N, Tsirigos A, Howell A, Martinez-Outschoorn UE, Sotgia F, Lisanti MP. Glycolytic cancer associated fibroblasts promote breast cancer tumor growth, without a measurable increase in angiogenesis: evidence for stromal-epithelial metabolic coupling. Cell Cycle. 2010; 9: 2412-2422.

68. Ko YH, Lin Z, Flomenberg N, Pestell RG, Howell A, Sotgia F, Lisanti MP, Martinez-Outschoorn UE. Glutamine fuels a vicious cycle of autophagy in the tumor stroma and oxidative mitochondrial metabolism in epithelial cancer cells: Implications for preventing chemotherapy resistance. Cancer Biol Ther. 2011; 12.

69. Martinez-Outschoorn UE, Pestell RG, Howell A, Tykocinski ML, Nagajyothi F, Machado FS, Tanowitz HB, Sotgia F, Lisanti MP. Energy transfer in "parasitic" cancer metabolism: mitochondria are the powerhouse and Achilles' heel of tumor cells. Cell Cycle. 2011; 10: 4208-4216.

70. Martinez-Outschoorn UE, Whitaker-Menezes D, Lin Z, Flomenberg N, Howell A, Pestell RG, Lisanti MP, Sotgia F. Cytokine production and inflammation drive autophagy in the tumor microenvironment: role of stromal caveolin-1 as a key regulator. Cell Cycle. 2011; 10: 1784-1793.

71. Capparelli C, Guido C, Whitaker-Menezes D, Bonuccelli G, Balliet R, Pestell TG, Goldberg AF, Pestell RG, Howell A, Sneddon S, Birbe R, Tsirigos A, Martinez-Outschoorn U, Sotgia F, Lisanti MP. Autophagy and senescence in cancer-associated fibroblasts metabolically supports tumor growth and metastasis via glycolysis and ketone production. Cell Cycle. 2012; 11: 2285-2302.

72. Mercier I, Camacho J, Titchen K, Gonzales DM, Quann K, Bryant KG, Molchansky A, Milliman JN, Whitaker-Menezes D, Sotgia F, Jasmin JF, Schwarting R, Pestell RG, Blagosklonny MV, Lisanti MP. Caveolin-1 and Accelerated Host Aging in the Breast Tumor Microenvironment: Chemoprevention with Rapamycin, an mTOR Inhibitor and Anti-Aging Drug. Am J Pathol. 2012; 181: 278-293.

73. Blagosklonny MV. Prevention of cancer by inhibiting aging. Cancer Biol Ther. 2008; 7: 1520-1524.

74. Hursting SD, Lavigne JA, Berrigan D, Perkins SN, Barrett JC. Calorie restriction, aging, and cancer prevention: mechanisms of action and applicability to humans. Annu Rev Med. 2003; 54: 131-152.

75. Longo VD, Fontana L. Calorie restriction and cancer prevention: metabolic and molecular mechanisms. Trends Pharmacol Sci. 2010; 31: 89-98.

76. Blagosklonny MV. Calorie restriction: Decelerating mTOR-driven aging from cells to organisms (including humans). Cell Cycle. 2010; 9: 683-688.

77. Hursting SD, Perkins SN, Phang JM. Calorie restriction delays spontaneous tumorigenesis in p53-knockout transgenic mice. Proc Natl Acad Sci U S A. 1994; 91: 7036-7040.

78. Berrigan D, Perkins SN, Haines DC, Hursting SD. Adult-onset calorie restriction and fasting delay spontaneous tumorigenesis in p53-deficient mice. Carcinogenesis. 2002; 23: 817-822.

79. Harrison DE, Strong R, Sharp ZD, Nelson JF, Astle CM, Flurkey K, Nadon NL, Wilkinson JE, Frenkel K, Carter CS, Pahor M, Javors MA, Fernandezr E, Miller RA. Rapamycin fed late in life extends lifespan in genetically heterogenous mice. Nature. 2009; 460: 392-396.

80. Anisimov VN, Zabezhinski MA, Popovich IG, Piskunova TS, Semenchenko AV, Tyndyk ML, Yurova MN, Antoch MP, Blagosklonny MV. Rapamycin extends maximal lifespan in cancer-prone mice. Am J Pathol. 2010; 176: 2092-2097.

81. Anisimov VN, Zabezhinski MA, Popovich IG, Piskunova TS, Semenchenko AV, Tyndyk ML, Yurova MN, Rosenfeld SV, Blagosklonny MV. Rapamycin increases lifespan and inhibits spontaneous tumorigenesis in inbred female mice. Cell Cycle. 2011; 10: 4230-4236.

82. Mathew T, Kreis H, Friend P. Two-year incidence of malignancy in sirolimus-treated renal transplant recipients: results from five multicenter studies. Clin Transplant. 2004; 18: 446-449.

83. Kauffman HM, Cherikh WS, Cheng Y, Hanto DW, Kahan BD. Maintenance immunosuppression with target-of-rapamycin inhibitors is associated with a reduced incidence of de novo malignancies. Transplantation. 2005; 80: 883-889.

84. Yakupoglu YK, Buell JF, Woodle S, Kahan BD. Individualization of Immunosuppressive Therapy. III. Sirolimus Associated With a Reduced Incidence of Malignancy. Transplant Proc. 2006; 38: 358-361.

85. Campistol JM, Eris J, Oberbauer R, Friend P, Hutchison B, Morales JM, Claesson K, Stallone G, Russ G, Rostaing L, Kreis H, Burke JT, Brault Y, Scarola JA, Neylan JF. Sirolimus Therapy after Early Cyclosporine Withdrawal Reduces the Risk for Cancer in Adult Renal Transplantation. J Am Soc Nephrol. 2006; 17: 581-589.

86. Stallone G, Schena A, Infante B, Di Paolo S, Loverre A, Maggio G, Ranieri E, Gesualdo L, Schena FP, Grandaliano G. Sirolimus for Kaposi's sarcoma in renal-transplant recipients. N Engl J Med. 2005; 352: 1317-1323.

87. Pinkston JM, Garigan D, Hansen M, Kenyon C. Mutations that increase the life span of C. elegans inhibit tumor growth. Science. 2006; 313: 971-975.

88. Poyurovsky MV, Prives C. P53 and aging: A fresh look at an old paradigm. Aging. 2010; 2: 380-382.

89. Blagosklonny MV. Revisiting the antagonistic pleiotropy theory of aging: TOR-driven program and quasi-program. Cell Cycle. 2010; 9: 3151-3156.

90. de Keizer PL, Laberge RM, Campisi J. p53: Pro-aging or pro-longevity? Aging. 2010; 2: 377-379.

91. Chao SK, Horwitz SB, McDaid HM. Insights into 4E-BP1 and p53 mediated regulation of accelerated cell senescence. Oncotarget. 2011; 2: 89-98.

92. Matheu A, Maraver A, Klatt P, Flores I, Garcia-Cao I, Borras C, Flores JM, Vi–a J, Blasco MA, Serrano M. Delayed ageing through damage protection by the Arf/p53 pathway. Nature. 2007; 448: 375-379.

93. Donehower LA, Harvey M, Slagle BL, McArthur MJ, Montgomery CA, Jr., Butel JS, Bradley A. Mice deficient for p53 are developmentally normal but susceptible to spontaneous tumours. Nature. 1992; 356: 215-221.

94. Harvey M, McArthur MJ, Montgomery CA, Jr., Butel JS, Bradley A, Donehower LA. Spontaneous and carcinogen-induced tumorigenesis in p53-deficient mice. Nat Genet. 1993; 5: 225-229.

95. Jacks T, Remington L, Williams BO, Schmitt EM, Halachmi S, Bronson RT, Weinberg RA. Tumor spectrum analysis in p53-mutant mice. Curr Biol. 1994; 4: 1-7.

96. Donehower LA, Harvey M, Vogel H, McArthur MJ, Montgomery CA, Jr., Park SH, Thompson T, Ford RJ, Bradley A. Effects of genetic background on tumorigenesis in p53-deficient mice. Mol Carcinog. 1995; 14: 16-22.

97. Venkatachalam S, Shi YP, Jones SN, Vogel H, Bradley A, Pinkel D, Donehower LA. Retention of wild-type p53 in tumors from p53 heterozygous mice: reduction of p53 dosage can promote cancer formation. Embo J. 1998; 17: 4657-4667.

98. Hinkal G, Parikh N, Donehower LA. Timed somatic deletion of p53 in mice reveals age-associated differences in tumor progression. PLoS One. 2009; 4: e6654.

99. Guevara NV, Kim HS, Antonova EI, Chan L. The absence of p53 accelerates atherosclerosis by increasing cell proliferation in vivo. Nat Med. 1999; 5: 335-339.

100. Mercer J, Figg N, Stoneman V, Braganza D, Bennett MR. Endogenous p53 protects vascular smooth muscle cells from apoptosis and reduces atherosclerosis in ApoE knockout mice. Circ Res. 2005; 96: 667-674.

101. Mercer J, Bennett M. The role of p53 in atherosclerosis. Cell Cycle. 2006; 5: 1907-1909.

102. van Vlijmen BJ, Gerritsen G, Franken AL, Boesten LS, Kockx MM, Gijbels MJ, Vierboom MP, van Eck M, van De Water B, van Berkel TJ, Havekes LM. Macrophage p53 deficiency leads to enhanced atherosclerosis in APOE*3-Leiden transgenic mice. Circ Res. 2001; 88: 780-786.

103. Edinger AL, Linardic CM, Chiang GG, Thompson CB, Abraham RT. Differential effects of rapamycin on mammalian target of rapamycin signaling functions in mammalian cells. Cancer Res. 2003; 63: 8451-8460.

104. Sipula IJ, Brown NF, Perdomo G. Rapamycin-mediated inhibition of mammalian target of rapamycin in skeletal muscle cells reduces glucose utilization and increases fatty acid oxidation. Metabolism. 2006; 55: 1637-1644.

105. Brown NF, Stefanovic-Racic M, Sipula IJ, Perdomo G. The mammalian target of rapamycin regulates lipid metabolism in primary cultures of rat hepatocytes. Metabolism. 2007; 56: 1500-1507.

106. Hu W, Feng Z, Teresky AK, Levine AJ. p53 regulates maternal reproduction through LIF. Nature. 2007; 450: 721-724.

107. Hu W, Feng Z, Atwal GS, Levine AJ. p53: a new player in reproduction. Cell Cycle. 2008; 7: 848-852.

108. Roemer K. Are the conspicuous interdependences of fecundity, longevity and cognitive abilities in humans caused in part by p53? Cell Cycle. 2010; 9: 3438-3441.

109. Levine AJ, Tomasini R, McKeon FD, Mak TW, Melino G. The p53 family: guardians of maternal reproduction. Nat Rev Mol Cell Biol. 2011; 12: 259-265.

110. Mantovani R. More on the pro-fertility activity of p53: the blastocyst side. Cell Cycle. 2011; 10: 4205.

111. Chen D, Zheng W, Lin A, Uyhazi K, Zhao H, Lin H. Pumilio 1 suppresses multiple activators of p53 to safeguard spermatogenesis. Curr Biol. 2012; 22: 420-425.

112. McGee MD, Day N, Graham J, Melov S. cep-1/p53-dependent dysplastic pathology of the aging C. elegans gonad. Aging. 2012; 4: 256-269.

113. Kang HJ, Feng Z, Sun Y, Atwal G, Murphy ME, Rebbeck TR, Rosenwaks Z, Levine AJ, Hu W. Single-nucleotide polymorphisms in the p53 pathway regulate fertility in humans. Proc Natl Acad Sci U S A. 2009; 106: 9761-9766.

Priority Research Paper

cep-1/p53-dependent dysplastic pathology of the aging *C. elegans* gonad

Mathew D. McGee, Nicholas Day, Jill Graham, and Simon Melov

Buck Institute for Research on Aging, Novato, CA 94945 USA

Key words: *aging, p53, pathology, C. elegans, gonad*
Received: *3/28/12; Accepted: 4/28/12; Published: 4/30/12*
Correspondence to: *Simon Melov, PhD;* ***E-mail:*** *smelov@buckinstitute.org*

Copyright: *© McGee et al. This is an open-access article distributed under the terms of the Creative Commons Attribution License, which permits unrestricted use, distribution, and reproduction in any medium, provided the original author and source are credited*

Abstract: The *C. elegans* germline and somatic gonad are actively developing until the animal reaches adulthood, and then continue to undergo striking changes as the animal ages. Reported changes include a depletion of available sperm, a decrease in oocyte quality up till mid-life, a reduction in germline nuclei, a decrease in fertility, and an accumulation of DNA in the midbody of aging *C. elegans*. Here, we have focused on the aging gonad in old animals, and show in detail that the aging gonad undergoes a massive uterine growth composed of endoreduplicating oocytes, yolk, and expanses of chromatin. We use a novel series of imaging techniques in combination with histological methodology for reconstructing aged worms in 3-dimensions, and show in old animals growing masses swelling inside the uterus to occupy most of the diameter of the worm. We link this accelerated growth to the *cep*-1/p53 tumor suppressor. Because *cep*-1 is required for DNA damage induced apoptosis, and *daf*-2 limits longevity, these results suggest a role for age-related DNA damage in dysplastic uterine growths, which in some respects resemble premalignant changes that can occur in aging mammals.

INTRODUCTION

Much of the pathobiology of aging *C. elegans* and the aging germline remains relatively poorly described despite the widespread use of *C. elegans* as a model system to study aging. The aging *C. elegans* germline has been reported to undergo a series of changes up to midlife [1,2]. After approximately 8 days of age, the pool of sperm that are produced during larval development are depleted and few viable embryos are produced despite a continuous supply of oocytes. In the absence of sperm, the buildup of RNP granules is thought to facilitate cell cycle arrest in unfertilized oocytes for up to several days [3,4]. Eventually, oocytes bypass the prophase I diakinesis arrest [5] but fail to fully complete anaphase I [6]. Because they lack the sperm-contributed centrioles required for cytokinesis [7,8], these unfertilized oocytes would likely undergo endoreduplication [9,10] as worms age, rather than mitosis.

In mid-life (approximately 8-12 days of age), concurrent with sperm depletion, is a decrease in oocyte quality that also prevents the development of viable embryos even in the presence of viable sperm [11,12]. This decrease in oocyte quality with age functions at least partially through the insulin signaling and TGF-β pathways from the somatic gonad. Low quality oocytes can have various defects including small size, apparent cavities, increased aneuploidy, or cluster together in the uterus [11,13]. The apoptotic pathway is also required to maintain oocyte quality, as a loss of apoptosis in the germline causes an early loss of reproductive capacity and an earlier incidence of abnormal oocytes [14,15]. This decline in oocyte quality is also accompanied by a substantive increase in genome copy number, which is due to proliferation of the genome in the germline with age [16].

Endoreduplication has been well described in young animals, but not in worms older than 11 days of age or so (middle aged worms). Animals with a substantive amount of endoreduplication result in what is generally called the Emo (endomitotic) phenotype. This effect was first described in animals that were depleted of sperm [10,17]. Subsequently, the phenotype was

observed in a Sec61p protein translocation mutant that causes defective ovulation [9]. Several other genes that affect ovulation can also cause an Emo phenotype [5], and is generally caused by inappropriate maturation of unfertilized oocytes. Therefore, many mutants or treatments that prevent fertilization could potentially cause an Emo phenotype. In an aging context, this has been described to some degree in a previous report from our laboratory [16], and more recently observed in oocytes from 8 day old animals [11].

Using imaging techniques in combination with a novel histological methodology for reconstructing aged worms in 3-dimensions, we characterize in detail here for the first time the development of large uterine masses in aging *C. elegans* which arise from unfertilized oocytes that fail to be expelled from the vulva. Although we and others have commented on early stages of this phenotype [11,16], we report here a more detailed analysis of the progression of the massive age-related uterine growths that swell the uterus and fill most of the diameter of the worm. This advanced age germline phenotype causes other internal organ systems, such as the intestine, to become compressed, which likely has multiple deleterious functional outcomes in worms of advanced age. We observe a high degree of individual variation in the aging germline phenotype, despite animals being raised in identical conditions with an identical genetic background. We also report here for the first time a detailed description of an advanced age Emo phenotype, with uterine masses appearing to be primarily a combination of endoreduplicating oocytes, clusters of cells and/or nuclei, masses of chromatin, and extracellular yolk protein. We report a retardation of age-related uterine growths in the *daf-2* insulin-signaling mutant, consistent with prior studies showing reduced germline tumor growth [18] and reduced endomitotic phenotype at older ages [11,16]. Perhaps more significantly, we report that the tumor suppressor *cep-1*/p53 mutant has a more severe endomitotic phenotype at younger ages than wild-type animals. We also mined a pre-existing whole-genome expression profiling study of aging in *C. elegans* [19] to show that the transcriptional abundance of *cep-1*/p53 statistically significantly declines with age. *Cep-1*/p53 is known to be involved in DNA damage-induced apoptosis in *C. elegans* [20,21] and there has been some evidence of impaired DNA damage response in older animals [22]. Our data therefore provides evidence for a pathological role for DNA damage in old animals. However, p53 has also been shown to be a regulator of growth via the IGF-1/mTOR pathway [23], and is an important part of the response to genotoxic stress [24,25]. Hence, it is likely that reducing levels of *cep-1*/p53 with age, results in a complex phenotype including a massive dysplastic growth in the uterus, concomitant with a profound increase in genome copy number, substantially higher than that seen in young *C. elegans* at the peak of reproductive potential.

RESULTS

Wild-type *C. elegans* accumulate large uterine growths with age

By using a combination of novel imaging techniques (Figure 1, Movies 1-5), we have refined the spatial position of the midbody DNA masses we previously reported [16] primarily to the uterus, through virtue of being able to analyze the animal in detail in 3-dimensions. The masses begin to grow as early as 8 days of age (Figures 1A-B, Movie 1). This is consistent with the approximate age *C. elegans* deplete their sperm [10,26] and oocyte quality declines such that fertility can only be extended a few days by mating [1,11,12]. Once oocytes fail to be fertilized in the spermatheca, they bypass diakinesis arrest [6] and begin endoreduplicating to swell the uterus by 16 days of age (Figures 1A, Movie S1). The DNA masses are sometimes pushed into the continuous spermatheca and proximal gonad arm from the uterus (Figure 1A), similar to tumors that arise in young adult *glp-1* mutants [27,28]. Large age-related uterine growths can sometimes rupture regions of the uterine wall, causing them to enter the pseudocoelom(data not shown). Aged wild-type worms raised at elevated temperature have generally less severe uterine masses by DAPI staining than those raised at normal temperatures (Figure 2), but the masses also generally become visible at earlier ages, compared to worms raised at standard temperature (20^{o}C). Further, these small masses are more often seen in the distal and proximal gonad arm rather than in the uterus (data not shown). We also observed uterine growths by DAPI staining in aged animals grown in sterile conditions, using axenic culture methods (Figure 3). Therefore, the growth of these uterine masses is not caused solely by bacterial infection. The reduced severity of uterine masses does not mean bacteria contribute to growth of uterine masses, since axenic growth conditions also cause slow growth. We observed no masses, even at advanced ages, in *glp-4* mutants that do not develop a full gonad (Figure 2C). We did observe germline masses in old, sperm-deficient *fem-2* worms similar to old wild-type worms (Figure 2A-B), and we previously demonstrated that no masses form in males [16]. This is also consistent with previous studies that reported an Emo phenotype in young worms devoid of sperm [10,17].

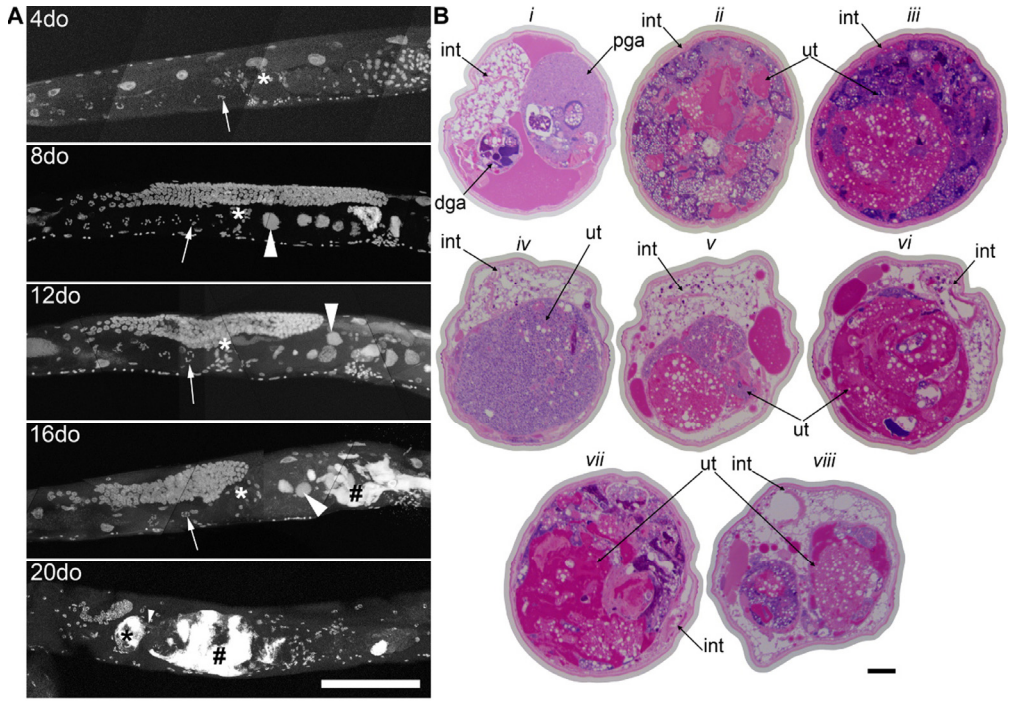

Figure 1. Germline masses accumulate with age. **a,** Partial maximum projection of mid-section of whole wild-type worms stained with DAPI at 4, 8, 12, 16, and 20-days-old raised at 20 degrees. Arrow indicates the -1 oocyte in diakinesis (none visible in 20-day-old worm). Asterisk indicates spermatheca. Large arrowhead indicates unfertilized, endomitotic nuclei. # indicates a mass that has no distinct cellular structure. Small arrowhead in the 20-day-old indicates site of invasion from uterus to spermatheca. Scale bar represents 100 microns. **b,** Cross sections of a 20-day-old wild-type worm stained with pararosaniline and methylene blue. Cross sections from the same worm starting at approximately -1 oocyte position along anterior half (*i*). Remaining sections are spaced 50 µm apart (*ii-viii*), moving towards posterior and ending at approximately -1 oocyte position along posterior half (*viii*). In some cross sections, the uterine growth has taken up nearly the whole diameter of the worm (*ii*, *iii*, *vii*). Growth recedes at midbody (*iv*). Intestine (int), distal gonad arm (dga), proximal gonad arm (pga), and uterus (ut) are indicated.

Table 1. Expected genome copy number of a wild-type adult hermaphrodite

	Germline Nuclei	Somatic Nuclei	Intestine	Hypodermis	Sperm	Embryos	TOTAL (no embryos)	TOTAL (6 embryos)
# Nuclei	1000	959	34	98	150	520		
Number	2	1	1	1	2	6		
Ploidy	1	2	32	4	1	2		
Total	2000	1918	1020	196	300	6240	5434	11674

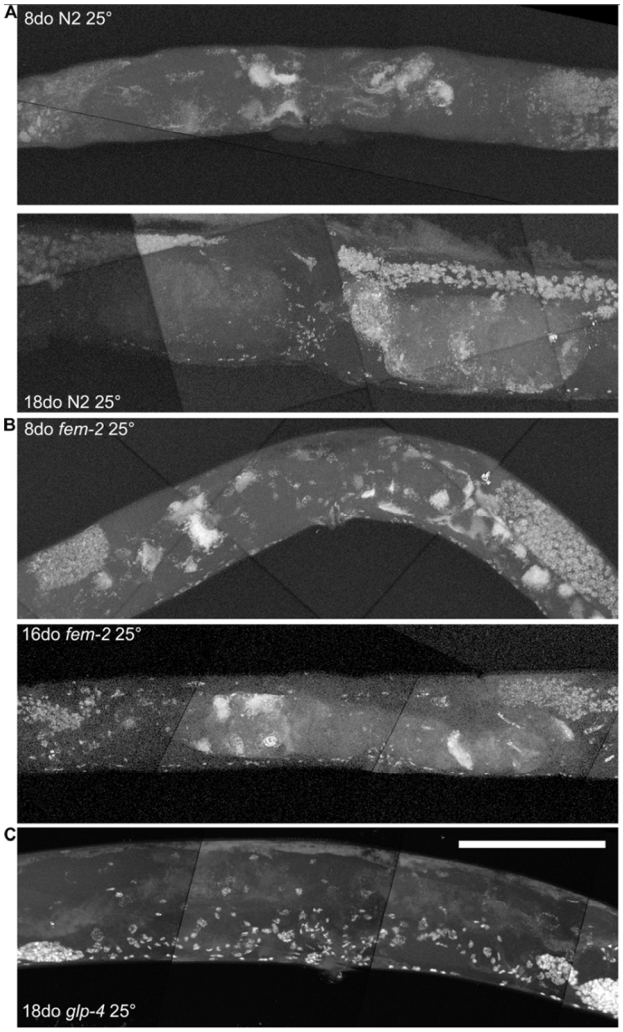

Figure 2. Age-related growths require a germline, but not competent sperm. a, Maximum projection of 8 and 18-day-old wild-type worm raised at 25 degrees and stained with DAPI. Growths visible at both ages, though generally never as severe as old wild-type worms raised at 20 degrees. **b,** Maximum projection of 8 and 16-day-old *fem-2* (no sperm) worms raised at 25 degree restrictive temperature and stained with DAPI. Masses are visible at both ages, similar to wild-type worms. **c**, Maximum projection of 18-day-old *glp-4* (underdeveloped gonad and germline) worm raised at 25 degree restrictive temperature and stained with DAPI. No masses are visible. Scale bar represents 100 microns.

Germline masses are responsible for an age-related genome copy number increase

In order to quantify the genomic DNA copy number of these growing uterine masses in aging animals, we used digital PCR of individual nematodes to estimate genome copy number at different ages. In a previous study by us, we used qPCR to estimate genome copy number in select strains [16]. However, here instead of qPCR, we use the digital PCR technique, as it is very sensitive, highly resistant to PCR inhibitors, and allows absolute quantitation of low copy number without reliance on standards [29]. The expected genome copy number of an adult hermaphrodite is ~5434 (3134 somatic) (Table 1), not including fertilized embryos.

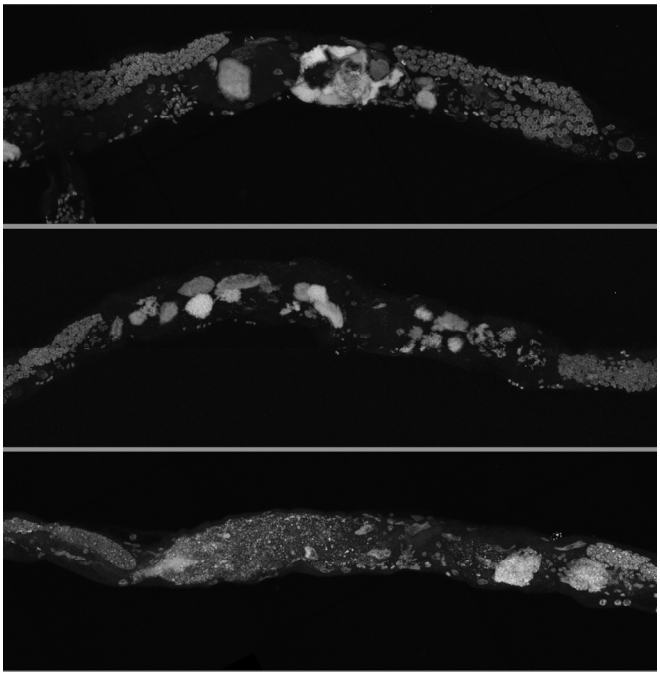

Figure 3. Germline masses in worms grown in axenic media. Partial maximum projection of mid-section of 26-day-old whole wild-type worms stained with DAPI. Worms were raised at 20 degrees in axenic media.

The number of embryos, which can be as many as 25-30 in the most extreme cases [26], and developmental stage of embryos in the uterus can vary greatly, causing a high degree of variability in the measured genome copy number of reproductive adults. To quantitate the amount of individual variation that is also visually apparent by microscopy (Movies 3-5), we assayed individual animals rather than pools of animals, giving us insight into the variance of age-related genome copy number variation between individual worms. We calculated a mean genome copy number of 17,160 (n = 10, +/- 3,102 S.E.M.) at 3 days of age (Table 2, Figure 4). Genome copy number does not significantly change from 3 days to 12 days of age, but there is almost a 4-

fold increase in genome copy number between 12 and 16 days of age ($p<0.0001$, Figure 4). It is worth noting that this 4-fold increase in genome copy number is substantially increased over that of younger animals, when reproduction is at peak capacity, and the animals are packed with developing oocytes and embryos. The trends we report here of genome copy number increases with age using digital PCR agree with our previous study [16] and also correlates with the onset of uterine growths (Figure 1A). *glp-4* mutants lack a gonad and have much lower genome copy number and reduced variance compared to wild-type worms (Figure 4). Average genome copy number in *glp-4* worms decreases between days 6 (6345, n = 10, +/- 312 S.E.M.) and 9 (3781, n = 9, +/- 718 S.E.M., p=0.0034) and then remains relatively constant through day 16. We previously were unable to calculate genome copy number in this strain by qPCR [16] likely due to overall low copy number or potential PCR inhibitors in preparing nucleic acids from individual worms. This data suggests the high variance in wild-type genome copy number is primarily due to germline effects. Initially the variance in genome copy number in young worms is likely due to developing embryos, while as the animal ages, the substantial variance increase arises due to massive proliferation of unfertilized, endoreduplicating oocytes, an age-related Emo phenotype.

Table 2. Measured genome copy number by digital PCR

Age (days)	N2	*glp-4*	*cep-1*	*daf-2*
3	17160 +/- 3102 (n=10)	5735 +/- 653 (n=10)	11644 +/- 1672 (n=9) (1 low)	-
6	24041 +/- 4333 (n=10)	6345 +/- 312 (n=10)	26337 +/- 3383 (n=10)	-
8	-	-	-	51068 +/- 8123 (n=10)
9	18130 +/- 3129 (n=10)	3781 +/- 718 (n=9)	33210 +/- 4674 (n=9)#	-
12	15360 +/- 2497 (n=10)	4054 +/- 404 (n=9)	45600 +/- 9960 (n=10)	-
16	60139 +/- 7004 (n=10)	3979 +/- 540 (n=9)	53411 +/- 13202 (n=8)&&	-
32	-	-	-	16609 +/- 2172 (n=10)
45	-	-	-	9427 +/- 1707 (n=10)
60	-	-	-	24086 +/- 7849 (n=10)

Error is S.E.M.

& Indicates censored animal that was below detection threshold

# Indicates censored animal that was above detection threshold

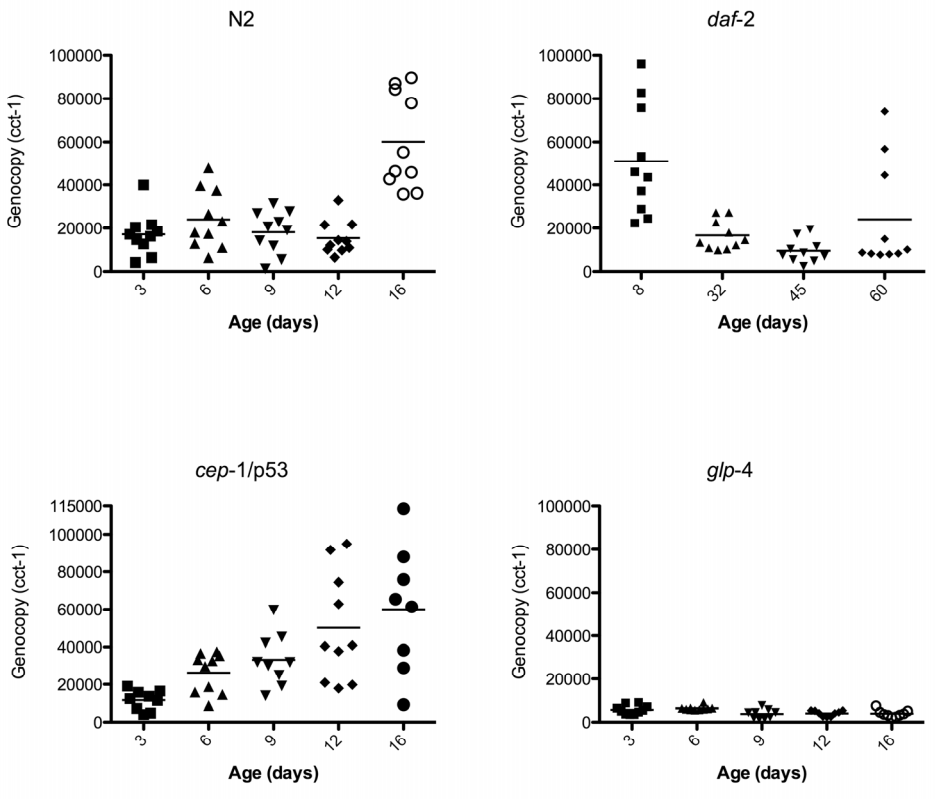

Figure 4. Genome copy number increases with the growth of uterine masses. Data points represent the genome copy number (y-axis) of individual worms at different ages (x-axis) as measured by digital PCR of individual worms with primers corresponding to genomic DNA of *cct-1* gene. Graphs are of wild-type N2, *glp-4*, *daf-2*, or *cep-1* worms.

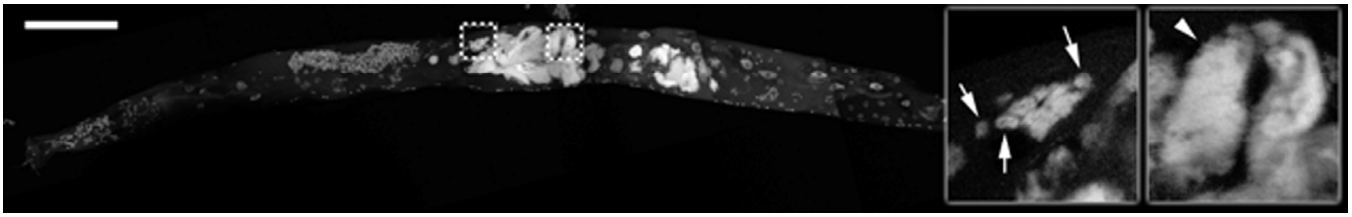

Figure 5. Uterine growths contain individual nuclei and large masses of chromatin. Partial maximum projection of a 16-day-old wild-type animal stained with DAPI and raised at 20 degrees. Insets are a single focal planes enlarged from the boxed regions. Arrows point to some of the visible individual nuclei in the uterus. Arrowhead points to a large chromatin mass in the uterus. Scale bar represents 100 microns.

Age-related germline masses have a complex composition

Examination of the germline masses by staining of sectioned tissues and imaging by light microscopy (Figures 1B, Movies 3-5) reveals three regions with distinct characteristics: cellularized areas with similar appearance to primary oocytes, chromatin masses associated with abnormal nuclei, and acellular accumulations in extracellular space of yolk and/or other matter. While the morphology of aged worms varies greatly, we found that 20-day-old animals have

very large uterine masses that compress many tissues. These masses appear to be smallest near the vulva, suggesting that the local microenvironment inhibits growth. This could be due to several causes, including extracellular signaling, or bacterial invasion through the vulva [30]. However, as masses are still present in worms grown in axenic media, this is unlikely. We found that while some nuclei in the uterine masses appear intact, other regions appear to be primarily acellular accumulations of chromatin and yolk based on histological staining. We also observed clusters of individual nuclei and large, endoreduplicating nuclei in these masses by DAPI staining (Figure 5). Defects in nuclear envelope morphology, such as blebbing, are a known age-related degenerative process in *C. elegans [31]* and could play a role in the growth of these masses. Lamin appears to surround the periphery of some, but not all, of these masses by antibody staining and lamin::gfp reporters (data not shown). Indeed, it is difficult to delineate individual cellular boundaries in these masses, suggesting that DNA replication is occurring within the uterus unbound by cell membranes.

Unfertilized oocytes in the proximal gonad arm of old animals are also clearly abnormal compared to those in young animals. Young healthy oocytes are large with distinct nuclei, while old animals often have smaller oocytes with less distinct nuclei and are filled with other unidentified matter not visible in young oocytes (Figure 6, Movies 2-5). The technique for visualizing individual animal morphology we have employed here in animals across the full lifespan of *C. elegans* allows a dynamic visual appreciation of the development of low quality oocytes, compared to more traditional imaging techniques and is in agreement with previous reports of smaller oocytes that are incapable of normal embryonic development in middle aged animals [11,12].

A large portion of the non-cellularized swelling of the midbody appears to be composed of yolk deposited in the pseudocoelom, which is magenta-colored in the stained cross sections (Figures 1B, 6). In young worms, yolk is produced in the intestine and transported through the pseudocoelom to the germline [32,33]. Although some yolk is always present in the pseudocoelom of adult worms, there is an accumulation of yolk outside the intestine with age, when the somatic gonad no longer holds enough mature oocytes to capture this material by endocytosis [30,32,34,35].

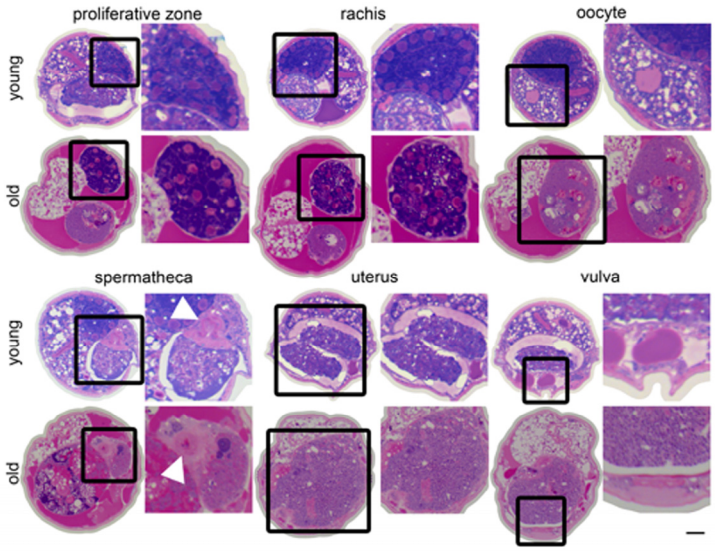

Figure 6. Changes in the germline with age. Cross sections from a 4-day-old (young) and a 20-day-old (old) wild-type worm. Regions of the germline indicated above the sections are representative and the structure is enlarged to the right of each section. White arrowhead indicates spermathecal epithelium. The region of the uterus shown in the old animal is near the vulva does not contain a massive uterine growth.

In addition to the uterine mass phenotype, the distal gonad is highly disorganized and shrunken in old animals compared to young. Instead of meiotic germline nuclei surrounding the periphery of the gonad with a well-developed central rachis as in young worms [22], nuclei appear to be spread throughout the gonad often with no visible rachis (Figure 6, Movies 2-5). These nuclei also appear to be generally less regular in size and composition. Twenty-day-old animals also have a shrunken distal gonad that is also visible by DAPI staining (Figure 1A).

The *daf-2* insulin-signaling mutant is able to reduce uterine masses at extreme age

Because long-lived *daf-2* worms are resistant to *gld-1* driven tumors in young animals [18] and we have previously seen lower genome copy number in old *daf-2* worms compared to wild-type [16], we evaluated in greater detail whether age-related uterine growths were delayed in *daf-2* animals. The increased resolution of imaging surprisingly showed that at 20 days of age, *daf-2* germline masses (Figures 7, Movie 6) are visually very similar to wild-type (Figure 1, Movies 3-5). These masses become less severe with age by both DAPI staining and genome copy number measurements after peaking in severity around 20 days of age (Figures 4, 7, Table 2). Fourty-five-day-old *daf-2* worms, well past the maximum life span of wild-type worms, have barely visible uterine masses by DAPI staining (Figure 7), and lower genome copy number measurements (Figure 4, Table 2). The uterus still appears swollen in 45-day-old animals even though DAPI intensity is drastically lowered (Figure 7), suggesting there could be a reduction of DNA in these masses but not an actual decrease in size. Eight-day-old *daf-2* worms have a strikingly elevated genome copy number (51,068, n = 10, +/- 8,123 S.E.M.) compared to 9-day-old wild-type animals, representing an almost 3-fold increase in genome copy number over wild-type levels, followed by a significant decrease at 32 (16,610, n = 10 +/- 2172 S.E.M., p=0.0007) and 45 (9,427 +/- 1,707 S.E.M., *p*=0.02) days of age. At 60 days of age the variance of genome copy number increases ($p = 0.0001$), and there may be some reoccurrence of endoreduplication at the end of life in the *daf-2* longevity mutant. Average genome copy number increases slightly, but not significantly between 45 and 60 days of age (24,090, n = 10, +/- 7,849 S.E.M., p=0.08). The substantial increase in genome copy number in *daf-2* animals at a young age is particularly unexpected, as it is known that this strain of *daf-2* is less fertile than N2 [36]. The origin of these extra genome copies in *daf-2* animals warrants further investigation, as it is either due to reduced oocyte quality, resulting in an early endomitotic phenotype not detectable by our methodology (DAPI staining or serial sectioning/3D reconstruction), or is somatic in origin.

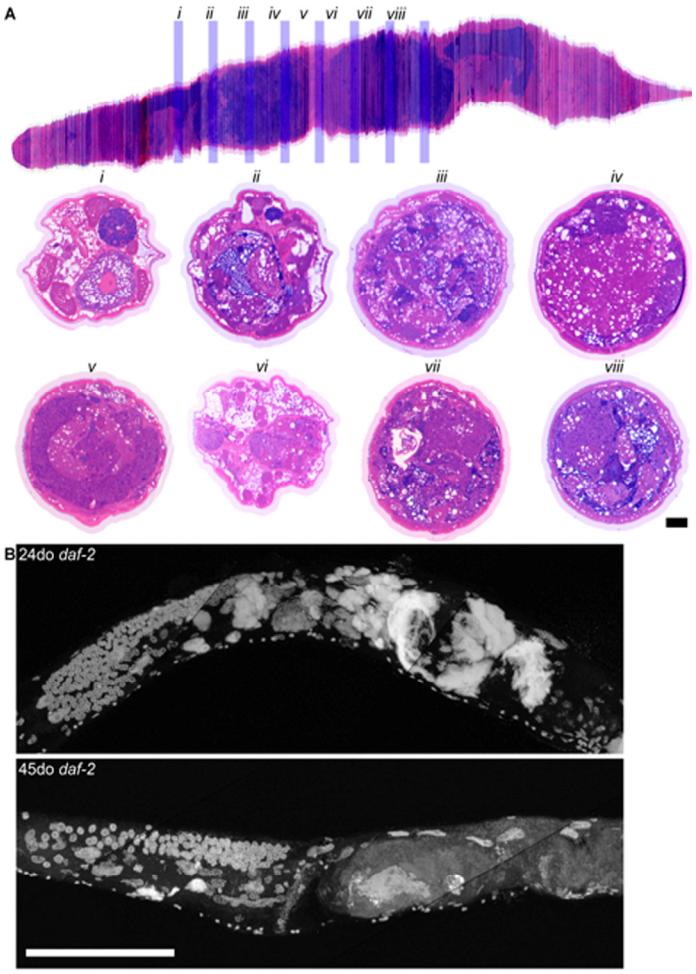

Figure 7. Long-lived *daf-2* mutants have decreased uterine masses with age. **a,** Aligned cross sections of a 20-day-old wild-type worm stained with pararosaniline and methylene blue. The aligned cross sections were resliced longitudinally in software (top) from the mid-pharynx (top left) to the tail (top right). Cross sections from the same worm containing the gonad are shown spaced 50 µm apart *(i-viii*) and are represented by blue bars in the longitudinal section (top). In some cross sections, the uterus has enlarged to take up nearly the whole diameter of the worm *(iii*, *iv*, *vii, viii*). Intestine (int), distal gonad arm (dga), proximal gonad arm (pga), and uterus (ut) are indicated. **b,** Maximum projection of 24 and 45-day-old long-lived *daf-2* worms raised at 20 degrees and stained with DAPI. Large uterine masses, similar to those seen in old wild-type worms, are visible at 24-days-old, but are reduced in size at 45-days-old. Scale bar represents 100 microns.

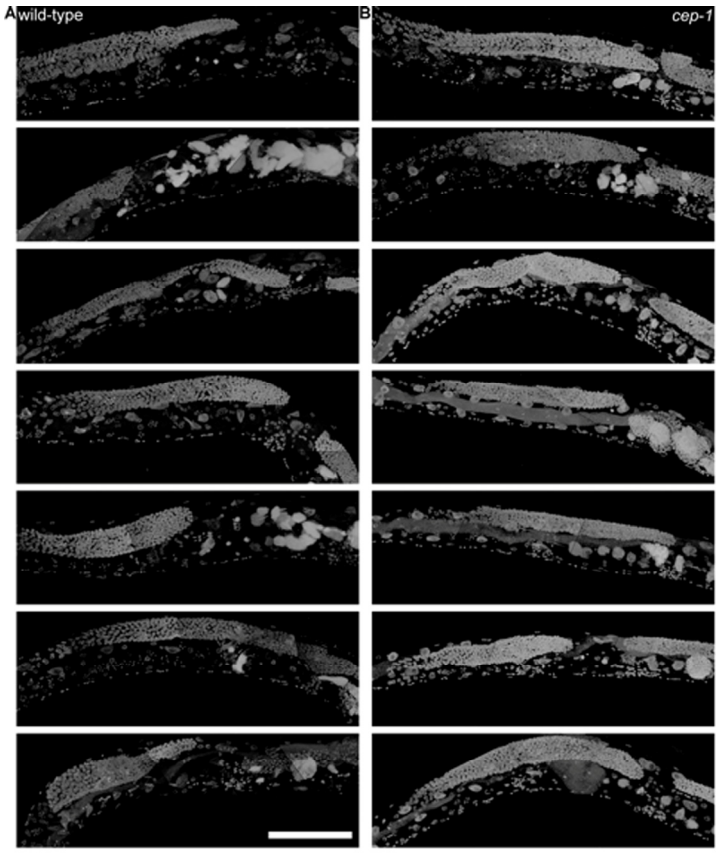

Figure 8. 8-day-old wild-type and *cep-1* worms have visibly detectable masses. **a,** Partial maximum projection of mid-section of 7 individual whole 8-day-old wild-type worms stained with DAPI raised at 20 degrees. **b,** Partial maximum projection of mid-section of 7 individual whole 8-day-old *cep-1* worms stained with DAPI raised at 20 degrees. Uterine masses are detectable at the same age in *cep-1* **(b)** and wild-type **(a)**. Scale bar represents 100 microns.

***cep-1*/p53 has earlier onset of endoreduplicating uterine growths, and *cep-1*/p53 declines with age**

Because *C. elegans cep-1* is known to function in DNA damage-induced apoptosis in the germline [37-39] and the mammalian homolog p53 is a well-known tumor-suppressor [40,41], we tested the hypothesis that *cep-1* limits the growth of these age-related uterine masses either through it's role in germline apoptosis or in transcriptional regulation of other genes. Indeed, we observed large chromatin masses in the uterus of most *cep-1* worms by middle age (12 days of age, Figures 8-9), whereas most wild-type worms do not have similar growths until about 16 days of age (Figure 1A, Movie 1). The age at which these masses can be morphologically visualized in *cep-1* mutants is roughly equivalent to when they appear in wild-type (Figure 8). Mating *cep-1* hermaphrodites to wild-type males did not appear to delay onset (data not shown), suggesting oocyte defects rather than unviable sperm causes endoreduplication as in middle aged wild-type worms [1,11]. *Cep-1* worms have a steady increase in genomic DNA copy number from 3 to 16 days of age (Figure 4, Table 1), whereas wild-type worms maintain relatively steady levels of genomic DNA before a large increase at 16 days of age (Figures 4, Table 1). *Cep-1* worms have a significantly higher genome copy number than wild-type worms at 9 ($p = 0.01$) and 12 ($p = 0.002$) days of age. Given wild-type animals accumulate uterine masses with age, and loss of *cep-1* increases the rate at which these masses appear, we wished to evaluate the transcriptional levels of *cep-1* with age to determine if there was any change in *cep-1* with increasing age. We had previously reported the largest study on gene expression profiling and aging in any species to date in *C. elegans [19]*, so we mined this pre-existing data set to look at the transcriptional profile of *cep-1* in wild-type aging of *C. elegans*. In our previous study, we noted that there were 5986 genes that were statistically significantly differentially expressed over the lifetime of *C. elegans*. These genes clustered into seven distinct profiles over lifespan, and *cep-1* is in cluster 5 (supplemental Table 8, [19]), and falls steadily in abundance over the life of *C. elegans* from a peak in young adulthood (Figure 10). Hence, there is a statistically significant decline in the transcript abundance of a key mediator of DNA damage and cell growth with age in *C. elegans*. To test whether DNA damage-induced apoptosis is important in removing oocytes likely to become uterine masses, we also examined *ced-3* mutants for uterine masses, which are incapable of physiological or DNA damage-induced apoptosis [42]. In agreement with previous studies that found loss of *ced-3* results in small, low-quality oocytes that will undergo endomitosis [14,15,43]. We observed an early onset of massive uterine growths in *ced-3* worms (Figure 11). This indicates that DNA damage may be occurring in these uterine growths and DNA damage-induced apoptosis may be a contributing mechanism to delay these massive uterine growths.

DISCUSSION

We have described in detail, a number of novel phenotypes in the aging *C. elegans* germline. Although age-related endoreduplication of unfertilized oocytes in middle aged animals has been commented on previously [1,11,16], we used a number of new techniques to describe the pathology of these masses and other age-related germline phenotypes in greater detail, and for the first time in older animals on different genetic backgrounds that may help shed light on the

mechanism of age-related germline phenotypes in future studies. Most striking is the massive growth in the uterus that arises from unfertilized oocytes. These masses grow large enough to swell the uterus to fill most of the diameter of the worm. They are primarily composed of endoreduplicating unfertilized oocytes, masses of chromatin from presumably lysed nuclei, small clusters of individuals cells and/or nuclei, and yolk proteins. The growth of these uterine masses is accelerated in the *cep-1*/p53 mutant known to be required for DNA damage-induced apoptosis in *C. elegans*.

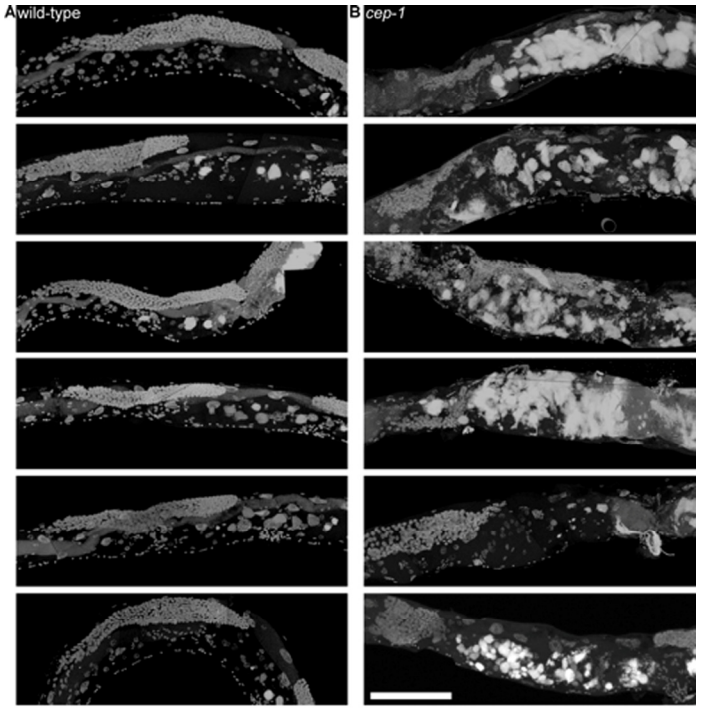

Figure 9. *cep-1* worms have earlier uterine mass onset. **a,** Partial maximum projection of mid-section of 6 individual whole wild-type worms stained with DAPI 12-days-old raised at 20 degrees. **b,** Partial maximum projection of mid-section of 6 individual whole *cep-1* worms stained with DAPI 12-days-old raised at 20 degrees. Uterine masses are visibly larger in *cep-1* **(b)** than wild-type **(a)**. Scale bar represents 100 microns.

Cep-1 is not a close homolog of mammalian p53 and was not identified as such until 2001 [20,21]. Although we show that loss of *cep-1* causes early age-related uterine masses, a previous study showed that *cep-1* does not affect the number of mitotic cells in germline tumor mutants or the shortened lifespan of these mutants [18]. Therefore it is likely that *cep-1*/p53 has a different mechanistic function in *C. elegans* tumors from *gld-1* and *glp-1* [28,44] mutants compared to mammals [45]. *Cep-1*/p53 controls the transcription of many downstream target genes and affects processes such as DNA damage-induced apoptosis [20,21], meiotic segregation in the germline [20], stress tolerance [46], genotoxic stress response [24], and cell growth [24,43]. We observed a statistically significant decrease in the transcriptional abundance of *cep-1*/p53 with age, concordant with an increase in endoreduplication within the gonad, contributing to late life pathology of the gonad. The reason for the decrease in *cep-1*/p53 with age within *C. elegans* is currently not known. However, in mammals, p53 activity also declines with age, and this decrease has been proposed to be a contributing factor to the increased tumor incidence in older populations [41], as well as being linked to cellular senescence [47], and antagonistic pleiotropy in aging [48]. Intriguing links between the activity of p53, mTOR, and senescence [49,50], hint at a more complex explanation for the increase in the Emo phenotype in late life than a simple decrease in apoptosis due to the decline in levels of *cep-1*/p53 with age. One possible explanation for the Emo phenotype in the aged *C. elegans* gonad, is the gradual decline in *cep-1*/p53 activity results in reduced apoptosis, combined with enhanced activity of the mTOR growth program, which then gives rise to the Emo phenotype with age. This decline in *cep-1*/p53 in aging *C. elegans*, coupled with a rapid increase in growth in the gonad (as evidenced by an upto 4 fold increase in overall genome copy number per worm) hints at possible commonalities in widely divergent species in age-related phenotypes due to the decline of p53 levels with age.

It also appears likely that DNA damage-induced apoptotic defects cause early uterine growths based on our observations and those of others [14,15,43]. The massive increase in DNA with age, in conjunction with decreased levels of *cep-1*/p53, coupled with clear pathological outcomes (compression of a variety of tissues with likely functional consequences) begs the question whether or not this age-related pathology could be considered to be analogous to age-related tumors seen in mammalian systems. By classical criteria, there are almost no tumors in *C. elegans* described to date that conform to a formal definition of cancer. The closest exception to this generalization may be the laminin mutants previously reported [51], where germ cells were documented to be actively invading somatic tissues, in conjunction with midbody swelling. What would be needed to legitimately link the age-related pathology we describe here in *C. elegans* to cancer are additional criteria, such as mutations in tumor suppressors with age that are then intimately linked to the development of the tumor-like pathology. The age-

related germline dysplasia we describe here shares several characteristics with those observed in tumor-prone mutants such as *gld-1*, but also have several distinctions. They are both abrogated in *daf-2* worms for a time and are the result of uncontrolled germline growth. However, *daf-2* worms do not have a delayed age-related germline tumor onset as seen in the tumor-prone mutants.

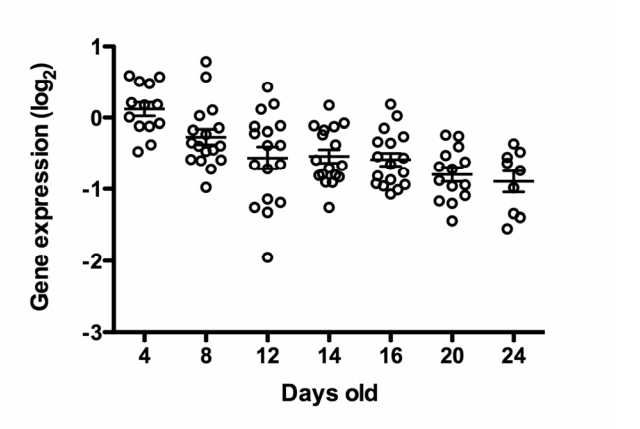

Figure 10. *cep-1*/p53 transcript abundance decreases with age. Whole genome expression profiling was used to identify genes that were differentially expressed with age (for complete description, see [19], cep-1/p53 is statistically significantly differentially expressed with age relative to young worms ($p<0.05$, *cep-1*/p53 is in Cluster 5 [19]). Each data point represents the *cep-1*/p53 message levels in a single animal, and expression level is represented relative to mRNA from a pool of young N2 animals [19].

Instead, it is likely there must be a mechanism to reduce tumors at extreme ages after they have already formed. Also distinct from age-related tumors, *gld-1* and *glp-1* tumors appear to have more rapid growth of intact germline nuclei while the age-related dysplastic pathology in the gonad grows more slowly and contains regions that are both cellularized and acellular, as well as accumulations of material such as yolk and chromatin.

The molecular characterization of this unique age-related gonadal pathology in *C. elegans* could potentially give more insight into age-related tumors in other species. Of particular interest will be whether age-related mutations in orthologs of mammalian tumor suppressors or oncogenes could be driving the growth of this dysplastic gonadal pathology, as we showed is possible in the *cep-1/*p53 mutant. Indeed, the rapid increase in genomic DNA at extreme age could be a source of genomic DNA changes and there are established methods to evaluate genomic DNA quality in *C. elegans* [52,53].

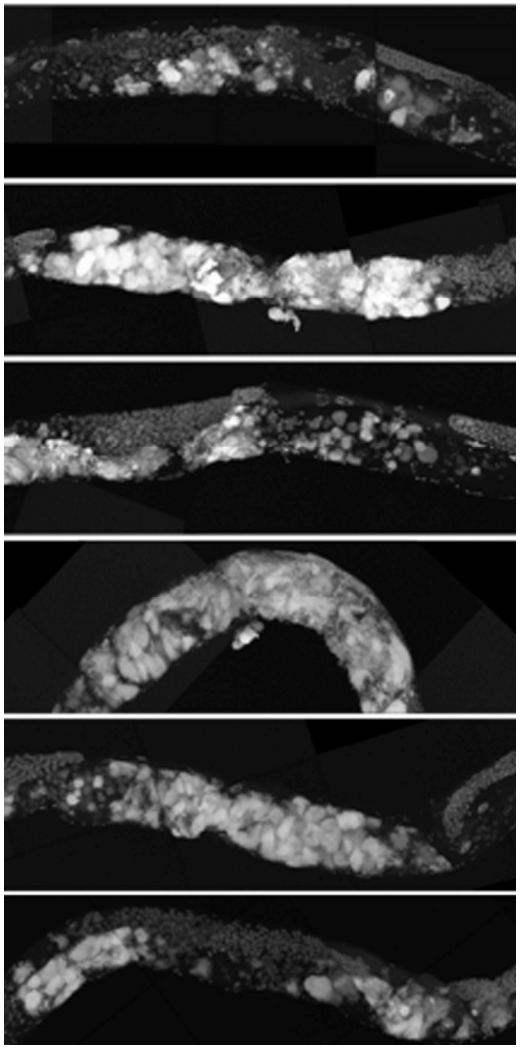

Figure 11. *ced-3* animals have early uterine mass onset. Partial maximum projection of mid-section of 6 individual 12-day-old *ced-3* worms stained with DAPI and raised at 20 degrees. 12-day-old *ced-3* animals have uterine masses visually similar to *cep-1* at the same age.

We propose that age-related uterine masses arise from a combination of several different events. Some regions of the uterine masses appear cellularized while others are acellular. Oocytes that normally arrest at diakinesis eventually bypass this arrest and begin endo-reduplicating. The nuclear envelope breaks down as the amount of DNA increases, causing the cell to eventually lyse. Many of these nuclei have a disrupted nuclear

envelope as observed by lamin::gfp (data not shown). Degradation of the nuclear envelope has been observed in aging *C. elegans* previously [31]. As oocytes begin to be ovulated at a slower rate in the aging mother, yolk is no longer being used at the same rate by primary oocytes, which would account for the buildup of yolk in the pseudocoelom and masses we and others have observed [30,33-35]. The intestine is apparently unable to regulate the amount of yolk produced to match actual demand [35]. This is possibly also influenced by the loss of intestinal nuclei which occurs as *C. elegans* ages, which we recently described [30].

We have demonstrated that several age-related changes occur in the *C. elegans* gonad. Most dramatically, we describe how uterine masses in *C. elegans* arise in the aging germline from unfertilized oocytes that begin endoreduplicating after bypassing the arrest at the end of diakinesis [5]. Uterine masses grow uncontrollably until they occupy most of the diameter of the worm and are accompanied by a massive increase in DNA copy number per worm in old adults, which greatly exceeds the genome copy number of worms at their reproductive peak at younger ages, and is coupled to a decline in levels of *cep-1*/p53. We also determined that loss of the CEP-1/p53 protein exacerbates the growth of uterine masses at earlier ages. DNA damage-induced apoptosis likely limits uterine growths, as *cep-1*/p53 is required for DNA damage-induced apoptosis in the germline [54]. Additionally, we and others have found that *ced-3* lowers oocyte quality and enhances the endomitotic phenotype. We have also found that the occurrence of these masses is not completely dependent on the bacterial food source or immune response [55], as worms grown in sterile axenic media still develop uterine masses with age. In summary, the aging *C. elegans* uterus develops massive growths from endoreduplicating oocytes that are modulated by the CEP-1/p53 protein, which has multiple functions including roles in DNA damage response, growth [41,45,48], genotoxic stress response [24], and cellular senescence [47].

EXPERIMENTAL PROCEDURES

C. elegans strains were cultured using standard conditions [22] (N2, *cep-1(gk138)I*, *daf-2(e1370)III, ced-3(n717)IV)* or at the restrictive temperature of 25 degrees (*glp-4(bn2)I*, *fem-2(b245)III*) and obtained from the *Caenorhabditis* Genetics Center. Synchronized populations were acquired by allowing adult parents to lay eggs for 2-4 h before removing them (day 0). Worms were transferred daily to fresh plates during the reproductive period. Confocal microscopy, staining of tissue sections, and 3-D visualization was performed as described [30].

Individual worms for genome copy number experiments were frozen in water and lysed in Proteinase K as described [16]. Digital PCR was performed on the lysate of individual animals using primers corresponding to the genomic DNA of the *cct-1* gene (5'-aatacggttgtgtttcaggtaatg-3' and 5'-taccggtgagggcaa gaat-3'). Digital PCR of *ced-7* and *fat-3* genes yielded similar results to *cct-1* (data not shown). Digital PCR signal was measured using UPL probe #78 (Roche) on a Biomark microfluidic system in 12.765 digital arrays (Fluidigm).

For Axenic liquid culture, *C. elegans* were first grown at 20C at a density of 15,000 worms/plate on NGM plates seeded with OP50 bacteria. Eggs were isolated from these cultures and grown in CeHR medium according to previous studies [56,57] with a minor modification. Heme was excluded from the axenic media and was added prior to use along with the UHT milk. Ten freshly hatched sterile L1 were seeded in 1 ml CeHR medium without antibiotics in a 24 well plate and grown at 20C shaking at 450 rpm on a small shaker. After the first generation, gravid adults were allowed to lay eggs for 4 hours in each well and were subsequently removed. Synchronized eggs were allowed to grow in sterile CeHR medium until Day 22 of adulthood. The media was changed three times weekly until day 8 of adulthood, and from there it was changed twice weekly. The first generation of nematodes grows slowly on CeHR (7-10) days, while successive generations grow at similar rates to those on solid media. Nematodes were allowed to adapt to CeHR media for at least one full generation before use.

ACKNOWLEDGMENTS

This work was supported by Geroscience funds awarded to SM from NIH (ULDE19608 & RL1AG032117), support from the Hillblom foundation, and a generous gift from the Glenn Foundation for Medical Research. MG was supported by a TL1 fellowship from the NIH (AG032116). We also thank Daniel Crippen, Cathy Vitelli, Darren Weber, and Adam Orr for help in the 3D worm reconstruction. We also would like to thank the paper polishing group at the Buck Institute for helpful discussions (Judith Campisi, Gordon Lithgow, Pankaj Kapahi). We are grateful to the Caenorhabditis Genetics Center for strains.

CONFLICT OF INTERESTS STATEMENT

The authors of this manuscript have no conflict of interest to declare.

REFERENCES

1. Hughes SE, Huang C, and Kornfeld K. Identification of mutations that delay somatic or reproductive aging of Caenorhabditis elegans. Genetics. 2011; 189:341-356.

2. Collins JJ, Huang C, Hughes S, and Kornfeld K. The measurement and analysis of age-related changes in Caenorhabditis elegans. WormBook. 2008; 1-21.

3. Patterson JR, Wood MP, and Schisa JA. Assembly of RNP granules in stressed and aging oocytes requires nucleoporins and is coordinated with nuclear membrane blebbing. Dev Biol. 2011; 353:173-185.

4. Schisa JA, Pitt JN, and Priess JR. Analysis of RNA associated with P granules in germ cells of C. elegans adults. Development. 2001; 128:1287-1298.

5. Greenstein D.Control of oocyte meiotic maturation and fertilization. WormBook. 2005; 1-12.

6. McNally KL, and McNally FJ. Fertilization initiates the transition from anaphase I to metaphase II during female meiosis in C. elegans. Dev Biol. 2005; 282:218-230.

7. Gonczy P, Echeverri C, Oegema K, Coulson A, Jones S, Copley R, Duperon J, Oegema J, Brehm M, Cassin E, Hannak E, Kirkham M, Pichler S, Flohrs K, Goessen A, Leidel S, et al. Functional genomic analysis of cell division in C. elegans using RNAi of genes on chromosome III. Nature. 2000; 408:331-336.

8. Sadler PL, and Shakes DC. Anucleate Caenorhabditis elegans sperm can crawl, fertilize oocytes and direct anterior-posterior polarization of the 1-cell embryo. Development. 2000; 127:355-366.

9. Iwasaki K, McCarter J, Francis R, and Schedl T. emo-1, a Caenorhabditis elegans Sec61p gamma homologue, is required for oocyte development and ovulation. J Cell Biol. 1996; 134:699-714.

10. Ward S, and Carrel JS. Fertilization and sperm competition in the nematode Caenorhabditis elegans. Dev Biol. 1979; 73:304-321.

11. Luo S, Kleemann GA, Ashraf JM, Shaw WM, and Murphy CT. TGF-β and insulin signaling regulate reproductive aging via oocyte and germline quality maintenance. Cell. 2010; 143:299-312.

12. Hughes SE, Evason K, Xiong C, and Kornfeld K. Genetic and pharmacological factors that influence reproductive aging in nematodes. PLoS Genetics. 2007; 3:e25.

13. Luo S, Shaw WM, Ashraf J, and Murphy CT. TGF-beta Sma/Mab signaling mutations uncouple reproductive aging from somatic aging. PLoS Genetics. 2009; 5:e1000789.

14. Andux S, and Ellis RE. Apoptosis maintains oocyte quality in aging Caenorhabditis elegans females. PLoS Genetics. 2008; 4:e1000295.

15. Gumienny TL, Lambie E, Hartwieg E, Horvitz HR, and Hengartner MO. Genetic control of programmed cell death in the Caenorhabditis elegans hermaphrodite germline. Development. 1999; 126:1011-1022.

16. Golden T, Beckman K, Lee A, Dudek N, Hubbard A, Samper E, and Melov S. Dramatic age-related changes in nuclear and genome copy number in the nematode Caenorhabditis elegans. Aging Cell. 2007; 6:179-188.

17. Ward S, and Miwa J. Characterization of temperature-sensitive, fertilization-defective mutants of the nematode caenorhabditis elegans. Genetics. 1978; 88:285-303.

18. Pinkston JM, Garigan D, Hansen M, and Kenyon C. Mutations that increase the life span of C. elegans inhibit tumor growth. Science (New York, NY). 2006; 313:971-975.

19. Golden T, Hubbard A, Dando C, Herren M, and Melov S. Age-related behaviors have distinct transcriptional profiles in C.elegans. Aging Cell. 2008; 7:850-865.

20. Derry WB, Putzke AP, and Rothman JH. Caenorhabditis elegans p53: role in apoptosis, meiosis, and stress resistance. Science. 2001; 294:591-595.

21. Schumacher B, Hofmann K, Boulton S, and Gartner A. The C. elegans homolog of the p53 tumor suppressor is required for DNA damage-induced apoptosis. Curr Biol. 2001; 11:1722-1727.

22. Luo S, Kleemann GA, Ashraf JM, Shaw WM, and Murphy CT. TGF-beta and insulin signaling regulate reproductive aging via oocyte and germline quality maintenance. Cell. 2010; 143:299-312.

23. Feng Z, and Levine AJ. The regulation of energy metabolism and the IGF-1/mTOR pathways by the p53 protein. Trends Cell Biol. 2010; 20:427-434.

24. Vousden KH, and Lane DP. p53 in health and disease. Nat Rev Mol Cell Biol. 2007; 8:275-283.

25. Budanov AV, and Karin M. p53 Target Genes Sestrin1 and Sestrin2 Connect Genotoxic Stress and mTOR Signaling. Cell. 2008; 134:451 - 460.

26. Maupas E.Modes et formes de reproduction des nematodes. Archives de Zoologie expérimentale et générale. 1901; 8:463-624.

27. Francis R, Maine E, and Schedl T. Analysis of the multiple roles of gld-1 in germline development: interactions with the sex determination cascade and the glp-1 signaling pathway. Genetics. 1995; 139:607-630.

28. Francis R, Barton MK, Kimble J, and Schedl T. gld-1, a tumor suppressor gene required for oocyte development in Caenorhabditis elegans. Genetics. 1995; 139:579-606.

29. Qin J, Jones RC, and Ramakrishnan R. Studying copy number variations using a nanofluidic platform. Nucleic Acids Res. 2008; 36:e116.

30. McGee MD, Weber D, Day N, Vitelli C, Crippen D, Herndon LA, Hall DH, and Melov S. Loss of intestinal nuclei and intestinal integrity in aging C. elegans. Aging Cell. 2011; 10:699-710.

31. Haithcock E, Dayani Y, Neufeld E, Zahand AJ, Feinstein N, Mattout A, Gruenbaum Y, and Liu J. Age-related changes of nuclear architecture in Caenorhabditis elegans. Proceedings of the National Academy of Sciences of the United States of America. 2005; 102:16690-16695.

32. Hall D, Winfrey V, Blaeuer G, Hoffman L, Furuta T, Rose K, Hobert O, and Greenstein D. Ultrastructural features of the adult hermaphrodite gonad of Caenorhabditis elegans: relations between the germ line and soma. Dev Biol. 1999; 212:101-123.

33. Kimble J, and Sharrock WJ. Tissue-specific synthesis of yolk proteins in Caenorhabditis elegans. Dev Biol. 1983; 96:189-196.

34. Garigan D, Hsu A-L, Fraser AG, Kamath RS, Ahringer J, and Kenyon C. Genetic analysis of tissue aging in Caenorhabditis elegans: a role for heat-shock factor and bacterial proliferation. Genetics. 2002; 161:1101-1112.

35. Herndon L, Schmeissner P, Dudaronek J, Brown P, Listner K, Sakano Y, Paupard M, Hall D, and Driscoll M. Stochastic and genetic factors influence tissue-specific decline in ageing C. elegans. Nature. 2002; 419:808-814.

36. Gems D, Sutton A, Sundermeyer M, Albert P, King K, Edgley M, Larsen P, and Riddle D. Two pleiotropic classes of daf-2

mutation affect larval arrest, adult behavior, reproduction and longevity in Caenorhabditis elegans. Genetics. 1998; 150:129-155.
37. Waters K, Yang AZ, and Reinke V. Genome-wide analysis of germ cell proliferation in C.elegans identifies VRK-1 as a key regulator of CEP-1/p53. Dev Biol. 2010; 344:1011-1025.
38. Quevedo C, Kaplan DR, and Derry WB. AKT-1 regulates DNA-damage-induced germline apoptosis in C. elegans. Curr Biol. 2007; 17:286-292.
39. Schumacher B, Hanazawa M, Lee M-H, Nayak S, Volkmann K, Hofmann ER, Hofmann R, Hengartner M, Schedl T, and Gartner A. Translational repression of C. elegans p53 by GLD-1 regulates DNA damage-induced apoptosis. Cell. 2005; 120:357-368.
40. Hollstein M, Sidransky D, Vogelstein B, and Harris C. p53 mutations in human cancers. Science. 1991; 253:49-53.
41. Feng Z, Hu W, Rajagopal G, and Levine AJ. The tumor suppressor p53: cancer and aging. Cell Cycle. 2008; 7:842-847.
42. Gartner A, Boag PR, and Blackwell TK. Germline survival and apoptosis. WormBook : the online review of C elegans biology. 2008; 1-20.
43. Rutkowski R, Dickinson R, Stewart G, Craig A, Schimpl M, Keyse SM, and Gartner A. Regulation of Caenorhabditis elegans p53/CEP-1-dependent germ cell apoptosis by Ras/MAPK signaling. PLoS Genet. 2011; 7:e1002238.
44. Francis R, Barton MK, Kimble J, and Schedl T. gld-1, a tumor suppressor gene required for oocyte development in Caenorhabditis elegans. Genetics. 1995; 139:579.
45. Levine A.p53, the cellular gatekeeper for growth and division. Cell. 1997; 88:323-331.
46. Sendoel A, Kohler I, Fellmann C, Lowe SW, and Hengartner MO. HIF-1 antagonizes p53-mediated apoptosis through a secreted neuronal tyrosinase. Nature. 2010; 465:577-583.
47. de Keizer PL, Laberge RM, and Campisi J. p53: Pro-aging or pro-longevity? Aging (Albany NY). 2010; 2:377-379.
48. Blagosklonny MV.Revisiting the antagonistic pleiotropy theory of aging: TOR-driven program and quasi-program. Cell Cycle. 2010; 9:3151-3156.
49. Korotchkina LG, Leontieva OV, Bukreeva EI, Demidenko ZN, Gudkov AV, and Blagosklonny MV. The choice between p53-induced senescence and quiescence is determined in part by the mTOR pathway. Aging (Albany NY). 2010; 2:344-352.
50. Demidenko ZN, Korotchkina LG, Gudkov AV, and Blagosklonny MV. Paradoxical suppression of cellular senescence by p53. Proc Natl Acad Sci U S A. 2010; 107:9660-9664.
51. Huang C-C, Hall DH, Hedgecock EM, Kao G, Karantza V, Vogel BE, Hutter H, Chisholm AD, Yurchenco PD, and Wadsworth WG. Laminin alpha subunits and their role in C. elegans development. Development. 2003; 130:3343-3358.
52. van Haaften G, Plasterk RHA, and Tijsterman M. Genomic instability and cancer: scanning the Caenorhabditis elegans genome for tumor suppressors. Oncogene. 2004; 23:8366-8375.
53. van Haaften G, Vastenhouw NL, Nollen EAA, Plasterk RHA, and Tijsterman M. Gene interactions in the DNA damage-response pathway identified by genome-wide RNA-interference analysis of synthetic lethality. Proceedings of the National Academy of Sciences of the United States of America. 2004; 101:12992-12996.
54. Derry WB, Bierings R, van Iersel M, Satkunendran T, Reinke V, and Rothman JH. Regulation of developmental rate and germ cell proliferation in Caenorhabditis elegans by the p53 gene network. Cell Death Differ. 2007; 14:662-670.
55. Kurz CL, and Tan M-W. Regulation of aging and innate immunity in C. elegans. Aging Cell. 2004; 3:185-193.
56. Clegg ED, Lapenotiere HF, French DY, and Szilagyi M. Use of CeHR axenic medium for exposure and gene expression studies. East Coast Worm Meeting. 2002; .
57. Szewczyk NJ, Kozak E, and Conley CA. Chemically defined medium and Caenorhabditis elegans. BMC Biotechnol. 2003; 3:19.

MOVIES

Please check the full text version to see six movies related to this manuscript.

Research Perspective

p53 governs *t*elomere *r*egulation *f*eedback *too*, via TRF2

Izumi Horikawa, Kaori Fujita, and Curtis C. Harris

Laboratory of Human Carcinogenesis, National Cancer Institute, National Institutes of Health, Bethesda, MD 20892, USA

Key words: *telomere uncapping, p53, ubiquitin ligase, TRF2, feedback regulation*
Received: *1/19/11; Accepted: 1/24/11; Published: 1/25/11*
Corresponding author: *Curtis C. Harris, MD;* ***E-mail:*** *Curtis_Harris@nih.gov*

Copyright: *© Horikawa et al. This is an open-access article distributed under the terms of the Creative Commons Attribution License, which permits unrestricted use, distribution, and reproduction in any medium, provided the original author and source are credited*

Abstract: p53 takes critical part in a number of positive and negative feedback loops to regulate carcinogenesis, aging and other biological processes. Uncapped or dysfunctional telomeres are an endogenous DNA damage that activates ATM kinase (ataxia telangiectasia mutated) and then p53 to induce cellular senescence or apoptosis. Our recent study shows that p53, a downstream effector of the telomere damage signaling, also functions upstream of the telomere-capping protein complex by inhibiting one of its components, TRF2 (telomeric repeat binding factor 2). Since TRF2 inhibition leads to ATM activation, a novel positive feedback loop exists to amplify uncapped telomere-induced, p53-mediated cellular responses. Siah1 (seven in absentia homolog 1), a p53-inducible E3 ubiquitin ligase, plays a key role in this feedback regulation by targeting TRF2 for ubiquitination and proteasomal degradation. Biological significance and therapeutic implications of this study are discussed.

Telomere DNA repeats and telomerase: Classical view of telomere biology

Chromosome ends have repetitive DNA sequences called telomere DNA repeats. The unit of the repeats is 5'-TTAGGG-3' in mammals, and the total length of the repeats reaches approximately 3 to 15 kilobase pairs (Kb) in humans, depending on cell types as well as other intrinsic and extrinsic factors. A major determinant of the telomere length in normal human differentiated cells (e.g., fibroblasts, which is a cell type most commonly used in cell culture experiments *in vitro*) is their replicative history, i.e., the number of cell divisions the cells have undergone [1]. Because of the inability of conventional DNA polymerases to replicate the very end of linear DNA molecules (so-called "end replication problem"), these normal cells experience a progressive decline in telomere length, as an indicator of "cellular aging", in a cell division number-dependent manner. The presence of critically eroded telomeres in these cells is associated with the end of their replicative lifespan, a permanent growth arrest state called "replicative senescence" [1]. In contrast, germ cells, stem cells and cancer cells have a mechanism of synthesizing telomere DNA repeats to compensate the cell division-dependent telomere attrition, thereby bypassing the replicative senescence and being capable of self-replicating indefinitely [2]. Although ~10% of human cancers use a recombination-based mechanism (i.e., alternative lengthening of telomeres, ALT) [2], the major mechanism for telomere maintenance in human cells is the activation of a telomere G-rich strand-synthesizing enzyme, telomerase, which consists of the catalytic protein subunit (human telomerase reverse transcriptase, hTERT), the RNA component (hTER) containing a C-rich template region, and other associated proteins [3]. During a transition from normal mortal cells to immortalized, transformed cells, the transcriptional activation of the *hTERT* gene is a limiting step on which various cellular and viral oncogenic mechanisms act [4], including p53 inactivation [5]. Consistently, an ectopic expression of *hTERT* could lead to immortalization of normal human cells [6], and inhibition of *hTERT* in immortalized cancer cells could induce them to undergo senescence [7]. All of these findings accumulated from 1980's to late 1990's have supported "telomere hypothesis of cellular aging" to explain replicative senescence and immortalization of human cells.

Telomeres as a DNA-multiprotein complex: Specific structure and functions

Since mid-late 1990's a growing body of evidence has established that not only telomere length but also its specific DNA structure is a key factor for normal telomere functions, and that a number of proteins associated with telomere DNA repeats play physiological roles at telomeres [8]. Telomere DNA was revealed to form a lariat structure, which is named "t-loop", hiding chromosome ends into the structure and thus preventing them from undergoing illegitimate degradation or fusion events and from activating unwanted DNA damage signaling [9]. For the formation of this t-loop structure, a single-stranded, G-rich 3'-overhang at the extreme end of telomere DNA repeats plays an essential role by invading the double-stranded part of the repeats. The coordinated synthesis and processing of C-rich strand are required for the generation of 3'-overhang and thus essential for the telomere-specific DNA structure [10].

An increasing number of proteins have been shown to interact with telomere DNA repeats. Six of them (TRF1, TRF2, POT1, TIN2, TPP1 and RAP1) form a single telomere DNA-interacting complex, named "shelterin" [8]. TRF1 and TRF2 directly bind the double-stranded telomere repeats, POT1 directly binds to the single-stranded 3'-overhang, and the other three components interconnect these telomere-binding components. The shelterin complex is indispensable for the formation and maintenance of the telomere-specific DNA structure described above, as well as for distinguished recognition of telomeres from broken DNA ends. Specifically, TRF2 has an activity to enhance the t-loop formation [11] and can prevent ATM (ataxia telangiectasia mutated) kinase from initiating the DNA damage signaling at functional telomeres [12]. TRF2 interacts with ATM and inhibits its autophosphorylation critical for activation [13]. POT1 governs the integrity of telomere DNA ends at both G-rich 3'-overhang and C-rich 5'-recessed strand [14], as well as inhibits another DNA damage signaling kinase ATR (ATM- and Rad3-related) [12].

Taken all these findings together, we now recognize telomeres as a DNA-multiprotein complex with specific structure and functions, rather than only as an end of linear DNA molecules, and the concept of "telomere capping" has been established. The "capped" state of telomeres is primarily attributed to the t-loop structure of telomere DNA repeats and the recruitment and function of the shelterin complex [8,9]. Functional inhibition or knockdown of the shelterin components such as TRF2 and POT1 thus induced the "uncapped", or dysfunctional, state of telomeres, which was characterized by loss of 3'-overhang, telomere fusion-induced chromosome instability and activated DNA damage signaling [15-17]. The classical view of telomere biology described above, however, still stands together with the updated view: either telomeres that are long enough (e.g., in normal, non-senescent cells) or activated telomerase (e.g., in cancer cells), or both (e.g., in germ cells and stem cells) could contribute to the strength and stable maintenance of the capped state of telomeres [18]. Long telomeres could provide a platform for enhanced recruitment of telomere-binding proteins (e.g., TRF2) and a high efficiency of t-loop formation in the absence of telomerase activity. The ability of telomerase to synthesize G-rich telomere DNA strand could generate 3'-overhang sufficient for short telomeres to form a t-loop. Consistently, the presence of neither long telomeres nor telomerase activity (for example, critically short telomeres at the end of replicative lifespan in telomerase-negative normal cells [19], and telomerase inhibition in cancer cells with short telomeres [20]) causes the telomere uncapping-associated phenotypes similar to those induced by inhibition of the shelterin components.

p53 as a downstream effector of the telomere damage signaling

The tumor suppressor protein p53 is activated by endogenous or exogenous DNA damage and other cellular stresses through its posttranslational modifications such as phosphorylation, acetylation and sumoylation [21]. The p53-induced cellular phenotypes include apoptotic cell death and cellular senescence, each of which functions as a tumor suppressor mechanism and may have a role in organismal aging [22]. Classically, along with the telomere hypothesis of cellular aging, inhibition of p53 allowed normal human fibroblasts to continue proliferating even with shorter telomeres than the threshold length, suggesting that p53 was indispensable for the onset of telomere-initiated replicative cellular senescence [1]. With the concept of telomere capping, we now define uncapped or dysfunctional telomeres, which are functionally synonymous with eroded telomeres at the end of the cellular replicative lifespan [18,19], as an endogenous DNA damage that physiologically activates p53. Two major signaling kinases that phosphorylate and thereby activate p53 are ATM and ATR, which, as described above, are controlled by two shelterin components TRF2 and POT1, respectively [12]. ATM and p53 mediate the telomere uncapping-induced apoptosis or cellular senescence (for example, apoptosis in lymphocytes [23] and cellular senescence in fibroblasts [24]), establishing the TRF2-ATM-p53 pathway as a

downstream effector pathway of the DNA damage response initiated at uncapped telomeres. Although ATR may be less essential to telomere damage signaling in human cells with functional ATM and its downstream targets, it is still capable of inducing p53-dependent cellular senescence independently of ATM [25]. Thus, the POT1-ATR-p53 pathway can also signal the DNA damage response from uncapped telomeres.

p53 represses TRF2 protein levels through a p53-inducible E3 ubiquitin ligase Siah1

Comparing the expression profiles of endogenous mRNA or proteins in normal human cells at proliferating phase (referred "young") *versus* at replicative senescence has identified a number of senescence-associated genes and proteins. Our cell system consists of an isogenic pair of young and replicatively senescent human fibroblasts, in the latter of which p53 activation is evidenced by its phosphorylation at serine 15 residue and the upregulation of p53 target genes such as $p21^{WAF1}$ [26,27]. Among those identified by our previous studies using this cell system are: Δ133p53 and p53β (p53 isoforms) [26], POT1v5 (a POT1 isoform) [17], ING2 (a p53- and chromatin-interacting protein) [28], miR-34a (a p53-inducible microRNA) [26], and WNT16B (a member of WNT family of secreted proteins) [29]. Our recent study [27] adds TRF2 to the list of proteins whose expression levels are changed during replicative senescence. The expression levels of TRF2 protein were reduced in replicatively senescent fibroblasts, but TRF2 mRNA levels did not change, suggesting the regulation at a post-transcriptional or protein level. A series of experimental manipulation of p53 expression and activity, including spontaneous allelic loss, short hairpin RNA (shRNA)-mediated knockdown, dominant-negative inhibition, nutlin-3a activation and retroviral overexpression, all suggested that p53 represses TRF2 protein levels, again without a change in TRF2 mRNA expression.

Siah1 is an E3 ubiquitin ligase with a C3HC4-type RING finger domain. The *Siah1* gene is transcriptionally induced by p53 [30]. Siah1 targets proteins containing a Myb DNA-binding domain [31], which is present in TRF2 [15], for proteasome-mediated degradation. We have also found that TRF2 is a ubiquitinated protein and is subject to proteasome-mediated degradation [27]. All of these findings prompted us to examine whether Siah1 is responsible for the p53-mediated repression of TRF2 at the protein level. In the replicative senescence with activated p53 and all the experimental settings described above, Siah1 expression levels (both mRNA and protein levels) were inversely correlated with TRF2 protein levels: TRF2 upregulation was coincident with Siah1 downregulation when p53 was lost or inhibited; and TRF2 downregulation was coincident with Siah1 upregulation when p53 was overexpressed or nutlin-3a-activated [27]. The shRNA knockdown of Siah1 stabilized TRF2 protein by extending its half-life and, most importantly, Siah1 was found to physically interact with and ubiquitinate TRF2 in a manner dependent on its RING finger domain [27]. These data identified Siah1 as an E3 ubiquitin ligase that directly links p53 activation to TRF2 degradation, for the first time revealing that p53, a well-known downstream effector of the damage signaling from uncapped telomeres, also functions upstream to regulate a component of the telomere capping protein complex. Knockdown of endogenous Siah1 expression [27], as well as overexpression of TRF2 [32], delayed the onset of replicative senescence in human fibroblasts, suggesting that Siah1 co-operates with the other p53 target genes (e.g., $p21^{WAF1}$ and miR-34a) [26] in p53-regulated senescence.

TRF2-ATM-p53 positive feedback loop

p53 is engaged in a number of positive and negative feedback loops to regulate carcinogenesis, aging and other biological processes [33]. p53 and MDM2, which is a p53-induced E3 ubiquitin ligase and targets p53 for ubiquitination and proteasomal degradation, form a minimum feedback unit that takes part in several larger and more complex feedback loops. These feedback loops also link the p53 signaling pathway to other signal transduction pathways, including those involving the cyclin E/cdk2 complex, the p38 MAP kinase, the WNT/β-catenin cascade and the PTEN/AKT cascade [33]. Given that TRF2 functions to negatively control ATM [12,13] (Figure 1, blue line) and that ATM phosphorylates and activates p53 [24] (Figure 1, green line), as described above, our finding of the p53-Siah1-TRF2 pathway [27] (Figure 1, red lines) uncovers a novel feedback loop involving these factors: This TRF2-ATM-p53 feedback loop contains two inhibitory regulations (TRF2 ⊣ ATM and Siah1 ⊣ TRF2), thus functioning as a positive feedback mechanism (we would prefer the word "positive feedback", rather than "double-negative feedback", to indicate the functional consequence of the whole loop). Once telomere uncapping occurs either endogenously at the end of cellular replicative lifespan or exogenously by reagents and conditions inducing telomere dysfunction, diminished amount and/or impaired activity of TRF2 results in ATM activation. ATM-mediated activation of p53 then transcriptionally activates Siah1, which ubiquitinates and degrades TRF2, leading to further

decrease in TRF2 levels and thereby the maintenance and reinforcement of the uncapped state of telomeres.

The TRF2-ATM-p53 feedback loop amplifies telomere-initiated, p53-mediated DNA damage responses leading to the rapid induction of cellular senescence or apoptosis, which may prevent DNA damage-carrying cells from contributing to tumor formation.

Given the TRF2-ATM-p53 positive feedback loop, it is interesting to hypothesize that non-telomeric DNA damage and cellular stresses activating ATM and/or p53 may induce telomere uncapping through the repression of TRF2 protein levels. Consistent with this hypothesis, our preliminary data showed that doxorubicin-induced global DNA damage resulted in ubiquitination and down-regulation of TRF2 [27]. It should also be noted that the TRF2-ATM-p53 positive feedback loop can functionally interact with the previously identified feedback regulations (Figure 1, black lines). β-catenin, another degradation target of Siah1 [30], is known to activate p19/p14ARF, which inhibits MDM2 and thereby activates p53 [34]. This regulatory circuit may act as a negative feedback element for the TRF2-ATM-p53 positive feedback loop. While ATM can also activate p53 indirectly through the phosphorylation and inhibition of MDM2 [35], ATM-mediated phosphorylation of Siah1 may negatively affect its activity [36]. These co-operating and apparently opposing mechanisms are likely to add further strength and complexity to the DNA damage signaling from uncapped telomeres.

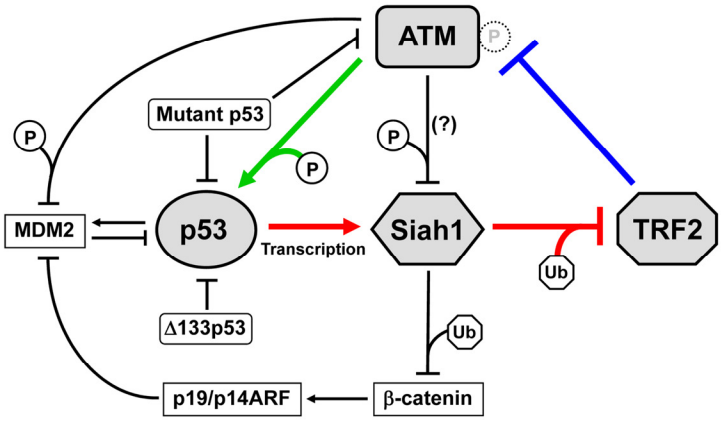

Figure 1. TRF2-ATM-p53 positive feedback loop. TRF2 interacts with ATM and inhibits its autophosphorylation and activation (blue line) [12,13]. ATM phosphorylates and activates p53 (green line) [23,24]. p53 transactivates Siah1, which targets TRF2 for ubiquitination and degradation (red lines) [27]. These regulatory mechanisms form a positive feedback loop. Mutant p53 abrogates this feedback loop through dominant-negative inhibition of wild-type p53 and a gain-of-function activity to inhibit ATM [48]. Δ133p53, a natural p53 isoform, also inhibits wild-type p53 [26]. The other factors that may functionally interact with this feedback loop (β-catenin, p19/p14ARF and MDM2) are also shown. P, phosphorylation. Ub, ubiquitination. Although ATM-mediated phosphorylation of Siah1 inhibits its interaction with a target protein (HIPK2) [36], it is unknown whether this mode of inhibition occurs for TRF2.

Perspectives

Our identification of the p53- and Siah1-mediated regulation of TRF2 largely depended on *in vitro* experiments using normal human fibroblasts in culture. However, there is evidence that this regulation also exists *in vivo*. Human colon adenomas, a premalignant tumor in which p53-mediated cellular senescence is pathologically induced *in vivo* [37,38], were shown to express higher levels of Siah1 and lower levels of TRF2 than normal non-senescent tissues [27], recapitulating the expression profile observed in senescent fibroblasts *in vitro*. Further studies will investigate the role of the TRF2-ATM-p53 feedback regulation in *in vivo* physiological senescence, aging-associated genome instability and organismal aging in humans.

An attribution of cellular senescence, or aging at the cellular level, to aging at the organ and organismal levels can be explained by an aging-associated decline in stem cell function [39-41]. Accumulated DNA damage at telomeric and non-telomeric loci in tissue-specific stem cells during aging could cause cellular senescence or apoptosis in those cells, leading to reduced tissue regeneration, impaired organ function and homeostasis, and eventually organismal senescence. Since a growing body of evidence suggests that p53 activity and telomere integrity are critical to the regulation of self-renewing and differentiating properties of embryonic and adult stem cells [39,42-44], the TRF2-ATM-p53 positive feedback loop should have significant relevance to stem cell biology and stem cell-based medicine.

p53 is the most frequently inactivated gene in human cancer [45,46], and therefore p53 replacement or restoration therapy is a therapeutic strategy against cancer. Telomeres have also been a promising target for cancer therapy: telomerase inhibitors can induce short telomeres in cancer cells to be uncapped [18]; and G-quadruplex ligands (e.g., telomestatin) reduce the amounts of G-rich 3'-overhang and remove POT1 and TRF2 from telomeric DNA, resulting in telomere uncapping [20,47]. We now know that these p53-based and telomere-based cancer therapies can co-operate in a single regulatory loop, namely the TRF2-ATM-p53 positive feedback loop. We expect that our findings will be experimental basis for combined application of p53-based therapy, telomere-based therapy and other strategies involving the associated factors such as β-catenin, p19/p14ARF and MDM2.

Some p53 missense mutations not only inhibit wild-type p53 activity but also gain a function that wild-type p53 does not have. One of such gain-of-function activities of mutant p53 is to inhibit ATM [48], which allows cancer cells to abrogate the TRF2-ATM-p53 feedback regulation in a more active manner than simply losing or inactivating wild-type p53. It will be of therapeutic interest to investigate whether small molecules that restore wild-type function to mutant p53 (e.g., CP-31398 and PRIMA-1) [49,50] can restore the TRF2-ATM-p53 positive feedback regulation in cancers with *p53* mutations. In cancers with wild-type *p53*, the expression of Δ133p53, a natural p53 isoform that inhibits wild-type p53 activity, is frequently elevated and thus Δ133p53 can be a therapeutic target [26]. Restoration of wild-type p53 activity by inhibition of Δ133p53 and the resulting degradation of TRF2 [26,27] may cause telomere uncapping-induced senescence or apoptosis through the TRF2-ATM-p53 positive feedback loop in cancers with wild-type *p53*.

Conclusion

p53 has long been linked to the regulation of telomeres. In the classical view of telomere length regulation, p53 was a mediator of telomere-induced replicative senescence, as well as a negative regulator of telomerase via hTERT inhibition. Upon identification of the telomere-capping shelterin complex, p53 has been established as a downstream effector of the DNA damage signaling emerging from a specific shelterin component at uncapped telomeres. With evidence that p53 directly controls the shelterin component in a feedback manner, much attention to p53 continues to come from basic research on telomere biology, as well as from translational and clinical research aiming at telomere-based therapies.

ACKNOWLEDGEMENTS

We thank Drs. David Lane, Jean-Christophe Bourdon, Borivoj Vojtesek, Ettore Appella, Lisa M. Jenkins and Abdul M. Mondal for fruitful collaborations.

CONFLICT OF INTERESTS STATEMENT

The authors of this manuscript have no conflict of interests to declare.

REFERENCES

1. Harley CB, Vaziri H, Counter CM, Allsopp RC. The telomere hypothesis of cellular aging. Exp Gerontol. 1992; 27: 375-382.

2. Colgin LM, Reddel RR. Telomere maintenance mechanisms and cellular immortalization. Curr Opin Genet Dev. 1999; 9: 97-103.

3. Collins K, Mitchell JR. Telomerase in the human organism. Oncogene. 2002; 21: 564-579.

4. Horikawa I, Barrett JC. Transcriptional regulation of the telomerase hTERT gene as a target for cellular and viral oncogenic mechanisms. Carcinogenesis. 2003; 24: 1167-1176.
5. Kanaya T, Kyo S, Hamada K, Takakura M, Kitagawa Y, Harada H et al. Adenoviral expression of p53 represses telomerase activity through down-regulation of human telomerase reverse transcriptase transcription. Clin Cancer Res. 2000; 6: 1239-1247.
6. Bodnar AG, Ouellette M, Frolkis M, Holt SE, Chiu CP, Morin GB et al. Extension of life-span by introduction of telomerase into normal human cells. Science. 1998; 279: 349-352.
7. Horikawa I, Oshimura M, Barrett JC. Repression of the telomerase catalytic subunit by a gene on human chromosome 3 that induces cellular senescence. Mol Carcinog. 1998; 22: 65-72.
8. de Lange T. Shelterin: the protein complex that shapes and safeguards human telomeres. Genes Dev. 2005; 19: 2100-2110.
9. de Lange T. Protection of mammalian telomeres. Oncogene. 2002; 21: 532-540.
10. Sfeir AJ, Chai W, Shay JW, Wright WE. Telomere-end processing: the terminal nucleotides of human chromosomes. Mol Cell. 2005; 18: 131-138.
11. Stansel RM, de Lange T, Griffith JD. T-loop assembly in vitro involves binding of TRF2 near the 3' telomeric overhang. EMBO J. 2001; 20: 5532-5540.
12. Denchi EL, de Lange T. Protection of telomeres through independent control of ATM and ATR by TRF2 and POT1. Nature. 2007; 448: 1068-1071.
13. Karlseder J, Hoke K, Mirzoeva OK, Bakkenist C, Kastan MB, Petrini JH et al. The telomeric protein TRF2 binds the ATM kinase and can inhibit the ATM-dependent DNA damage response. PLoS Biol. 2004; 2: E240.
14. Hockemeyer D, Sfeir AJ, Shay JW, Wright WE, de Lange T. POT1 protects telomeres from a transient DNA damage response and determines how human chromosomes end. EMBO J. 2005; 24: 2667-2678.
15. van Steensel B, Smogorzewska A, de Lange T. TRF2 protects human telomeres from end-to-end fusions. Cell. 1998; 92: 401-413.
16. Yang Q, Zheng YL, Harris CC. POT1 and TRF2 cooperate to maintain telomeric integrity. Mol Cell Biol. 2005; 25: 1070-1080.
17. Yang Q, Zhang R, Horikawa I, Fujita K, Afshar Y, Kokko A et al. Functional diversity of human protection of telomeres 1 isoforms in telomere protection and cellular senescence. Cancer Res. 2007; 67: 11677-11686.
18. Blackburn EH. Switching and signaling at the telomere. Cell. 2001; 106: 661-673.
19. Stewart SA, Ben Porath I, Carey VJ, O'Connor BF, Hahn WC, Weinberg RA. Erosion of the telomeric single-strand overhang at replicative senescence. Nat Genet. 2003; 33: 492-496.
20. Tahara H, Shin-Ya K, Seimiya H, Yamada H, Tsuruo T, Ide T. G-Quadruplex stabilization by telomestatin induces TRF2 protein dissociation from telomeres and anaphase bridge formation accompanied by loss of the 3' telomeric overhang in cancer cells. Oncogene. 2006; 25: 1955-1966.
21. Meek DW, Anderson CW. Posttranslational modification of p53: cooperative integrators of function. Cold Spring Harb Perspect Biol. 2009; 1: a000950.
22. Collado M, Blasco MA, Serrano M. Cellular senescence in cancer and aging. Cell. 2007; 130: 223-233.
23. Karlseder J, Broccoli D, Dai Y, Hardy S, de Lange T. p53- and ATM-dependent apoptosis induced by telomeres lacking TRF2. Science. 1999; 283: 1321-1325.
24. Herbig U, Jobling WA, Chen BP, Chen DJ, Sedivy JM. Telomere shortening triggers senescence of human cells through a pathway involving ATM, p53, and $p21^{CIP1}$, but not $p16^{INK4a}$. Mol Cell. 2004; 14: 501-513.
25. Toledo LI, Murga M, Gutierrez-Martinez P, Soria R, Fernandez-Capetillo O. ATR signaling can drive cells into senescence in the absence of DNA breaks. Genes Dev. 2008; 22: 297-302.
26. Fujita K, Mondal AM, Horikawa I, Nguyen GH, Kumamoto K, Sohn JJ et al. p53 isoforms Δ133p53 and p53β are endogenous regulators of replicative cellular senescence. Nat Cell Biol. 2009; 11: 1135-1142.
27. Fujita K, Horikawa I, Mondal AM, Jenkins LM, Appella E, Vojtesek B et al. Positive feedback between p53 and TRF2 during telomere-damage signalling and cellular senescence. Nat Cell Biol. 2010; 12: 1205-1212.
28. Pedeux R, Sengupta S, Shen JC, Demidov ON, Saito S, Onogi H et al. ING2 regulates the onset of replicative senescence by induction of p300-dependent p53 acetylation. Mol Cell Biol. 2005; 25: 6639-6648.
29. Binet R, Ythier D, Robles AI, Collado M, Larrieu D, Fonti C et al. WNT16B is a new marker of cellular senescence that regulates p53 activity and the phosphoinositide 3-kinase/AKT pathway. Cancer Res. 2009; 69: 9183-9191.
30. Matsuzawa SI, Reed JC. Siah-1, SIP, and Ebi collaborate in a novel pathway for β-catenin degradation linked to p53 responses. Mol Cell. 2001; 7: 915-926.
31. Tanikawa J, Ichikawa-Iwata E, Kanei-Ishii C, Nakai A, Matsuzawa S, Reed JC et al. p53 suppresses the c-Myb-induced activation of heat shock transcription factor 3. J Biol Chem. 2000; 275: 15578-15585.
32. Karlseder J, Smogorzewska A, de Lange T. Senescence induced by altered telomere state, not telomere loss. Science. 2002; 295: 2446-2449.
33. Harris SL, Levine AJ. The p53 pathway: positive and negative feedback loops. Oncogene. 2005; 24: 2899-2908.
34. Saegusa M, Hashimura M, Kuwata T, Hamano M, Okayasu I. β-catenin simultaneously induces activation of the p53-$p21^{WAF1}$ pathway and overexpression of cyclin D1 during squamous differentiation of endometrial carcinoma cells. Am J Pathol. 2004; 164: 1739-1749.
35. Maya R, Balass M, Kim ST, Shkedy D, Leal JF, Shifman O et al. ATM-dependent phosphorylation of Mdm2 on serine 395: role in p53 activation by DNA damage. Genes Dev. 2001; 15: 1067-1077.
36. Winter M, Sombroek D, Dauth I, Moehlenbrink J, Scheuermann K, Crone J et al. Control of HIPK2 stability by ubiquitin ligase Siah-1 and checkpoint kinases ATM and ATR. Nat Cell Biol. 2008; 10: 812-824.
37. Collado M, Gil J, Efeyan A, Guerra C, Schuhmacher AJ, Barradas M et al. Tumour biology: senescence in premalignant tumours. Nature. 2005; 436: 642.
38. Kuilman T, Michaloglou C, Vredeveld LC, Douma S, van Doorn R, Desmet CJ et al. Oncogene-induced senescence relayed by an interleukin-dependent inflammatory network. Cell. 2008; 133: 1019-1031.

39. Jaskelioff M, Muller FL, Paik JH, Thomas E, Jiang S, Adams AC et al. Telomerase reactivation reverses tissue degeneration in aged telomerase-deficient mice. Nature. 2011; 469: 102-106.
40. Rossi DJ, Jamieson CH, Weissman IL. Stems cells and the pathways to aging and cancer. Cell. 2008; 132: 681-696.
41. Sharpless NE, DePinho RA. How stem cells age and why this makes us grow old. Nat Rev Mol Cell Biol. 2007; 8: 703-713.
42. Begus-Nahrmann Y, Lechel A, Obenauf AC, Nalapareddy K, Peit E, Hoffmann E et al. p53 deletion impairs clearance of chromosomal-instable stem cells in aging telomere-dysfunctional mice. Nat Genet. 2009; 41: 1138-1143.
43. Cicalese A, Bonizzi G, Pasi CE, Faretta M, Ronzoni S, Giulini B et al. The tumor suppressor p53 regulates polarity of self-renewing divisions in mammary stem cells. Cell. 2009; 138: 1083-1095.
44. Nalapareddy K, Jiang H, Guachalla Gutierrez LM, Rudolph KL. Determining the influence of telomere dysfunction and DNA damage on stem and progenitor cell aging: what markers can we use? Exp Gerontol. 2008; 43: 998-1004.
45. Hollstein M, Sidransky D, Vogelstein B, Harris CC. p53 mutations in human cancers. Science. 1991; 253: 49-53.
46. Hollstein M, Shomer B, Greenblatt M, Soussi T, Hovig E, Montesano R et al. Somatic point mutations in the p53 gene of human tumors and cell lines: updated compilation. Nucleic Acids Res. 1996; 24: 141-146.
47. Gomez D, Wenner T, Brassart B, Douarre C, O'Donohue MF, El K, V et al. Telomestatin-induced telomere uncapping is modulated by POT1 through G-overhang extension in HT1080 human tumor cells. J Biol Chem. 2006; 281: 38721-38729.
48. Song H, Hollstein M, Xu Y. p53 gain-of-function cancer mutants induce genetic instability by inactivating ATM. Nat Cell Biol. 2007; 9: 573-580.
49. Foster BA, Coffey HA, Morin MJ, Rastinejad F. Pharmacological rescue of mutant p53 conformation and function. Science. 1999; 286: 2507-2510.
50. Lambert JM, Gorzov P, Veprintsev DB, Soderqvist M, Segerback D, Bergman J et al. PRIMA-1 reactivates mutant p53 by covalent binding to the core domain. Cancer Cell. 2009; 15: 376-388.

Research Paper

HIF-1α antagonizes p53-mediated apoptosis by triggering HIPK2 degradation

Lavinia Nardinocchi[1], Rosa Puca[1,2], Gabriella D'Orazi[1,2]

[1] *Department of Experimental Oncology, Molecular Oncogenesis Laboratory, National Cancer Institute "Regina Elena", Rome, Italy*

[2] *Department of Oncology and Experimental Medicine, University "G. d'Annunzio", Chieti, Italy*

Key words: *HIF-1α, HIPK2, zinc, proteasomal degradation, p53 transcriptional activity, p53Ser46*
Received: *12/13/10; Accepted: 12/28/10; Published: 1/18/11*
Corresponding author: *Gabriella D'Orazi, MD/PhD;* ***E-mail:*** *gdorazi@unich.it*

Copyright: *© Nardinocchi et al. This is an open-access article distributed under the terms of the Creative Commons Attribution License, which permits unrestricted use, distribution, and reproduction in any medium, provided the original author and source are credited*

Abstract: Many human diseases are characterized by the development of tissue hypoxia. Hypoxia-inducible factor (HIF) is a transcription factor that regulates fundamental cellular processes in response to changes in oxygen concentration, such as angiogenesis, survival, and alterations in metabolism. The levels of HIF-1α subunit are increased in most solid tumors not only by low oxygen but also by growth factors and oncogenes and correlate with patient prognosis and treatment failure. The link between HIF-1α and apoptosis, a major determinant of cancer progression and treatment outcome, is poorly understood. Here we show that HIF-1α protects against drug-induced apoptosis by antagonizing the function of the tumor suppressor p53. HIF-1α upregulation induced proteasomal degradation of homeodomain-interacting protein kinase-2 (HIPK2), the p53 apoptotic activator. Inhibition of HIF-1α by siRNA, HIF-1α-dominant negative or by zinc re-established the HIPK2 levels and the p53-mediated chemosensitivity in tumor cells. Our findings identify a novel circuitry between HIF-1α and p53, and provide a paradigm for HIPK2 dictating cell response to antitumor therapies.

INTRODUCTION

HIPK2 is a potential tumor suppressor gene; it is a nuclear serine/threonine kinase that acts as co-repressors for transcription factors [1] and is considered a central switch in the targeting of cells toward apoptosis upon genotoxic stress by phosphorylating tumor suppressor p53 at serine 46 (Ser46) [2,3]. The p53Ser46 modification triggers irreversible apoptosis by determining p53-dependent promoter selection [4]. HIPK2 contributes to p53 apoptotic activation by inducing Ser46 phosphorylation but also lysine 382 (Lys382) acetylation [2,3,5]. Thus, we found that HIPK2, through repression of Nox1 gene, strongly regulates p53 acetylation/deacetylation balance that along with (p)Ser46 is important for full p53 apoptotic activity [6]. A major determinant of tumor progression and cancer therapy is the ability of cancer cells to activate apoptotic cell death, mainly through intact p53 function. Understanding how aberrant signalling within tumors can interfere with p53 apoptotic activation is therefore of particular importance. Although mutations in the p53 gene are detected in ~50% of human cancers, indirect mechanism also leads to p53 inactivation [7]. Previous work has shown that knock-down of HIPK2, mainly by siRNA, leads to loss of p53 function, reduced apoptotic drug-response and increased tumor progression [8]. Therefore, an intact HIPK2 function is crucial for the apoptotic activation of wtp53 in tumors.

A physiological condition that inhibits HIPK2 functions in solid tumor is hypoxia which is a hallmark of tumor progression and failure of tumor therapies. Hypoxia-induced ubiquitin ligases such as Siah2 [9] or p53 targets MDM2 [10] and Siah1 [11] trigger HIPK2 degradation strongly affecting drug-induced p53 apoptotic activity. The key molecule expressed under hypoxia is hypoxia inducible factor-1 (HIF-1), a

heterodimeric transcription factor that consists of the HIF-1β subunit, constitutively expressed in cells, and the oxygen-sensitive HIF-1α subunit. Under normal oxygen levels, HIF-1α is hydroxylated at key proline residues facilitating interaction to von Hippel-Lindau protein (pVHL) which allows HIF-1α proteasomal degradation. Under hypoxic conditions, prolyl hydroxylation is inhibited, HIF-1α accumulates, dimerizes with HIF-1β forming the active HIF-1 complex for regulation of transcription of several genes involved in many aspects of cancer progression, including angiogenesis, metabolic adaptation, apoptosis resistance, invasion and metastasis [12]. HIF-1α synthesis and transactivation can also be activated by non-hypoxia-mediated mechanisms such as genetic alterations in a variety of cancer types. In this regard, we have shown that HIPK2 represses the HIF-1α transcription, thus, HIPK2 knock-down leads to HIF-1α upregulation with induction of a "constitutive hypoxic" phenotype [13]. Increased HIF-1α levels have been shown to be associated with increased resistance to conventional chemo- and radiotherapy in many solid tumors and play a negative role in patient prognosis. Thus, the downregulation of the activity of HIF-1α could have an immediate effect on its target genes contributing to blocking tumor angiogenesis, glycolysis and tumor growth and also improve the efficacy of classical therapies [14].

HIF-1α interacts with p53 and stimulates p53 transcriptional activity [15] although it antagonizes p53-mediated apoptosis [16]. Here we report a previously unknown regulatory circuitry between HIF-1α, HIPK2 and p53 apoptotic activity as the molecular mechanisms underlying HIPK2 regulation by HIF-1α have never been addressed.

RESULTS AND DISCUSSION

We first analyzed the effect of HIF-1α on DNA-damage-induced p53 apoptotic activation by using an *ex vivo* experimental model consisting of cell populations derived from explants of prostate cancer patients characterized by stabilized HIF-1α protein in normoxia ("constitutively hypoxic" phenotype) and associated with bad prognosis (namely C27 cells), and cell populations with a phenotype negative for HIF-1α expression under aerobic condition associated with good prognosis (namely C38 cells) [17]. The presence of HIF-1α overexpression at mRNA (Figure 1A) and protein level (see Figure 2F) in C27 cells led to a marked inhibition of drug-induced luciferase activity of the p53AIP1 reporter gene (Figure 1B and Supplementary Figure 1a) which is a well established target of p53-Ser46 modification and of p53 apoptotic activity [4]. Thus, in response to X-ray or to the radiomimetic drug bleomycin, both Ser46 phosphorylation, the cleavage of the apoptotic marker PARP, and p53 apoptotic gene

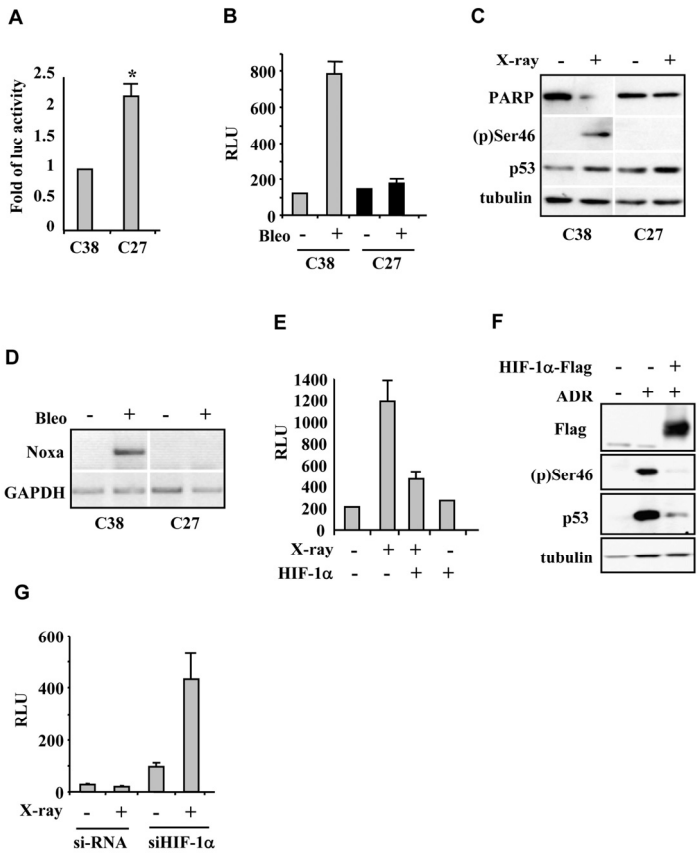

Figure 1. HIF-1α antagonizes p53 apoptotic activity. (**A**) Luciferase assay in C38 and C27 prostate cancer cells showed significantly higher HIF-1α-luc promoter activity in C27 cells. **P*=0.0159. (**B**) Luciferase assay of p53AIP1-luc reporter in C38 and C27 prostate cancer cells after bleomycin (Bleo) treatment showing impairment of p53 transcriptional activity in C27 cells. (**C**) Immunoblot of C38 and C27 cells after 40 Gy X-irradiation revealed PARP cleavage and Ser46 phosphorylation only in C38 cells. Blot image was cut and pasted. (**D**) RT-PCR analysis of p53 apoptotic target genes in C38 and C27 prostate cancer cells after bleomycin (Bleo) treatment. Gel image was cut and pasted. (**E**) Luciferase assay of p53 target Noxa-luc reporter in C38 cells after X-irradiation revealed impairment of luciferase activity after HIF-1α overexpression. (**F**) Immunoblot of RKO cells after adriamycin (ADR) treatment showed abolishment of (p)Ser46 after HIF-1α-Flag overexpression. (**G**) Luciferase assay of p53AIP1-luc reporter in C27 cells showed induction of luciferase activity after HIF-1α silencing with siRNA.

transcription were impaired in HIF-1α upregulated C27 cells, compared to C38 cells negative for HIF-1α expression under aerobic condition (Figure 1C, 1D**)**. Two lines of evidence indicate that the p53 apoptotic defect in C27 cells is due to stabilization of HIF-1α rather than to alternative mechanism of drug resistance or impairment of p53 downstream signalling. First, increasing HIF-1α levels in C38 prostate and RKO colon cancer cells by protein overexpression also conferred resistance to X-ray- or to drug-induced p53 transcriptional activity (Figure 1E and Supplementary Figure S1b, S1c) and inhibited Ser46 phosphorylation (Figure 1F). Second, loss of HIF-1 function by HIF-1α knock-down, restored the sensitivity to X-ray-induced p53AIP1-luciferase activity in C27 cells (Figure 1G). These results show that HIF-1α levels are relevant to the p53-mediated cellular response because they antagonized drug-induced p53Ser46 apoptotic transcriptional activity.

P53Ser46 phosphorylation is triggered by several kinases including HIPK2 whose knock-down strongly inhibits p53 apoptotic activity [5,8]. Therefore, an intact HIPK2 function is crucial for the apoptotic activation of wtp53 in tumors. We first evaluated whether HIF-1α affected HIPK2 mRNA expression. RT-PCR analyses of ADR-treated RKO cells showed that endogenous HIPK2 messenger RNA levels were not altered by HIF-1α upregulation (Supplementary Figure S1c**)**, although HIF-1α inhibited the drug-induced p53(p)Ser46 (Figure 1F), arguing for HIF-1α-mediated regulation of HIPK2 at the post-transcriptional level. We then performed experiments under conditions of HIF-1α and HIPK2 overexpression. Expression of increasing amounts of HIF-1α in 293 cells correlated with abolishment of HIPK2 protein levels (Figure 2A). A test for protein degradation showed that HIF-1α-induced HIPK2 downregulation in prostate C38 cells could be rescued by cell treatment with the proteasome inhibitor MG132 (Figure 2B), confirming a HIPK2 post-translational regulation. Thus, HIF-1α co-overexpression did not affect HIPK2 gene transcription in RKO colon cancer cells (Figure 2C). We next analysed these issues in C27 prostate cancer cells whereas HIF-1α upregulation antagonizes drug-induced p53Ser46 apoptotic transcriptional activity, suggesting that they should harbour reduced HIPK2 levels. Indeed, western blot analysis showed reduced HIPK2 protein levels in "constitutively hypoxic" C27 cells compared to the C38 cells with a phenotype negative for HIF-1α expression under aerobic condition (Figure 2D), while the HIPK2 mRNA levels were comparable expressed between the two cell lines (Figure 2E). Was the reduction of HIPK2 levels caused by HIF-1α upregulation? We addressed this issue by silencing of HIF-1α with siRNA that indeed rescued HIPK2 protein levels in C27 cells (Figure 2F). We thus conclude that HIF-1α regulates HIPK2 stability.

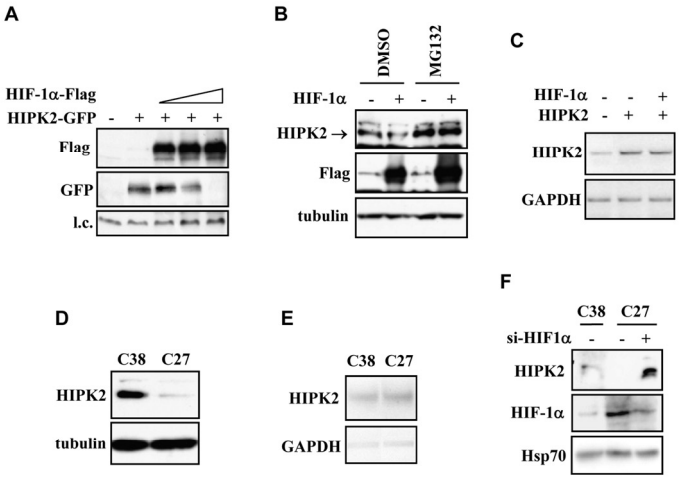

Figure 2. HIF-1α regulates HIPK2 protein degradation. (**A**) HIF-1α-Flag (4, 6, and 8 μg) and HIPK2-GFP (4 μg) expression vectors were co-transfected in 293 cells where immunoblot analyses showed that increased amounts of HIF-1α induced HIPK2 abolishment. (**B**) Immunoblot analysis of C38 cells transfected with HIF-1α expression and treated with proteasome inhibitor MG132 (10 μM for 4 h) or DMSO vehicle. The endogenous HIPK2 levels downregulated by HIF-1α were rescued by MG132. (**C**) RT-PCR analysis of HIPK2 in RKO colon cancer cells co-transfected with HIF-1α and HIPK2 expression vector. (**D**) Immunoblot of endogenous HIPK2 protein in C38 and C27 prostate cancer cells, showing lower HIPK2 levels in "constitutive hypoxic" C27 cells. (**E**) The HIPK2 mRNA levels were comparable between C38 and C27 cells. (**F**) Immunoblot in C27 cells showed rescue of endogenous HIPK2 protein levels after HIF-1α knock-down by siRNA.

How could HIF-1α inhibit HIPK2? First, being a transcription factor, HIF-1 might promote the expression of target genes that induce HIPK2 degradation. Alternatively, HIF-1 might directly interact with and regulate HIPK2. To discriminate between these two scenarios, exogenous HIPK2 and HIF-1α proteins were co-expressed in 293 cells for co-immunoprecipitation analysis. We found absence of interaction between HIPK2 and HIF-1α (Supplementary Figure S2a), suggesting rather a transcription-dependent regulation. The latter hypothesis was evaluated by the use of a HIF-1α mutant encoding the dominant negative form of HIF-1α without DNA binding and trans-activation domains (HIF-1αDN) [18]. The results unequivocally showed that the HIF-1αDN mutant could not inhibit HIPK2 stability (Supplementary Figure S2b).

Previous studies showed that HIF-1 may induce p53 transcriptional activity [15], although not the apoptotic one [16], and that p53 target genes such as MDM2 [10] or Siah1 [11] may trigger HIPK2 degradation under hypoxia. Moreover, the putative HIF-1 target WD40-repeat/SOCS box protein WSB-1 [19] has been shown to trigger HIPK2 degradation [20]. To evaluate whether p53 transcriptional activity plays a role in HIF-1α-induced HIPK2 degradation, HIF-1α and HIPK2 proteins were co-expressed in H1299 lung cancer (p53 null) cells and assayed for western immunoblotting. In the absence of p53, HIF-1α was still able to reduce HIPK2 protein levels (Supplementary Figure S2c). We conclude that HIF-1α inhibits HIPK2 *via* transcriptional upregulation of one or more target genes.

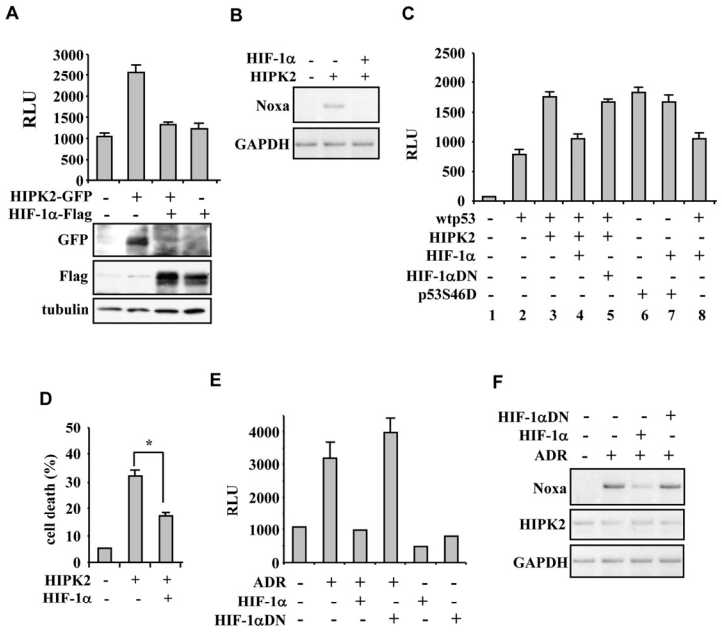

Figure 3. **HIPK2-induced p53 apoptotic activity is impaired by HIF-1α**. (**A**) Luciferase assay in 293 cells co-transfected with Noxa-luc reporter and HIPK2-GFP (4 μg) expression vector alone or in combination with HIF-1α-Flag (8 μg). Results represent mean ± s.d. from three experiments. The expression of the ectopic proteins was assayed by immunoblot. (**B**) Lysates from RKO cells co-transfected with HIF-1α and HIPK2 expression vectors were assayed for RT-PCR of p53 target gene Noxa. GAPDH is a loading control (**C**) Luciferase assay in H1299 cells co-transfected with Noxa-luc reporter and low amount of wtp53 expression vector or of p53S46D mutant, in combination with HIPK2, HIF-1α or HIF-1αDN mutant. Results represent mean ± s.d. from three experiments. (**D**) Tunel assay of RKO cells where HIF-1α overexpression significantly reduced the HIPK2-induced apoptotic cell death. **P*=0.001. (**E**) Luciferase assay in RKO cells stable transfected with p53AIP1-luc reporter where the adryamicin (ADR)-induced luciferase activity was inhibited by HIF-1α overexpression but not by HIF-1α dominat negative (DN) mutant. Results represent mean ± s.d. from three experiments. (**F**) Lysates from RKO cells treated as indicated were assayed for RT-PCR analyses of p53 apoptotic target Noxa and for HIPK2 expression. GAPDH is a loading control.

The above results demonstrate that HIF-1α upregulation reduces both HIPK2 protein levels and p53 apoptotic activation. The direct effect of HIF-1α on HIPK2-induced p53 activation was then analysed under conditions of proteins overexpression. The luciferase assay performed in 293 cells clearly showed that the positive effect of HIPK2 on endogenous p53 apoptotic transcriptional activity was eliminated by HIF-1α co-expression that indeed abolished HIPK2 levels (Figure 3A). The abolishment of p53 transcriptional activity was confirmed *in vivo* in RKO cells by RT-PCR analysis (Figure 3B). We then performed experiments with p53 overexpression in H1299 cells. HIF-1α abolished the HIPK2 additive effect on p53-induced Noxa-luc activity (Figure 3C, compare lane 3 with lane 2 and lane 4 with lane 3), while HIF-1αDN mutant failed to do so (Figure 3C, compare lane 5 with lane 4), suggesting that HIF-1α is acting on HIPK2 function. To finally demonstrate this issue, the transcriptional activity of a p53S46D mutant, which expresses constitutive Ser46 phosphorylation, was not inhibited by HIF-1α (Figure 3C, compare lane 7 with lane 6), confirming that HIPK2 is indeed the target of HIF-1α-induced p53 regulation. Next, we investigated the effect of HIPK2 inhibition on apoptosis. The results clearly showed that HIF-1α significantly counteracted HIPK2-induced cell death (Figure 3D). Finally, HIF-1α overexpression led to marked reduction of ADR-induced p53AIP1-luc activity in RKO cells, while the HIF-1α-DN mutant did not show such effect (Figure 3E), as also tested by *in vivo* by RT-PCR analyses (Figure 3F). These results recapitulate the negative effect of constitutive hypoxic phenotype on HIPK2-induced p53 apoptotic transcriptional activity and cell response to drug.

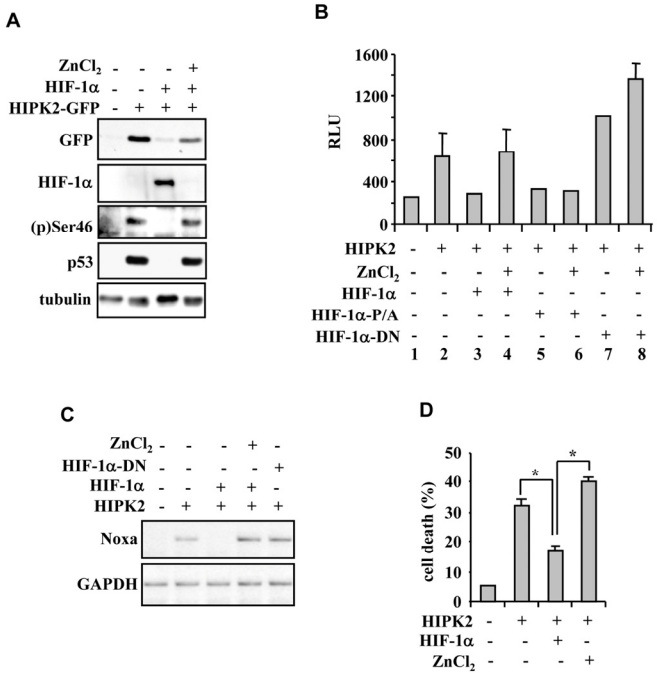

Figure 4. Zinc reactivates the HIF-1α-inhibited HIPK2/p53 signalling. (**A**) Immunoblot of RKO cells in which the effect of HIPK2 overexpression on p53Ser46 phosphorylation was abolished by HIF-1α co-expression and restored by concomitant zinc (100 μm for 24 h) treatment. (**B**) Luciferase assay in RKO cells stable transfected with p53AIP1-luc reporter showing that the HIPK2-induced luciferase activity was inhibited by HIF-1α and rescued by zinc treatment (100 μm for 24 h); zinc did not rescued the HIPK2 inhibition triggered by the HIF-1αP/A mutant and the HIF-1αDNA mutant did not inhibit HIPK2-induced transcriptional activity. Results represent mean ± s.d. from three experiments. (**C**) Lysates from RKO cells treated as indicated were assayed for RT-PCR analyses of p53 apoptotic target Noxa. GAPDH is a loading control. (**D**) Tunel assay of RKO cells showing that the HIPK2-induced apoptotic cell death was significantly inhibited by HIF-1α and strongly rescued by zinc treatment. **P*=0.001.

We recently reported that zinc inhibits HIF-1α stability *in vitro* and *in vivo* by acting on prolyl hydroxylation and VHL interaction [21]. We also showed that zinc inhibits MDM2 ubiquitin ligase activity, counteracting MDM2-induced p53 degradation and re-establishing HIPK2 stability [22]. Restoration of wtp53 function is decisive for the success of anti-tumor therapies and for tumor regression *in vivo* [23,24]. Therefore, zinc treatment of tumor cells with HIF-1α upregulation and that retain wild-type p53 should result in (*i*) reconstitution of HIPK2-induced p53Se46 phosphorylation, (*ii*) activation of p53-apoptotic genes and (*iii*) restoration of drug-induced apoptosis. The HIPK2-induced p53(p)Ser46 in RKO cells, abolished by HIF-1α co-expression, was completely re-established by zinc treatment that, as expected, concomitantly rescued the HIF-1α-induced HIPK2 downregulation (Figure 4A). The HIPK2-induced p53 transcription of p53AIP1-luc reporter, inhibited by HIF-1α, was strongly recovered by zinc treatment (Figure 4B, compare lane 4 with lane 3), while the inhibition triggered by a HIF-1α expression vector with prolyl mutations P402A and P564A (HIF-1αP/A) was not rescued by zinc (Figure 4B, compare lane 6 with lane 5), in agreement with our findings that the HIF-1αP/A mutant is not downregulated by zinc [21]; finally, the HIF-1αDN mutant did not inhibit the HIPK2-induced p53AIP1-luc activity (Figure 4B, compare lane 7 with lanes 5 or 3) that was rather superinduced by zinc (Figure 4B, compare lane 8 with lane 7), suggesting inhibition of endogenous HIF-1α by the HIF-1αDN mutant. The positive effect of zinc on rescue of HIPK2/p53 activity in the presence of HIF-1α upregulation was confirmed by *in vivo* RT-PCR analysis of p53 apoptotic target genes (Figure 4C) and by cell death analysis (Figure 4D).

The above results demonstrate that zinc treatment counteracts the HIF-1α-mediated inhibition of HIPK2, allowing restoration of p53 response to antitumor therapies. Thus, this issue was addressed in C27 prostate cancer cells in which both HIPK2 and p53 are disabled by constitutive HIF-1α upregulation. The results clearly showed that zinc restored (*i*) the endogenous p53 transcriptional activity in response to X-irradiation, (*ii*) the *in vivo* transcription of p53 target genes in response to drug and (*iii*) the cell death to genotoxicity (Supplementary Figure S3a-c), again implicating the HIF-1α/HIPK2 circuitry as shown by rescue of endogenous HIPK2 stability by zinc (Supplementary Figure S3d). These results are consistent with several observations by us showing that zinc supplementation can increase tumor response to drugs and counteract the negative effect of hypoxia, by acting on several interconnected signalling molecules such as HIPK2, HIF-1 and p53 [25].

Restoration of HIPK2 activity was finally monitored by chromatin immunoprecipitation assay as HIPK2 is able to modulate the transcription of several factors involved in cell survival and apoptosis [1]. The results showed that HIPK2 recruitment onto target genes such as *Bcl-2* [26] or *CYP1B1* [9] was present in basal condition only in C38 cells compared to the C27 cells where it was instead rescued by zinc treatment (Supplementary Figure S4). HIPK2 recruitment onto *Bcl-2* promoter is again indicative of functioning p53 as HIPK2 has been shown to be involved in the transcriptional repression of *Bcl-2* promoter exerted by p53 [26].

HIF-1α stabilization due to low oxygen or because genetic alterations is responsible of increased chemo-resistance and tumor cell viability in part due to inhibition of p53 apoptotic gene transcription [10]. The discovery here of the HIF-1α/HIPK2 circuitry gives a mechanistic explanation of the p53 apoptotic inhibition in response to drug under hypoxia in those tumors that retain a not functional wild-type p53. Thus, for the first time, it is shown a direct effect of HIF-1α on HIPK2 protein stability. Moreover, our findings also open novel and unexpected scenarios in tumor development and ask to whether HIPK2 might participate to the regulation of cancer stem cells (SCs). Hypoxia and HIFs-α subunits are considered a critical component of a cancer stem cell niche in different tumors including glioblastoma [27] and stem-like cells may be integral to the development and maintenance of human cancers [28]. Our data raise the possibility that HIPK2, because of the HIF-1α relationship is involved in the homeostasis of cancer SCs and in its subversion in tumors. Recent findings showed that loss of p53 favours symmetric divisions of cancer SCs, contributing to tumor growth [29]. As HIPK2 inhibition negatively affects p53 activity [8,30] it would be interesting to evaluate whether loss of p53 function in cancer SCs depends on HIF-1α-induced HIPK2 inhibition and propose an additional mechanism of tumorigenesis. Identification of the cell types capable of initiating and sustaining growth of the neoplastic clone *in vivo* is a fundamental problem in cancer research. Understanding the nature of the more quiescent cancer stem-like cells and their niches has the potential to development of novel cancer therapeutic protocols including pharmacological targeting of self-renewal pathways. Therefore, our data strengthen the notion that unleashing the growth suppressor activity of both HIPK2 and p53 by targeting HIF-1α with zinc is a

potentially valuable adjuvant strategy for cancer treatment.

METHODS

Cell culture and treatments. Human patients-derived prostate cancer cell lines C38 and C27, [17,31] (kindly provided by A. Farsetti, National Research Council, Rome, Italy), human embryo kidney 293, were maintained in DMEM (Life Technology-Invitrogen), while human lung cancer H1299 (p53 null) and colon cancer RKO were maintained in RPMI-1640 (Life Technology-Invitrogen), all supplemented with 10% heat-inactivated fetal bovine serum plus glutamine and antibiotics.

Subconfluent cells were treated with adriamycin (ADR) diluted into the medium to a final concentration of 1.5 μg/ml, bleomycin (Bleo) diluted into the medium to a final concentration of 120 μM, zinc chloride ($ZnCl_2$) diluted into the medium to a final concentration of 100 μM, or X-ray irradiated with 40 Gy, for the indicated period of time. Proteasome inhibitor MG132 at final concentration of 10 μM was added for 4 h.

Western blotting and co-immunoprecipitation. Total cell extracts and nuclear extracts were prepared essentially as described [13]. Proteins were transferred to a polyvinylidene difluoride (PVDF) (Millipore) or nitrocellulose (Biorad) membranes. Immunoblottings were performed with the following antibodies: mouse monoclonal anti-HIF-1α, (Novus Biologicals), mouse monoclonal anti-p53 (DO1) (Santa Cruz Biotechnology), rabbit polyclonal anti-phospho-Ser46, (Cell Signaling Technology), rabbit polyclonal anti-HIPK2 (kindly provided by M.L. Schmitz, Justus-Liebig-University, Giessen, Germany), mouse monoclonal anti-poly(ADP-ribose) polymerase (PARP, BD Pharmingen), monoclonal anti-GFP (Roche Diagnostic), mouse monoclonal anti-Flag (Sigma), mouse monoclonal anti-tubulin (Immunological Sciences), and mouse monoclonal anti-Hsp70 (Stressgene). Immunoreactivity was detected by enhanced chemiluminescence kit (ECL; Amersham). For HIF-1α/HIPK2 co-immunoprecipitation 293 cells were co-transfected with 4 μg HIPK2-GFP and 8 μg HIF-1α-Flag expression vector for 24 h. Total cell extracts were prepared by incubating at 4^0 C for 30 min in lysis buffer (20 mmol/L Hepes, 100 mmol/L NaCl, 5 mM EDTA (pH 8.0), 10% glicerol). Following preclearing for 1 h at 4^0 C, immunoprecipitation was performed by incubating total cell extracts with anti-Flag antibody pre-adsorbed to protein G-Agarose (Pierce), rocking for 2 h at 4^0 C. The beads were then resuspended in 5x Laemmli buffer and subjected to Western blot with the indicated primary antibodies.

RNA extraction and reverse transcription (RT)-PCR analysis. Cells were harvested in TRIzol Reagent (Invitrogen) and total RNA was isolated following the manufacturer's instructions essentially as described [30]. PCR was performed by using gene specific oligonucleotides under conditions of linear amplification. PCR products were run on a 2% agarose gel and visualized by ethidium bromide staining using UV light. The housekeeping GAPDH mRNA was used as internal control.

Transfection, plasmids and transactivation assay. Cells (RKO, C27 C38) were transfected with the cationic polymer LipofectaminePlus method (Invitrogen) according to manufacturers' instructions or (293 and H1299) with the N,N-bis-(2- hydroxyethyl)-2-amino-ethanesulphonic acid-buffered saline (BBS) version of the calcium phosphate procedure [32].

For luciferase activity the plasmid reporter used were: the HIF-1α-pH800-luc promoter (kindly provided by C. Michiels, FUNDP-University of Namur, Belgium), the p53-dependent promoters Noxa-luc (kindly provided by T. Taniguchi, University of Tokyo, Japan) and p53AIP1-luc (kindly provided by H. Arakawa, National Cancer Center, Tokyo, Japan). The amount of plasmid DNA in each sample was equalized by supplementing with empty vector. Transfection efficiency was normalized with the use of a co-transfected β-galactosidase (β-gal) plasmid. Luciferase activity was assayed on whole cell extract and the luciferase values were normalized to β-galactosidase activity and protein content and expressed as relative luciferase unit (RLU). The expression vectors used were: the Flag-tagged HIF-1α and the Flag-tagged HIF-1α with prolyl mutations P402A and P564A [33] (kindly provided by G.L. Semenza, The Johns Hopkins University School of Medicine, Baltimore, MD, USA), the dominant negative form of HIF-1α without DNA binding domain and transactivation domain (pCEP4-HIF-1αDN) [18] (kindly provided by B.H. Jiang, Nanjing Medical University, China), HIPK2-GFP [2], pCMV-wtp53, and the p53Ser46D (constitutively phosphorylated) (kindly provided by Dr. L Mayo, Case Western Reserve University, Cleveland, Ohio, USA) mutant.

siRNA interference. Cells were plated at semiconfluence in 35 mm dishes the day before transfection. Control-siRNA and siHIF-1α (Dharmacon) were transfected overnight using LipofectaminePlus reagent (Invitrogen) and 24 h later cells were trypsinized and replated and

transfected for the indicated period before harvesting for luciferase activity.

Chromatin Immunoprecipitation (ChIP) assay. Chromatin Immunoprecipitation (ChIP) analysis was carried out essentially as described [30]. Protein complexes were cross-linked to DNA in living cells by adding formaldehyde directly to the cell vulture medium at 1% final concentration. Chromatin extracts containing DNA fragments with an average size of 500 bp were incubated overnight at 4^0 C with milk shaking using rabbit polyclonal anti-HIPK2 (Santa Cruz Biotechnology) antibody. Before use, protein G (Pierce) was blocked with 1 μg/μL sheared herring sperm DNA and 1 μg/μL BSA for 3 h at 4^0 C and then incubated with chromatin and antibodies for 2 h at 4^0 C. PCR was performed with HOT-MASTER Taq (Eppendorf) using 2 μL of immuniprecipitated DNA and promoter-specific primers for human *Bcl-2* [26], and *CYP1B1* [9] promoters. Immunoprecipitation with non-specific immunoglobulins (IgG; Santa Cruz Biotechnology) was performed as negative controls. The amount of precipitated chromatin measured in each PCR was normalized with the amount of chromatin present in the input of each immunoprecipitation. PCR products were run on a 2% agarose gel and visualized by ethidium bromide staining using UV light.

TUNEL assay. For TUNEL assay, $4x10^4$ cells were spun on a slide by cytocentrifugation and subsequently fixed in 4 % paraformaldehyde for 30 min at room temperature. After rinsing with PBS the samples were permeabilized in a solution of 0.1 % Triton X-100 in sodium citrate for 2 min. Samples, washed with PBS, were then incubated in the TUNEL reaction mix for 1 h at 37^0C, according to the manufacturer's instructions (Roche, Germany). Cells were counter-stained with Hoechst 33342 before analysis with a fluorescent microscope (Zeiss). Standard deviations of three independent experiments were indicated.

Statistics. All experiment unless indicated were performed at least three times. All experimental results were expressed as the arithmetic mean and standard deviation (s.d.) of measurements was shown. Student's *t*-test was used for statistical significance of the differences between treatment groups. Statistical analysis was performed using analysis of variance at 5% ($p<0.05$) or 1% ($p<0.01$).

ACKNOWLEDGEMENTS

This work was supported by the Italian Association for Cancer Research (AIRC, no.1086). L.N. is supported by a Fellowship from L'Oreal Italia-UNESCO for Women in Science. R.P. is supported by a Fellowship from the Italian Foundation for Cancer Research (FIRC) and by a EMBO Short-term Fellowship. We thank A. Aiello and M. Di Salvio for experimental help, A. Farsetti for the prostate cancer cell model and D. Givol for scientific support.

CONFLICT OF INTERESTS STATEMENT

The authors of this manuscript have no conflicts of interest to declare.

REFERENCES

1. Rinaldo C, Prodosmo A, Siepi F, Soddu S. HIPK2: a multitalented partner for transcription factors in DNA damage response and development. Biochem Cell Biol. 2007; 85: 411418.

2. D'Orazi G, Cecchinelli B, Bruno T, Manni I, Higashimoto Y, Saito S, Gostissa M, Coen S, Marchetti A, Del Sal G, Piaggio G, Fanciulli M, and Soddu S. Homeodomain-interacting protein kinase-2 phosphorylates p53 at Ser46 and mediates apoptosis. Nature Cell Biol. 2002; 4: 11-19.

3. Hofmann TG, Moller A, Sirma H, Zentgraf H, Taya Y, Droge W, Schmitz ML. Regulation of p53 activity by its interaction with homeodomain-interacting protein kinase-2. Nature Cell Biol. 2002; 4: 1-10.

4. Oda K, Arakawa H, Tanaka T, Matsuda K, Tanikawa C, Mori T, Nishimori H, Tamai K, Tokino T, Nakamura Y, Taya Y. P53AIP1, a potential mediator of p53-dependent apoptosis, and its regulation by Ser-46-phosphorylated p53. Cell**.** 2000; 102: 849-862.

5. Puca R, Nardinocchi L, Sacchi A, Rechavi G, Givol D, D'Orazi G. HIPK2 modulates p53 activity towards pro-apoptotic transcription. Mol Cancer. 2009; 8:85.

6. Puca R, Nardinocchi L, Starace G, Rechavi G, Sacchi A, Givol D, D'Orazi. Nox1 is involved in p53 deacetylation and suppression of its transcriptional activity and apoptosis. Free Rad Biol Med. 2010; 48: 1338-1346.

7. Vousden KH and Prives C. P53 and prognosis: New insights and further complexity. Cell. 2005; 120: 7-10.

8. Puca R, Nardinocchi L, Givol D, D'Orazi G. Regulation of p53 activity by HIPK2: molecular mechanisms and therapeutical implications in human cancer cells Oncogene. 2010; 29: 4378-4387.

9. Calzado MA, de la Vega L, Moller A, Bowtell DD, Schmitz ML. An inducible autoregulatory loop between HIPK2 and Siah2 at the apex of the hypoxic response. Nature Cell Biol. 2009; 11: 85-91.

10. Nardinocchi L, Puca R, Sacchi A, Rechavi G, Givol D, D'Orazi G. Targeting hypoxia in cancer cells by restoring homeodomain interacting protein kinase 2 and p53 activity and suppressing HIF-1alpha. Plos ONE. 2009; 4(8):e6819.

11. Winter M, Sombroek D, Dauth I, Moehlenbrink J, Scheuermann K, Crone J, Hofmann TG.ATR. Control of HIPK2 stability by ubiquitin ligase Siah-1 and checkpoint kinases ATM and ATR. Nat Cell Biol. 2009; 10: 812-824.

12. Semenza GL. Targeting HIF-1 for cancer therapy. Nature Rev. Cancer. 2003; 3: 721-732.

13. Nardinocchi L, Puca R, Guidolin D, Belloni AS, Bossi G, Michiels C, Sacchi A, Onisto M, D'Orazi G. Transcriptional regulation of hypoxia-inducible factor 1alpha by HIPK2 suggests a novel mechanism to restrain tumor growth. Biochem Biophys Acta. 2009; 1793: 368-377.

14.Semenza GL. Defining the role of hypoxia-inducible factor 1 in cancer biology and therapeutics. Oncogene. 2010; 29: 625-634.

15. An WG, Kanekal M, Simon MC, Maltepe E, Blagosklonny MV, Neckers LM. Stabilization of wild-type p53 by hypoxia-inducible factor 1α. Nature. 1998; 392: 405-408.

16. Sendoel A, Kohler I, Fellmann C, Lowe SW, Hengsrtner MO. HIF-1 antagonizes p53-mediated apoptosis through a secreted neuronal tyrosinase. Nature 2010; 465:577-583.

17. Nanni S, Priolo C, Grasselli A, D'Eletto M, Merola R, Moretti F, Gallucci M, De Carli P, Sentinelli S, Cianciulli AM, Mottolese M, Carlini P, Arcelli D, et al. Epithelial-restricted gene profile of primary cultures from human prostate tumors: a molecular approach to predict clinical behavior of prostate cancer. Mol Cancer Res. 2006; 4: 79-92.

18. Zhong X-S, Liu LZ, Skinner HD, Cao Z, Ding M, Jiang BH. Mechanism of vascular endothelial growth factor expression mediated by cisplatin in human ovarian cancer cells. Biochem Biophys Res Commun. 2007; .358: 92-98.

19. Benita Y, Kikuchi H, Smith AD, Zhang MQ, Chung DC, Xavier RJ. An integrative genomics approach identifies Hypoxia Inducible Factor-1 (HIF-1)-target genes that form the core response to hypoxia. Nucleic Acids Res. 2009; 37: 4587-602.

20. Choi DW, Seo YM, Kim EA, Sung KS, Ahn JW, Park SJ, Lee SR, Choi CY. Ubiquitination and degradation of homeodomain-interacting protein kinase-2 by WD40 repeat/SOCS box protein WSB-1. J Biol Chem. 2008; 283: 4682-4689.

21. Nardinocchi L, Pantisano V, Puca R, Porru M, Aiello A, Grasselli A, Leonetti C, Safran M, Rechavi G, Givol D, Farsetti A, D'Orazi G. Zinc downregulates HIF-1α and inhibits its activity in tumor cells in vitro and in vivo. PLoS ONE. 2010; 5:e15048.

22. Nardinocchi L, Puca R, Givol D, D'Orazi G. Counteracting MDM2-induced HIPK2 degradation restores HIPK2/p53 apoptotic signalling in cancer cells. FEBS Lett. 2010; 584: 4253-4258.

23. Ventura A, Kirsch DG, McLaughlin ME, Tuveson DA, Grimm J, Lintault L, Newman J, Reczek EE, Weissleder R, Jacks T. Restoration of p53 function leads to tumour regression in vivo. Nature. 2007; 445: 661-665.

24. Brown CJ, Lain S, Verma CS, Fersht AR, Lane DP. Awakening guardian angels: drugging the p53 pathway. Nat Rev Cancer. 2009; 9: 862-873.

25. Nardinocchi L, Puca R, Givol D, D'Orazi G. HIPK2: A therapeutical target to be (re)activated for tumor suppression. Role in p53 activation and HIF-1α inhibition. Cell Cycle. 2010; 9: 1-6.

26. Esposito F, Tornincasa M, Chieffi P, De Martino I, Pierantoni GM, Fusco A. High-mobility group A1 proteins regulate p53-mediated transcription of Bcl-2 gene. Cancer Res. 2010; 70: 5379-5388.

27. Li Z, Bao S, Wu Q, Wang H, Eyler C, Sathornsumetee S, Shi Q, Cao Y, Lathia J, McLendon RE, Hjelmeland AB, Rich JN. Hypoxia-Inducible Factors Regulate Tumorigenic Capacity of Glioma Stem Cells. Cancer Cell. 2009; 15: 501-513.

28. Keith B and Simon MC. Hypoxia-inducible factors, stem cells, and cancer. Cell. 2007; 129: 465-472.

29. Cicalese A, Bonizzi G, Pasi CE, Faretta M, Ronzoni S, Giuliani B, Brisken C, Minucci S, Di Fiore PP, Pelicci PG. The tumor suppressor p53 regulates polarity of self-renewing divisions in mammary stem cells. Cell 2009; 138: 1083-1095.

30. Puca R, Nardinocchi L, Gal H, Rechavi G, Amariglio N, Domany E, Notterman DA, Scarsella M, Leonetti C, Sacchi A, Blandino G, Givol D, D'Orazi G. Reversible dysfunction of wild-type p53 following homeodomain-interacting protein kinase-2 knockdown. Cancer Res. 2008; 68: 3707-3714.

31. Nanni S, Benvenuti V, Grasselli A, Priolo C, Aiello A, Mattiussi S, Colussi C, Lirangi V, Illi B, D'Eletto M, Cianciulli AM, Gallucci M, De Carli P, et al. Endothelial NOS, estrogen receptor β, and HIFs cooperate in the activation of a prognostic transcriptional pattern in aggressive human prostate cancer. J Clin Invest. 2009; 119: 1093-108.

32. Chen C. and Okayama H. High-efficiency transformation of mammalian cells by plasmid DNA. Mol Cell Biol. 1987; 7: 2754-2756.

33. Liu YV, Baek JH, Zhang H, Diez R, Cole RN, Semenza GL. RACK1 competes with HSP90 for binding to HIF-1alpha and is required for O(2)-independent and HSP90 inhibitor-induced degradation of HIF-1alpha. Mol Cell. 2007; 25: 207-217.

SUPPLEMENTARY FIGURES

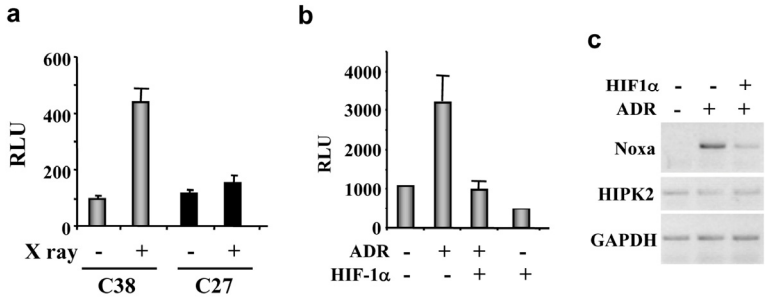

Figure S1. HIF-1α confers resistance to drug-induced p53 apoptotic activation. (**a**) Luciferase assay showed impaired p53AIP1-luc activity in C27 cells in response to X-ray irradiation, compared to the C38 cells. Results represent mean ± s.d. from three experiments. (**b**) Luciferase assay of RKO cells stable transfected with p53AIP1-luc reporter where HIF-1α overexpression inhibited the adryamicin (ADR)-induced p53 transcriptional activity. Results represent mean ± s.d. from three experiments. (**c**) RT-PCR analysis of p53 apoptotic target genes in RKO colon cancer cells where HIF-1α overexpression inhibited the adryamicin (ADR)-induced p53 target gene transcription. GAPDH was a loading control.

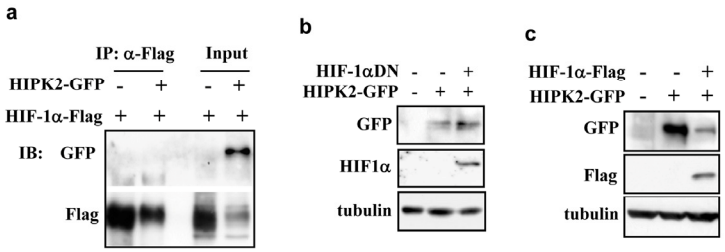

Figure S2. HIF-1α inhibits HIPK2 through its transcriptional activity. (**a**) 293 cells were co-transfected with 4 μg HIPK2-GFP and 8 μg HIF-1α-Flag and 24 h after later equal amount of total cell extracts were immune-precipitated with anti-Flag antibody and immunoblotted with anti-GFP antibody to detect protein/protein interaction. Input is 1/10 of the total cell extracts used for immune-precipitation. (**b**) Immunoblot of 293 cells co-transfected with HIPK2-GFP (4 μg) alone or in combination with the HIF-1αDN (8 μg) expression vectors. The HIPK2 protein levels were not abolished by HIF-1αDN. Anti-tubulin was used as protein loading control. (**c**) Immunoblot in H1299 cells (p53 null) co-transfected as in (b). The HIPK2 protein levels were strongly abolished by HIF-1α. Anti-tubulin was used as protein loading control.

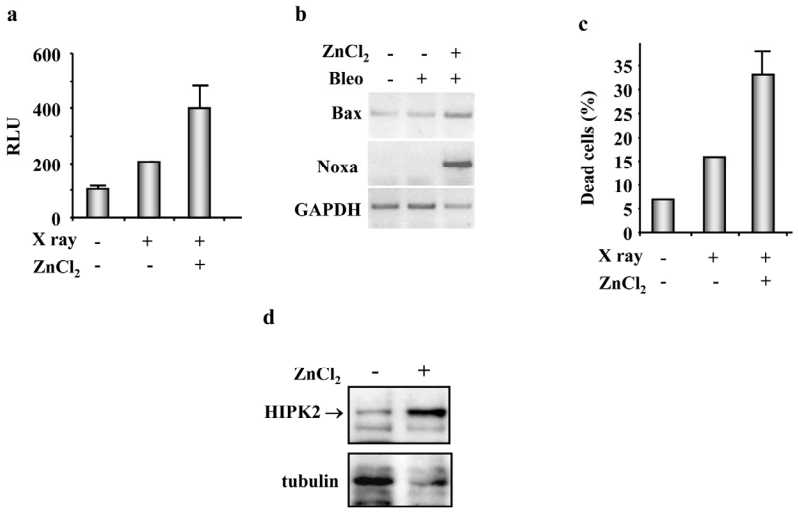

Figure S3. Zinc restores p53 activity in HIF-1α-upregulated cells. (**a**) Luciferase assay showed that the impaired Noxa-luc activity in C27 cells in response to X-ray irradiation was counteracted by zinc treatment. Results represent mean ± s.d. from three experiments. (**b**) Similar result was obtained in C27 cells by RT-PCR analysis where zinc restored the p53 apoptotic gene transcription in response to bleomycin (Bleo). GAPDH was used as internal control. (**c**) Tunel assay of C27 cells showing increased apoptotic cell death only after zinc supplementation to Bleo treatment. (**d**) Immunoblot showing increased endogenous HIPK2 levels in C27 after zinc treatment. Anti-tubulin was used as protein loading control.

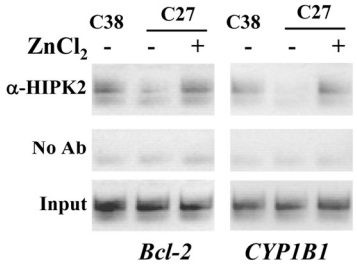

Figure S4. Zinc restores HIPK2 recruitment onto target promoter in HIF-1α-upregulated cells. Chromatin immunoprecipitation (ChIP) analysis performed with anti-HIPK2 antibody on C38 cells and C27 cells untreated or treated with zinc (100 μM for 24 h). PCR analyses were performed on the immunoprecipitated DNA samples using specific primers for the human Bcl-2 and CYP1B1 gene promoters. A sample representing linear amplification of the total input chromatin (Input) was included as control. Additional controls included immunoprecipitation performed with non-specific immunoglobulins (No Ab).

Review

p53, ROS and senescence in the control of aging

Arnaud Vigneron and Karen H Vousden

The Beatson Institute for Cancer Research, Glasgow, G61 1BD, UK

Corresponding author: *Karen H Vousden, PhD;* ***E-mail:*** *k.vousden@beatson.gla.ac.uk*

Abstract: In addition to its function as a tumour suppressor, p53 is also involved in an increasing number of pathology associated with aging. Several activities of p53 appear contribute to its role in aging; one function that might be particularly relevant in this context is the regulation of senescence. The control of ROS and senescence by p53 may help to explain how p53 can function to both restrain and promote aging.

p53 functions as a longevity assurance gene (by virtue of its strong tumor suppressor activity) and a regulator of aging. In several mouse models, persistent low-level activation of p53, either through deregulated expression of p53 itself or in response to constitutive stress like DNA damage/telomere erosion, leads to premature aging [1,2]. However, mice with normal basal p53 levels that have been engineered to a show a heightened ability to mount a p53 response show a very strong resistance to tumourigenesis without evidence of premature aging [3]. Indeed, in several of these models a decreased level of aging related damage is observed, indicating that p53 may also help to promote longevity. The control of aging reflects numerous activities of p53, including the modulation of the IGFR pathway through interplay between full-length p53 and N-terminally truncated splice variants of p53 [4] and the ability of p53 to restrict stem cell function [5]. p53 is also a key regulator of senescence, a central stress response that plays an important role in tumour suppression, but may also help to promote cancer development by inducing an inflammatory response [6]. The ability to control senescence is consistent with p53's function in restraining cancer development, but can the mechanisms through which p53 regulates senescence also contribute to the control of aging?

Induction of senescence by p53 is associated with the regulation of p53-dependent genes that can participate in cell cycle arrest. While depletion of these components can impact senescence induction – supporting their role in mediating this response – the inhibition of cell cycle progression alone does not explain how this arrest can be turned into the definitive and permanent proliferation block that is characteristic of senescence. Furthermore, despite the clear documentation of p53's ability to induce senescence, more recent evidence shows that p53 can also function to inhibit senescence while promoting cell cycle arrest [7]. So how can p53 both suppress and promote senescence? An important component of this may be the ability of p53 to control cell growth and metabolic stress through different pathways, including the regulation of ROS levels and the activity of mTOR (Figure 1). The ability of p53 to promote ROS production has been shown to participate in the induction of apoptosis by p53 [8]. But ROS are also known to be critical for senescence [9] and the p53 target genes that increase ROS may also play an important role in senescence induction. However, p53 also promotes the expression of a number of antioxidant genes, accounting for p53's ability to control oxidative stress in cells and mice [10]. So p53's ability to decrease and increase oxidative stress likely contributes to its dual effect on senescence. Another factor that influences the outcome to p53 activation is mTOR. While mTOR is normally associated with cell growth, activation of mTOR can contribute to and be essential for certain types of senescence [11,12], and the maintenance of mTOR signalling under conditions of cell cycle arrest leads to senescence in cultured cells [13]. p53 inhibits the mTOR pathway at several levels [14], contributing to the anti-senescence activity of p53 [15]. Furthermore, mTOR can be activated by ROS [16], so p53's antioxidant activities may reinforce the dampening of mTOR and senescence (Figure 1).

One of the main responses to mTOR inhibition is the induction of autophagy, a response that allows survival

under conditions of nutrient deprivation. There are several possible links between autophagy and senescence. Inhibition of autophagy results in the accumulation of protein aggregates, ER stress and mitochondrial dysfunction, each of which could promote senescence. However, other studies suggest that autophagy may be required for an efficient senescence response [17]. In either case, the ability of p53 to both enhance and inhibit autophagy [18] provides a further mechanism for the modulation of senescence.

The activity of p53 is regulated through many mechanisms, but of particular interest with respect to the control of senescence and aging is a role for the histone deacetylase Sirt1, whose expression is strongly down regulated in senescent cells [19]. In contrast nutrient deprivation, which inhibits mTOR and can impede cellular senescence [13], has been shown to increase Sirt1 levels [20]. One way in which Sirt1 functions is to deacetylate p53, modulating p53 activity and decreasing senesence [21]. Deactylation inhibits p53's ability to transcriptionally activate some, but not all, target genes - including those involved in apoptosis induction, ROS production [22,23], and presumably also senescence (Figure 1). The presence of a chronic DNA damage response (as may be seen in cancer cells), which is linked to the induction of senescence [24], can directly increase p53 acetylation by inducing the phosphorylation of the N-terminus of p53 and so promoting the interaction with the acetyl transferases CBP/p300. Mouse models have shown that expression of phosphorylation resistant p53 inhibits the induction of senescence [25], while cells harbouring p53 with acetyl-mimicking mutations of the last seven lysine residues have an accelerated entry into senescence and are very resistant to senescence bypass [26], although the cell cycle arrest response in these cells remains normal. Phosphorylation and acetylation of p53 is also seen to be important during Ras-induced or replicative senescence [27,28]. Under these circumstances, it would seem that deacetylation of p53 by Sirt1 impedes the induction of senescence, as well as apoptosis. Taken together there is good evidence that acetylation of p53 promotes sense-cence and apoptosis, so inhibitors of the deacetylation enzymes might be useful drugs for the reactivation of these p53 responses for cancer therapy [29].

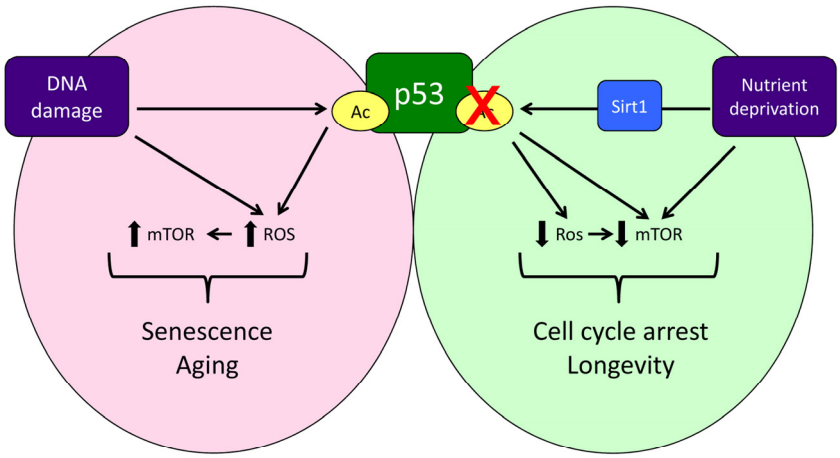

Figure 1. A model of how acetylation, oxidative stress and mTOR activity might influence the response to p53. Note that this model does not account for all published observations (e.g. reduction of the initial burst of mTOR activity during oncogene induced senescence [17]) and represents an oversimplification of these signalling pathways.

Several of the mechanisms implicated in the induction of senescence by p53 have also been linked to the regulation of longevity. Induction of mTOR and oxidative stress – and the complex interplay between them – is associated with aging [16] and Sirt1 is emerging as a key supporter of longevity in many organisms [30]. The induction of cellular senescence itself may result in loss of tissue renewal and architecture, organ dysfunction and organismal aging [31], while autophagy can protect from aging [32]. So it seems reasonable to propose that p53's ability to influence aging is reflected – at least in part - by the mechanisms through which p53 controls senescence. But as we have discussed, p53 can promote and impede both senescence and aging - so which output prevails? The answer is not yet clear, but one determining factor may be the type or extent of the p53-inducing stress. Current models suggest that mild or constitutive stress induced by normal growth and proliferation lead to p53-induced antioxidant and repair functions, while strong or persistent p53 activity may tip the balance towards the induction of apoptosis or senescence, thereby favoring aging. The mouse models also clearly suggest that inappropriate p53 activity promotes aging while a robust but normally regulated p53 response protects from the aging process. One prediction of this model is that the persistent stress encountered in tumors would favor p53-induced senescence over a more transient cell cycle arrest – and indeed the activation of p53 in established tumors has been shown to promote senescence in some tissue types [33].

p53 is emerging as an important, but complex, player in the regulation of senescence and longevity. The ability of p53 to both activate and inhibit senescence is reflected in the ability to promote and inhibit oxidative stress and autophagy, and the ultimate establishment of senescence or quiescence is highly dependent on collaborating factors such as mTOR activity or oxidative stress. Ultimately, these bipolar activities of p53 become manifest in the contradictory effects on longevity and aging. p53 based cancer therapies may be rendered more effective by an increased propensity of transformed cells to undergo senescence, compared to normal cells. However, the idea that p53 can both promote and prevent aging adds even more spice to the consideration of how to use drugs that can induce or inhibit p53 activity.

ACKNOWLEDGEMENTS

We are very grateful to Peter Adams for his helpful comments and advice.

REFERENCES

1. Tyner SD, Venkatachalam S, Choi J, Ghebranious N, Igelmann H, et al. p53 mutant mice that display early ageing-associated phenotypes. Nature. 2002; 415: 45-53.

2. Maier B, Gluba W, Bernier B, Turner T, Mohammad K, et al. Modulation of mammalian life span by the short isoform of p53. Genes Dev. 2004; 18: 306-319.

3. Matheu A, Maraver A, Klatt P, Flores I, Garcia-Cao I, et al. Delayed ageing through damage protection by the Arf/p53 pathway. Nature. 2007; 448: 375-379.

4. Pehar M, O'Riordan KJ, Burns-Cusato M, Andrzejewski ME, del Alcazar CG, et al. Altered longevity-assurance activity of p53:p44 in the mouse causes memory loss, neurodegeneration and premature death. Aging Cell. 2010; 9: 174-190.

5. Zhao T and Xu Y. p53 and stem cells: new developments and new concerns. Trends Cell Biol. 2010; 20: 170-175.

6. Coppe JP, Desprez PY, Krtolica A, Campisi J. The senescence-associated secretory phenotype: the dark side of tumor suppression. Annu Rev Pathol. 2010; 5: 99-118.

7. Demidenko ZN, Korotchkina LG, Gudkov AV, Blagosklonny MV. Paradoxical suppression of cellular senescence by p53. Proc Natl Acad Sci USA. 2010; 107: 9660-9664.

8. Johnson TM, Yu Z-X, Ferrans VJ, Lowenstein RA, Finkel T. Reactive oxygen species are downstream mediators of p53-dependent apoptosis. Proc Natl Acad Sci USA. 1996; 93: 11848-11852.

9. Lu T and Finkel T. Free radicals and senescence. Exp Cell Res. 2008; 314: 1918-1922.

10. Olovnikov IA, Kravchenko JE, Chumakov PM. Homeostatic functions of the p53 tumor suppressor: regulation of energy metabolism and antioxidant defense. Semin Cancer Biol. 2009; 19: 32-41.

11. Nardella C, Chen Z, Salmena L, Carracedo A, Alimonti A, et al. Aberrant Rheb-mediated mTORC1 activation and Pten haploinsufficiency are cooperative oncogenic events. Genes Dev. 2008; 22: 2172-2177.

12. Alimonti A, Nardella C, Chen Z, Clohessy JG, Carracedo A, et al. A novel type of cellular senescence that can be enhanced in mouse models and human tumor xenografts to suppress prostate tumorigenesis. J Clin Invest. 2010; 120: 681-693.

13. Demidenko ZN and Blagosklonny MV. Growth stimulation leads to cellular senescence when the cell cycle is blocked. Cell Cycle. 2008; 7: 3355-3361.

14. Feng Z and Levine AJ. The regulation of energy metabolism and the IGF-1/mTOR pathways by the p53 protein. Trends Cell Biol. 2010; 20: 427-434.

15. Korotchkina LG, Leontieva OV, Bukreeva EI, Demidenko ZN, Gudkov AV, et al. The choice between p53-induced senescence and quiescence is determined in part by the mTOR pathway. Aging. 2010; 2: 344-352.

16. Blagosklonny MV. Aging: ROS or TOR. Cell Cycle. 2008 7: 3344-3354.

17. Young AR, Narita M, Ferreira M, Kirschner K, Sadaie M, et al. Autophagy mediates the mitotic senescence transition. Genes Dev. 2009; 23: 798-803.

18. Maiuri MC, Galluzzi L, Morselli E, Kepp O, Malik SA, et al. Autophagy regulation by p53. Curr Opin Cell Biol. 2010; 22: 181-185.

19. Sasaki T, Maier B, Bartke A, Scrable H. Progressive loss of SIRT1 with cell cycle withdrawal. Aging Cell. 2006; 5: 413-422.
20. Kanfi Y, Peshti V, Gozlan YM, Rathaus M, Gil R, et al. Regulation of SIRT1 protein levels by nutrient availability. FEBS Lett. 2008 582: 2417-2423.
21. Langley E, Pearson M, Faretta M, Bauer UM, Frye RA, et al. Human SIR2 deacetylates p53 and antagonizes PML/p53-induced cellular senescence. Embo J. 2002; 21: 2383-2396.
22. Luo J, Nikolaev AY, Imai S, Chen D, Su F, et al. Negative control of p53 by Sir2alpha promotes cell survival under stress. Cell. 2001; 107: 137-148.
23. Vaziri H, Dessain SK, Ng Eaton E, Imai SI, Frye RA, et al. hSIR2(SIRT1) functions as an NAD-dependent p53 deacetylase. Cell. 2001; 107: 149-159.
24. Pospelova TV, Demidenko ZN, Bukreeva EI, Pospelov VA, Gudkov AV, et al. Pseudo-DNA damage response in senescent cells. Cell Cycle. 2009; 8: 4112-4118.
25. Armata HL, Garlick DS, Sluss HK. The ataxia telangiectasia-mutated target site Ser18 is required for p53-mediated tumor suppression. Cancer Res. 2007; 67: 11696-11703.
26. Krummel KA, Lee CJ, Toledo F, Wahl GM. The C-terminal lysines fine-tune p53 stress response in a mouse model but are not required for stability control or transactivation. Proc Natl Acad Sci USA. 2005; 102: 10188-10193.
27. Pedeux R, Sengupta S, Shen JC, Demidov ON, Saito S, et al. ING2 regulates the onset of replicative senescence by induction of p300-dependent p53 acetylation. Mol Cell Biol. 2005; 25: 6639-6648.
28. Pearson M, Carbone R, Sebastiani C, Cioce M, Fagioli M, et al. PML regulates p53 acetylation and premature senescence induced by oncogenic ras. Nature. 2000; 406: 207-210.
29. Lain S, Hollick JJ, Campbell J, Staples OD, Higgins M, et al. Discovery, in vivo activity, and mechanism of action of a small-molecule p53 activator. Cancer Cell. 2008; 13: 454-463.
30. Finkel T, Deng CX, Mostoslavsky R. Recent progress in the biology and physiology of sirtuins. Nature. 2009; 460: 587-591.
31. Campisi J. Senescent cells, tumor suppression, and organismal aging: good citizens, bad neighbors. Cell. 2005; 120: 513-522.
32. Salminen A and Kaarniranta K. Regulation of the aging process by autophagy. Trends Mol Med. 2009; 15: 217-224.
33. Xue W, Zender L, Miething C, Dickins RA, Hernando E, et al. Senescence and tumour clearance is triggered by p53 restoration in murine liver carcinomas. Nature. 2007; 445: 656-660.

Editorial

P53 and aging: A fresh look at an old paradigm

Masha V. Poyurovsky and Carol Prives

Department of Biological Sciences, Columbia University, New York, NY 10017

E-mail: *carol@biology.columbia.edu*

Apoptosis and cellular senescence, two key tumor suppression mechanisms, are thought to be antagonistically pleiotropic. Antagonistic pleiotropy holds that functions that are advantageous for a young and reproductively fit organism (eg. cancer protection and proper development) can be deleterious when that same organism becomes old (eg. loss of stem cell proliferation and tissue degeneration leading to diseases associated with age) [1]. This theory predicts that in an older animal (or human), the activity of tumor suppressors would be associated with enhanced aging phenotypes. However, confirmation of a direct connection between apoptosis, senescence and aging remains elusive [2]. In fact, at least in the case of p53 there is mounting data challenging the antagonistic pleiotropy model.

Multiple lines of evidence from animal models suggest that a functional p53 pathway favors prolonged survival. Aging mice show a decrease in p53 activity correlated with increased tumor incidence as well as an overall reduction in longevity [3]. On the other hand, mice with an extra gene dosage of Arf and p53 show significant tumor protection, decreased oxidative damage and delayed aging [4]. Animals expressing the $p53^{S18A}$ mutation present with accelerated aging, and cells from these mice undergo early senescence [5]. As phosphorylation of p53 at Ser18 (Ser15 in humans) is associated with activation, these results highlight a requirement for intact p53 signaling in longevity [6]. In the nematode *Caenorhabditis elegans*, mutations that lead to longevity preferentially antagonize tumor growth, likely due to an increase in DAF-16/p53–dependent apoptosis [7].

The mTOR pathway is intimately connected with organismal aging. In fact inhibition of mTOR either by treatment with rapamycin or by the inhibition of upstream signaling molecules, extends lifespan in yeast, worms and flies suggesting that this pathway may be one of the main mechanisms that decrease lifespan [8]. p53 is able to regulate activity of mTOR following DNA damage or oncogenic stress by activation of PTEN, AMP kinase and TSC-2, each of which signals to diminish the activity of mTOR (Figure 1) [9, 10]. p53 may also function downstream of mTOR by activating antioxidant genes and thus protecting cells against increased ROS levels in cells, one of the consequences of heightened mTOR activity [11-13].

As the ability of p53 to increase longevity becomes more evident, we should consider the role of its negative regulator, Mdm2, if not in the process of aging directly, at least in its effects on the activity of mTOR. Growth factor and oncogene signaling activate PI-3 kinase and its downstream effector AKT, a protein kinase that activates mTOR via inhibition of TSC-1 protein. AKT also phosphorylates Mdm2 leading to enhanced Mdm2 ubiquitin ligase activity and more rapid degradation of p53 (Figure 1) [8, 14]. Additionally, AKT stimulates FOXO phosphorylation, which results in FOXO nuclear exportation and ubiquitin dependent proteasomal degradation [15]. FOXO proteins have conserved abilities to increase longevity in worms and flies [16]. Indeed, Mdm2 was reported to function as an E3 ubiquitin ligase to promote FOXO degradation, following activation of AKT, thus forging an additional link between Mdm2 and changes in longevity [17].

Additionally, mTOR is able to positively regulate Mdm2 through an increase in translation of Mdm2 mRNA. Consistently, an increase in p53 dependent apoptosis in the liver of mouse embryos treated with Rapamycin *in utero* is attributed mTOR's ability to control translation of Mdm2 [18]. However, because the interplay between apoptosis and aging is likely to be highly context specific, it is important to note that mice expressing only ~30% of the wild type Mdm2 levels do not have an aging phenotype, while exhibiting clear en-

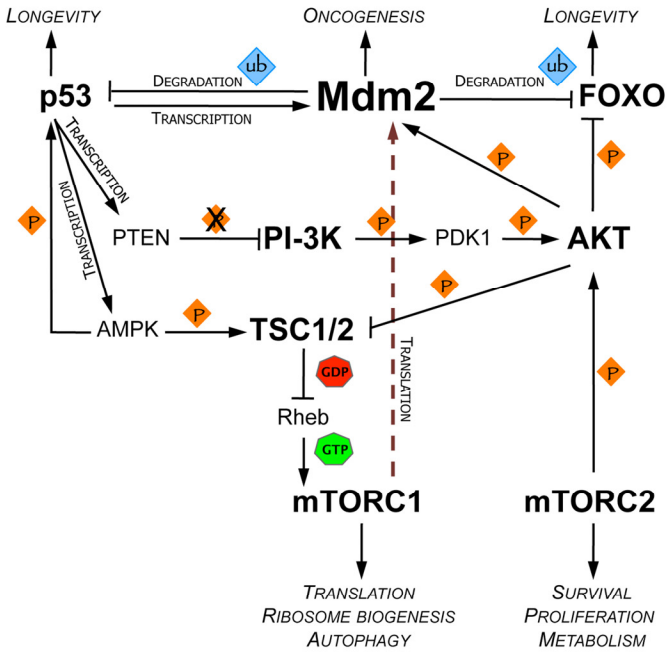

Figure 1. Signaling circuitry connecting Mdm2 with the regulation of longevity and metabolism. Both mTORC1 and 2 (mammalian target of rapamycin complex 1/2) are able to positively regulate the activity of Mdm2, either through enhancement of translation of Mdm2 mRNA or via activation of AKT. Conversely, Mdm2 can activate mTORC1 by targeting p53 for degradation. p53 negatively regulates mTORC1 by activating TSC1/2 (tuberous sclerosis 1/2) complex, which acts as a GTPase activating protein (GAP) for Rheb (Ras homologue enriched in brain). p53 can also repress the activity of PI-3K (phosphatidylinositol 3-kinase) by induction of PTEN (phosphatase and tensin homologue), leading to further downregulation of mTORC1. Arrows represent up-regulation. Orange diamonds represent kinase activity. Blue diamonds represent E3 ubiquitin ligase activity of Mdm2. AMPK, AMP-activated protein kinase; FOXO, Forkhead box; PDK1, 3-phosphoinositide-dependent protein kinase 1.

hancement in tumor protection [19]. It would be of interest to look at the effects of nutrient deprivation on the mice carrying an Mdm2 hypomorphic allele.

In conclusion, as our notion of p53 function in aging and senescence changes, it is very tempting to imagine that just a slight inhibition of Mdm2 function in cells could both prolong full tumor surveillance mechanisms of p53, and in some circumstances increase longevity. Numerous molecular inhibitors of Mdm2 are in various stages of development with the goal of reactivating p53 activity in cancer [20]. The idea that controlled pharmacological modulation of Mdm2 function might also have positive consequences in extension of human lifespan could be an unexpected benefit and an additional incentive for design of new compounds targeting Mdm2.

ACKNOWLEDGEMENTS

We would like to thank the members of the Prives lab for their valuable input and stimulating discussion.

REFERENCES

1. Campisi J. Aging, tumor suppression and cancer: high wire-act! Mech Ageing Dev 2005; 126:51-58.

2. Johnson FB, Sinclair DA, Guarente L. Molecular biology of aging. Cell 1999; 96:291-302.

3. Feng Z, Hu W, Teresky AK, Hernando E, Cordon-Cardo C, Levine AJ. Declining p53 function in the aging process: a possible mechanism for the increased tumor incidence in older populations. Proc Natl Acad Sci U S A 2007; 104:16633-16638.

4. Matheu A, Maraver A, Klatt P, Flores I, Garcia-Cao I, Borras C, Flores JM, Vina J, Blasco MA, Serrano M. Delayed ageing through

damage protection by the Arf/p53 pathway. Nature 2007; 448:375-379.

5. Armata HL, Garlick DS, Sluss HK. The ataxia telangiectasia-mutated target site Ser18 is required for p53-mediated tumor suppression. Cancer Res 2007; 67:11696-11703.

6. Bode AM, Dong Z. Post-translational modification of p53 in tumorigenesis. Nat Rev Cancer 2004; 4:793-805.

7. Pinkston JM, Garigan D, Hansen M, Kenyon C. Mutations that increase the life span of C. elegans inhibit tumor growth. Science 2006; 313:971-975.

8. Hands SL, Proud CG, Wyttenbach A. mTOR's role in ageing: protein synthesis or autophagy? Aging (Albany NY) 2009; 1:586-597.

9. Levine AJ, Feng Z, Mak TW, You H, Jin S. Coordination and communication between the p53 and IGF-1-AKT-TOR signal transduction pathways. Genes Dev 2006; 20:267-275.

10. Demidenko ZN, Korotchkina LG, Gudkov AV, Blagosklonny MV. Paradoxical suppression of cellular senescence by p53. Proc Natl Acad Sci U S A 2010; 107:9660-9664.

11. Hu W, Zhang C, Wu R, Sun Y, Levine A, Feng Z. Glutaminase 2, a novel p53 target gene regulating energy metabolism and antioxidant function. Proc Natl Acad Sci U S A 2010; 107:7455-7460.

12. Suzuki S, Tanaka T, Poyurovsky MV, Nagano H, Mayama T, Ohkubo S, Lokshin M, Hosokawa H, Nakayama T, Suzuki Y, Sugano S, Sato E, Nagao T, Yokote K, Tatsuno I, Prives C. Phosphate-activated glutaminase (GLS2), a p53-inducible regulator of glutamine metabolism and reactive oxygen species. Proc Natl Acad Sci U S A 2010; 107:7461-7466.

13. Bensaad K, Cheung EC, Vousden KH. Modulation of intracellular ROS levels by TIGAR controls autophagy. EMBO J 2009; 28:3015-3026.

14. Ogawara Y, Kishishita S, Obata T, Isazawa Y, Suzuki T, Tanaka K, Masuyama N, Gotoh Y. Akt enhances Mdm2-mediated ubiquitination and degradation of p53. J Biol Chem 2002; 277:21843-21850.

15. Aoki M, Jiang H, Vogt PK. Proteasomal degradation of the FoxO1 transcriptional regulator in cells transformed by the P3k and Akt oncoproteins. Proc Natl Acad Sci U S A 2004; 101:13613-13617.

16. Kenyon C. The plasticity of aging: insights from long-lived mutants. Cell 2005; 120:449-460.

17. Fu W, Ma Q, Chen L, Li P, Zhang M, Ramamoorthy S, Nawaz Z, Shimojima T, Wang H, Yang Y, Shen Z, Zhang Y, Zhang X, Nicosia SV, Pledger JW, Chen J, Bai W. MDM2 acts downstream of p53 as an E3 ligase to promote FOXO ubiquitination and degradation. J Biol Chem 2009; 284:13987-14000.

18. Moumen A, Patane S, Porras A, Dono R, Maina F. Met acts on Mdm2 via mTOR to signal cell survival during development. Development 2007; 134:1443-1451.

19. Mendrysa SM, O'Leary KA, McElwee MK, Michalowski J, Eisenman RN, Powell DA, Perry ME. Tumor suppression and normal aging in mice with constitutively high p53 activity. Genes Dev 2006; 20:16-21.

20. Vassilev LT. Small-molecule antagonists of p53-MDM2 binding: research tools and potential therapeutics. Cell Cycle 2004; 3:419-421.

Research Perspective

SOCS1, a novel interaction partner of p53 controlling oncogene-induced senescence

Frédérick A. Mallette[1,2], Viviane Calabrese[1], Subburaj Ilangumaran[3] and Gerardo Ferbeyre[1]

[1] Département de Biochimie, Université de Montréal, Montréal, Québec H3C 3J7, Canada
[2] Present address: Terry Fox Molecular Oncology Group and the Bloomfield Center for Research on Aging, Sir Mortimer B Davis Jewish General Hospital, Lady Davis Institute for Medical Research, Montréal, Québec H3T 1E2, Canada
[3] Immunology Division, Department of Pediatrics; Faculty of Medicine and Health Sciences, University of Sherbrooke, Sherbrooke, Canada

Key words: *SOCS1, senescence, p53, ATM, ATR, STAT5, cytokines*
Received: *06/14/10; accepted: 06/24/10; published on line: 06/26/10*
Corresponding author: *g.ferbeyre@umontreal.ca*
Copyright: *© Mallette et al. This is an open-access article distributed under the terms of the Creative Commons Attribution License, which permits unrestricted use, distribution, and reproduction in any medium, provided the original author and source are credited*

Abstract: Members of the signal transducers and activators of transcription (STATs) family of proteins, which connect cytokine signaling to activation of transcription, are frequently activated in human cancers. Suppressors of cytokine signaling (SOCS) are transcriptional targets of activated STAT proteins that negatively control STAT signaling. SOCS1 expression is silenced in multiple human cancers suggesting a tumor suppressor role for this protein. However, SOCS1 not only regulates STAT signaling but can also localize to the nucleus and directly interact with the p53 tumor suppressor through its central SH2 domain. Furthermore, SOCS1 contributes to p53 activation and phosphorylation on serine 15 by forming a ternary complex with ATM or ATR. Through this mechanism SOCS1 regulates the process of oncogene-induced senescence, which is a very important tumor suppressor response. A mutant SOCS1 lacking the SOCS box cannot interact with ATM/ATR, stimulate p53 or induce the senescence phenotype, suggesting that the SOCS box recruits DNA damage activated kinases to its interaction partners bound to its SH2 domain. Proteomic analysis of SOCS1 interaction partners revealed other potential targets of SOCS1 in the DNA damage response. These newly discovered functions of SOCS1 help to explain the increased susceptibility of *Socs1* null mice to develop cancer as well as their propensity to develop autoimmune diseases. Consistently, we found that mice lacking SOCS1 displayed defects in the regulation of p53 target genes including *Mdm2*, *Pmp22*, *PUMA* and *Gadd45a*. The involvement of SOCS1 in p53 activation and the DNA damage response defines a novel tumor suppressor pathway and intervention point for future cancer therapeutics.

SOCS1, cancer and senescence

Cytokines are secreted proteins that regulate different cellular processes including survival, proliferation and differentiation. Following binding to their receptors, cytokines activate the Janus kinases (JAK1, JAK2, JAK3 and Tyk2) leading to the phosphorylation of tyrosine residues on the cytoplasmic portion of the receptor creating docking sites for signaling molecules containing a SH2 domain [1,2]. Members of the STAT family of proteins that are recruited to the phosphorylated cytokine receptors themselves become phosphorylation substrates for JAK kinases. Phosphorylated STAT proteins homo- or hetero-dimerize and translocate to the nucleus to activate transcription of target genes by binding to specific response elements in their promoter regions. Among these cytokine-induced proteins, members of the SOCS family constitute important negative regulators of the JAK/STAT signaling pathway.

There are eight members of the SOCS family of proteins (CIS, SOCS1-7), each of which harbor a central SH2 domain and a C-terminal SOCS box region [3] (Figure 1). The suppressor of cytokine signaling SOCS1 was initially identified as a cytokine-inducible inhibitor of STAT signaling [4,5,6]. Through its SH2 domain, SOCS1 can directly bind phosphorylated JAK2 to prevent the phosphorylation of STAT. SOCS1 also possesses a kinase inhibitory region (KIR), a domain composed of less than 30 amino acids, which shares homology with the pseudosubstrate inhibitory region of JAK and leads to inhibition of the catalytic activity of JAK [7,8]. The SOCS box allows recruitment of elongin B/C and Cullin 2 to form an ubiquitin E3 ligase complex [9,10]. This allows the SOCS protein to operate as an adaptor to trigger ubiquitination and degradation of proteins involved in cellular signaling including JAK [11], TEL-JAK2 [12], IRS-1/2 [13], FAK [14], Vav [15] and Mal [16]. It is currently thought that SOCS1 contributes to tumor suppression due to its ability to control and terminate the activation of STATs [17,18,19,20,21,22,23,24,25]. On the other hand, the relationship between SOCS1 and other tumor suppressor pathways and the cellular mechanisms by which SOCS1 might exert its tumor suppression remain largely unexplored.

To prevent the formation of cancer, normal cells possess intrinsic tumor suppressor mechanisms that are triggered upon oncogene activation. Like apoptosis, cellular senescence opposes cellular transformation by limiting the proliferation of cells expressing oncogenes. In normal human diploid cells, oncogene activation causes a permanent growth arrest with features of cellular senescence [26]. We have recently extended the list of oncogenes known to trigger the senescence response to include the JAK/STAT5 pathway. The transcription factor STAT5 is implicated in tumor formation by regulating important cellular processes including cell cycle progression, apoptosis, angiogenesis and metastasis [27]. However, in normal cells, expression of Tel/Jak2 or constitutively activated allele of STAT5A and B initiated a cell cycle arrest in G1 associated with markers of premature cellular senescence and activation of the tumor suppressors Rb and p53 [28,29,30].

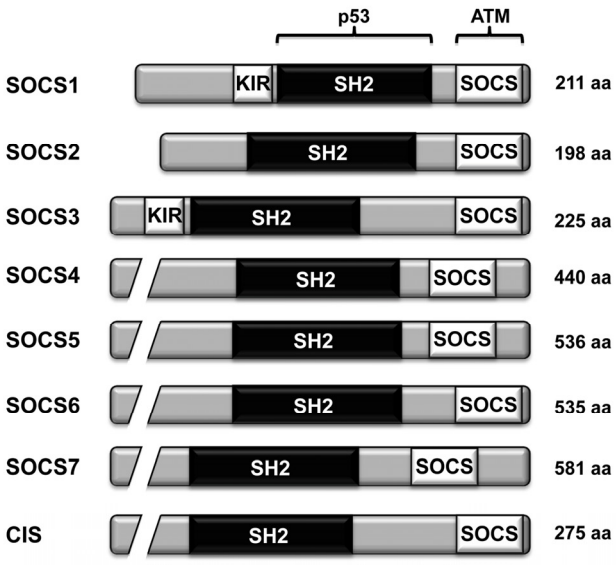

Figure 1. The domain architecture of the different members of the SOCS family of proteins. All eight members of the SOCS family harbor a central SH2 domain and a C-terminal SOCS box. Both SOCS1 and SOCS3 also contain a kinase inhibitory region (KIR). The region of SOCS1 interacting with p53 and ATM are shown [34].

SOCS box proteins and the regulation of p53

The activation of the p53 pathway following oncogene activation is crucial to induce senescence in normal cells. In mice, stimulation of p53 is dependent on p19ARF (Alternative Reading Frame), which is induced by several oncogenes [31,32]. However, the role of ARF in oncogene-induced senescence in human cells is still unclear [33]. In order to identify new regulators of p53 activation following constitutively activated STAT5 expression in normal cells, we performed microarray analysis covering the entire human transcriptome. We observed that the expression of SOCS1 was highly increased at both mRNA and protein level during STAT5-induced senescence [34]. Unexpectedly, SOCS1 expression in normal human fibroblasts was sufficient to trigger a p53-dependent cell cycle arrest displaying features of the senescence phenotype. This function of SOCS1 was dependent on the integrity of its SOCS box. In addition, SOCS1, but not a mutant lacking the SOCS box domain, led to the accumulation of phosphorylated p53 on serine 15 and increased transcription of the p53 target gene p21CIP. The knockdown of SOCS1 during STAT5-induced senescence reduced the phosphorylation of p53 on Ser15, diminished the nuclear accumulation of p53 and compromised the development of senescence phenotype [34]. The remaining activated p53 and partial bypass of the senescence response observed following the knockdown of SOCS1 might arise from the ability of STAT5 to engage multiple signaling pathways to ensure p53 activation. For example, STAT5 can directly transactivate the promoter of the PML gene and stimulate its expression in a p53-independent fashion [30]. The PML protein can then inhibit Mdm2 and stimulate p53 [35,36] contributing to the senescence phenotype [37,38].

SOCS1 mediated STAT5-induced senescence via an unexpected protein-protein interaction between the SH2 domain of SOCS1 and the transactivation domain of p53 [34]. Because the transactivation domain of p53 harbors no tyrosine residues, the binding should occur independently of tyrosine phosphorylation, as reported before for SOCS1 binding to Vav [15] and for other SH2 domains as well [39,40]. The von Hippel-Lindau protein (VHL), another SOCS box-containing protein, has been recently shown to interact with p53. This interaction does not rely on an SH2 domain but on the SOCS box domain of VHL. However, like SOCS1, VHL facilitates p53 interaction with the DNA damage activated kinase ATM [41]. Hence, SOCS1 links DNA damage signals stimulated by oncogenic activity to p53.

Interestingly, SOCS1 is not the only protein inhibitor of STAT implicated in the regulation of p53 activity. The protein inhibitors of activated STAT, PIAS1 and PIASy both promote the sumoylation and transcriptional activity of p53 [42,43,44]. However, the mechanism of activation of p53 by PIAS is still unclear. While the sumoylation of p53 by PIAS1 has been demonstrated [43], a mutated PIAS1 lacking the RING finger-like domain and defective in promoting p53 sumoylation was sufficient to activate p53 [44]. Furthermore, by controlling the activity of both p53 and Rb, PIASy regulates Ras-induced senescence and apoptosis [42]. These data suggest that the control of STAT signaling is tightly linked to the activation of p53 to possibly control the JAK/STAT oncogenic pathway.

Inhibitors of STATs activity and the DNA damage response

The stimulation of p53 during oncogene-induced senescence is associated with the activation of the DNA damage response [28,45,46]. The DNA damage observed in normal cells expressing activated oncogenes may be due to reactive oxygen species [47] and/or some type of replicative stress [45,46]. SOCS1-induced senescence was accompanied by the activation of the DNA damage-regulated kinases ATM and Chk2. Since the stimulation of p53 reporters by SOCS1 was partially blocked in cells depleted of ATM, ATM might participate in the SOCS1-dependent activation of p53. Using pulldown assays, we demonstrated that SOCS1 interacted with both ATM and ATR through its SOCS box (Figure 1) [34]. ATM is an important mediator of the senescence response by activating the p53 pathway, mainly through phosphorylation of the Ser 15 residue [28,45,46]. Depletion of SOCS1 during STAT5-induced senescence caused a dramatic decrease in Ser15 phosphorylation of p53. In order to form a ternary complex with p53 and ATM, SOCS1 must localize to the nucleus. We confirmed that SOCS1 is able to localize to the nucleus and that endogenous SOCS1 colocalized to DNA damage foci with ATM during STAT5-induced senescence [34], thus reinforcing the notion that SOCS1 is a mediator of the DNA damage response. Not only SOCS1 but also other proteins controlling JAK/STAT signaling are known to localize to DNA damage sites. PIAS1 and PIAS4 were also shown to localize to DNA breaks and contribute to the DNA damage response by sumoylating BRCA1 [48,49]. Together, these findings strongly suggest a close link between cytokine signaling and the DNA damage response.

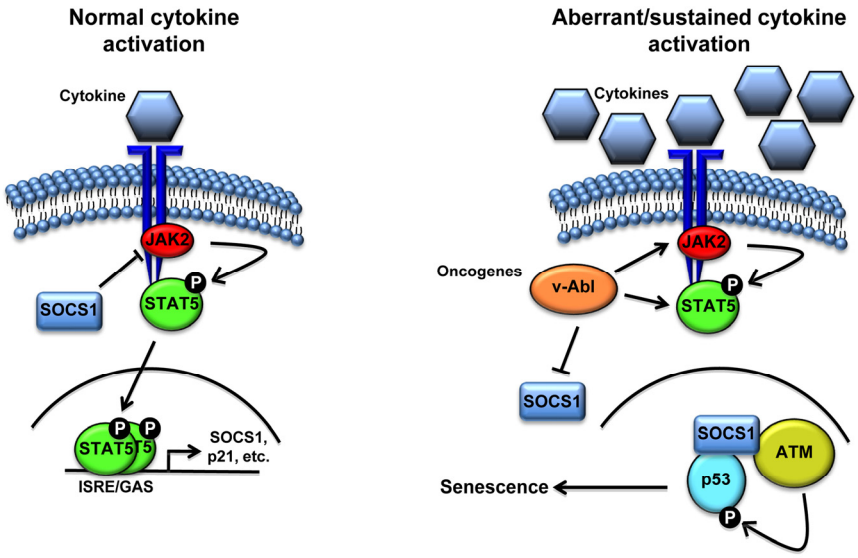

Figure 2. Schematic representation of the cell proliferation control exerted by SOCS1. Following activation of the receptor by cytokine binding, JAK phosphorylates the receptor creating a docking site for STATs. JAK then phopshorylates STATs causing its release from the receptor, allowing dimerization and translocation to the nucleus to activate the transcription of specific genes including members of the SOCS family. Subsequently, SOCS terminates cytokine signaling by blocking JAK activity and STAT recruitment to the receptor. However, aberrant activation of STAT5 triggered by oncogenic fusion kinases like TEL-JAK2 might result in sustained levels of SOCS1 that can activate p53 by forming a complex with ATM and p53.

Cytokines, senescence and SOCS1: an emergency switch to control proliferation

Senescent cells secrete numerous cytokines and other mediators that modify the tissue microenvironment. The sum of these secreted factors constitutes what has been named the senescence-associated secretory phenotype (SASP) [50]. Among the SASP factors, IL-6 is required for the oncogene-induced senescence and induction of the tumor suppressor p15INK4B [51]. Furthermore, persistent, but not transient, DNA damage signaling triggers the ATM-dependent IL-6 secretion, presumably to call attention to the presence of damaged cells [52]. During oncogene-induced senescence, IL-6 also amplifies the secretion of IL-8 [51], which with GROα activates the CXCR2 receptor to reinforce senescence [53]. Among the factors secreted by senescent cells, IGFBP7 [54] and PAI-1 [55] contribute to the growth arrest response, while p53 regulates expression of chemokines directing the immune system to permit the clearance of senescent cells [56]. Collectively, these reports suggest that cytokine signaling could prevent tumor formation by promoting cellular senescence.

The capacity of SOCS1 to activate the p53 pathway can establish an emergency anti-proliferative program in cells exposed to sustain or aberrant cytokine stimulation (Figure 2). Following normal activation of the JAK/STAT pathway, SOCS1 blocks the phosphorylation of STAT by inhibiting or degrading JAK2. However, aberrant and sustained stimulation of STAT might induce a molecular switch allowing SOCS1 to localize to DNA breaks and stimulate ATM-dependent activation of p53.

A general role for SOCS1 in the DNA damage response

The localization of SOCS1 to DNA breaks during STAT5-induced senescence raises numerous questions. First, does the SOCS1 ubiquitin ligase activity contribute to the DNA damage response? A novel cascade of ubiquitination controlled by the E3 ubiquitin ligases RNF8/RNF168 and HERC2 have recently been reported to control the recruitment of BRCA1 and 53BP1 by ubiquitinating the histones H2A and H2AX [57,58,59,60,61,62]. The presence of SOCS1 at DNA

breaks could not only regulate ATM-mediated p53 activation but also control the DNA repair process. Second, what are the mechanisms underlying the nuclear transport of SOCS1 and its presence at DNA damage foci? Since most of its interacting partners were localized to the plasma membrane, SOCS1 was considered to be mostly a cytoplasmic protein, but recent evidences suggest that it can localize to the nucleus under certain conditions including STAT5-induced senescence [34,63]. A bipartite nuclear localization signal (NLS) located between the SH2 domain and the SOCS box allows nuclear localization of SOCS1 [63,64]. However, the mechanism controlling the active transport of SOCS1 remains unclear. A clearer understanding of the mechanisms controlling SOCS1 nuclear localization would be crucial to determine how SOCS1 mediates its tumor suppressor activity. Post-translational modifications like ubiquitination and phosphorylation that have been shown to control the nuclear localization of p53 [65,66,67] and STAT [68] could also control the nucleo-cytoplasmic shuttling of SOCS1. Exclusion of SOCS1 from the nucleus would prevent the formation of the ternary complex with p53 and ATM, preventing the activation of p53. Furthermore, the phosphorylation status of SOCS1 could regulate its activity since aberrant SOCS1 phosphorylation is associated with cellular transformation. Actually, phosphorylation of SOCS1 triggered by the oncogenic v-Abl kinase impedes the SOCS1-Elongin B/C interaction, leading to sustained JAK/STAT signaling [69]. v-Abl signaling induces multiple serine/threonine kinases including members of the Pim kinase family. Pim-1 and Pim-2 are required for efficient cellular transformation mediated by v-Abl [70] and are able to phosphorylate SOCS1 and disrupt its binding to Elongin C [71]. Because SOCS1 requires the SOCS box to form a complex with ATM, v-Abl- or Pim kinase-mediated phosphorylation could potentially interfere with this interaction and block p53 activation. Therefore, it appears that aberrant phosphorylation by oncogenic kinases could interfere with the tumor suppressor activities of SOCS1 by at least two different mechanisms: phosphorylated SOCS1 would not be able to inhibit the JAK/STAT pathway and to interact with ATM and promote p53 activation.

Table I. Identification of SOCS1 interaction partners by mass spectrometry*

Protein	Function
Elongin C	Interacts with SOCS box [10]
Elongin B	Interacts with SOCS box [10]
Pericentrin	Cells depleted of pericentrin enter senescence due to p53 activation [72]
SHC (Src homology 2 domain containing) transforming protein 1 (**SHC1**)	Member of the Shc protein family of molecular adaptors, SHC1 promotes apoptosis by its redox activity. SHC1 is implicated in the control of oxidative stress and life span in mammals [73].
Tripartite motif-containing 28 (**TRIM28** or **KAP1**)	TRIM28 is implicated in transcriptional control through its interaction with the Kruppel-associated box repression domain. TRIM28 contributes to DNA repair mechanisms [74].
5'-nucleotidase, cytosolic II (**NT5C2**)	NT5C2 hydrolyzes 5-prime-monophosphate (IMP) and other purine nucleotides. NT5C2 is implicated in the maintenance of a constant composition of intracellular purine/pyrimidine nucleotides [75].
BCL2-associated transcription factor 1 (**BCLAF1**)	BCLAF1, a transcriptional repressor that interacts with members of the BCL2 family of proteins, promotes apoptosis [76].
Human positive cofactor 4 (**PC4**)	Suppressor of oxidative mutator phenotype [77]. Accumulates at DNA damage foci [78].

***For LC-MS/MS analysis, 3XFlag-SOCS1 was overexpressed in U2OS cells and immunoprecipitated two days post-transfection using the anti-Flag M2 Affinity Gel (Sigma). The total immunoprecipitate was send to the Proteomics Core Facility of the Institute for Research in Immunology and Cancer (IRIC, Montreal, Canada; www.iric.ca) for analysis.**

Finally, the role of SOCS1 as a mediator facilitating the interactions of ATM and ATR with their targets suggests that other interaction partners of SOCS1 could also become the substrates of ATM/ATR-dependent phosphorylation during the DNA damage response. Proteomic analysis of SOCS1 complexes revealed putative interactions with several proteins that play a role in the DNA damage response, apoptosis or oxidative stress pathways (Table I). Future work will determine which functions of SOCS1 apply to every one of its interaction partners: ubiquitination followed by proteolytic degradation or DNA damage stimulated phosphorylation.

CONCLUSIONS

Studies on molecular mechanisms underlying cellular senescence have made significant contributions to the discovery of novel regulators of tumor suppressor pathways. Using microarrays or cDNA / siRNA screens, multiple researchers have identified novel regulators of p53 or Rb in controlling tumor formation. Using this approach to study STAT5-induced senescence, we identified SOCS1 as an important activator of the p53 and the DNA damage response. Surprisingly, the SOCS box represents a binding motif for ATM and ATR [34]. To date, about 40 proteins are known to harbor a SOCS box domain. Clearly further work will determine whether SOCS box-containing proteins also participate in the DNA damage response and control oncogenesis.

ACKNOWLEDGEMENTS

We thank Gillian Vogel for critical reading of the manuscript and helpful suggestions. F.A.M. and G.F. are supported by the Fonds de Recherche en Santé du Québec and V.C. by the Natural Sciences and Engineering Research Council of Canada (NSERC). This work was funded by grants from the Canadian Institutes of Health Research (CIHR MOP82887 to G.F. and MOP84234 to S.I.).

CONFLICT OF INTERESTS STATEMENT

The authors of this manuscript have no conflict of interests to declare.

REFERENCES

1. Hanada T, Yoshimura A. Regulation of cytokine signaling and inflammation. Cytokine Growth Factor Rev. 2002; 13: 413-421.

2. Ward AC, Touw I, Yoshimura A. The Jak-Stat pathway in normal and perturbed hematopoiesis. Blood. 2000; 95: 19-29.

3. Alexander WS. Suppressors of cytokine signalling (SOCS) in the immune system. Nat Rev Immunol. 2002; 2: 410-416.

4. Endo TA, Masuhara M, Yokouchi M, Suzuki R, Sakamoto H, Mitsui K, Matsumoto A, Tanimura S, Ohtsubo M, Misawa H, Miyazaki T, Leonor N, Taniguchi T, et al. A new protein containing an SH2 domain that inhibits JAK kinases. Nature. 1997; 387: 921-924.

5. Naka T, Narazaki M, Hirata M, Matsumoto T, Minamoto S, Aono A, Nishimoto N, Kajita T, Taga T, Yoshizaki K, Akira S, Kishimoto T. Structure and function of a new STAT-induced STAT inhibitor. Nature. 1997; 387: 924-929.

6. Starr R, Willson TA, Viney EM, Murray LJ, Rayner JR, Jenkins BJ, Gonda TJ, Alexander WS, Metcalf D, Nicola NA, Hilton DJ. A family of cytokine-inducible inhibitors of signalling. Nature. 1997; 387: 917-921.

7. Nicholson SE, Willson TA, Farley A, Starr R, Zhang JG, Baca M, Alexander WS, Metcalf D, Hilton DJ, Nicola NA. Mutational analyses of the SOCS proteins suggest a dual domain requirement but distinct mechanisms for inhibition of LIF and IL-6 signal transduction. EMBO J. 1999; 18: 375-385.

8. Yasukawa H, Misawa H, Sakamoto H, Masuhara M, Sasaki A, Wakioka T, Ohtsuka S, Imaizumi T, Matsuda T, Ihle JN, Yoshimura A. The JAK-binding protein JAB inhibits Janus tyrosine kinase activity through binding in the activation loop. EMBO J. 1999; 18: 1309-1320.

9. Kamura T, Maenaka K, Kotoshiba S, Matsumoto M, Kohda D, Conaway RC, Conaway JW, Nakayama KI. VHL-box and SOCS-box domains determine binding specificity for Cul2-Rbx1 and Cul5-Rbx2 modules of ubiquitin ligases. Genes Dev. 2004; 18: 3055-3065.

10. Kamura T, Sato S, Haque D, Liu L, Kaelin WG, Jr., Conaway RC, Conaway JW. The Elongin BC complex interacts with the conserved SOCS-box motif present in members of the SOCS, ras, WD-40 repeat, and ankyrin repeat families. Genes Dev. 1998; 12: 3872-3881.

11. Ungureanu D, Saharinen P, Junttila I, Hilton DJ, Silvennoinen O. Regulation of Jak2 through the ubiquitin-proteasome pathway involves phosphorylation of Jak2 on Y1007 and interaction with SOCS-1. Mol Cell Biol. 2002; 22: 3316-3326.

12. Kamizono S, Hanada T, Yasukawa H, Minoguchi S, Kato R, Minoguchi M, Hattori K, Hatakeyama S, Yada M, Morita S, Kitamura T, Kato H, Nakayama K, et al. The SOCS box of SOCS-1 accelerates ubiquitin-dependent proteolysis of TEL-JAK2. J Biol Chem. 2001; 276: 12530-12538.

13. Rui L, Yuan M, Frantz D, Shoelson S, White MF. SOCS-1 and SOCS-3 block insulin signaling by ubiquitin-mediated degradation of IRS1 and IRS2. J Biol Chem. 2002; 277: 42394-42398.

14. Liu E, Cote JF, Vuori K. Negative regulation of FAK signaling by SOCS proteins. EMBO J. 2003; 22: 5036-5046.

15. De Sepulveda P, Ilangumaran S, Rottapel R. Suppressor of cytokine signaling-1 inhibits VAV function through protein degradation. J Biol Chem. 2000; 275: 14005-14008.

16. Mansell A, Smith R, Doyle SL, Gray P, Fenner JE, Crack PJ, Nicholson SE, Hilton DJ, O'Neill LA, Hertzog PJ. Suppressor of cytokine signaling 1 negatively regulates Toll-like receptor signaling by mediating Mal degradation. Nat Immunol. 2006; 7: 148-155.

17. Rottapel R, Ilangumaran S, Neale C, La Rose J, Ho JM, Nguyen MH, Barber D, Dubreuil P, de Sepulveda P. The tumor suppressor activity of SOCS-1. Oncogene. 2002; 21: 4351-4362.

18. Fukushima N, Sato N, Sahin F, Su GH, Hruban RH, Goggins M. Aberrant methylation of suppressor of cytokine signalling-1

(SOCS-1) gene in pancreatic ductal neoplasms. Br J Cancer. 2003; 89: 338-343.

19. Galm O, Yoshikawa H, Esteller M, Osieka R, Herman JG. SOCS-1, a negative regulator of cytokine signaling, is frequently silenced by methylation in multiple myeloma. Blood. 2003; 101: 2784-2788.

20. Jiang S, Zhang HW, Lu MH, He XH, Li Y, Gu H, Liu MF, Wang ED. MicroRNA-155 functions as an OncomiR in breast cancer by targeting the suppressor of cytokine signaling 1 gene. Cancer Res. 2010; 70: 3119-3127.

21. Melzner I, Bucur AJ, Bruderlein S, Dorsch K, Hasel C, Barth TF, Leithauser F, Moller P. Biallelic mutation of SOCS-1 impairs JAK2 degradation and sustains phospho-JAK2 action in the MedB-1 mediastinal lymphoma line. Blood. 2005; 105: 2535-2542.

22. Pichiorri F, Suh SS, Ladetto M, Kuehl M, Palumbo T, Drandi D, Taccioli C, Zanesi N, Alder H, Hagan JP, Munker R, Volinia S, Boccadoro M, et al. MicroRNAs regulate critical genes associated with multiple myeloma pathogenesis. Proc Natl Acad Sci U S A. 2008; 105: 12885-12890.

23. Sutherland KD, Lindeman GJ, Choong DY, Wittlin S, Brentzell L, Phillips W, Campbell IG, Visvader JE. Differential hypermethylation of SOCS genes in ovarian and breast carcinomas. Oncogene. 2004; 23: 7726-7733.

24. Weniger MA, Melzner I, Menz CK, Wegener S, Bucur AJ, Dorsch K, Mattfeldt T, Barth TF, Moller P. Mutations of the tumor suppressor gene SOCS-1 in classical Hodgkin lymphoma are frequent and associated with nuclear phospho-STAT5 accumulation. Oncogene. 2006; 25: 2679-2684.

25. Yoshikawa H, Matsubara K, Qian GS, Jackson P, Groopman JD, Manning JE, Harris CC, Herman JG. SOCS-1, a negative regulator of the JAK/STAT pathway, is silenced by methylation in human hepatocellular carcinoma and shows growth-suppression activity. Nat Genet. 2001; 28: 29-35.

26. Evan GI, d'Adda di Fagagna F. Cellular senescence: hot or what? Curr Opin Genet Dev. 2009; 19: 25-31.

27. Yu H, Jove R. The STATs of cancer--new molecular targets come of age. Nat Rev Cancer. 2004; 4: 97-105.

28. Mallette FA, Gaumont-Leclerc MF, Ferbeyre G. The DNA damage signaling pathway is a critical mediator of oncogene-induced senescence. Genes Dev. 2007; 21: 43-48.

29. Mallette FA, Gaumont-Leclerc MF, Huot G, Ferbeyre G. Myc down-regulation as a mechanism to activate the Rb pathway in STAT5A-induced senescence. J Biol Chem. 2007; 282: 34938-34944.

30. Mallette FA, Moiseeva O, Calabrese V, Mao B, Gaumont-Leclerc MF, Ferbeyre G. Transcriptome analysis and tumor suppressor requirements of STAT5-induced senescence. Ann N Y Acad Sci. 2010; 1197: 142-151.

31. de Stanchina E, McCurrach ME, Zindy F, Shieh SY, Ferbeyre G, Samuelson AV, Prives C, Roussel MF, Sherr CJ, Lowe SW. E1A signaling to p53 involves the p19(ARF) tumor suppressor. Genes Dev. 1998; 12: 2434-2442.

32. Zindy F, Eischen CM, Randle DH, Kamijo T, Cleveland JL, Sherr CJ, Roussel MF. Myc signaling via the ARF tumor suppressor regulates p53-dependent apoptosis and immortalization. Genes Dev. 1998; 12: 2424-2433.

33. Wei W, Hemmer RM, Sedivy JM. Role of p14(ARF) in replicative and induced senescence of human fibroblasts. Mol Cell Biol. 2001; 21: 6748-6757.

34. Calabrese V, Mallette FA, Deschenes-Simard X, Ramanathan S, Gagnon J, Moores A, Ilangumaran S, Ferbeyre G. SOCS1 links cytokine signaling to p53 and senescence. Mol Cell. 2009; 36: 754-767.

35. de Stanchina E, Querido E, Narita M, Davuluri RV, Pandolfi PP, Ferbeyre G, Lowe SW. PML is a direct p53 target that modulates p53 effector functions. Mol Cell. 2004; 13: 523-535.

36. Bourdeau V, Baudry D, Ferbeyre G. PML links aberrant cytokine signaling and oncogenic stress to cellular senescence. Front Biosci. 2009; 14: 475-485.

37. Ferbeyre G, de Stanchina E, Querido E, Baptiste N, Prives C, Lowe SW. PML is induced by oncogenic ras and promotes premature senescence. Genes Dev. 2000; 14: 2015-2027.

38. Pearson M, Carbone R, Sebastiani C, Cioce M, Fagioli M, Saito S, Higashimoto Y, Appella E, Minucci S, Pandolfi PP, Pelicci PG. PML regulates p53 acetylation and premature senescence induced by oncogenic Ras. Nature. 2000; 406: 207-210.

39. Cleghon V, Morrison DK. Raf-1 interacts with Fyn and Src in a non-phosphotyrosine-dependent manner. J Biol Chem. 1994; 269: 17749-17755.

40. Park I, Chung J, Walsh CT, Yun Y, Strominger JL, Shin J. Phosphotyrosine-independent binding of a 62-kDa protein to the src homology 2 (SH2) domain of p56lck and its regulation by phosphorylation of Ser-59 in the lck unique N-terminal region. Proc Natl Acad Sci U S A. 1995; 92: 12338-12342.

41. Roe JS, Kim H, Lee SM, Kim ST, Cho EJ, Youn HD. p53 stabilization and transactivation by a von Hippel-Lindau protein. Mol Cell. 2006; 22: 395-405.

42. Bischof O, Schwamborn K, Martin N, Werner A, Sustmann C, Grosschedl R, Dejean A. The E3 SUMO ligase PIASy is a regulator of cellular senescence and apoptosis. Mol Cell. 2006; 22: 783-794.

43. Kahyo T, Nishida T, Yasuda H Involvement of PIAS1 in the sumoylation of tumor suppressor p53. Mol Cell. 2001; 8: 713-718.

44. Megidish T, Xu JH, Xu CW. Activation of p53 by protein inhibitor of activated Stat1 (PIAS1). J Biol Chem. 2002; 277: 8255-8259.

45. Bartkova J, Rezaei N, Liontos M, Karakaidos P, Kletsas D, Issaeva N, Vassiliou LV, Kolettas E, Niforou K, Zoumpourlis VC, Takaoka M, Nakagawa H, Tort F, et al. Oncogene-induced senescence is part of the tumorigenesis barrier imposed by DNA damage checkpoints. Nature. 2006; 444: 633-637.

46. Di Micco R, Fumagalli M, Cicalese A, Piccinin S, Gasparini P, Luise C, Schurra C, Garre M, Nuciforo PG, Bensimon A, Maestro R, Pelicci PG, d'Adda di Fagagna F. Oncogene-induced senescence is a DNA damage response triggered by DNA hyper-replication. Nature. 2006; 444: 638-642.

47. Mallette FA, Ferbeyre G. The DNA damage signaling pathway connects oncogenic stress to cellular senescence. Cell Cycle. 2007; 6: 1831-1836.

48. Galanty Y, Belotserkovskaya R, Coates J, Polo S, Miller KM, Jackson SP. Mammalian SUMO E3-ligases PIAS1 and PIAS4 promote responses to DNA double-strand breaks. Nature. 2009; 462: 935-939.

49. Morris JR, Boutell C, Keppler M, Densham R, Weekes D, Alamshah A, Butler L, Galanty Y, Pangon L, Kiuchi T, Ng T, Solomon E. The SUMO modification pathway is involved in the BRCA1 response to genotoxic stress. Nature. 2009; 462: 886-890.

50. Coppe JP, Patil CK, Rodier F, Sun Y, Munoz DP, Goldstein J, Nelson PS, Desprez PY, Campisi J. Senescence-associated secretory phenotypes reveal cell-nonautonomous functions of oncogenic RAS and the p53 tumor suppressor. PLoS Biol. 2008; 6: 2853-2868.

51. Kuilman T, Michaloglou C, Vredeveld LC, Douma S, van Doorn R, Desmet CJ, Aarden LA, Mooi WJ, Peeper DS. Oncogene-induced senescence relayed by an interleukin-dependent inflammatory network. Cell. 2008; 133: 1019-1031.

52. Rodier F, Coppe JP, Patil CK, Hoeijmakers WA, Munoz DP, Raza SR, Freund A, Campeau E, Davalos AR, Campisi J. Persistent DNA damage signalling triggers senescence-associated inflammatory cytokine secretion. Nat Cell Biol. 2009; 11: 973-979.

53. Acosta JC, O'Loghlen A, Banito A, Guijarro MV, Augert A, Raguz S, Fumagalli M, Da Costa M, Brown C, Popov N, Takatsu Y, Melamed J, d'Adda di Fagagna F, et al. Chemokine signaling via the CXCR2 receptor reinforces senescence. Cell. 2008; 133: 1006-1018.

54. Wajapeyee N, Serra RW, Zhu X, Mahalingam M, Green MR. Oncogenic BRAF induces senescence and apoptosis through pathways mediated by the secreted protein IGFBP7. Cell. 2008; 132: 363-374.

55. Kortlever RM, Higgins PJ, Bernards R. Plasminogen activator inhibitor-1 is a critical downstream target of p53 in the induction of replicative senescence. Nat Cell Biol. 2006; 8: 877-884.

56. Xue W, Zender L, Miething C, Dickins RA, Hernando E, Krizhanovsky V, Cordon-Cardo C, Lowe SW. Senescence and tumour clearance is triggered by p53 restoration in murine liver carcinomas. Nature. 2007; 445: 656-660.

57. Bekker-Jensen S, Rendtlew Danielsen J, Fugger K, Gromova I, Nerstedt A, Lukas C, Bartek J, Lukas J, Mailand N. HERC2 coordinates ubiquitin-dependent assembly of DNA repair factors on damaged chromosomes. Nat Cell Biol. 2010; 12: 80-86; sup pp 81-12.

58. Doil C, Mailand N, Bekker-Jensen S, Menard P, Larsen DH, Pepperkok R, Ellenberg J, Panier S, Durocher D, Bartek J, Lukas J, Lukas C. RNF168 binds and amplifies ubiquitin conjugates on damaged chromosomes to allow accumulation of repair proteins. Cell. 2009; 136: 435-446.

59. Huen MS, Grant R, Manke I, Minn K, Yu X, Yaffe MB, Chen J. RNF8 transduces the DNA-damage signal via histone ubiquitylation and checkpoint protein assembly. Cell. 2007; 131: 901-914.

60. Kolas NK, Chapman JR, Nakada S, Ylanko J, Chahwan R, Sweeney FD, Panier S, Mendez M, Wildenhain J, Thomson TM, Pelletier L, Jackson SP, Durocher D Orchestration of the DNA-damage response by the RNF8 ubiquitin ligase. Science. 2007; 318: 1637-1640.

61. Mailand N, Bekker-Jensen S, Faustrup H, Melander F, Bartek J, Lukas C, Lukas J. RNF8 ubiquitylates histones at DNA double-strand breaks and promotes assembly of repair proteins. Cell. 2007; 131: 887-900.

62. Stewart GS, Panier S, Townsend K, Al-Hakim AK, Kolas NK, Miller ES, Nakada S, Ylanko J, Olivarius S, Mendez M, Oldreive C, Wildenhain J, Tagliaferro A, et al. The RIDDLE syndrome protein mediates a ubiquitin-dependent signaling cascade at sites of DNA damage. Cell. 2009; 136: 420-434.

63. Koelsche C, Strebovsky J, Baetz A, Dalpke AH. Structural and functional analysis of a nuclear localization signal in SOCS1. Mol Immunol. 2009; 46: 2474-2480.

64. Baetz A, Koelsche C, Strebovsky J, Heeg K, Dalpke AH. Identification of a nuclear localization signal in suppressor of cytokine signaling 1. FASEB J. 2008; 22: 4296-4305.

65. Boyd SD, Tsai KY, Jacks T. An intact HDM2 RING-finger domain is required for nuclear exclusion of p53. Nat Cell Biol. 2000; 2: 563-568.

66. Geyer RK, Yu ZK, Maki CG. The MDM2 RING-finger domain is required to promote p53 nuclear export. Nat Cell Biol. 2000; 2: 569-573.

67. Li M, Brooks CL, Wu-Baer F, Chen D, Baer R, Gu W. Mono-versus polyubiquitination: differential control of p53 fate by Mdm2. Science. 2003; 302: 1972-1975.

68. Sekimoto T, Imamoto N, Nakajima K, Hirano T, Yoneda Y. Extracellular signal-dependent nuclear import of Stat1 is mediated by nuclear pore-targeting complex formation with NPI-1, but not Rch1. EMBO J. 1997; 16: 7067-7077.

69. Limnander A, Danial NN, Rothman PB. v-Abl signaling disrupts SOCS-1 function in transformed pre-B cells. Mol Cell. 2004; 15: 329-341.

70. Chen JL, Limnander A, Rothman PB. Pim-1 and Pim-2 kinases are required for efficient pre-B-cell transformation by v-Abl oncogene. Blood. 2008; 111: 1677-1685.

71. Chen XP, Losman JA, Cowan S, Donahue E, Fay S, Vuong BQ, Nawijn MC, Capece D, Cohan VL, Rothman P. Pim serine/threonine kinases regulate the stability of Socs-1 protein. Proc Natl Acad Sci U S A. 2002; 99: 2175-2180.

72. Srsen V, Gnadt N, Dammermann A, Merdes A. Inhibition of centrosome protein assembly leads to p53-dependent exit from the cell cycle. J Cell Biol. 2006; 174: 625-630.

73. Trinei M, Giorgio M, Cicalese A, Barozzi S, Ventura A, Migliaccio E, Milia E, Padura IM, Raker VA, Maccarana M, Petronilli V, Minucci S, Bernardi P, et al. A p53-p66Shc signalling pathway controls intracellular redox status, levels of oxidation-damaged DNA and oxidative stress-induced apoptosis. Oncogene. 2002; 21: 3872-3878.

74. White DE, Negorev D, Peng H, Ivanov AV, Maul GG, Rauscher FJ. 3rd KAP1, a novel substrate for PIKK family members, colocalizes with numerous damage response factors at DNA lesions. Cancer Res. 2006; 66: 11594-11599.

75. Yamauchi T, Negoro E, Kishi S, Takagi K, Yoshida A, Urasaki Y, Iwasaki H, Ueda T. Intracellular cytarabine triphosphate production correlates to deoxycytidine kinase/cytosolic 5'-nucleotidase II expression ratio in primary acute myeloid leukemia cells. Biochem Pharmacol. 2009; 77: 1780-1786.

76. Letsas KP, Frangou-Lazaridis M, Skyrlas A, Tsatsoulis A, Malamou-Mitsi V. Transcription factor-mediated proliferation and apoptosis in benign and malignant thyroid lesions. Pathol Int. 2005; 55: 694-702.

77. Wang JY, Sarker AH, Cooper PK, Volkert MR. The single-strand DNA binding activity of human PC4 prevents mutagenesis and killing by oxidative DNA damage. Mol Cell Biol. 2004; 24: 6084-6093.

78. Mortusewicz O, Roth W, Li N, Cardoso MC, Meisterernst M, Leonhardt H. Recruitment of RNA polymerase II cofactor PC4 to DNA damage sites. J Cell Biol. 2008; 183: 769-776.

Research Paper

The choice between p53-induced senescence and quiescence is determined in part by the mTOR pathway

Lioubov G. Korotchkina, Olga V. Leontieva, Elena I. Bukreeva, Zoya N. Demidenko, Andrei V. Gudkov and Mikhail V. Blagosklonny

Department of Cell Stress Biology, Roswell Park Cancer Institute, BLSC, L3-312, Buffalo, NY 14263, USA

Key words: *p53, senescence, rapamycin, mTOR, cancer, cell cycle*
Received: *06/05/10; accepted: 06/23/10; published on line: 06/25/10*
Corresponding author: *blagosklonny@oncotarget.com*
Copyright: *© Korotchkina et al. This is an open-access article distributed under the terms of the Creative Commons Attribution License, which permits unrestricted use, distribution, and reproduction in any medium, provided the original author and source are credited*

Abstract: Transient induction of p53 can cause reversible quiescence and irreversible senescence. Using nutlin-3a (a small molecule that activates p53 without causing DNA damage), we have previously identified cell lines in which nutlin-3a caused quiescence. Importantly, nutlin-3a caused quiescence by actively suppressing the senescence program (while still causing cell cycle arrest). Noteworthy, in these cells nutlin-3a inhibited the mTOR (mammalian Target of Rapamycin) pathway, which is known to be involved in the senescence program. Here we showed that shRNA-mediated knockdown of TSC2, a negative regulator of mTOR, partially converted quiescence into senescence in these nutlin-arrested cells. In accord, in melanoma cell lines and mouse embryo fibroblasts, which easily undergo senescence in response to p53 activation, nutlin-3a failed to inhibit mTOR. In these senescence-prone cells, the mTOR inhibitor rapamycin converted nutlin-3a-induced senescence into quiescence. We conclude that status of the mTOR pathway can determine, at least in part, the choice between senescence and quiescence in p53-arrested cells.

INTRODUCTION

Depending on the cell type and other factors p53 activation can result in apoptosis, reversible (quiescence) and irreversible (senescence) cell cycle arrest [1-8]. While the choice between apoptosis and cell cycle arrest has been intensively scrutinized, the choice between quiescence and senescence was not systematically addressed and remains elusive. In order to observe whether p53 activation causes either senescence or quiescence, others and we employed nutlin-3a. Nutlin-3a, a small molecular therapeutic, inhibits Mdm2/p53 interaction and induces p53 at physiological levels without causing DNA damage [9-11]. It was reported that nutlin-3a caused senescent morphology and permanent loss of proliferative potential [12, 13]. However, in other cell lines nutlin-3a caused quiescence so that cells resumed proliferation, when nutlin-3a was removed [14-16]. Moreover, we recently reported that in human fibroblasts (WI-38tert) and fibrosarcoma cells (HT-1080-p21-9), in which nutlin-3a caused quiescence [16], p53 acted as a suppressor of senescence [17]. Thus, ectopic expression of p21 in these cells caused senescence, while simultaneous induction of p53 converted senescence into quiescence [17]. In agreement with previous reports [18-20], we found that p53 inhibited the mTOR pathway [17]. Importantly, the mTOR pathway is involved in cellular senescence [21-26]. We suggested that p53-mediated arrest remains reversible as long as p53 inhibits mTOR. If this model is correct, then senescence would occur in those cells, in which p53 is incapable of suppressing mTOR. Here we provide experimental evidence supporting this prediction and demonstrate that irreversibility of p53-mediated arrest may result from its failure to suppress the mTOR pathway.

RESULTS

Depletion of TSC2 favors senescence by p53

We have shown that nutlin-3a caused quiescence in HT-p21-9 cells and WI-38tert cells [16]. In these cells, nutlin-3a actively suppressed senescence and this suppression was associated with inhibition of the mTOR pathway by p53 [17]. Next, we investigated whether nutlin-3a can cause senescence in cells lacking tuberous sclerosis 2 (TSC2) (Figure 1A), given that regulation of mTOR by p53 requires TSC2 [18]. The transduced cells were transiently treated with nutlin-3a as shown (Figure 1B). The Tsc2-depleted cells acquired a large/flat morphology and could not resume proliferation, whereas cells treated with vector and nutlin-3a did not become senescent and resumed proliferation, forming colonies after removal of nutlin-3a (Figure 1C-D). The potency of shTSC2 with different sequences varied and two other shTSC2 were less potent but still depleted TSC2 at some time points (Supplemental Figure 1) and partially decreased the proliferative potential in nutlin-3a-arrested cells (Supplemental Figure 1).

We next extended this observation to WI-38tert cells transduced with shTSC2 (Figure 2A). In control, nutlin-3a caused a lean morphology, a characteristic of quiescence [16]. Depletion of TSC2 by shTSC2 converted quiescent morphology to senescent morphology (Figure 2B). Furthermore, this was associated with permanent loss of proliferative potential (Figure 2C). In control, cells resumed proliferation after removal of nutlin-3a, whereas nutlin-3a caused permanent loss of proliferative potential in shTSC2-treated cells (Figure 2C). In agreement with our results, it was previously observed that knockout of Tsc2 cooperates with p53 in induction of cellular senescence in MEFs [27].

Nutlin-3 causes senescence in Mel-10 and -9 cells

We next wished to identify senescence-prone cells, which undergo senescence in response to nutlin-3a. In MEL-10 and Mel-9, two melanoma-derived cell lines, nutlin-3a induced p53 and p21 (Figure 3A) and caused senescent morphology (Figure 3B) and cells did not resume proliferation, when nutlin-3a was removed (Supplemental Figure 2). In contrast, rapamycin did not cause senescent morphology and cells resumed proliferation, when rapamycin was removed (Figure 3B and Supplemental Figure 2). Unlike rapamycin, nutlin-3a did not inhibit S6 phosphorylation (Figure 3A), a marker of rapamycin-sensitive mTOR activity.

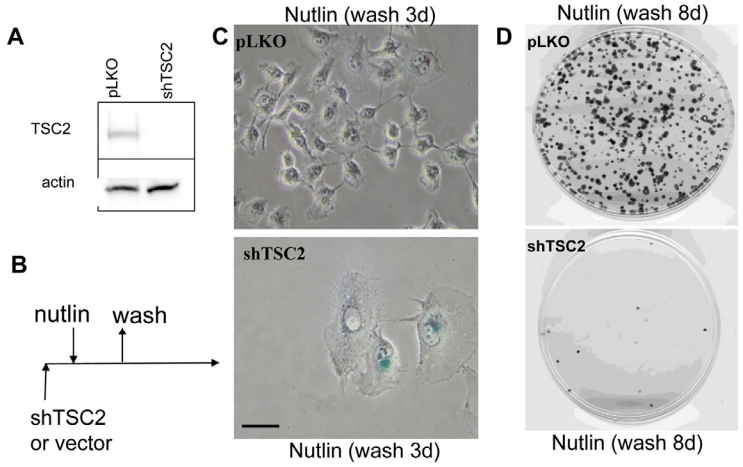

Figure 1. Depletion of TSC2 converts quiescence into senescence in HT-p21-9 cells. (**A**) HT-p21-9 cells were transduced with control lentivirus (pLKO) or lentivirus expressing shTSC2 (sequence # 10) and selected with puromycin for 5 days and then immunoblot was performed. (**B**) Schema: Testing the reversibility of nutlin-3a effects. (**C**) HT-p21-9 cells were transduced with control pLKO or shTSC2 and 5000 cells were plated in 24-well plates and, the next day, were treated with 10 uM nutlin-3a for 3 days. Then nutlin-3a was washed out and the cells were cultivated in fresh medium for 3 days and then stained for beta-Gal and microphotographed. Bars 50 um. (**D**) HT-p21-9 cells were transduced with control pLKO or shTSC2 (and selected for 4 days with puromycin). Then 1000 cells were plated per 60-mm dishes and, the next day, were treated with nutlin-3a for 3 days. Then nutlin-3a was washed out and cells were cultivated in fresh medium for 8 days. Colonies were stained with crystal violet.

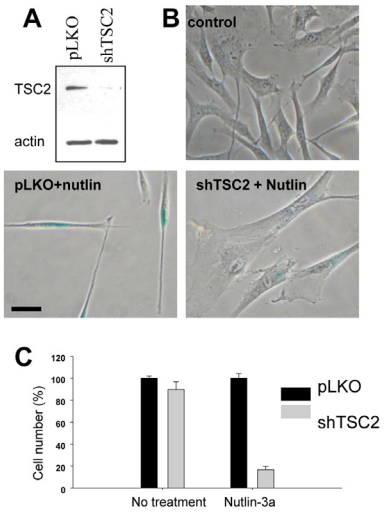

Figure 2. Depletion of TSC2 converts quiescence into senescence in WI-38tert cells. (**A**) Immunoblot. WI-38tert cells were transduced with shTSC or control pLKO and cultured for 5 days. (**B**) WI-38tert cells were transduced with lentiviruses. Next day, medium was replaced and Nutlin (10 uM) with our without rapamycin was added. After 4 days cells were washed and stained for beta-Gal. Bars 50 um. (**C**) WI-38tert cells were transduced with lentiviruses. Next day, medium was replaced and Nutlin (10 uM) was added. After 4 days cells were washed and counted after 6 days.

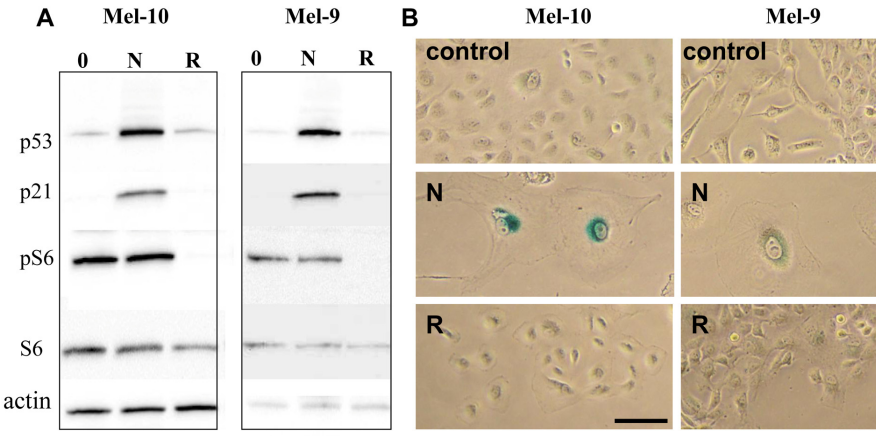

Figure 3. Effects of nutlin-3a and rapamycin on melanoma cells. (A) Mel-10 and Mel-9 cells were incubated with 10 uM nutlin (N) and 500 nM rapamycin (R) for 1 day and immunoblot was performed. (**B)** Mel-10 and Mel-9 cells were incubated with 10 uM nutlin and 500 nM rapamycin for 4 days, then drugs were washed out and cells were incubated for additional 4 days and stained for beta-Gal. Bars 50 um**.**

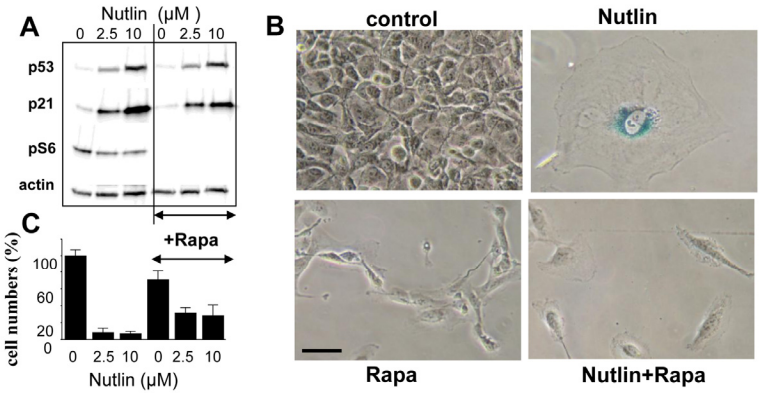

Figure 4. Effect of rapamycin on nutlin-induced senescence in melanoma cells. (A) Mel-10 cells were incubated with 2.5 and 10 uM nutlin with or without 500 nM rapamycin for 1 day and then immunoblot was performed. (**B**) Beta-Gal staining. Mel-10 cells were incubated with 10 M nutlin alone and 500 nM rapamycin for 4 days, then drugs were washed out and cells were incubated for additional 3 days and stained for beta-Gal. Bars 50 um**.**

Rapamycin suppresses nutlin-3a-induced senescence

To establish a causal link between mTOR and senescence, we next investigated whether inhibition of the mTOR pathway by rapamycin could convert nutlin-3a-induced senescence into quiescence. Rapamycin did not affect p53 and p21 induction caused by nutlin-3a but abrogated S6 phosphorylation (Figure 4A), associated with conversion from senescent morphology to quiescent morphology (Figure 4B). Importantly, cells were capable to resume proliferation following removal of nutlin-3a and rapamycin, indicating that the condition was reversible (Figure 4C). Similar results were obtained with Mel-9 cells (data not shown).

Next, we extended this observation to cells of different tissue and species origin. As shown previously, nutlin-3a caused senescence in mouse embryonic fibroblasts (MEFs) [13]. Here we showed that nulin-3a failed to inhibit mTOR pathway in MEF (Figure 5A), and caused senescence (Figure 5 B). Rapamycin inhibited the mTOR pathway and converted senescent morphology to quiescent morphology (Figure 5). This suggests that failure to suppress a rapamycin-sensitive pathway determines nutlin-3a-induced senescence instead of quiescence.

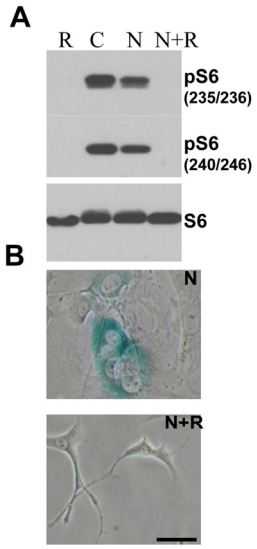

Figure 5. Effect of rapamycin on nutlin-induced senescence in melanoma cells. (**A**) Immunoblot. MEF cells were incubated with 10 nutlin-3a with or without 10 nM rapamycin for 1 day and immunoblot using rabbit anti-phospho-S6 (Ser240/244) and (Ser235/236) and mouse anti-S6 was performed. (**B**) Beta-Gal staining. MEF cells were incubated with 10 uM nutlin alone or with 500 nM rapamycin for 4 days, then drugs were washed out and cells were incubated for additional 4 days and stained for beta-Gal. Bars 50 um**.**

DISCUSSION

The role of p53 in organismal aging and longevity is complex [28-32], indicating that p53 may act as anti-aging factor in some conditions. We have recently de-

monstrated that p53 can suppress cellular senescence, converting it into quiescence [17]. In these quiescence-prone cells, p53 inhibited the mTOR pathway, which is involved in senescence program (Figure 6A). Still p53 induces senescence in numerous cell types. Here we showed that in those cell types, in which nutlin-3a caused senescence, it failed to inhibit the mTOR pathway (Figure 6B). The role of active mTOR as a senescence-inducing factor in these cells was demonstrated by using rapamycin, which partially converted nutlin-3a-induced senescence into quiescence (Figure 6B, lower panel). This indicates that rapamycin-sensitive mTOR activity is necessary for senescence during nutlin-3a-induced cell cycle arrest. And vice versa, in quiescence-prone cells, depletion of TSC2 converted quiescence into senescence (Figure 6A, lower panel). Taken together, data suggest that activation of the mTOR pathway favors senescence (Figure 7). In agreement, Ras accelerated senescence in nutlin-arrested cells [13]. Similarly, activation of Ras and MEK in murine fibroblasts converted p53-induced quiescence into senescence [33]. Interestingly, p53 levels did not correlate with the senescence phenotype, suggesting that factors other than p53 may determine senescence [33]. These important observations are in agreement with our model that senescence requires two factors: cell cycle arrest caused by p53 and simultaneous activation of the growth-promoting mTOR pathway (Note: Ras is an activator of the mTOR pathway). And vice versa it was observed that induction of p53 maintains quiescence upon serum starvation, without causing senescence [34]. In agreement, our model predicts that, by deactivating mTOR, serum starvation prevents senescence.

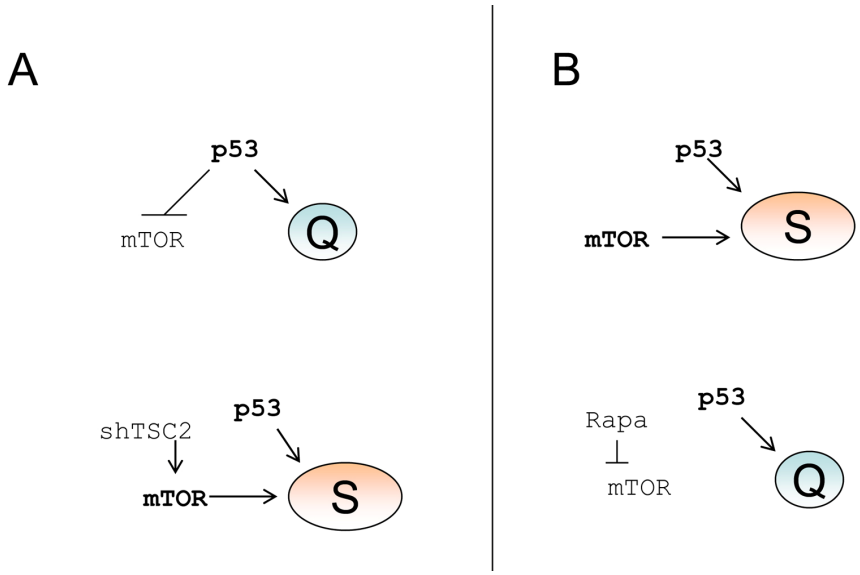

Figure 6. p53 causes senescence by failing to suppress senescence. (**A**) Quiescence-prone cells. Upper panel. P53 causes cell cycle arrest and inhibits the mTOR pathway, thus ensuring quiescence. Lower panel. Transduction of cells with shTSC2 activates mTOR thus converting quiescence into senescence. (**B**) Senescence-prone cells. Upper panel. P53 causes cell cycle arrest without inhibiting the mTOR pathway, thus ensuring senescence. Lower panel. Rapamycin inhibits mTOR thus converting senescence into quiescence

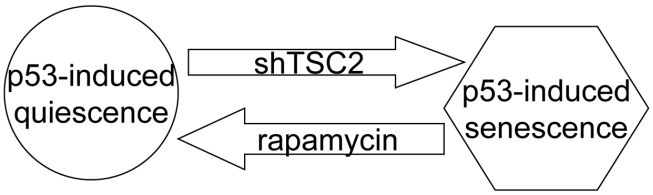

Figure 7. Activation of the mTOR pathway favors senescence in nutlin-3a-arrested cells

Another factor that favors senescence is the duration of cell cycle arrest [13, 35]. Importantly, the duration of the arrest may exceed the duration of treatment with nutlin-3a because of persistent induction of p21 even after removal of nutlin-3a in some cancer cell lines [35]. Additional pathways may be involved in the senescence program. For example, nutlin-3a induces cytoskeletal rearrangement [36]. We speculate that p53 affects not only rapamycin-sensitive mTORC1 but also the mTORC2 complex, given that mTORC2 controls the actin cytoskeleton [37]. Also, p53 inhibits downstream branches of the mTOR pathway [38, 39]. P53 stimulates autophagy [18, 40], which in turn is essential for life-extension by pharmacological manipulations (see [41-44]). Finally, p53 affects cellular metabolism [45-48] and this effect may contribute to suppression of cellular senescence and synergistically potentate metabolic changes caused by mTOR inhibition. The relative contribution of all these mutually dependent factors needs further investigations. The key role of mTOR in cellular senescence links cellular and organismal aging and age-related diseases.

MATERIAL AND METHODS

Cell lines and reagents. HT-p21-9 cells are derivatives of HT1080 human fibrosarcoma cells, where p21 expression can be turned on or off using a physiologically neutral agent isopropyl--thio-galactosidase (IPTG) [16, 49-51]. HT-p21-9 cells express GFP. WI-38-Tert, WI-38 fibroblasts immortalized by telomerase were described previously [16, 17]. Melanoma cell lines, MEL-9 (SK-Mel-103) and MEL-10 (SK-Mel-147), were described previously [52, 53]. RPE cells were described previously [21, 22]. MEF, mouse fibroblasts isolated from 13-day embryos, were provided by Marina Antoch (RPCI) and maintained in DMEM supplemented with 10% FCS. Rapamycin (LC Laboratories, MA, USA), IPTG (Sigma-Aldrich, St. Louis, MO), nutlin-3a (Sigma-Aldrich) were used as previously described [17].

Lentiviral shRNA construction. Bacterial glycerol stocks [clone NM_000548.2-1437s1c1 (#10), NM_000548.x-4581s1c1 (#7) and NM_000548.2-4551s1c1 (#9)] containing lentivirus plasmid vector pLKO.1-puro with shRNA specific for TSC2 was purchased from Sigma. The targeting sequences are: CCGGGCTCATCAACAGGCAGTTCTACTCGAGTA GAACTGCCTGTTGATGAGCTTTTTG (#10), CCGG CAATGAGTCACAGTCCTTTGACTCGAGTCAAAG GACTGTGACTCATTGTTTTTG (#7) and CCGGCG ACGAGTCAAACAAGCCAATCTCGAGATTGGCTT GTTTGACTCGTCGTTTTTG (#9).

pLKO.1-puro lentiviral vector without shRNA was used as a control. Lentiviruses were produced in HEK293T cells after co-transfection of lentivirus plasmid vector with shRNA or control vector with packaging plasmids using Lipofectamine2000 (Invitrogen). After 48h and 72h medium containing lentivirus was collected, centrifuged at 2000g and filtered through 0.22 uM filter. Filtered virus containing medium was used for cell infection or stored at -80 C. Cells were transduced with lentivirus in the presence of 8 mg/ml polybrene and selected with puromycin (1-2 mg/ml) for 4-6 days. Cells were treated with drugs either 24h after transduction or after puromycin selection for infected cells.

Colony formation assay. Plates were fixed and stained with 1.0 % crystal violet (Sigma-Aldrich).

Immunoblot analysis. The following antibodies were used: anti-p53 and anti-p21 antibodies from Cell signaling and anti-actin antibodies from Santa Cruz Biotechnology, rabbit anti-phospho-S6 (Ser240/244) and (Ser235/236), mouse anti-S6, mouse anti-phospho-

p70 S6 kinase (Thr389), mouse anti-p21, rabbit anti-phospho-4E-BP1 (Thr37/46) from Cell Signaling; mouse anti-4E-BP1 from Invitrogen; mouse anti-p53 (Ab-6) from Calbiochem.

Beta-galactosidase staining. beta-Gal staining was performed using Senescence -galactosidase staining kit (Cell Signaling Technology) according to manufacturer's protocol.

CONFLICT OF INTERESTS STATEMENT

The authors of this manuscript have no conflict of interests to declare.

REFERENCES

1. Vogelstein B, Lane DP, Levine AJ. Surfing the p53 network. Nature 2000; 408: 307-310.

2. Itahana K, Dimri G, Campisi J. Regulation of cellular senescence by p53. Eur J Biochem 2001; 268: 2784-2791.

3. Vousden KH. Outcomes of p53 activation--spoilt for choice. J Cell Sci 2006; 119: 5015-5020.

4. Vousden KH, Prives C. Blinded by the Light: The Growing Complexity of p53. Cell 2009; 137: 413-431.

5. Levine AJ, Oren M. The first 30 years of p53: growing ever more complex. Nat Rev Cancer 2009; 9: 749-758.

6. Brown CJ, Lain S, Verma CS, Fersht AR, Lane DP. Awakening guardian angels: drugging the p53 pathway. Nat Rev Cancer 2009; 9: 862-873.

7. Liebermann DA, Hoffman B, Vesely D. p53 induced growth arrest versus apoptosis and its modulation by survival cytokines. Cell Cycle 2007; 6: 166-170.

8. Paris R, Henry RE, Stephens SJ, McBryde M, Espinosa JM. Multiple p53-independent gene silencing mechanisms define the cellular response to p53 activation. Cell Cycle 2008; 7: 2427-2433.

9. Vassilev LT. Small-molecule antagonists of p53-MDM2 binding: research tools and potential therapeutics. Cell Cycle 2004; 3: 419-421.

10. Vassilev LT, Vu BT, Graves B, Carvajal D, Podlaski F, Filipovic Z, Kong N, Kammlott U, Lukacs C, Klein C, Fotouhi N, Liu EA. In vivo activation of the p53 pathway by small-molecule antagonists of MDM2. Science 2004; 303: 844-848.

11. Huang B, Vassilev LT. Reduced transcriptional activity in the p53 pathway of senescent cells revealed by the MDM2 antagonist nutlin-3. Aging 2009; 1: 845-854.

12. Van Maerken T, Speleman F, Vermeulen J, Lambertz I, De Clercq S, De Smet E, Yigit N, Coppens V, Philippé J, De Paepe A, Marine JC, Vandesompele J. Small-molecule MDM2 antagonists as a new therapy concept for neuroblastoma. Cancer Res. 2006; 66: 9646-9655.

13. Efeyan A, Ortega-Molina A, Velasco-Miguel S, Herranz D, Vassilev LT, Serrano M. Induction of p53-dependent senescence by the MDM2 antagonist nutlin-3a in mouse cells of fibroblast origin. Cancer Res. 2007; 67: 7350-7357.

14. Huang B, Deo D, Xia M, Vassilev LT. Pharmacologic p53 Activation Blocks Cell Cycle Progression but Fails to Induce Senescence in Epithelial Cancer Cells. Mol Cancer Res. 2009; 7: 1497-1509.

15. Cheok CF, Kua N, Kaldis P, Lane DP. Combination of nutlin-3 and VX-680 selectively targets p53 mutant cells with reversible effects on cells expressing wild-type p53. Cell Death Differ. 2010; in press.

16. Korotchkina LG, Demidenko ZN, Gudkov AV, Blagosklonny MV. Cellular quiescence caused by the Mdm2 inhibitor nutlin-3a. Cell Cycle 2009; 8: 3777-3781.

17. Demidenko ZN, Korotchkina LG, Gudkov AV, Blagosklonny MV. Paradoxical suppression of cellular senescence by p53. Proc Natl Acad Sci U S A 2010; 9660-4: 9660-9664.

18. Feng Z, Zhang H, Levine AJ, Jin S. The coordinate regulation of the p53 and mTOR pathways in cells. Proc Natl Acad Sci U S A 2005; 102: 8204-8209.

19. Budanov AV, Karin M. p53 target genes sestrin1 and sestrin2 connect genotoxic stress and mTOR signaling. Cell 2008; 134: 451-460.

20. Matthew EM, Hart LS, Astrinidis A, Navaraj A, Dolloff NG, Dicker DT, Henske EP, El-Deiry WS. The p53 target Plk2 interacts with TSC proteins impacting mTOR signaling, tumor growth and chemosensitivity under hypoxic conditions. Cell Cycle 2009; 8: 4168-4175.

21. Demidenko ZN, Blagosklonny MV. Growth stimulation leads to cellular senescence when the cell cycle is blocked. Cell Cycle 2008; 7: 3355-3361.

22. Demidenko ZN, Zubova SG, Bukreeva EI, Pospelov VA, Pospelova TV, Blagosklonny MV. Rapamycin decelerates cellular senescence. Cell Cycle 2009; 8: 1888-1895.

23. Demidenko ZN, Shtutman M, Blagosklonny MV. Pharmacologic inhibition of MEK and PI-3K converges on the mTOR/S6 pathway to decelerate cellular senescence. Cell Cycle 2009; 8: 1896-1900.

24. Demidenko ZN, Blagosklonny MV. At concentrations that inhibit mTOR, resveratrol suppresses cellular senescence. Cell Cycle 2009; 8: 1901-1904.

25. Demidenko ZN, Blagosklonny MV. Quantifying pharmacologic suppression of cellular senescence: prevention of cellular hypertrophy versus preservation of proliferative potential. Aging 2009; 1: 1008-1016.

26. Pospelova TV, Demidenko ZN, Bukreeva EI, Pospelov VA, Gudkov AV, Blagosklonny MV. Pseudo-DNA damage response in senescent cells. Cell Cycle 2009; 8: 4112-4118.

27. Zhang H, Cicchetti G, Onda H, Koon HB, Asrican K, Bajraszewski N, Vazquez F, Carpenter CL, Kwiatkowski DJ. Loss of Tsc1/Tsc2 activates mTOR and disrupts PI3K-Akt signaling through downregulation of PDGFR. J Clin Invest. 2003; 112: 1223-1233.

28. Matheu A, Maraver A, Klatt P, Flores I, Garcia-Cao I, Borras C, Flores JM, Vina J, Blasco MA, Serrano M. Delayed ageing through damage protection by the Arf/p53 pathway. Nature 2007; 448: 375-379.

29. Waskar M, Landis GN, Shen J, Curtis C, Tozer K, Abdueva D, Skvortsov D, Tavare S, Tower J. Drosophila melanogaster p53 has developmental stage-specific and sex-specific effects on adult life span indicative of sexual antagonistic pleiotropy. Aging 2009; 1: 903-936.

30. Biteau B, Jasper H. It's all about balance: p53 and aging. Aging 2009; 1: 884-886.

31. Hur JH, Walker DW. p53, sex, and aging: lessons from the fruit fly. Aging 2009; 1: 881-883.
32. Donehower LA. Longevity regulation in flies: a role for p53. Aging 2009; 1: 6-8.
33. Ferbeyre G, de Stanchina E, Lin AW, Querido E, McCurrach ME, Hannon GJ, Lowe SW. Oncogenic ras and p53 cooperate to induce cellular senescence. Mol Cell Biol. 2002; 22: 3497-3508.
34. Itahana K, Dimri GP, Hara E, Itahana Y, Zou Y, Desprez PY, Campisi J. A role for p53 in maintaining and establishing the quiescence growth arrest in human cells. J Biol Chem 2002; 277: 18206-18214.
35. Shen H, Maki CG. Persistent p21 expression after Nutlin-3a removal is associated with senescence-like arrest in 4N cells. J Biol Chem 2010.
36. Moran DM, Maki CG. Nutlin-3a induces cytoskeletal rearrangement and inhibits the migration and invasion capacity of p53 wild-type cancer cells. Mol Cancer Ther 2010; 9: 895-905.
37. Jacinto E, Loewith R, Schmidt A, Lin S, Ruegg MA, Hall A, Hall MN. Mammalian TOR complex 2 controls the actin cytoskeleton and is rapamycin insensitive. Nat Cell Biol 2004; 6: 1122-1128.
38. Constantinou C, Clemens MJ. Regulation of the phosphorylation and integrity of protein synthesis initiation factor eIF4GI and the translational repressor 4E-BP1 by p53. Oncogene 2005; 24: 4839-4850.
39. Constantinou C, Elia A, Clemens MJ. Activation of p53 stimulates proteasome-dependent truncation of eIF4E-binding protein 1 (4E-BP1). Biol Cell 2008; 100: 279-289.
40. Maiuri MC, Malik SA, Morselli E, Kepp O, Criollo A, Mouchel PL, Carnuccio R, Kroemer G. Stimulation of autophagy by the p53 target gene Sestrin2. Cell Cycle 2009; 8: 1571-1576.
41. Morselli E, Galluzzi L, Kepp O, Criollo A, Maiuri MC, Tavernarakis N, Madeo F, Kroemer G. Autophagy mediates pharmacological lifespan extension by spermidine and resveratrol. Aging 2009; 1: 961-970.
42. Alvers AL, Wood MS, Hu D, Kaywell AC, Dunn WA, Jr., Aris JP. Autophagy is required for extension of yeast chronological life span by rapamycin. Autophagy 2009; 5: 847-849.
43. Bjedov I, Toivonen JM, Kerr F, Slack C, Jacobson J, Foley A, Partridge L. Mechanisms of life span extension by rapamycin in the fruit fly Drosophila melanogaster. Cell Metab 2010; 11: 35-46.
44. Hands SL, Proud CG, Wyttenbach A. mTOR's role in ageing: protein synthesis or autophagy? Aging 2009; 586-597.
45. Vousden KH, Ryan KM. p53 and metabolism. Nat Rev Cancer 2009; 9: 691-700.
46. Feng Z, Levine AJ. The regulation of energy metabolism and the IGF-1/mTOR pathways by the p53 protein. Trends Cell Biol 2010;
47. Hu W, Zhang C, Wu R, Sun Y, Levine A, Feng Z. Glutaminase 2, a novel p53 target gene regulating energy metabolism and antioxidant function. Proc Natl Acad Sci U S A 107: 7455-7460.
48. Suzuki S, Tanaka T, Poyurovsky MV, Nagano H, Mayama T, Ohkubo S, Lokshin M, Hosokawa H, Nakayama T, Suzuki Y, Sugano S, Sato E, Nagao T, Yokote K, Tatsuno I, Prives C. Phosphate-activated glutaminase (GLS2), a p53-inducible regulator of glutamine metabolism and reactive oxygen species. Proc Natl Acad Sci U S A 107: 7461-7466.
49. Chang BD, Broude EV, Dokmanovic M, Zhu H, Ruth A, Xuan Y, Kandel ES, Lausch E, Christov K, Roninson IB. A senescence-like phenotype distinguishes tumor cells that undergo terminal proliferation arrest after exposure to anticancer agents. Cancer Res. 1999; 59: 3761-3767.
50. Chang BD, Broude EV, Fang J, Kalinichenko TV, Abdryashitov R, Poole JC, Roninson IB. p21Waf1/Cip1/Sdi1-induced growth arrest is associated with depletion of mitosis-control proteins and leads to abnormal mitosis and endoreduplication in recovering cells. Oncogene 2000; 19: 2165-2170.
51. Broude EV, Swift ME, Vivo C, Chang BD, Davis BM, Kalurupalle S, Blagosklonny MV, Roninson IB. p21(Waf1/Cip1/Sdi1) mediates retinoblastoma protein degradation. Oncogene 2007; 26: 6954-6958.
52. Mannava S, Grachtchouk V, Wheeler LJ, Im M, Zhuang D, Slavina EG, Mathews CK, Shewach DS, Nikiforov MA. Direct role of nucleotide metabolism in C-MYC-dependent proliferation of melanoma cells. Cell Cycle 2008; 7: 2392-2400.
53. Zhuang D, Mannava S, Grachtchouk V, Tang WH, Patil S, Wawrzyniak JA, Berman AE, Giordano TJ, Prochownik EV, Soengas MS, Nikiforov MA. C-MYC overexpression is required for continuous suppression of oncogene-induced senescence in melanoma cells. Oncogene 2008; 27: 6623-6634.

SUPPLEMENTAL FIGURES

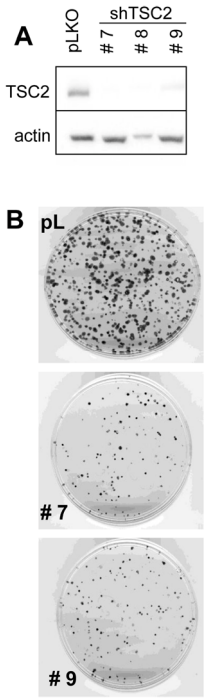

Supplemental Figure 1. Depletion of TSC2 converts quiescence into senescence in HT-p21-9 cells. (**A**) HT-p21-9 cells were transduced with control lentivirus (pLKO) or lentivirus expressing shTSC2 (sequence # 7, 8, 9) and selected with puromycin for 10 days and then immunoblot was performed. (**B**) HT-p21-9 cells were transduced with control pLKO or shTSC2 (and selected for 4 days with puromycin). Then 1000 cells were plated per 60-mm dishes and, the next day, were treated with nutlin-3a for 3 days. Then nutlin-3a was washed out and cells were cultivated in fresh medium for 8 days. Colonies were stained with crystal violet.

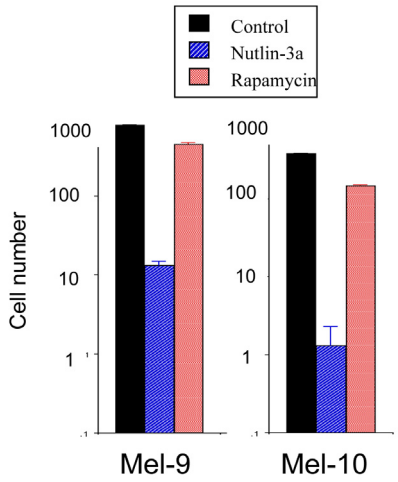

Supplemental Figure 2. Irreversible and reversible effects of nutlin-3a and rapamycin: Mel-10 and Mel-9 cells were incubated with 10 uM nutlin (N) and 500 nM rapamycin (R) for 4 day and then nutlin-3a was washed. After a week, cells were counted.

Research paper

Drosophila melanogaster p53 has developmental stage-specific and sex-specific effects on adult life span indicative of sexual antagonistic pleiotropy

Morris Waskar[1,6], Gary N. Landis[1], Jie Shen[1], Christina Curtis[1,2], Kevin Tozer[1], Diana Abdueva[1,3], Dmitriy Skvortsov[1,4], Simon Tavaré[1,2] , and John Tower[1]

[1] Molecular and Computational Biology Program, Department of Biological Sciences, University of Southern California, Los Angeles, CA 90089-2910

[2] Department of Oncology, University of Cambridge Cancer Research UK Cambridge Research Institute, Li Ka Shing Centre, Robinson Way Cambridge CB2 0RE, England

[3] Current address: Department of Pathology and Laboratory Medicine, Children's Hospital Los Angeles, Keck School of Medicine, University of Southern California, Los Angeles, CA 90089-9034, USA

[4] Current address: Department of Human Genetics, UCLA School of Medicine, University of California, Los Angeles, USA

[6] Current address: Unilever Research Center, Bangalore 560066, India

Running title: *p53 sexual antagonistic pleiotropy*

Key words: *aging, sexual conflict, Geneswitch, maternal effects, tumor suppressor*

Correspondence: *John Tower, PhD, Molecular and Computational Biology Program, Department of Biological Sciences, University of Southern California, 1050 Childs Way, Room 201, Los Angeles, CA 90089-2910*

Received: *09/24/09; accepted: 10/26/09; published on line: 10/27/09*

E-mail: *jower@usc.edu*

Copyright: *© 2009 Waskar et al. This is an open-access article distributed under the terms of the Creative Commons Attribution License, which permits unrestricted use, distribution, and reproduction in any medium, provided the original author and source are credited*

Abstract: Truncated and mutant forms of *p53* affect life span in *Drosophila*, nematodes and mice, however the role of wild-type *p53* in aging remains unclear. Here conditional over-expression of both wild-type and mutant *p53* transgenes indicated that, in adult flies, *p53* limits life span in females but favors life span in males. In contrast, during larval development, moderate over-expression of *p53* produced both male and female adults with increased life span. Mutations of the endogenous *p53* gene also had sex-specific effects on life span under control and stress conditions: null mutation of *p53* increased life span in females, and had smaller, more variable effects in males. These developmental stage-specific and sex-specific effects of *p53* on adult life span are consistent with a sexual antagonistic pleiotropy model.

INTRODUCTION

The *p53* gene encodes a transcription factor that regulates apoptosis and metabolism and is mutated in the majority of human cancers [1, 2]. The p53 protein functions as a tetramer with various protein domains mediating oligomerization, DNA binding and transcriptional transactivation. *Drosophila* contains a single *p53* gene with a structure similar to humans [3-6] including two promoters, and the major protein products are of similar size: 393 amino acid residues for the human protein, Hp53, and 385 amino acid residues for the *Drosophila* protein, Dmp53 (*Drosophila* protein diagrammed in Figure 1A). The central DNA binding

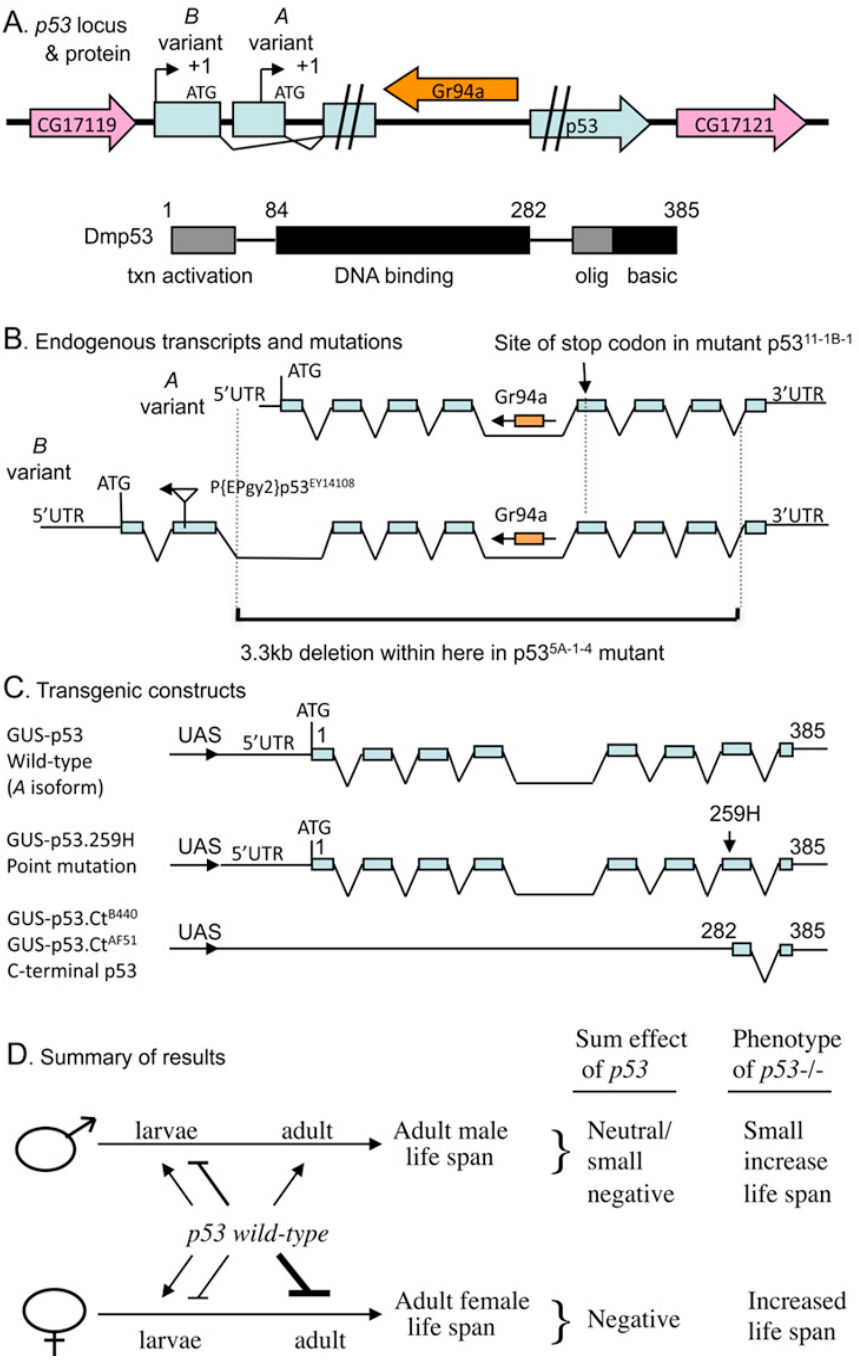

Figure 1. Summary of *Drosophila p53* locus, mutations, transgenes and life span effects. (**A**) Diagram of *p53* locus and major protein product Dmp53. The *p53* gene is indicated in blue, including the two promoters, indicated by black arrows. The internal intron/exon structure of *p53* is omitted here for clarity, but is shown below in (**B**). The pink arrows in indicate the genes that flank *p53* on the 5' and 3' side, genes *CG17119* and *CG17121*, respectively. The orange arrow indicates the gustatory receptor gene *Gr94a*, located in the *p53* intron. The 385 aa Dmp53 protein is diagrammed using black and gray boxes, including the N-terminal transcriptional activation domain, the central DNA binding domain, and the C-terminal oligomerization domain and basic region. (**B**) Diagram of endogenous *p53* transcripts and mutations. The intron/exon structure of the A and B variant transcripts is indicated. The Gr94a gene is indicated in orange with an arrow indicating orientation. The location of insertion of the P element P{EPgy2}p53^{EY14108} in the second exon of the *B* isoform is indicated by a triangle, with an arrow indicating the orientation of the insert. The lower black bracket indicates the breakpoints of the 3.3kb deletion in the p53[5A-1-4] mutation. (**C**) Diagram of transgenic *p53* constructs. (**D**) Summary of *p53* effects on adult life span. The effect on adult life span of *p53* wild type (*A* variant) over-expression during larval development and in adults is diagrammed: Bars represent negative effects of *p53* wild-type on adult life span, while arrows represent positive effects on adult life span; thickness of the lines indicates relative strength of the effect. "Sum effect of *p53*" is the expected summation of effects of *p53* on adult life span, which is consistent with the life span phenotype of *p53* null mutation (*p53*-/-), as indicated.

domain of Dmp53 protein shows partial sequence conservation with Hp53 [3]. The other domains of Dmp53 show less obvious sequence similarity to Hp53, but appear conserved in function. Similar to the N-terminal transcriptional activation domain of Hp53, the N-terminus of Dmp53 contains a high proportion of acidic residues, and Dmp53 has been shown to bind to conserved p53 response elements and activate transcription [3]. The C-terminus of Hp53 contains a basic region (9/26 residues) that can bind either DNA or RNA, and the C-terminus of Dmp53 is also relatively basic (6/24 residues). Finally, the oligomerization domain is located in the C-terminal portion of Hp53, and the corresponding region of Dmp53 contains a conserved critical Gly "hinge" residue, and appears active in oligimerization based on yeast two hybrid assays. The *p53* message is expressed at very low levels in adult tissues, with some enrichment indicated for the eye, malphigian tubule (similar to mammalian kidney), and female germ cells [7, 8].

Mutant forms of p53 lacking function of a particular domain can have powerful dose-dependent effects that are often dependent upon the presence of wild-type p53 [3, 9-11]. For example, specific truncated forms of mouse p53 can cause enhanced cancer resistance and accelerated aging phenotypes, generally interpreted as a state of p53 hyperactivation [12]. Based on studies in mammals it has been suggested that *p53* may exhibit antagonistic pleiotropy between life-cycle stages, in that it favors normal development, fecundity and cancer resistance in young animals, but may promote aging in old animals [9, 13-15]. Recently *p53* gene activity was found to limit the life span of *C. elegans* hermaphrodites, and this effect was dependent upon the activity of the insulin/IGF1-like signaling (IIS) transcription factor gene *Daf-16/FOXO* [16]. In *Drosophila*, several dominant *p53* mutations and transgenes have been characterized, that generally appear to antagonize *p53* activity [3]. Nervous-tissue expression of one of these dominant *p53* transgenes (*p53* point mutation 259H) was found to inhibit IIS and extend life span in females [17, 18]. However it remains unclear if and how *p53* might normally affect the life span of *Drosophila* males and females. Here the wild-type form of *p53*, as well as mutant forms, were assayed for effects on *Drosophila* life span, in both male and female flies.

RESULTS

Transgenic manipulation of *p53* in adult flies

Drosophila p53 transgenes were assayed for effects on life span both in adults and during larval development (see below). The conditional transgenic system Geneswitch [19-21] was used to over-express both wild-type and mutant forms of *p53*. With the Geneswitch system transgene expression is triggered by feeding flies (or larvae) the drug RU486/Mifepristone. A Geneswitch driver strain called Act-GS-255B was used (Table 1, strain 9), where the tissue-general *actin5C* promoter drives expression of the Geneswitch transcription factor. In the presence of RU486, the Act-

Table 1. *Drosophila* strains

Strain #	Genotype	Group (notes)
2	w[1118] ; + ; Df(3R)Exel6193, P{XP-U}Exel6193 /TM6B, Tb (BL7672)	- (Chromosomal Def uncovers p53)
3	y[1] w[1118] ; + ; p53[5A-1-4] (BL6815)	- (deletion of p53 gene)
4	y[1] w[1118] ; + ; p53[11-1B-1] (BL6816)	M (pt mutant)
5	w[1118] ; p53[1] / TM6B, Tb	M (the same pt mutant as line 4)
6	w[1118] ; + ; +	+
7	Oregon R (+ ; + ; +)	+
8	y[1] w[67c23]; P{EPgy2}p53[EY14108] (BL 20906)	M (the P-insertion disrupts the B variant)
9	w ; P{Switch}Actin 255B	(GeneSwitch Act-GS-255B driver)
16	y[1]w[1118]; P{w[+mC]=UAS-p53.Ex}3/T(2;3)TSTL, CyO:TM6B, Tb	(UAS-p53 wild type)
17	w ; P{w[+mC]=GUS-p53}2.1	(UAS-p53 wild type - CDM26)
18	w; P{w[+mC]=GUS-p53.Ct}AF51	(C-terminal p53 - AF51)
19	w[1118]; +; P{w[+mC]=GUS-p53.Ct}B440/TM6B, Tb	(C-terminal p53 - B440)
20	w[1118]; P{w[+mC]=GUS-p53.259H}	(p53 point mutation - 259H)

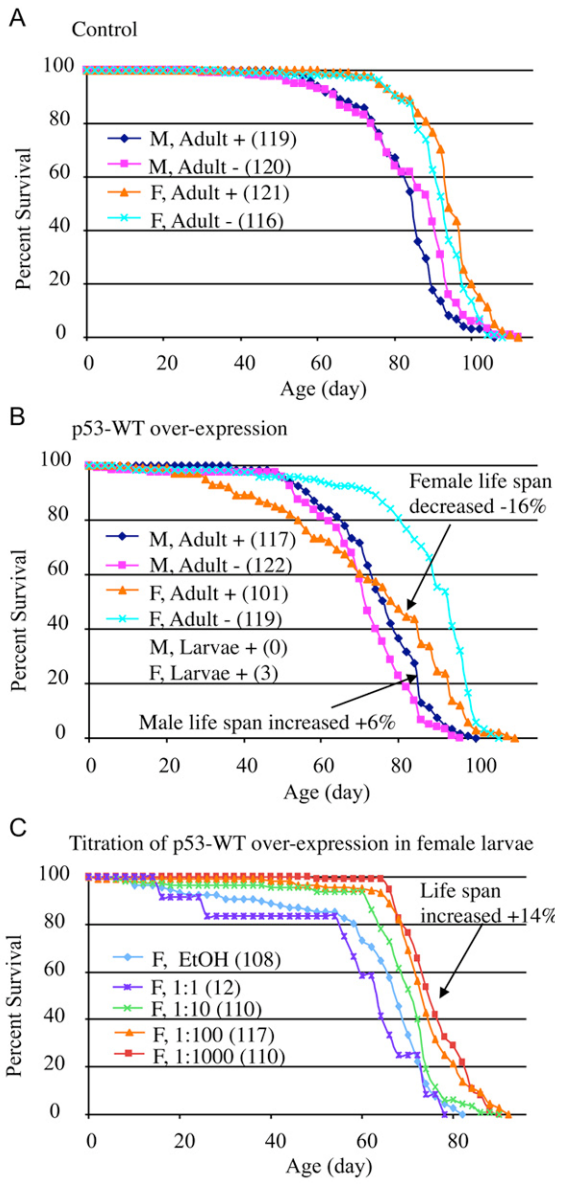

Figure 2. Conditional over-expression of wild-type *p53* transgenes using Geneswitch system. All flies were the progeny of either Oregon R control (**A**) or p53-WT transgenic strain (**B**, **C**) crossed to the tissue-general Geneswitch driver Act-GS-255B. The flies were cultured in the presence and absence of drug, as larvae or adults, as indicated: M = males, F = females, + indicates culture in presence of drug, - indicates culture in absence of drug. The number of flies in each group are indicated in parentheses. (**A**, **B**) Blue diamonds indicate male adults plus drug, pink squares indicate male adults minus drug, orange triangles indicate female adult plus drug, turquoise x indicates female adults minus drug. (**A**) Control flies, progeny of Oregon R wild-type and Act-GS-255B. (**B**) *p53* wild-type transgene over-expression. Note male larvae plus drug produced no adult flies, whereas female larvae plus drug produced only three escapers. (**C**) Titration of *p53* wild-type over-expression during female larval development and effect on subsequent adult life span. EtOH indicates the ethanol solvent for the drug alone (vector control, indi-cated with light blue diamonds). Repeats of the titration experiments, including data for males are presented in Supplementary Figure S1.

GS-255B driver produces expression of UAS-containing target constructs in all the tissues of either larvae or adults [19, 22]: detailed characterization of the system using UAS-GFP reporter constructs demonstrates that the Act-GS-255B driver produces abundant transgene expression throughout all of the tissues of both adult flies and larvae, for both male and female animals, with slightly less (but still abundant) expression in adult males relative to females [22]. All of the flies examined in this study are the progeny of a cross; for example "16-9" flies are the progeny of a cross of males of strain 16 (containing the UAS-p53 wild-type transgene) with females of strain 9 (containing the Act-GS-255B Geneswitch driver) to generate progeny containing both constructs (strains summarized in Table 1); in all cases crosses are indicated with the male parent genotype first, and the female parent genotype second. The RU486 drug itself had no significant effect on male or female life span when administered to adults (Figure 2A; statistical analyses summarized in Supplementary Table S1). When wild-type *p53* was over-expressed specifically in adult flies, it had a negative effect (-16%) on mean life span in females (cross 16-9: 95% bootstrap CI for the ratio of the means [-21.11 - 11.61], log-rank p-value = 2.21×10^{-6}), and a positive effect (+6%) on mean life span in males (cross 16-9: 95% bootstrap CI [2.36 - 10.37], log-rank p-value = 6.97×10^{-3}) (Figure 2B; Supplementary Table S1). Slightly larger changes were observed for median life spans (Supplementary Table S1), and similar results were obtained with multiple independent transgenic insertions of *p53* wild-type (data not shown). In contrast, adult-specific over-expression of the dominant mutant *p53* (point mutation p53-259H) transgene did not have a negative effect on female life span, and instead female life span tended to be increased (cross 20-9: +7%, 95% bootstrap CI [4.09 - 9.72], log-rank p-value = 4.05×10^{-8}) (Supplementary Figure S1B; Supplementary Table S1) [22], and similar results were obtained with *p53* dominant mutant transgene p53-Ct[B440] (Supplementary Figure S1C; Supplementary Table S1). Because these *Drosophila p53* dominant mutation transgenes are generally expected to antagonize the activity of wild-type *p53*, the data are consistent with wild-type *p53* having a negative effect on adult female life span. The negative effect on life span of wild-type *p53* over-expression in adult females and the lack of negative effect with dominant mutant *p53* transgenes was also confirmed using the FLP-*out* conditional system [23] to cause transgene over-expression (data not shown). Taken together, these data indicate that in adult flies, *p53* inhibits life span in females and favors life span in males.

Transgenic manipulation of *p53* during development

A strikingly different set of results was obtained when *Drosophila p53* transgenes were expressed specifically during larval development. When administered only during larval development, the drug RU486 itself had no effect on subsequent adult female life span, and a small negative effect on subsequent adult male life span (~-4%; Supplementary Table S1). Over-expression of wild-type *p53* at high levels during larval development was toxic to both males and females, in that no male adults were produced, and only three female adults (escapers) were obtained (Figure 2B). Intriguingly, the three female escapers had unusually long life spans: 86 days, 92 days, and 96 days, respectively. To determine if this apparent life span increase was significant, and to investigate the developmental effects of wild-type *p53* over-expression in greater detail, the over-expression was modulated by titration of the RU486/Mifepristone drug, in replicated experiments. Titration of wild-type *p53* over-expression during development again indicated toxicity at high levels of expression, with greater toxicity evident for males (Supplementary Table S2). Strikingly, at lower levels of induction, wild-type *p53* produced both female and male adults with increased mean and maximal life span (Figure 2C; Supplementary Figure S1E-F; Table S2; female: +14%, 95% bootstrap CI [9.29 – 19.27]; log-rank p-value ≈ 0; male: +15%, 95% bootstrap CI [10.54 – 19.30]; log-rank p-value = 4.97×10^{-7}). These data demonstrate that high-level expression of *p53* can be toxic during development, whereas moderate over-expression of *p53* during development can cause increased life span in the resulting male and female adults. Consistent with this conclusion, expression of the dominant mutant transgenes during development tended to decrease the life span of the resultant male and female adults (Supplementary Figure S1A-D, Table S1).

Effect of mutations in the endogenous *p53* gene

To confirm the effects of *p53* on *Drosophila* life span, flies were examined that had a deletion or mutation of the endogenous *p53* gene (mutations diagrammed in Figure 1B; strains listed in Table 1) [24]. Multiple trans-heterozygous *p53* wild-type and mutant allele combinations were assayed for life span simultaneously as a control for genetic background effects and environmental effects (the "L" cohort, data summarized in Supplementary Tables S3, S4). This was done using two *p53* wild-type strains (called the "+" group; strains 6 and 7), two strains containing *p53* null mutation (called the "-" group; strains 2 and 3), and three strains containing *p53* dominant mutations (called the "M" group; strains 4, 5 and 8), and crossing each strain to each of the others in a "round-robin" approach. In this way each of the various *p53* genotypes (+/+, -/-, +/-, +/M, -/M, M/M) represents the average of multiple specific genetic backgrounds. This approach avoids the potential complication of identifying *p53* effects that might be specific to only one particular genetic background, such as would be created by using a backcrossing strategy.

In flies with mutations of the endogenous *p53* gene, the effect on life span should be the sum of the effects of *p53* at various life-cycle stages, both positive and negative (diagrammed in Figure 1D); and indeed, *p53* mutations were found to have a significant effect on life span in both sexes (ANOVA, $p < 0.0001$; Supplementary Table S5): Null mutation (-/-) of the *p53* gene increased mean female life span by +13% (95% bootstrap CI [9.00 -17.28]; log-rank p-value ≈ 0) relative to wild-type (+/+) controls (Figure 3A; Supplementary Figure S2A; Supplementary Table S4). In the heterozygous *p53* mutant genotype (-/+) average female life span was also increased relative to wild-type controls by +11% (95% bootstrap CI [8.41 - 13.59]; log-rank p-value ≈ 0). In male flies null mutation (-/-) of the *p53* gene increased mean life span by +12% (95% bootstrap CI [4.92-14.50]; log-rank p-value ≈ 0), whereas the effect of heterozygous mutation was smaller, yielding mean life span increases of +5.5% (95% bootstrap CI [2.15 – 7.53]; log-rank p-value ≈ 0) (Figure 3B; Supplementary Figure S2B; Supplementary Table S4). However, as seen below (Figure 4A, Supplementary Figure S4), the life span increases in *p53* mutant males were not consistently observed when crosses were done in the opposite direction, and therefore may not be biologically significant. Similar effects of *p53* null (-/-) and heterozygous (+/-) genotypes were obtained when the experiments were repeated using different culture conditions (richer food source and presence of mates) that yield shorter overall life spans (the "W" cohort; Supplementary Figure S3; Supplementary Tables S6, S7). Taken together, these data with endogenous *p53* gene mutations support the conclusion that, in sum, *p53* limits the life span of female flies, with smaller and more variable effects in male flies.

Several *Drosophila p53* dominant mutations (M) were examined and found to have complex effects on adult life span, depending upon the particular allele, and whether or not a wild-type copy of *p53* was present in the background (Figure 3; Supplementary Figures S2, S3). Some of the variability in life span across genotypes is expected to result from differences in genetic

background. Indeed, the complexity of *p53* dominant mutations and their interactions with genetic background has recently been reviewed [25]. Strikingly, when the data for the various *p53* genotypes in the L cohort were grouped to control for genetic background effects, the dominant mutations tended to increase life span in females (+/M, -/M, M/M), and to decrease life span in males (+/M, M/M) (Figure 3; Supplementary Figure S2; Supplementary Table S4). Since the *Drosophila p53* dominant mutations are generally expected to antagonize wild type *p53* function, the increased life span of +/M females relative to wild type (+/+) is consistent with the results obtained above suggesting that, in sum, *p53* limits the life span of females. However, for the M/M genotype flies, a wild-type copy of the entire *p53* gene is not present, and these genotypes produced the greatest increase in life span in females and the greatest decrease in life span in males. Therefore, these data suggest that the mutant forms of *p53* may have sexually antagonistic effects on *Drosophila* life span that are not necessarily dependent upon the presence of a wild-type *p53*. Strikingly, these effects of dominant mutations on life span were highly dependent upon environment, since in the W cohort the dominant mutations tended to decrease life span in both males and females (Supplementary Figure S3; Supplementary Table S7). It will be of interest in the future to determine what is the mechanism for these opposite effects of dominant *p53* mutations in males versus fe-males, and to determine if the dramatic gene-by-environ-ment effect of *p53* dominant mutations in females is due to the presence of mates, the richer food source, or both.

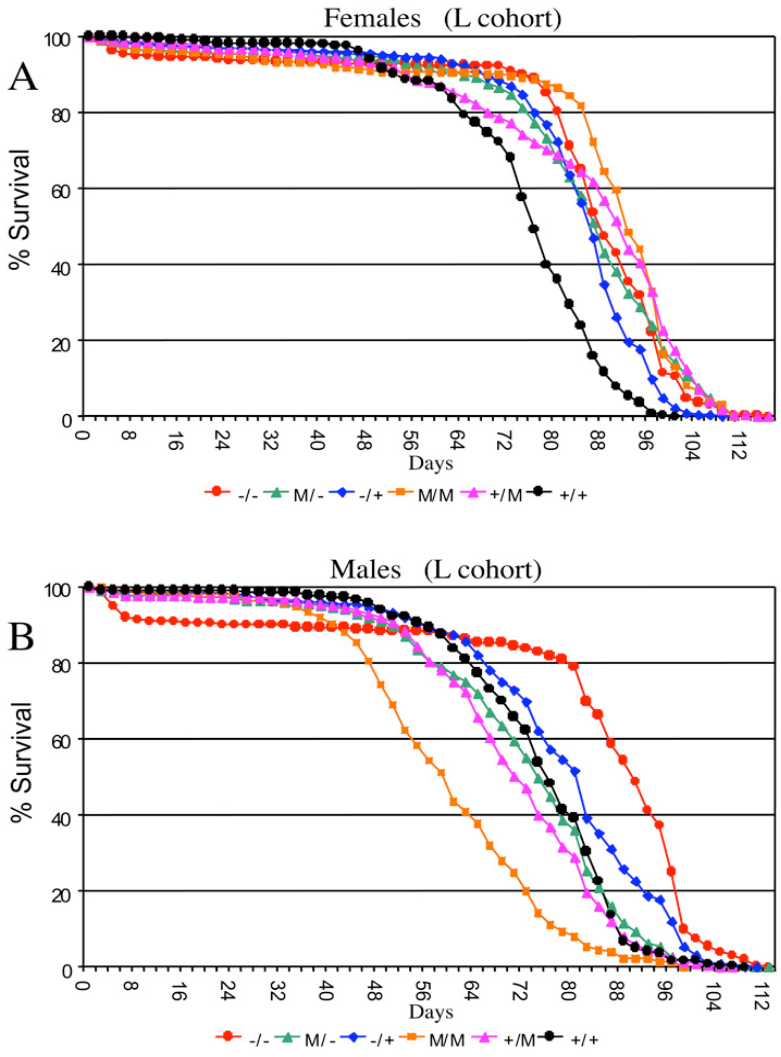

Figure 3. Effect of *p53* mutations on life span. Cumulative survival curves for L cohort. A key of *p53* genotypes is presented below the graphs. Males are indicated with solid symbols and females are indicated with open symbols. (**A**) Females. (**B**) Males.

Controls for maternal effects and *X* chromosome effects

In an effort to control for possible maternal effects and *X* chromosome effects, several life span assays were repeated with the crosses done in both directions simultaneously, i.e., varying which strain serves as mother or father for the cross (Supplementary Figure S4). An increase in life span of *p53* null mutant (-/-) flies relative to wild-type (+/+) controls was obtained in female progeny regardless of cross direction (Supplementary Figure S4; Supplementary Table S8), thereby ruling out a primary effect of maternal genotype. In males a consistent change in life span was not observed, in that although the null mutants exhibited slight differences in life span compared to controls, the direction of change differed depending on the direction of the cross. Furthermore, while the survival curves of many of the reverse cross pairs differed from one another in both sexes (log-rank test, data not shown), in females there was strong concordance and highly significant results from comparisons of survival curves in both cross directions and relative to both controls, while this was not the case for males (Supplementary Table S8). These results demonstrate that the increased life span in females due to *p53* mutation cannot be simply due to maternal or *X* chromosome effects, and in conjunction with the above findings, these data again suggest that *p53* preferentially limits the life span of female flies.

Sex-specific effects *p53* on fly stress resistance

Drosophila p53 is required for normal resistance of larval cells and tissues to certain kinds of stress, for example, ionizing radiation and UV toxicity [26, 27], and third-instar larvae that are null for *p53* exhibit decreased survival when challenged with 4,000 Rads of ionizing radiation [28]. To determine if *p53* genotype might have sex-specific effects on stress resistance in adult flies, male and female flies that were either wild-type or mutant for *p53* were subjected to two types of life-shortening stress, ionizing radiation and 100% oxygen atmosphere, in replicated experiments (Figure 4, Supplementary Table S9). Treatment with 90,000 Rads of gamma-irradiation on day 10 of adult age reduced adult life spans by half, and *p53* mutant female flies were again found to have greater mean life span than wild-type controls (+/-: +18%, 95% bootstrap CI [13.13 - 23.36]; log-rank p-value = 0; -/-: +13%, 95% bootstrap CI [9.09 - 16.71]; log-rank p-value = 2.98×10^{-4}). In contrast, *p53* mutations were found to slightly reduce the survival of female flies subject to 100% oxygen atmosphere (-/+: not significantly different than wild-type; -/-: -4%, 95% bootstrap CI [−5.06 - −3.34]; log-rank p-value = 1.28×10^{-13}). In males, *p53* null mutants subject to ionizing radiation had significantly reduced mean life span, whereas heterozygotes fared slightly better than wild-type (+/-: +4%, 95% bootstrap CI [1.80 – 6.00]; log-rank p-value = 2.02×10^{-7}; -/-: -19%, 95% bootstrap CI [−20.68 - −17.06]; log-rank p-value ≈ 0). As with females, *p53* gene mutations tended to reduce male survival in response to a 100% oxygen environment (+/-: −4%, 95% bootstrap CI [−4.38 - −3.05]; log-rank p-value = $4.44 \times 10^{-16;}$ -/-: −15%, 95% bootstrap CI [−16.13 - −14.10]; log-rank p-value ≈ 0). Therefore, wild-type *p53* tended to favor the survival of both sexes under 100% oxygen stress conditions, yet was detrimental to female life span in flies subject to ionizing radiation. Therefore the results for adults subject to ionizing radiation were similar to those observed during normal aging: normal *p53* function increased survival of males and decreased survival of females. The fact that *p53* favored the survival of both sexes under the more severe life-shortening condition of 100% oxygen stress may be indicative of a threshold effect on survival that is sex-specific.

DISCUSSION

In these experiments a combination of genetic and transgenic approaches were used to study how *p53* affects the life span of male and female *Drosophila*. The conditional transgenic system Geneswitch was employed to produce tissue-general expression of *p53*, either during development or specifically in adults. Detailed characterization of the Geneswitch driver strain ("Actin-GS-255B") using GFP reporter constructs demonstrated that the system yields truly tissue-general expression during larval development, as well as tissue-general expression in both male and female adults [22]. The data indicate that *Drosophila p53* has effects on adult life span that are antagonistically pleiotropic between developmental stages and sexes (summarized in Figure 1A). One advance of the present study is that life span effects were identified using transgenes encoding the full length, wild-type form of *Drosophila* p53 protein, as well as ones encoding mutant forms. In adults, wild-type *p53* over-expression limited life span in females and favored life span in males. In contrast, during development, *p53* over-expression acted in a dose-dependent manner to either reduce or increase the subsequent longevity of both male and female adults: high level expression during development was detrimental, whereas moderate over-expression produced increased life span. The dominant mutation transgenes generally produced the opposite effect of wild type *p53* transgenes, in both males and females.

This indicates that the opposing effects of *p53* transgenes on male and female life span cannot be simply due to some cryptic difference in the efficiency of transgene expression in males versus females, or to some differential toxicity of the encoded proteins in males versus females.

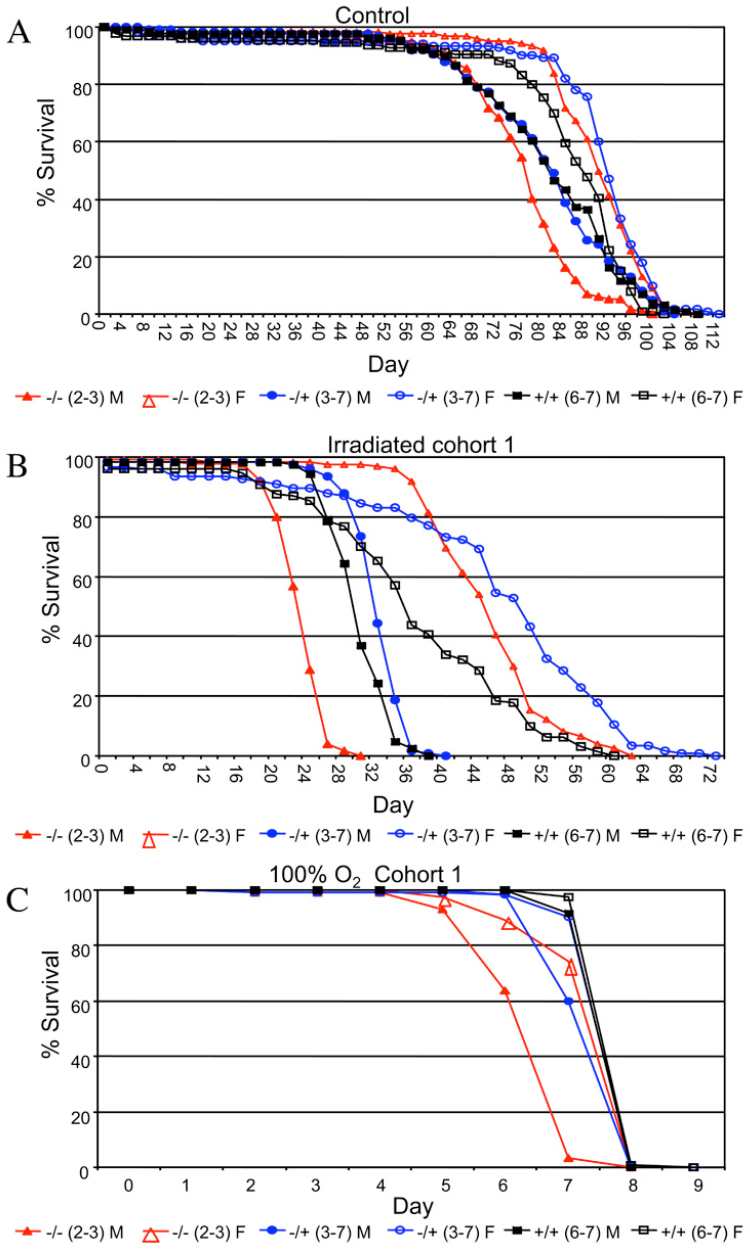

Figure 4. Survival curves for the indicated genotypes under stress conditions. (**A**) Ionizing radiation. (**B**) 100% oxygen survival. A key of *p53* genotypes is presented below the graphs. Males are indicated with solid symbols and females are indicated with open symbols. Survival curves for replicate experiments (cohort 2) are presented in Supplementary Figure S5. Survival statistics for these and replicate experiments are summarized in Table S9.

Results consistent with the transgenic manipulations were obtained from analysis of the endogenous *p53* gene: Null mutation of the endogenous *p53* gene increased life span in females, and had smaller, more variable effects on male life span. The effects of *p53* on adult fly survival under stress conditions were also sex-biased: wild-type *p53* was found to favor the survival of both sexes under 100% oxygen stress conditions, yet to be detrimental to female life span in flies subject to ionizing radiation. In these experiments *p53* expression and function is being altered in all of the tissues of the animal simultaneously, and therefore the effects observed are the sum of any possible tissue-specific effects of *p53*. Indeed our results suggest that the positive and negative effects of *p53* on life span observed here with tissue-general alterations are comprised of a mix of both positive and negative tissue-specific effects, that combine to result in the observed opposite effects in males versus females (J.S. and J.T., 2009 Experimental Gerontology, in press).

The data presented here indicate that *p53* null mutation increases life span in female flies, with smaller, more variable increases observed for male flies. Helfand and coworkers have previously reported that *p53* null mutant male and female flies were sickly, with a shortened life span, however, statistical analysis was not presented [17]. One possibility is that the apparent reduction in life span and vigor previously reported for *p53* null flies may have resulted from inbreeding depression in the homozygous mutant flies used in that study. In contrast, in the experiments presented here, multiple trans-heterozygous *p53* null mutant genotypes were examined, so as to reduce possible inbreeding effects, and thereby reveal the life span benefit of *p53* null mutations. Helfand and coworkers also analyzed the effect on life span of nervous system-specific expression of two *p53* dominant mutant transgenes, a C-terminal fragment transgene (p53-Ct), and the point mutant (p53-259H). They found that nervous system expression of p53-Ct throughout both development and adulthood increased female life span by +58%, and increased male life span by +32% [17]. Because the dominant mutations are generally expected to antagonize p53 activity, their results are consistent with our conclusion that, in sum, *p53* limits life span in females, with smaller effect in males (summarized in Figure 1D). Using the Elav-Geneswitch driver to restrict expression to the adult nervous system, Helfand and coworkers found that the p53-Ct transgene increased female life span by +18% to +26%, and the p53-259H transgene increased female life span by +11% to +13%, again consistent with our finding that *p53* limits the life span of adult females. Indeed, using the tissue-general Act-GS-255B driver to restrict transgene expression to adults, we also found that the p53-Ct and p53-259H transgenes produced an increase in median life span in females (Supplementary Figure S1A-D) [22]. For adult-specific expression in male nervous system, Helfand and coworkers reported life span data for only two assays, both using the p53-Ct transgene: using a high-calorie food condition, male life span was reported to be increased by +13%, whereas using a low-calorie food, male life span was unchanged, and results for normal food were not presented [17]. That result might at first appear to be partly inconsistent with our conclusion that *p53* favors life span in adult males, however, there are several possible explanations that might reconcile these results. First, the previous experiment involved the p53-Ct transgene, encoding the p53 C-terminal fragment, and data from mammals suggests that certain dominant p53 mutants are capable of either antagonizing or promoting p53 activity, depending upon the level of expression and the cellular context [11]. Second, the life span increase was observed only under a high-calorie food condition, and our data suggest sex-specific interactions between dominant *p53* mutations and diet/environment with regard to life span (Figure 3, Supplementary Figure S2). Under our conditions and using tissue-general expression, we found that adult-specific expression of the dominant mutant *p53* transgenes tended to decrease male life span (Supplementary Figure S1, Table S1), consistent with our conclusion that *p53* normally favors adult male life span. Finally, the effects of tissue-general expression, as tested here, will be the sum of all tissue-specific effects, be they positive or negative. Indeed our results suggest that the positive and negative effects of *p53* on life span observed here with tissue-general alterations are comprised of a mix of both positive and negative tissue-specific effects (J.S. and J.T., 2009 Experimental Gerontology, in press), that combine to result in opposite effects in males versus females (summarized in Figure 1D). Therefore, the previous results from the Helfand group (with the possible exception of a single assay of males under a high-calorie food condition), are generally consistent with the results presented here.

One possible mechanism by which *p53* might act in adult flies to preferentially limit female life span is by stimulating IIS, since IIS appears to preferentially limit life span in females of *Drosophila* and other species [29, 30]. Studies in mammals provide precedent for crosstalk between *p53* and the IIS pathway, including the target transcription factor FOXO, in regulating both aging and cancer [31, 32]. Consistent with this idea, life span extension in *Drosophila* females produced by nervous system-specific expression of the dominant mutant *p53-259H* transgene was found to correlate with

a reduction in IIS signaling [18]. In *C. elegans*, mutation of the *p53* homolog *cep-1* increased life span of adult hermaphrodites, and this increase required the function of the IIS target transcription factor gene *Daf-16/FOXO* [16]. To definitively rule in (or out) a role for IIS in *Drosophila p53* life span effects will require future assays in the presence and absence of the Foxo transcription factor.

Another possible mechanism by which *p53* might affect life span is by altering proliferation or causing apoptosis in particular cell types. For example, ablation of germ-line cells in adult animals by forced over-expression of the *bam* gene caused increased life span in males and females [33]. However, while germ line ablation might be attractive as a possible mechanism for the increased life span observed in *p53*-over-expressing males, it is not consistent with the life span decrease observed in females. Alternatively, over-expression of wild-type *p53* specifically in adult diploid cells using an *escargot*-GAL4 driver caused ablation of most stem cells in the gut, and gut stem cell proliferation appears to be more rapid in females than in males [34]. While this might be attractive as a possible mechanism for the life span decrease observed in *p53*-over-expressing females, it is not consistent with the life span increase observed in males; indeed other experiments involving disruption of adult diploid cell function caused an equally dramatic decrease in life span in both sexes [35]. It will be of interest in the future to ask if *p53* might be affecting life span through highly sex-specific or sexually opposite effects on cell proliferation and survival. Notably, over-expression of strong caspase inhibitors and other apoptosis and senescence regulatory genes in adult flies did not yield increased life span in either sex, and where negative effects on life span were observed, such as with *wingless* and *activated Ras*, the negative effects were similar in males and females [22]. Those results tend to suggest that *p53* may be acting through some other mechanisms, such as alterations in metabolism or autophagy. Additional possible mechanisms by which *p53* might affect life span include sex-specific alterations in behavior, such as food intake, or potentially costly activities such as movement or aggression.

In these experiments *Drosophila p53* was also found to have sex-specific effects on survival under stress conditions. Wild-type *p53* favored the survival of both sexes under 100% oxygen stress, yet was detrimental to female life span in flies subject to ionizing radiation. This may be indicative of a threshold effect on survival that is sex-specific. Mechanistically the ability of *p53* to either favor survival or mortality may be related to *p53*'s ability to regulate both repair and apoptotic pathways [1, 36-38], and perhaps the functional connection between *p53* and FOXO in response to oxidative stress [25]. In line with our findings, *C. elegans* hermaphrodites that are long-lived due to *p53* (*cep-1*) mutation did not demonstrate increased resistance to oxidative (or UV) stress [16], however resistance to gamma irradiation was not examined. Strikingly, in *C. elegans* hermaphrodites, *p53* has recently been found to increase life span in response to mild mitochondrial stress, and to decrease life span in response to severe mitochondrial stress, consistent with a threshold effect on survival [39] ; however effects in males have not been reported. In mice, reduced *p53* function results in resistance to lethality caused by moderate gamma irradiation and increased sensitivity to severe irradiation [40,41], again suggestive of a threshold effect, however any potential sex-bias has not been reported. Finally, long-lived female *Drosophila* that over-expressed dominant-mutant *p53* in neurons exhibited increased resistance to the oxidative stressor paraquat [17]; however effects in males were not reported. Taken together the data are consistent with a model in which *p53* has a threshold effect on survival under stress, and the threshold for the transition from favorable to detrimental depends upon the type of stress and the sex of the animal. Such a threshold model is consistent with extensive data from mammals and model systems demonstrating that *p53* can either favor oxidative stress resistance and cell survival, or favor oxidative stress and cell death, depending upon the cellular and environmental context, and the degree of activation of *p53* [38]. In mammals, physiological levels of *p53* activity appear to maintain normal cellular redox status, through sustained expression of antioxidant genes (e.g., *Sesn1&2, GPX1, AIF*) and metabolic genes (e.g., *SCO2, PGM, TIGAR*). In contrast, hypo-physiological levels of *p53* activity can suppress expression of antioxidant genes (e.g., *Sesn1&2, GPX1*) and cause increased oxidative stress. Similarly, hyper-physiological levels of *p53* activity can induce pro-oxidant and apoptosis-promoting genes (e.g., *NQO1, POX, BAX, PUMA, p66shc*), and/or cause an imbalance in expression of antioxidant genes (e.g., *MnSOD, PIG12, ALDH4, GPX*), and again cause increased oxidative stress [38].

Antagonistic pleiotropy of gene function between younger and older animals is generally accepted as one of the most likely genetic mechanisms underlying aging [42]; however, specific genes exhibiting such pleiotropy have generally not been identified. One notable exception is data from mammals that suggests *p53* exhibits antagonistic pleiotropy between developmental stages. At young ages *p53* favors fecundity and favors survival by acting as a tumor suppressor, yet at late ages

it may limit survival by promoting cell senescence, or through other mechanisms [13, 43]. Increasing evidence suggests that genes can also exhibit antagonistic plieotropy of function between the sexes, affecting a variety of traits including reproductive fitness and life span [30, 44-47]. The data presented here suggest that *Drosophila p53* exhibits a combination of both developmental stage-specific and sex-specific antagonistic pleiotropy with regard to life span. If this result were to translate to humans, it would have implications for human aging related diseases such as cancer. Consistent with our results using flies, the effects of human *p53* and *p53*-interacting genes such as *MDM2* on cancer incidence and longevity are often sex-biased [48], and *p53* has recently been implicated in regulating mammalian maternal fecundity [49]. Moreover, during mouse development, *p53* null mutations cause a high frequency of neural tube defects and lethality that preferentially affects female embryos [50, 51], and interestingly, this sex difference appears to result from the number of *X* chromosomes rather than the presence or absence of the *Y* [52]. The sex-specific effects of *p53* may be related to recent observations that in humans the *X*-chromosome dosage-compensation gene *MOF* can regulate *p53* [53]; and notably the *MOF* gene is conserved and also *X*-linked in flies. Taken together the data support a sexual antagonistic pleiotropy model in which *p53* function may be maintained by positive selection for fecundity and/or survival benefit during development, in young animals, and under certain stress conditions, despite acting at another stage of the life cycle and in the other sex to limit adult life span (summarized in Figure 1D).

METHODS

Drosophila culture. *Drosophila* culture and life span assays were performed as previously described [19]. Briefly, crosses were conducted in 250 ml urine-specimen bottles (Genessee Scientific) containing 35 ml of medium. Adult flies were maintained in narrow polystyrene vials (Genesee Scientific) containing 5 ml medium. *Drosophila* culture media contained cornmeal, agar, dextrose, yeast, and propionic acid to inhibit bacterial growth and tegosept to inhibit fungal growth [54]; except for the W cohort which were cultured on an older recipe containing molasses rather than dextrose (food recipes summarized in Supplementary Table S10). Flies were maintained at 25^{o}C and on a 12:12 dark/light cycle, and were removed to room temperature for less than 1 hour every 2 days to provide fresh medium and remove and enumerate dead flies. To estimate life expectancy, single-sex mortality vials were established, with ~25 flies per vial (sample sizes were occasionally reduced due to rare escapers) and 5 or 10 replicate vials (depending on the experiment) per sex for every cohort. The L cohort deletion experiment used 10 replicate vials per sex, the reverse-cross experiments used 5 vials per sex, the stress experiments used 5 vials per sex, the Geneswitch experiments used 5 vials per sex, and the drug-titration experiments used 5 vials per sex. Note that for each line in the W cohort ~125 flies were maintained at ~25 flies per vial with mates.

Drosophila strains. All *Drosophila* strains and genotypes are listed in Table 1, and several mutants and transgenes are diagrammed in Figure 1. Wild-type (*A*-isoform) and dominant-mutant *p53* transgene stocks were obtained from Michael Brodsky [3] and Bloomington *Drosophila* Stock Center. P{UAS-p53.Ex}, *p53* wild-type. P{GUS-p53.Ct}AF51, C-terminal fragment AA285-385, chromosome 2. P{GUS-p53.Ct}B440, C-terminal fragment AA285-385, chromosome 3. P{GUS-p53.259H}, AA substitution, chromosome 3. The *p53* mutant strains were obtained from Kent Golic and Bloomington *Drosophila* Stock Center [55]. Df(3R)slo3 is deletion of entire *p53* gene ("-"). Df(3R)Exel, P{XP-U}Exel is deletion of entire *p53* gene ("-"). *p53*[5A-1-4] is 3.3kb internal deletion ("-"), and it's structure was confirmed by PCR amplification and sequencing (diagrammed in Figure 1B). *p53*[11-1B-1] is a point mutation that introduces a stop codon at nucleotide residue 211, and is predicted to yield a 70AA truncated protein ("M"). P{EPgy2}p53[EY14108] is a P element insert mutation obtained from Bloomington *Drosophila* Stock Center (BL 20906), and the insertion was mapped to the first exon of the *p53* B-variant using inverse PCR (diagrammed in Figure 1B) [56]. Because the p53[EY14108] mutation is predicted to produce an altered complement of p53 protein isoforms, it is grouped here with the dominant mutants ("M").

Geneswitch conditional gene expression system. Geneswitch strains and protocols are as previously described [19-21]. The strain Act-GS-255B [19, 22] contains two inserts on the second chromosome of a construct in which the *actin5C* promoter drives expression of the Geneswitch coding region. RU486 (Mifepristone, Sigma) was fed to adult flies or developing larvae by adjusting the food to ~160ug/ml final concentration. A stock solution of 3.2mg/ml of RU486 was prepared by dissolving drug in ethanol (100%). Control food received ethanol solvent alone. In certain experiments RU486 concentrations were titrated as indicated. All ages are expressed as days from eclosion at 25^{o}C. To generate flies containing both the Act-GS-255B driver and the UAS-transgenes, virgins from the Act-GS-255B strain were crossed to males

from each transgenic strain and the Oregon R wild-type strain as a control. Certain crosses were done in the opposite direction, as indicated in the "reverse cross" experiments. The life span assay result for p53-259H transgene over-expression in adult flies using Act-GS-255B driver has been previously published [22], and is included here with additional statistical analysis for comparison purposes (Supplementary Table S1).

Statistical analyses. Initial cohort size was taken to be the number of flies in the vials at the beginning of the second two-day interval. Deaths during the first interval after transfer were considered to be due to injury during collection and therefore were excluded from the calculations. Survivorship was scored every other day and final cohort size was taken as summed deaths. The effect of *p53* deletion, mutation, and over-expression on *Drosophila* life span was assayed in multiple trials for several lines. Life span summary statistics for each of the experiments (data pooled across replicate vials) and detailed statistical analyses are presented in the Supplementary Materials (Tables S1-S9). A non-parametric log-rank test was employed to compare the survival functions between *p53* deficient or over-expression genotypes and controls [57]. To further assess the effect of *p53* on mean, median, and "maximal lifespan" (defined operationally here as the 90^{th} percentile of life span), 95% double bootstrap-t confidence intervals for the ratio of the means (or ratio of the percentiles) of the experimental and control samples were computed using a custom Fortran script. Mixed effects models were fit to data from each sex separately to ascertain the effects of mutation type (M) and genotype (G) (fixed main effects) on life expectancy, with replicate vials (R) treated as a random effect using the *nlme* package in R. Mixed-effects models allow for a flexible representation of the covariance structure due to the grouping of the data and enabled the variation induced in the survival response by replicate vials to be characterized. As appropriate, the models were $y = \mu + M + R(M) + \varepsilon$ (where M = +/+, +/-, etc and G = 6-7, 2-6, etc was treated as an "inner" grouping) and $y = \mu + G + R(G) + \varepsilon$, where ε indicates the within vial error variance. Post-hoc Tukey tests were performed to assess significant differences among means after correcting for multiple testing. Analyses were performed using the R statistical environment [58], unless otherwise noted.

ACKNOWLEDGEMENTS

We thank Michelle Arbeitman and Heidi Scrable for helpful comments. This work was supported by a Senior Scholar Award from the Ellison Medical Foundation to JT, and by grants from the Department of Health and Human Services to ST (GM067243) and to JT (AG011833), and by a pilot project award to JT from the USC ADRC (1P50 AG05142). ST is a Royal Society-Wolfson Research Merit Award holder.

CONFLICT OF INTERESTS STATEMENT

The authors of this manuscript have no conflicts of interest to declare.

REFERENCES

1. Soussi T. p53 alterations in human cancer: more questions than answers. Oncogene 2007; 26:2145-2156.

2. Yaswen P, Campisi J. Oncogene-induced senescence pathways weave an intricate tapestry. Cell 2007; 128:233-234.

3. Brodsky MH, Nordstrom W, Tsang G, Kwan E, Rubin GM, Abrams JM. *Drosophila* p53 binds a damage response element at the reaper locus. Cell 2000; 101:103-113.

4. Ollmann M, Young LM, Di Como CJ, Karim F, Belvin M, Roberts S, Whittaker K, Demsky M, Fisher WW, Buchman A, et al. *Drosophila* p53 is a structural and functional homolog of the tumor suppressor p53. Cell 2000; 101:91-101.

5. Akdemir F, Christich A, Sogame N, Chapo J, Abrams JM. p53 directs focused genomic responses in *Drosophila*. Oncogene 2007; 26:5184-5193.

6. Bourdon JC, Fernandes K, Murray-Zmijewski F, Liu G, Diot A, Xirodimas DP, Saville MK, Lane DP. p53 isoforms can regulate p53 transcriptional activity. Genes Dev 2005; 19:2122-2137.

7. Chintapalli VR, Wang J, Dow JA. Using FlyAtlas to identify better *Drosophila melanogaster* models of human disease. Nat Genet 2007; 39:715-720.

8. Jin S, Martinek S, Joo WS, Wortman JR, Mirkovic N, Sali A, Yandell MD, Pavletich NP, Young MW, Levine AJ. Identification and characterization of a p53 homologue in *Drosophila melanogaster*. Proc Natl Acad Sci U S A 2000; 97:7301-7306.

9. Sharpless NE, DePinho RA. Telomeres, stem cells, senescence, and cancer. J Clin Invest 2004; 113:160-168.

10. Campisi J. Senescent cells, tumor suppression, and organismal aging: good citizens, bad neighbors. Cell 2005; 120:513-522.

11. Moore L, Lu X, Ghebranious N, Tyner S, Donehower LA. Aging-associated truncated form of p53 interacts with wild-type p53 and alters p53 stability, localization, and activity. Mech Ageing Dev 2007; 128:717-730.

12. Gatza C, Hinkel G, Moore L, Dumble M, Donehower LA. p53 and mouse aging models. In: Masoro EJ, Austad SN, eds. Handbook of the Biology of Aging. Burlington, MA: Elsevier, 2006:149-171.

13. Kang HJ, Feng Z, Sun Y, Atwal G, Murphy ME, Rebbeck TR, Rosenwaks Z, Levine AJ, Hu W. Single-nucleotide polymorphisms in the p53 pathway regulate fertility in humans. Proc Natl Acad Sci U S A 2009; 106:9761-9766.

14. Campisi J. Cancer and ageing: rival demons? Nat Rev Cancer 2003; 3:339-349.

15. Aranda-Anzaldo A, Dent MA. Reassessing the role of p53 in cancer and ageing from an evolutionary perspective. Mech Ageing Dev 2007; 128:293-302.

16. Arum O, Johnson TE. Reduced expression of the *Caenorhabditis elegans* p53 ortholog *cep-1* results in increased longevity. J Gerontol A Biol Sci Med Sci 2007; 62:951-959.

17. Bauer JH, Poon PC, Glatt-Deeley H, Abrams JM, Helfand SL. Neuronal expression of p53 dominant-negative proteins in adult *Drosophila melanogaster* extends life span. Curr Biol 2005; 15:2063-2068.

18. Bauer JH, Chang C, Morris SN, Hozier S, Andersen S, Waitzman JS, Helfand SL. Expression of dominant-negative Dmp53 in the adult fly brain inhibits insulin signaling. Proc Natl Acad Sci U S A 2007; 104:13355-61330.

19. Ford D, Hoe N, Landis GN, Tozer K, Luu A, Bhole D, Badrinath A, Tower J. Alteration of *Drosophila* life span using conditional, tissue-specific expression of transgenes triggered by doxycycline or RU486/Mifepristone. Exp Gerontol 2007; 42:483-497.

20. Osterwalder T, Yoon KS, White BH, Keshishian H. A conditional tissue-specific transgene expression system using inducible GAL4. Proc Natl Acad Sci U S A 2001; 98:12596-12601.

21. Roman G, Endo K, Zong L, Davis RL. P[Switch], a system for spatial and temporal control of gene expression in *Drosophila melanogaster*. Proc Natl Acad Sci U S A 2001; 98:12602-12607.

22. Shen J, Curtis C, Tavaré S, Tower J. A screen of apoptosis and senescence regulatory genes for life span effects when over-expressed in *Drosophila*. Impact Aging 2009; 1:191-211.

23. Sun J, Tower J. FLP recombinase-mediated induction of Cu/Zn-superoxide dismutase transgene expression can extend the life span of adult *Drosophila melanogaster* flies. Mol Cell Biol 1999; 19:216-228.

24. Rong YS, Titen SW, Xie HB, Golic MM, Bastiani M, Bandyopadhyay P, Olivera BM, Brodsky M, Rubin GM, Golic KG. Targeted mutagenesis by homologous recombination in *D. melanogaster*. Genes Dev 2002; 16:1568-1581.

25. van der Horst A, Burgering BM. Stressing the role of FoxO proteins in lifespan and disease. Nat Rev Mol Cell Biol 2007; 8:440-450.

26. Brodsky MH, Weinert BT, Tsang G, Rong YS, McGinnis NM, Golic KG, Rio DC, Rubin GM. *Drosophila melanogaster* MNK/Chk2 and p53 regulate multiple DNA repair and apoptotic pathways following DNA damage. Mol Cell Biol 2004; 24:1219-1231.

27. Jassim OW, Fink JL, Cagan RL. Dmp53 protects the *Drosophila* retina during a developmentally regulated DNA damage response. Embo J 2003; 22:5622-5632.

28. Sogame N, Kim M, Abrams JM. *Drosophila* p53 preserves genomic stability by regulating cell death. Proc Natl Acad Sci U S A 2003; 100:4696-4701.

29. Toivonen JM, Partridge L. Endocrine regulation of ageing and reproduction in *Drosophila*. Mol Cell Endocrinol 2009; 299:39-50.

30. Tower J. Sex-specific regulation of aging and apoptosis. Mech Ageing Dev 2006; 127:705-718.

31. You H, Mak TW. Crosstalk between p53 and FOXO transcription factors. Cell Cycle 2005; 4:37-38.

32. Maier B, Gluba W, Bernier B, Turner T, Mohammad K, Guise T, Sutherland A, Thorner M, Scrable H. Modulation of mammalian life span by the short isoform of p53. Genes Dev 2004; 18:306-319.

33. Flatt T, Min KJ, D'Alterio C, Villa-Cuesta E, Cumbers J, Lehmann R, Jones DL, Tatar M. *Drosophila* germ-line modulation of insulin signaling and lifespan. Proc Natl Acad Sci U S A 2008; 105:6368-6373.

34. Jiang H, Patel PH, Kohlmaier A, Grenley MO, McEwen DG, Edgar BA. Cytokine/Jak/Stat signaling mediates regeneration and homeostasis in the *Drosophila* midgut. Cell 2009; 137:1343-1355.

35. Biteau B, Hochmuth CE, Jasper H. JNK activity in somatic stem cells causes loss of tissue homeostasis in the aging *Drosophila* gut. Cell Stem Cell 2008; 3:442-455.

36. Sablina AA, Budanov AV, Ilyinskaya GV, Agapova LS, Kravchenko JE, Chumakov PM. The antioxidant function of the p53 tumor suppressor. Nat Med 2005; 11:1306-1313.

37. Edwards MG, Anderson RM, Yuan M, Kendziorski CM, Weindruch R, Prolla TA. Gene expression profiling of aging reveals activation of a p53-mediated transcriptional program. BMC Genomics 2007; 8:80.

38. Liu B, Chen Y, St Clair DK. ROS and p53: a versatile partnership. Free Radic Biol Med 2008; 44:1529-1535.

39. Ventura N, Rea SL, Schiavi A, Torgovnick A, Testi R, Johnson TE. p53/CEP-1 increases or decreases lifespan, depending on level of mitochondrial bioenergetic stress. Aging Cell 2009; 8:380-393.

40. Komarova EA, Kondratov RV, Wang K, Christov K, Golovkina TV, Goldblum JR, Gudkov AV. Dual effect of p53 on radiation sensitivity in vivo: p53 promotes hematopoietic injury, but protects from gastro-intestinal syndrome in mice. Oncogene 2004; 23:3265-3271.

41. Strom E, Sathe S, Komarov PG, Chernova OB, Pavlovska I, Shyshynova I, Bosykh DA, Burdelya LG, Macklis RM, Skaliter R, Komarova EA, Gudkov AV. Small-molecule inhibitor of p53 binding to mitochondria protects mice from gamma radiation. Nat Chem Biol 2006; 2:474-479.

42. Hughes KA, Reynolds RM. Evolutionary and mechanistic theories of aging. Annu Rev Entomol 2005; 50:421-445.

43. Rodier F, Campisi J, Bhaumik D. Two faces of p53: aging and tumor suppression. Nucleic Acids Res 2007; 35:7475-7484.

44. Nuzhdin SV, Pasyukova EG, Dilda CL, Zeng ZB, Mackay TF. Sex-specific quantitative trait loci affecting longevity in *Drosophila melanogaster*. Proc Natl Acad Sci U S A 1997; 94:9734-9739.

45. Tower J, Arbeitman M. The genetics of gender and life span. J Biol 2009; 8:38.

46. Rice WR, Gavrilets S, Friberg U. Sexually antagonistic "zygotic drive" of the sex chromosomes. PLoS Genet 2008; 4:e1000313.

47. Morrow EH, Stewart AD, Rice WR. Assessing the extent of genome-wide intralocus sexual conflict via experimentally enforced gender-limited selection. J Evol Biol 2008; 21:1046-54.

48. Feng Z, Hu W, Rajagopal G, Levine AJ. The tumor suppressor p53: cancer and aging. Cell Cycle 2008; 7:842-847.

49. Hu W, Feng Z, Atwal GS, Levine AJ. p53: a new player in reproduction. Cell Cycle 2008; 7:848-852.

50. Sah VP, Attardi LD, Mulligan GJ, Williams BO, Bronson RT, Jacks T. A subset of p53-deficient embryos exhibit exencephaly. Nat Genet 1995; 10:175-180.

51. Armstrong JF, Kaufman MH, Harrison DJ, Clarke AR. High-frequency developmental abnormalities in p53-deficient mice. Curr Biol 1995; 5:931936.

52. Chen X, Watkins R, Delot E, Reliene R, Schiestl RH, Burgoyne PS, Arnold AP. Sex difference in neural tube defects in p53-null mice is caused by differences in the complement of X not Y genes. Dev Neurobiol 2008; 68:265-273.

53. Rea S, Xouri G, Akhtar A. Males absent on the first (MOF): from flies to humans. Oncogene 2007; 26:5385-5394.

54. Ren C, Webster P, Finkel SE, Tower J. Increased internal and external bacterial load during *Drosophila* aging without life-span trade-off. Cell Metab 2007; 6:144-152.

55. Xie HB, Golic KG. Gene deletions by ends-in targeting in *Drosophila melanogaster*. Genetics 2004; 168:1477-1489.

56. Landis GN, Bhole D, Tower J. A search for doxycycline-dependent mutations that increase *Drosophila melanogaster* life span identifies the *VhaSFD*, *Sugar baby*, *filamin*, *fwd* and *Cct1* genes. Genome Biol 2003; 4:R8.

57. Miller RG. Survival Analysis. New York: John Wiley & Sons, 1981.

58. RDevelopment CoreTeam. R: A language and environment for statistical computing.: R Foundation for Statistical Computing, Vienna, Austria, 2006.

SUPPLEMENTARY FIGURES

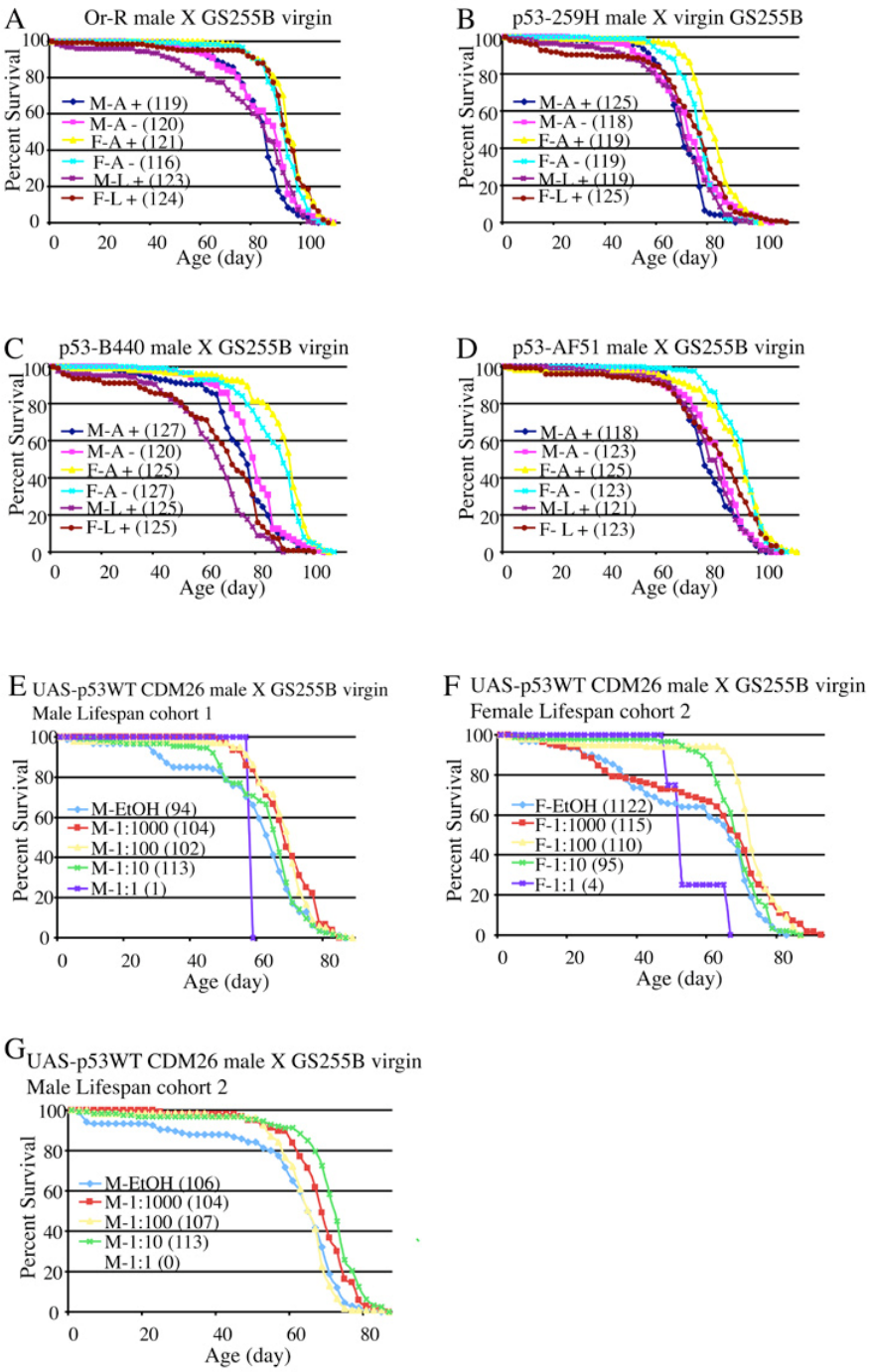

Supplementary Figure S1. Conditional over-expression of wild-type and dominant-mutant *p53* transgenes using Geneswitch system. All flies were the progeny of the indicated transgenic strains crossed to the ubiquitous Geneswitch driver Act-GS-255B. The flies were cultured in the presence and absence of drug, as larvae or adults, as indicated: M = males, F = females, A = adults, L = larvae, "+" indicates culture in presence of drug, "-" indicates culture in absence of drug. (**A**) Controls: progeny of Act-GS-255B driver crossed to Or-R wild type. (**B-D**) *p53* dominant-mutant transgene over-expression. (**B**) UAS-p53-259H. (**C**) UAS-p53-B440. (**D**) UAS-p53-AF51. (**E-G**). Titration of *p53* wild-type (UAS-p53WT-CDM26) over-expression during development and effect on subsequent adult life span. (**E**) Males, cohort 1. Females of cohort 1 are shown in Figure 2. (**F**) Females, cohort 2. (**G**) Males, cohort 2.

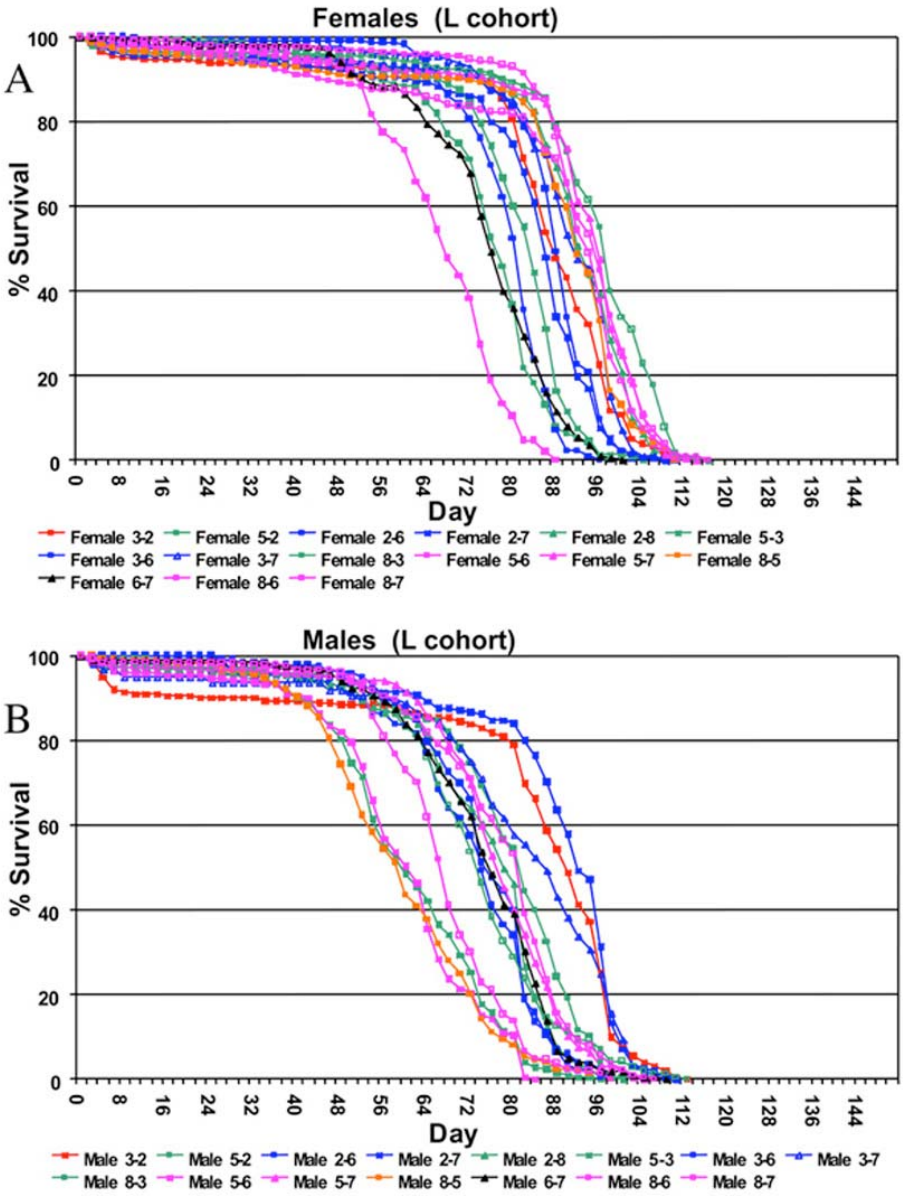

Supplementary Figure S2. Survival data for each genotype in cohort L. Survival curves. (**A**) Females. (**B**) Males.

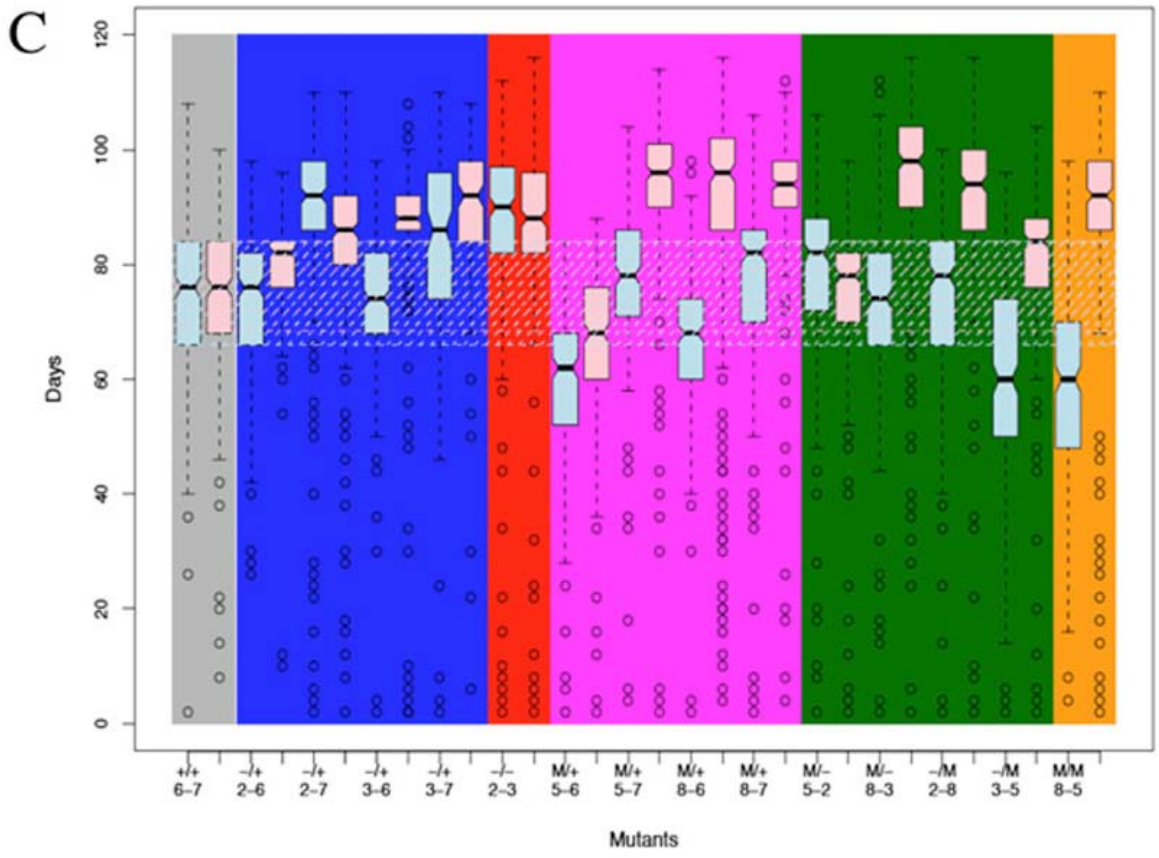

Supplementary Figure S2. Survival data for each genotype in cohort L. (**C**) Box plot presentation of survival data for each genotype in cohort L. Blue boxes indicate males, pink boxes indicate females.

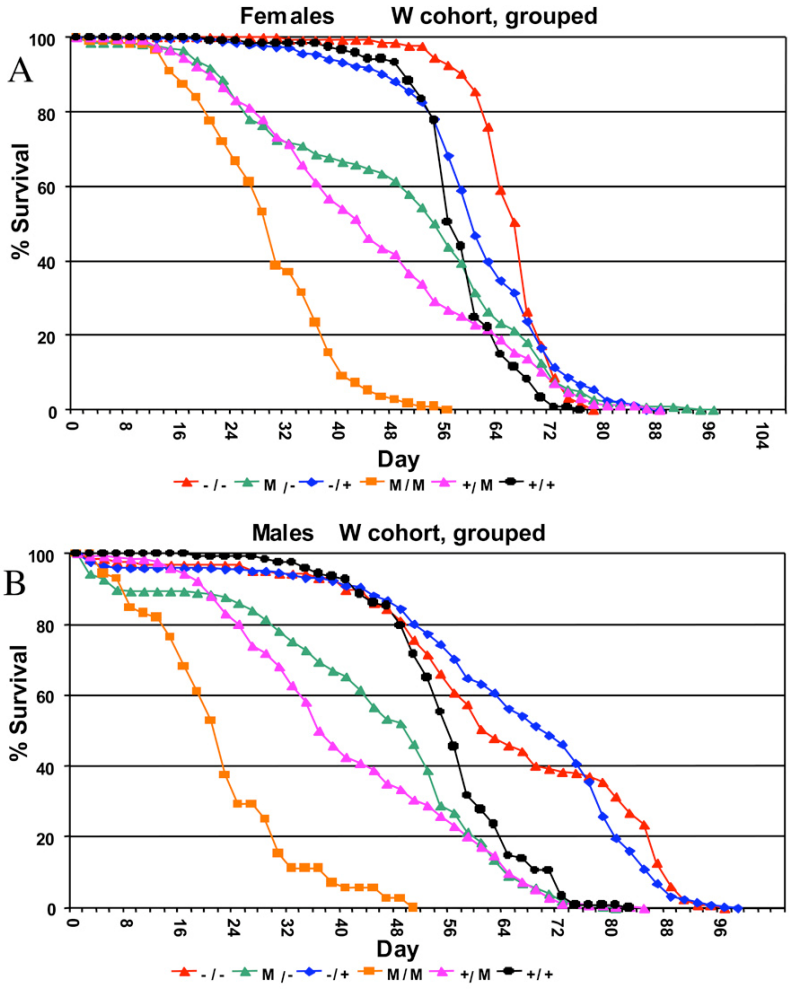

Supplementary Figure S3. Survival curves for flies in cohort W. Grouped data. (**A**) Females. (**B**) Males.

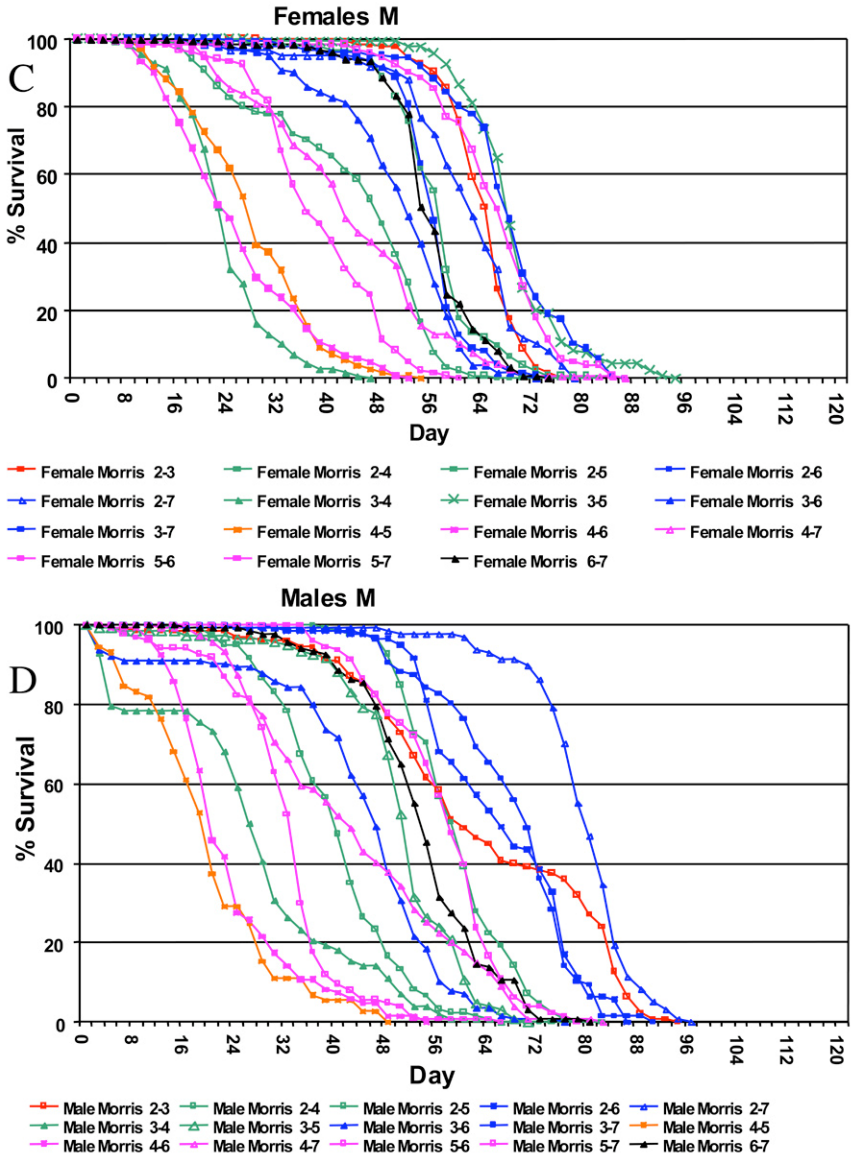

Supplementary Figure S3. Survival curves for flies in cohort W. Survival curves for each genotype. (**C**) Females. (**D**) Males

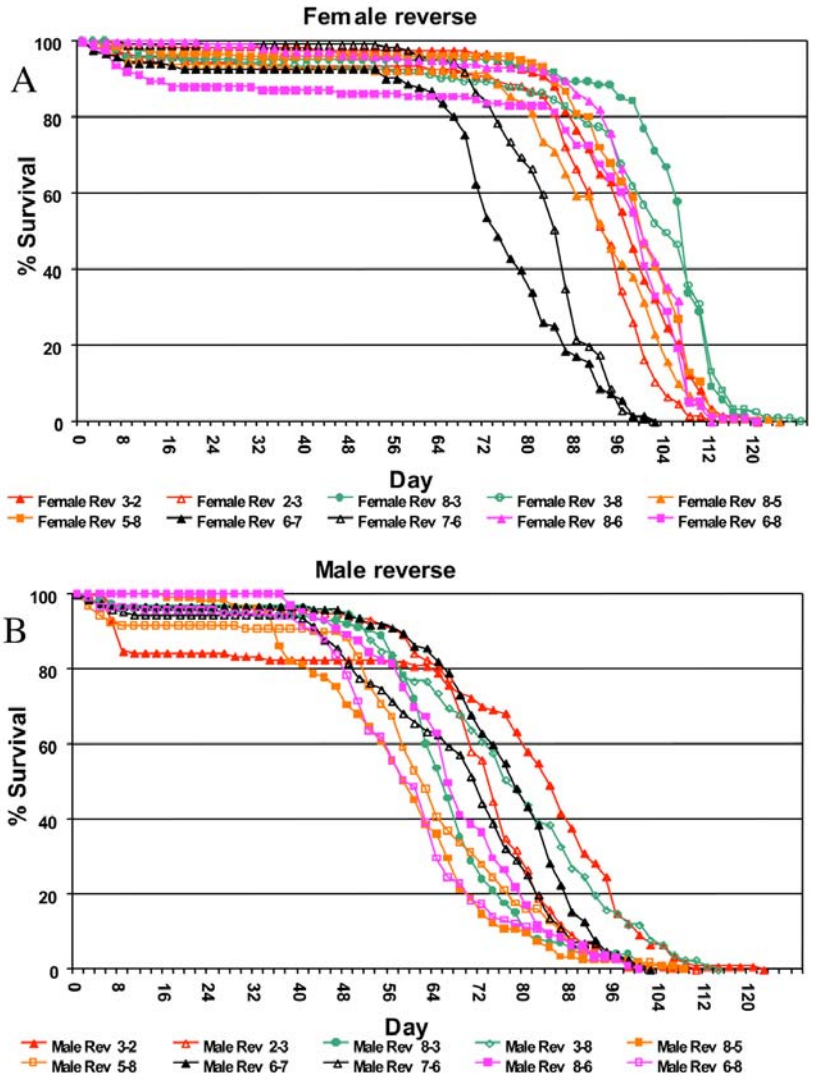

Supplementary Figure S4. Reciprocal crosses. (**A**) Females, (**B**) Males.

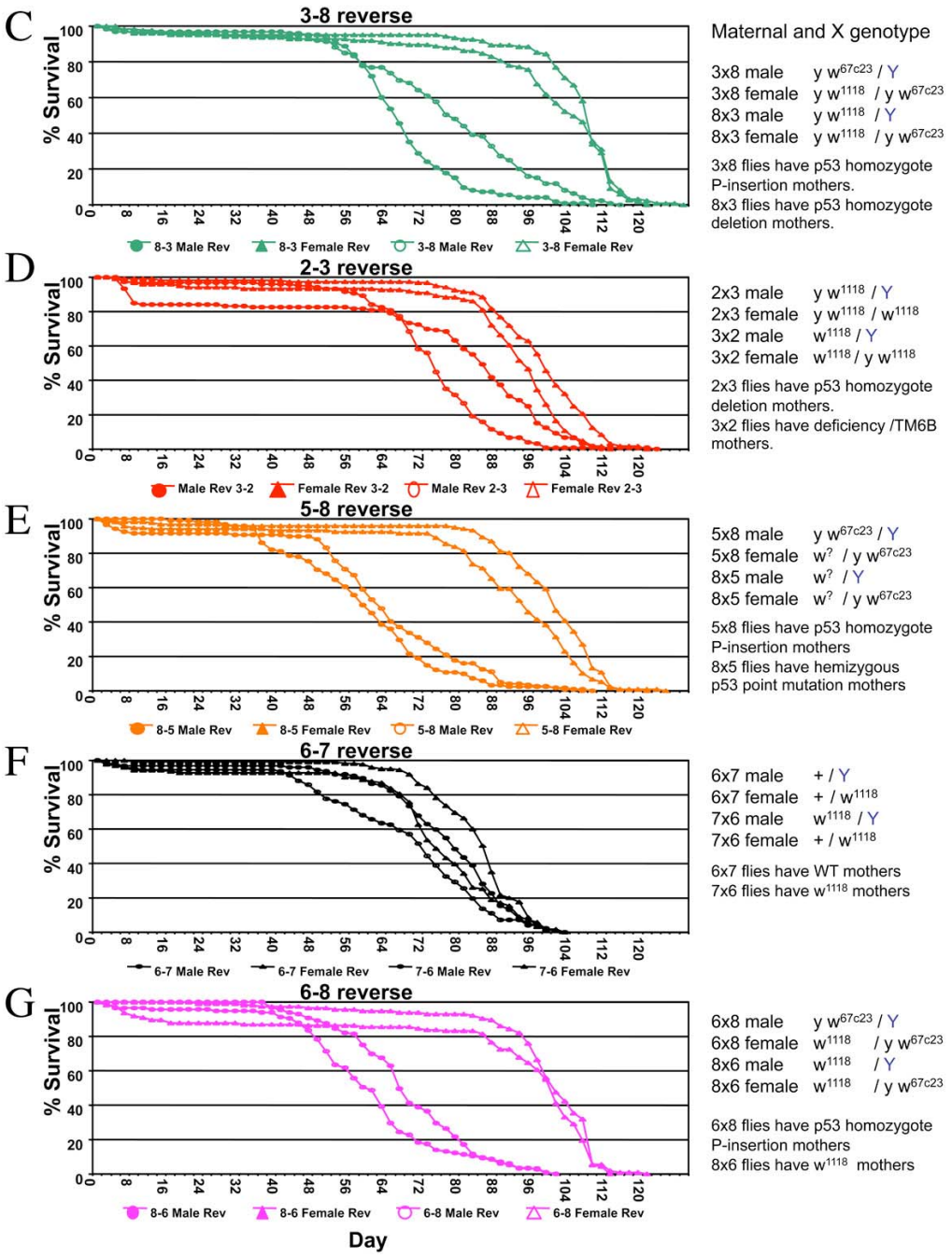

Supplementary Figure S4. Reciprocal crosses. (**C-G**) Comparisons of reciprocal crosses for specific genotypes. *X* and *Y* chromosomal composition of the flies is summarized to the right, along with the maternal *p53* genotypes.

H

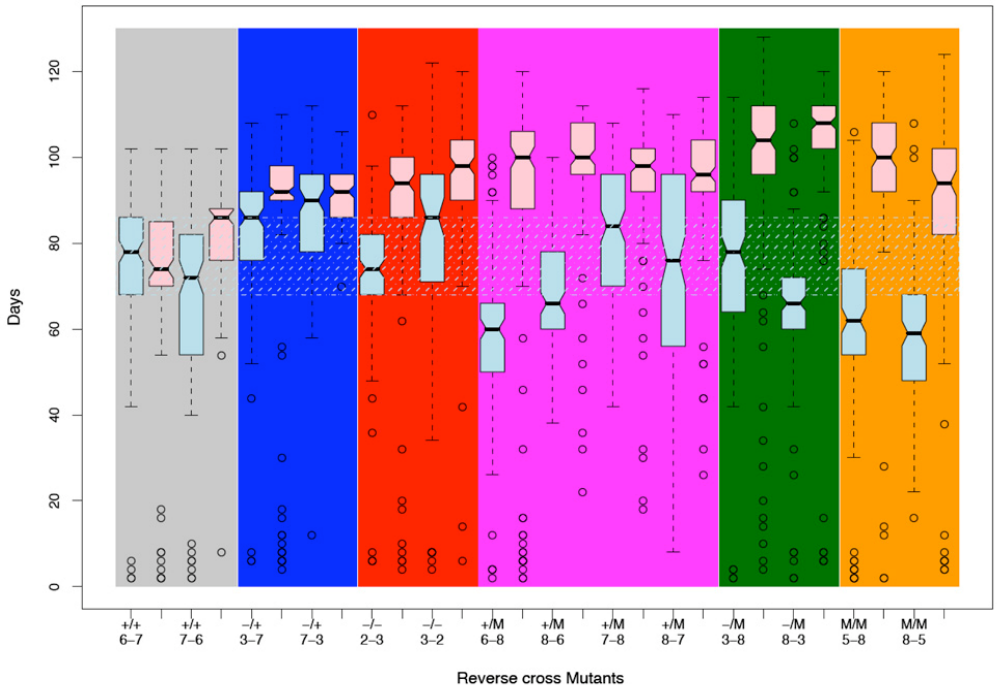

Supplementary Figure S4. Reciprocal crosses. (**H**) Box plot presentation of survival data for reciprocal crosses. Blue boxes indicate males, pink boxes indicate females.

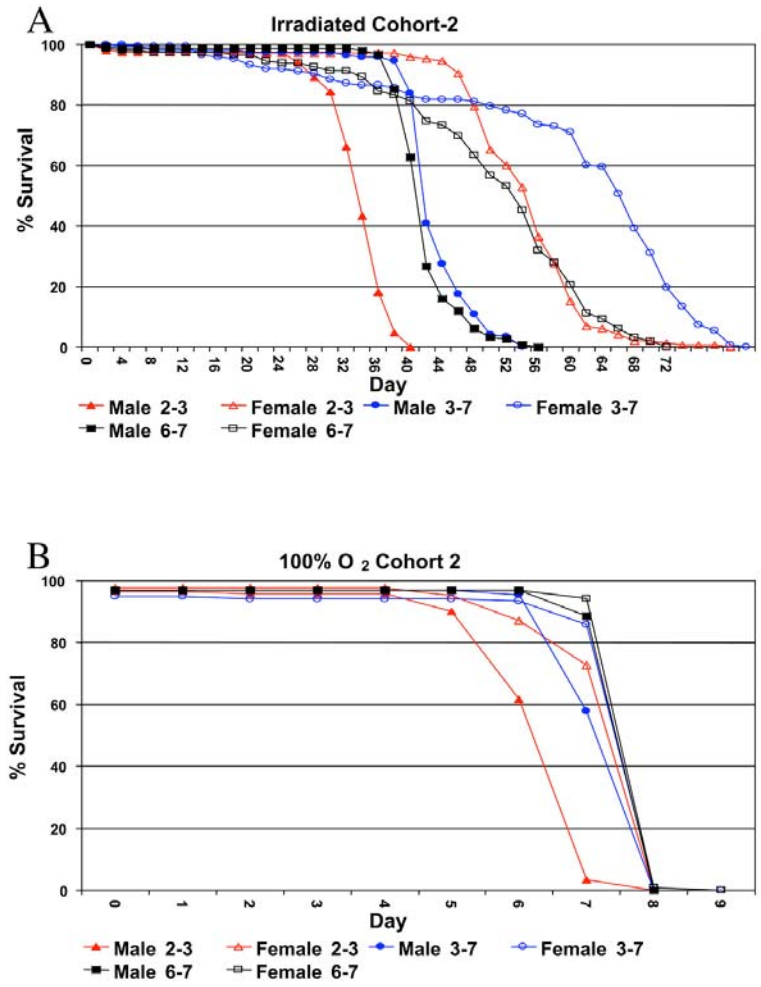

Supplementary Figure S5. Survival data for flies subjected to stress. (**A**) Irradiation, cohort 2. (**B**) 100% oxygen atmosphere, cohort 2.

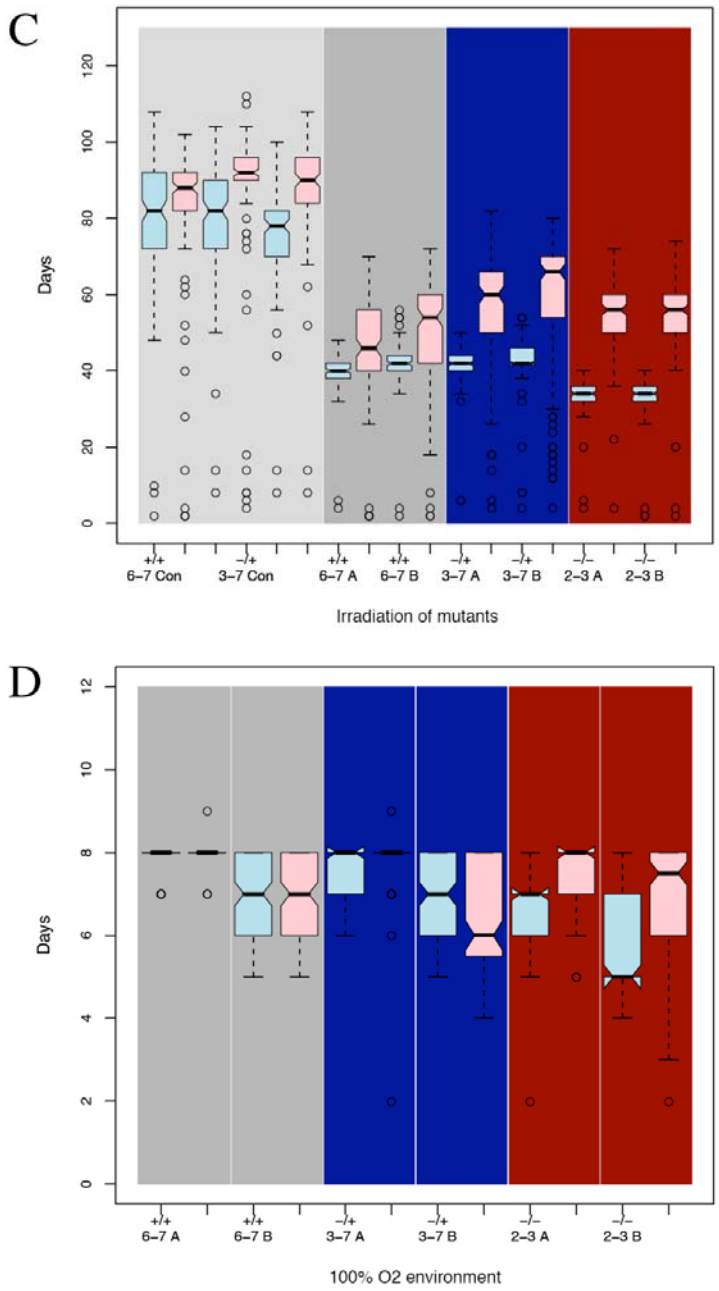

Supplementary Figure S5. Survival data for flies subjected to stress. Box plot presentation of survival data for flies subjected to stress; data is the sum of cohorts 1 and 2. (**C**) Irradiation. (**D**) 100% oxygen atmosphere. Blue boxes indicate males, pink boxes indicate females.

SUPPLEMENTARY TABLES

Table S1. Summary of the effect on life span of wild-type *p53* over-expression using the GeneSwitch system

p53 GeneSwitch over-expression experiments Male												
M-F	Target transgene	Gr	N	± SD	Mean life span		Med life span		Max life span		P-val	Sig
					Mean	CI %Δ	Med	CI %Δ	Max	CI %Δ		
7-9	+	L-A-	120	14.25	84.6	NA	90	NA	98	NA	NA	NA
		L+A-	123	22.48	78.44	–4.77 - –2.78	86	–9.58 - –1.58	98	–3.67 - –2.28	0.204	__
		L-A+	119	10.94	83.08	–4.76 - 1.25	86	–7.34 - –1.95	94	–8.41 - –1.59	6.58×10^{-3}	*
16-9	p53-WT[Ex]	L-A-	122	14.76	71.11	NA	72	NA	86	NA	NA	NA
		L+A-	0⊗	NA	NA	NA	NA	NA	NA	NA	NA	NA
		L-A+	117	12.54	75.38	2.36 - 10.37	78	5.83 - 15.51	90	1.67 – 10.11	6.97×10^{-3}	*
18-9	p53-Ct[AF51]	L-A-	123	13.77	82.05	NA	86	NA	95.6	NA	NA	NA
		L+A-	121	14.59	79.72	–6.11 - 0.77	80	–14.59 - –6.97	96	–4.65 - 6.52	0.159	_
		L-A+	118	11.15	79.71	–5.73 - 0.55	78	–12.89 - –9.30	96	–4.01 - 4.57	0.032	_
19-9	p53-Ct[B440]	L-A-	99	13.05	76.71	NA	78	NA	90	NA	NA	NA
		L+A-	125	18.47	61.7	–23.45 - –15.28	66	–18.34 - –10.18	80	–19.48 - –5.97	8.16×10^{-12}	***
		L-A+	127	16.1	73.1	–8.26 - –0.79	76	–6. 88 - –1.93	88.8	–7.08 - 9.28	0.194	__
20-9	p53-259H	L-A-	118	13.86	71.54	NA	72	NA	88	NA	NA	NA
		L+A-	119	16.92	67.73	–10.46 - –0.72	70	–5.33 - 0.00	84	–10.19 - 2.22	0.069	__
		L-A+	125	10.41	68.9	–7.11 - –0.02	70	–2.77 - 1.76	78	–15.77 - –5.53	2.11×10^{-3}	*

p53 GeneSwitch over-expression experiments Female												
M-F	Target transgene	Gr	N	± SD	Mean life span		Med life span		Max life span		P-val	Sig
					Mean	CI %Δ	Med	CI %Δ	Max	CI %Δ		
7-9	+	L-A-	116	9.64	92.02	NA	94	NA	102	NA	NA	NA
		L+A-	124	8.61	91.97	–3.33 - –0.72	94	–2.88 - 2.79	106	–1.41 - 3.62	2.55×10^{-2}	__
		L-A+	121	15.74	94.69	0.866 - 2.72	94	–4.76 - 0.00	104	2.33 – 7.41	3.10×10^{-3}	*
16-9	p53-WT[Ex]	L-A-	119	16.09	88.35	NA	94	NA	100	NA	NA	NA
		L+A-	3⊗	5.03	91.33	NA	92	NA	95.2	NA	NA	NA
		L-A+	101	22.07	74.02	–21.11 - –11.61	80	–23.06 - –8.69	98	–3.39- 2.09	2.21×10^{-6}	***
18-9	p53-Ct[AF51]	L-A-	123	8.861	92.2	NA	94	NA	102	NA	NA	NA
		L+A-	123	20.08	81.82	–14.90 - –8.03	86	–12.87 - –5.66	100	–5.59 - –1.96	3.40×10^{-3}	*
		L-A+	125	16.53	89.18	–6.71 - –0.35	94	0.00 - 3.19	104	–3.83 - 2.28	8.57×10^{-1}	__
19-9	p53-Ct[B440]	L-A-	127	13.54	86.3	NA	90	NA	98	NA	NA	NA
		L+A-	125	22.35	64.56	–29.62 - –20.83	70	–26.06 - –18.68	85.2	–16.43 - –7.00	0	***
		L-A+	125	14.39	89.31	1.96 - 6.81	94	4.38 - 9.12	100	0.35 - 4.09	4.72×10^{-2}	__
20-9	p53-259H	L-A-	119	8.495	75.39	NA	76	NA	84	NA	NA	NA
		L+A-	125	22.02	70.24	–11.94 - –2.49	76	–3.71 - 5.72	88	1.80 - 8.56	2.02×10^{-1}	__
		L-A+	119	10.98	80.66	4.09 - 9.72	82	4.52 - 14.04	92	4.26 - 13.18	4.05×10^{-8}	***

95% double bootstrap-t confidence intervals for the ratio of the means (or ratio of the percentiles) of the mutant and wild-type samples were computed as listed. The mean, median, and maximal life span values are reported for each genotype as well as the P-values representing the significance of the log-rank test of the null hypothesis that there is no difference in the probability of death between functions between wild-type untreated and *p53* over-expressing flies. Note that * indicates $1.00 \times 10^{-3} < P < 5.00 \times 10^{-2}$, ** indicates $1.00 \times 10^{-8} P < 1.00 \times 10^{-3}$, *** indicates $P < 1.00 \times 10^{-8}$.

Table S2. Summary of the effect of wild-type *p53* over-expression titrated at various levels during development on Drosophila life span

p53 wild-type dilution experiment, cohort 1 and cohort 2 combined, Male											
Gr	**M-F**	**N**	**± SD**	**Mean life span**		**Med life span**		**Max life span**		**P-val**	**Sig**
				Mean	**CI %Δ**	**Med**	**CI %Δ**	**Max**	**CI %Δ**		
No Drug	17-9	200	17.75	59.08	NA	64	NA	74	NA	NA	NA
1:1000	17-9	204	9.92	67.68	10.54 – 19.30	68	3.63 - 8.99	78	2.48 – 8.52	4.97×10^{-7}	**
1:100	17-9	209	11.23	65.13	6.12 – 15.09	68	6.07 - 11.26	74	–4.77 - 3.03	1.73×10^{-2}	*
1:10	17-9	203	65.13	67.89	7.60 – 19.77	70	6.84 – 12.35	78	1.27 – 8.37	2.68×10^{-10}	***
1:1	17-9	1[⊗]	NA	NA	NA	NA	NA	NA	NA	NA	NA
p53 wild-type dilution experiment, cohort 1 and cohort 2 combined, Female											
Gr	**M-F**	**N**	**± SD**	**Mean life span**		**Med life span**		**Max life span**		**P-val**	**Sig**
				Mean	**CI %Δ**	**Med**	**CI %Δ**	**Max**	**CI %Δ**		
No Drug	17-9	230	18.97	59.56	NA	68	NA	76	NA	NA	NA
1:1000	17-9	221	18.39	68.15	9.29 – 19.27	72	–0.78 – 5.88	84	5.51 -10.53	6.66×10^{-16}	***
1:100	17-9	217	12.90	72.26	16.92 – 26.49	74	5.29 - 12.74	84	6.79 - 13.81	0	***
1:10	17-9	205	12.40	67.89	9.33 – 18.73	70	–0.33 – 5.89	78	–0.52 - 4.92	1.35×10^{-4}	**
1:1	17-9	16	16.69	57.62	–21.09 – 8.51	62	–26.15 - –2.34	74	–11.67 - 7.36	0.17	__

Wild-type *p53* over-expression was induced using the GeneSwitch system and titrated at various levels with the drug RU486. [⊗]Note that for the 1:1 dilution, only 1 male pupae eclosed. 95% double bootstrap-t confidence intervals for the ratio of the means (or ratio of the percentiles) of the mutant and wild-type samples in each condition were computed as listed for each *p53* concentration in the combined data from two trials. The mean, median, and maximal lifespan values are reported for each genotype as well as the P-values representing the significance of the log-rank test of the null hypothesis that there is no difference in the probability of death between functions between wild-type untreated and *p53* over-expressing flies. Note that * indicates $1.00 \times 10^{-3} < P < 5.00 \times 10^{-2}$, ** indicates $1.00 \times 10^{-8} P < 1.00 \times 10^{-3}$, *** indicates $P < 1.00 \times 10^{-8}$.

Table S3. Summary of the significance of *p53* deletion or mutation on life span

L cohort [b] Male											
M-F	**Gr**	**N**	**± SD**	**Mean life span**		**Med life span**		**Max life span**		**P-val**	**Sig**
				Mean	**CI %Δ**	**Med**	**CI %Δ**	**Max**	**CI %Δ**		
6-7	+/+	234	14.82	74.05	NA	76	NA	88	NA	NA	NA
3-2	-/-	$^{\otimes}$178	24.53	83.07	7.13 - 16.53	90	14.26 - 23.92	98	8.84 - 11.36	0	***
2-6	-/+	$^{\otimes}$210	13.03	73.97	–3.15 - 2.80	77	–6.11 - 4.74	86.2	–5.04 - –2.27	0.39	___
2-7	-/+	195	19.83	86.86	13.22 - 21.24	92	14.31 - 24.91	100	11.88 - 15.32	0	***
3-6	-/+	236	13.19	73.69	–3.26 - 2.47	74	–6.92 - 0.51	88	–1.80 - 2.91	0.13	___
3-7	-/+	97	23.28	80.29	2.31 - 13.61	86	6.61 - 19.99	100	10.76 - 15.32	6.47×10^{-10}	***
5-6	M/+	211	16.95	58.93	–23.65 - –17.35	62	–22.11 - –11.32	82	NA	0	***
5-7	M/+	187	14.93	76.47	–0.25 - 6.59	78	–0.35 - 7.45	90.8	2.35 - 8.69	0.074	___
8-6	M/+	241	13.77	66.85	–12.58 - –6.90	68	–13.15 - –5.58	82	–7.74 - –5.90	1.32×10^{-11}	***
8-7	M/+	231	17.79	76.44	–0.36 - 6.88	82	4.69 - 12.06	92	0.46 - 7.46	3.20×10^{-3}	*
2-8	-/M	227	17.53	73.43	–4.19 - 2.36	78	–3.37 - 5.65	88	–1.78 - 2.03	0.92	____
5-3	M/-	202	16.83	60.09	–22.03 - –15.76	60	–26.13 - –14.92	81.8	–6.82 - –1.26	0	***
5-2	M/-	235	16.79	78.09	–5.00 - 1.51	82	4.83 - 11.49	95.2	9.10 - 15.26	6.94×10^{-6}	**
8-3	M/-	211	17.47	72.72	–4.98 - 2.52	74	–5.63 - 0.65	92	–2.43 - 11.30	0.92	___
8-5	M/M	226	16.05	59.09	–23.01 - –17.26	60	–23.30 - –15.94	78	–16.17 - –7.75	0	***

L cohort [b] Female											
M-F	**Gr**	**N**	**± SD**	**Mean life span**		**Med life span**		**Max life span**		**P-val**	**Sig**
				Mean	**CI %Δ**	**Med**	**CI %Δ**	**Max**	**CI %Δ**		
6-7	+/+	238	14.54	74.68	NA	76	NA	90	NA	NA	NA
3-2	-/-	242	22.22	84.47	9.00 - 16.99	88	13.07 - 21.08	102	10.47 - 19.52	0	***
2-6	-/+	237	9.92	79.11	3.40 - 8.62	82	7.89 - 13.22	88	–4.63 - –0.15	0.05	*
2-7	-/+	238	20.11	81.39	5.29 - 12.64	86	10.36 - 16.84	96	3.85 - 8.92	0	***
3-6	-/+	225	19.67	84.29	8.96 - 16.55	88	12.47 - 19.58	96	2.24 - 8.88	0	***
3-7	-/+	126	14.82	89.03	15.20 - 22.93	92	15.58 - 28.32	100	8.41 - 13.49	0	***
5-6	M/+	212	15.32	65.82	–14.91 - –8.90	68	–13.10 - –7.01	81.8	–10.96 - –4.47	6.53×10^{-14}	***
5-7	M/+	227	19.18	91.32	18.39 - 26.10	96	23.53 - 30.09	106	15.00 - 21.18	0	***
8-6	M/+	$^{\otimes}$208	21.00	89.36	15.18 - 23.80	96	23.93 - 31.21	106	14.98 - 22.09	0	***
8-7	M/+	210	15.27	92	19.74 - 26.56	94	NA	104	NA	0	***
2-8	-/M	215	20.74	89.01	15.09 - 23.10	94	23.68 - 30.52	102	8.87 - 15.67	0	***
5-3	M/-	225	18.15	78.90	1.89 - 9.10	84	10.53 - 13.95	92	–0.165 - 4.88	4.28×10^{-7}	**
5-2	M/-	221	16.31	74.37	–3.69 - 2.68	78	–0.026 - 8.22	88	–4.65 - 0.11	0.95	___
8-3	M/-	231	17.70	93.8	21.72 - 29.48	98	28.95 - 33.40	102	16.92 - 22.64	0	***
8-5	M/M	231	22.60	86.94	12.14 - 20.48	92	18.42 - 25.00	102	10.14 - 15.88	0	***

To assess the effect of *p53* mutation on mean, median, and maximal lifespan, 95% double bootstrap t confidence intervals for the ratio of the means (or ratio of the percentiles) of the mutant and wild-type samples were computed as listed for the combined data for the L-cohort and stress assays. The log-rank test was employed to test the null hypothesis that there is no difference in the probability of death between wild-type and *p53* mutant flies. P-values indicating the significance of the tests are reported. $^{\otimes}$Indicates exclusion of an outlier vial.

Table S4. Summary of the effect *p53* deletion or mutation on life span in grouped data

L cohort grouped Male										
Gr	**N**	**± SD**	**Mean lifespan**		**Med life span**		**Max life span**		**P-val**	**Sig**
			Mean	**CI %Δ**	**Med**	**CI %Δ**	**Max**	**CI %Δ**		
+/+	234	14.82	74.05	NA	76	NA	88	NA	NA	NA
-/-	⊗178	24.53	83.07	4.92 - 14.50	90	13.09 - 22.05	98	8.84 - 11.36	0	***
-/+	⊗738	17.60	78.12	2.15 - 7.53	82	4.53 - 12.49	98	11.36 - 12.39	2.04×10^{-8}	***
+/M	870	17.48	69.54	–8.41 - –3.61	72	–7.82 -0.18	88	–1.20 - 0.00	5.00×10^{-3}	*
-/M	875	18.35	71.43	–5.86 - –0.91	74	–7.57 -0.29	90	–0.28 - 3.94	0.73	__
M/M	226	16.05	49.09	–23.06 - –17.11	60	–23.27 - –15.95	78	–16.07 - –8.02	0	***

L cohort grouped Female										
Gr	**N**	**± SD**	**Mean lifespan**		**Med life span**		**Max life span**		**P-val**	**Sig**
			Mean	**CI %Δ**	**Med**	**CI %Δ**	**Max**	**CI %Δ**		
+/+	238	14.54	74.68	NA	76	NA	90	NA	NA	NA
-/-	242	22.22	84.47	9.00 -17.28	88	13.09 - 20.58	102	10.50 – 19.74	0	***
-/+	826	17.14	82.69	8.41 - 13.59	86	13.16 - 16.86	96	1.90 – 8.85	0	***
+/M	⊗857	20.90	84.7	10.65 - 16.25	92	21.05 - 26.32	104	12.78 – 18.12	0	***
-/M	892	19.83	84.07	10.01 - 15.28	88	15.79 - 21.45	104	12.82 – 18.70	0	***
M/M	231	22.60	86.94	12.19 - 20.76	92	18.42 - 24.16	102	10.26 – 15.97	0	***

To assess the effect of *p53* mutation on mean, median, and maximal lifespan, 95% double bootstrap t confidence intervals for the ratio of the means (or ratio of the percentiles) of the mutant and wild-type samples were computed as listed for the grouped L-cohort data. The mean, median, and maximal lifespan values are reported for each genotype as well as the P-values for the log-rank test of the null hypothesis of identical survival functions between wild-type and *p53* mutant flies. Note that * indicates $1.00 \times 10^{-3} < P < 5.00 \times 10^{-2}$, ** indicates $1.00 \times 10^{-8} P < 1.00 \times 10^{-3}$, *** indicates $P < 1.00 \times 10^{-8}$. ⊗ Indicates exclusion of an outlier vial.

Table S5. Effect of *p53* mutation on Drosophila life span

a. Mutation type Male							
Effects	**DF Num**	**DF Den**	**F-val**	**P-val**	**Sig**		
(Intercept)	1	3106	23222.526	<0.0001	***		
Mutation type	5	3106	57.277	<0.0001	***		
Mutation type	**Coef**	**DF**	**Std.Error**	**t-value**	**P-val**	**Adj P-val**	**Sig**
(+/+) (Intercept)	74.033	3106	1.223	60.543	<<0.0001		***
(-/+)	4.065	3106	1.345	3.023	0.0025	0.028	*
(-/-)	8.831	3106	1.787	4.943	<<0.0001	<0.001	***
(M/+)	-4.521	3106	1.320	-3.426	0.0006	0.007	**
(M/-)	-2.610	3106	1.320	-1.978	0.0480	0.338	--
(M/M)	-14.940	3106	1.672	-8.938	<<0.0001	<0.001	***

b. Genotype Male							
Effects	**DF num**	**DF den**	**F-val**	**P-val**	**Sig**		
(Intercept)	1	3097	27262.577	<0.0001	***		
Mutation type	14	3097	49.205	<0.0001	***		
Genotype	**Coef**	**DF**	**Std.Error**	**t-value**	**P-val**	**Adj P-val**	**Sig**
6-7 (intercept)	74.0435	3097	1.153	64.194	<<0.0001		***
3-2	-0.139	3097	1.614	-0.086	0.931	1.000	--
2-6	-0.362	3097	1.565	-0.231	0.817	1.000	--
2-7	12.803	3097	1.647	7.775	<<.0001	<0.001	***
3-6	6.501	3097	2.061	3.154	0.002	0.0186	*
3-7	8,860	3097	1.691	5.238	<<0.0001	<0.001	***
5-6	-15.088	3097	1.611	-9.364	<<0.0001	<0.001	***
5-7	-7.187	3097	1.557	-4.615	<<0.0001	<0.001	***
8-6	2.288	3097	1.666	1.373	0.170	0.840	--
8-7	2.397	3097	1.573	1.523	0.128	0.694	--
2-8	4.064	3097	1.568	2.593	0.010	0.0931	--
5-3	-13.976	3097	1.632	-8.566	<<0.0001	<0.001	***
5-2	-1.370	3097	1.612	-0.850	0.395	0.993	--
8-3	-0.646	3097	1.581	-0.409	0.683	1.000	--
8-5	-14.952	3097	1.583	-9.448	<<0.0001	<0.001	***

c. Mutation type Female							
Effects	**DF Num**	**DF Den**	**F-val**	**P-val**	**Sig**		
(Intercept)	1	3271	37307.36	<0.0001	***		
Mutation type	5	3271	12.41	<0.0001	***		
Mutation type	**Coef**	**DF**	**Std.Error**	**t-value**	**P-val**	**Adj P-val**	**Sig**
(+/+) (Intercept)	74.667	3271	1.294	57.726	<<0.0001	<0.001	***
(-/+)	8.040	3271	1.437	5.595	<<0.0001	<0.001	***
(-/-)	9.817	3271	1.783	5.506	<<0.0001	<0.001	***
(M/+)	10.068	3271	1.431	7.034	<<0.0001	<0.001	***
(M/-)	9.412	3271	1.425	6.605	<<0.0001	<0.001	***
(M/M)	12.282	3271	1.804	6.810	<<0.0001	<0.001	***

Table S5. (cont.)

d. Genotype Female							
Effects	**DF num**	**DF den**	**F-val**	**P-val**	**Sig**		
(Intercept)	1	3262	28493.444	<0.0001	***		
Mutation type	14	3262	40.714	<0.0001	***		
Genotype	**Coef**	**DF**	**Std.Error**	**t-value**	**P-val**	**Adj P-val**	**Sig**
6-7 (intercept)	74.662	3262	1.240	60.228	<<0.0001		***
3-2	9.601	3262	1.694	5.669	<<0.0001	<0.001	***
2-6	4.442	3262	1.671	2.658	0.008	0.0776	--
2-7	6.714	3262	1.669	4.038	0.0001	<0.001	***
3-6	14.751	3262	2.017	7.312	<<0.0001	<0.001	***
3-7	9.823	3262	1.662	5.909	<<0.0001	<0.001	***
5-6	-8.906	3262	1.721	-5.172	<<0.0001	<0.001	***
5-7	14.672	3262	1.731	8.478	<<0.0001	<0.001	***
8-6	16.652	3262	1.689	9.856	<<0.0001	<0.001	***
8-7	17.510	3262	1.726	10.146	<<0.0001	<0.001	***
2-8	-0.291	3262	1.701	-0.171	0.8644	1.000	--
5-3	4.183	3262	1.694	2.470	0.0136	0.124	--
5-2	19.126	3262	1.682	11.372	<<0.0001	<0.001	***
8-3	14.410	3262	1.714	8.410	<<0.0001	<0.001	***
8-5	12.294	3262	1.682	7.309	<<0.0001	<0.001	***

ANOVA results for differences in mean life span in Drosophila with differing *p53* mutation types, where the main effect is the mutation type, comprised of grouped genotypes, and replicate vials are treated as a random effect in males (a) and females (c). Similar tests were also performed where the main effect is genotype in males (b) and females (d). Significant differences in group means were identified using Tukey's Honestly Significant Difference (HSD) multiple comparison and adjusted p-values based on the single-step method are reported for the relevant comparisons of various mutation types to wild-type.

Table S6. Summary of the significance of *p53* deletion or mutation effects on life span in W cohort

W cohort [c] Male											
M-F	**Gr**	**N**	**± SD**	**Mean life span**		**Med life span**		**Max life span**		**P-val**	**Sig**
				Mean	**CI %Δ**	**Med**	**CI %Δ**	**Max**	**CI %Δ**		
6-7	+/+	123	10.48	53.64	NA	54	NA	69.2	NA	NA	NA
2-3	-/-	125	18.89	63.2	11.33 - 24.50	60	1.89 – 21.56	86	6.72 – 26.42	2.62×10^{-10}	***
2-6	-/+	122	11.7	66.18	18.72 - 28.60	66	12.94 – 30.20	80	1.64 -18.95	0	***
2-7	-/+	130	9.27	79.11	42.19 -52.75	80	41.55 – 54.53	88	9.94 -29.94	0	***
3-6	-/+	114	15.55	43.33	–24.71 - –14.15	46	–20.74 - –11.38	57.4	–27.18 - –12.22	1.30×10^{-8}	**
3-7	-/+	127	11.33	67.54	21.00 - 30.88	70	23.40 – 34.64	78.8	0.34 – 19.58	0	***
4-6	M/+	120	9.617	23.3	–59.34 - –53.76	20	–65.84 - –61.16	38	–53.86 - –35.26	0	***
4-7	M/+	119	15.74	43.14	–24.28 - –13.92	42	–29.24 - –14.46	66	–17.60 - –2.42	1.60×10^{-4}	**
5-6	M/+	124	9.25	32.02	–43.68 - –37.22	34	–39.34 - –31.90	40	–51.62 - –38.42	0	***
5-7	M/+	126	9.38	56.98	2.01 - 10.35	58	2.87 – 11.76	68	–14.53 - 1.27	0.038	*
2-4	-/M	120	9.66	39.97	–28.86 - –22.20	40	–30.94 - –22.77	52	–35.37 - –22.50	0	***
2-5	-/M	125	7.96	59.12	6.31 – 14.34	60	6.94 – 19.48	70	–12.64 - 2.11	7.69×10^{-4}	**
3-4	-/M	98	15.58	26.53	–55.51 - –45.30	27	–57.20 - –49.80	50	–37.31 - –22.61	0	***
3-5	-/M	120	10.56	50.28	–10.41 - –2.46	52	–7.44 - 3.31	62	–20.46 - –6.79	1.32×10^{-3}	*
4-5	M/M	72	10.77	19.89	–66.79 - –58.37	20	–64.24 - –58.24	35.4	–57.32 - –28.56	0	***

W cohort [c] Female											
M-F	**Gr**	**N**	**± SD**	**Mean life span**		**Med life span**		**Max life span**		**P-val**	**Sig**
				Mean	**CI %Δ**	**Med**	**CI %Δ**	**Max**	**CI %Δ**		
6-7	+/+	121	8.00	55.8	NA	56	NA	66	NA	NA	NA
2-3	-/-	125	6.83	63.86	11.65 - 17.66	66	11.08 – 24.48	70	–0.19 - 10.22	2.22×10^{-16}	***
2-6	-/+	125	7.76	55.7	–3.17 - 2.87	56	–8.38 - 3.75	62	–14.66 - –0.93	0.736	---
2-7	-/+	126	11.67	60.81	4.73 - 12.84	62	1.63 - 14.65	73	4.97 - 22.97	9.69×10^{-10}	***
3-6	-/+	121	10.29	50.38	–13.09 - –6.07	52	–15.61 - –3.58	60	–15.45 - –5.63	1.38×10^{-4}	**
3-7	-/+	126	10.35	67.44	17.10 - 24.67	68	11.41 – 25.88	79	13.61 - 28.76	0	***
4-6	M/+	121	10.58	25.19	–57.65 - –51.46	24	–63.50 - –51.89	40	–45.03 - –32.68	0	***
4-7	M/+	116	14.03	42.78	–27.51 - –19.19	42	–30.78 - –22.13	61	–12.87 - 5.36	1.39×10^{-10}	***
5-6	M/+	121	9.88	38	–34.90 - –28.56	36	–44.66 - –32.95	50	–29.34 - –18.38	0	***
5-7	M/+	122	11.15	65.11	12.61 - 20.35	67	6.01 – 21.98	76	9.90 – 21.58	0	***
2-4	-/M	121	13.23	43.09	–26.96 - –18.55	48	–21.58 - –10.11	56	–20.64 - –11.77	0	***
2-5	-/M	125	7.80	56.77	–1.19 - 4.95	58	–3.89 - 7.78	66	–8.45 – 7.60	0.282	
3-4	-/M	117	7.14	23.5	–60.12 - –55.36	24	–58.54 - –51.52	32.8	–52.38 – –39.97	0	***
3-5	-/M	120	8.53	68.77	19.78 - 26.57	68	12.29 – 25.49	78	11.42 – 26.35	0	***
4-5	M/M	110	9.68	27.45	–53.79 - –47.70	28	–52.55 - –46.49	38	–48.59 – –39.77	0	***

To assess the effect of *p53* mutation on mean, median, and maximal lifespan, 95% double bootstrap t confidence intervals for the ratio of the means (or ratio of the percentiles) of the mutant and wild-type samples were computed as listed for the W-cohort. The log-rank test was employed to test the null hypothesis that there is no difference in the probability of death between wild-type and *p53* mutant flies. P-values indicating the significance of the tests are reported.

Table S7. Grouped life span data from W cohort experiments with log rank, average, standard deviations, medians and standard deviations of medians

Group	Genotype	Sex	N	Mean Life span phenotype[a]	Median Life span phenotype[b]	Log Rank (vs +/+)
W cohort						
	-/-	Male	127	63.2±20.25	60±20.66	2.62e-10
	M/-	Male	492	44.68±18.88	48±19.23	5.65e-05
	+/-	Male	504	64.65±19.73	68±19.91	0.00
	M/M	Male	72	19.89±10.84	20±10.82	0.00
	+/M	Male	492	39.02±17.21	36±17.78	8e-09
	+/+	Male	123	53.64±10.58	54±10.52	
	-/-	Female	125	63.9±6.49	66±6.18	2.22e-16
	M/-	Female	490	48.27±19.90	54±20.34	0.947
	+/-	Female	498	58.67±12.00	58±12.13	8.27e-07
	M/M	Female	111	27.45±10.38	28±9.96	0.00
	+/M	Female	480	42.82±18.56	42±18.67	0.000628
	+/+	Female	121	55.80±8.15	56±8.10	

[a] Mean life span, days +/- SD.

[b] Median life span, days +/- SD Life Span, days.

Table S8. Summary of the effect of *p53* deletion or mutation on life span for the reverse-cross data

Reverse cross Male										
M-F	**Gr**	**N**	**± SD**	**Mean**	**Med**	**Max**	**P-val[a]**	**Sig[a]**	**P-val[b]**	**Sig[b]**
6-7	+/+	124	17.89	75.19	78	92	NA	NA	1.96×10^{-3}	*
7-6	+/+	126	21.08	66.4	72	88	1.96×10^{-3}	*	NA	NA
2-3	-/-	120	16.81	72.08	74	88	2.74×10^{-2}	*	2.64×10^{-1}	--
3-2	-/-	⊗71	26.35	78.65	86	102	6.43×10^{-5}	**	1.58×10^{-8}	***
3-7	-/+	131	16.95	82.15	86	98	7.14×10^{-6}	*	2.90×10^{-12}	***
7-3	-/+	120	13.94	85.85	90	100	1.11×10^{-9}	***	2.22×10^{-16}	***
6-8	+/M	115	18.34	59.04	60	83.2	5.35×10^{-11}	***	4.15×10^{-4}	**
8-6	+/M	129	13.99	67.64	66	84	2.89×10^{-6}	**	2.06×10^{-1}	--
7-8	+/M	122	17.02	81.25	84	100	9.69×10^{-6}	**	7.28×10^{-11}	***
8-7	+/M	117	22.92	74.97	76	102	3.77×10^{-3}	*	3.33×10^{-6}	***
3-8	-/M	125	21.50	75.98	78	102	2.80×10^{-2}	*	5.31×10^{-6}	***
8-3	-/M	125	17.39	65.10	66	80	1.92×10^{-7}	**	5.74×10^{-2}	--
5-8	M/M	119	22.11	61.28	62	88	1.85×10^{-6}	**	1.07×10^{-1}	--
8-5	M/M	122	16.77	58.21	59	79.6	1.70×10^{-13}	***	3.31×10^{-5}	**

Reverse cross Female										
M-F	**Gr**	**N**	**± SD**	**Mean**	**Med**	**Max**	**P-val[a]**	**Sig[a]**	**P-val[b]**	**Sig[b]**
6-7	+/+	123	21.24	72.44	74	92	NA	NA	4.09×10^{-4}	**
7-6	+/+	125	11.62	82.54	86	94	4.09×10^{-4}	**	NA	NA
2-3	-/-	122	21.9	88.23	94	103.8	0	***	1.35×10^{-14}	***
3-2	-/-	121	15.84	95.77	98	110	0	***	0	***
3-7	-/+	123	27.64	84.59	92	101.6	0	***	1.58×10^{-14}	***
7-3	-/+	126	5.985	90.94	92	100	0	***	2.96×10^{-10}	***
6-8	+/M	124	31.88	87.37	100	108	0	***	0	***
8-6	+/M	116	15.76	97.45	100	108	0	***	0	***
7-8	+/M	125	15.99	93.94	98	106	0	***	0	***
8-7	+/M	122	14.68	94.84	96	107.8	0	***	0	***
3-8	-/M	123	25.27	96.6	104	114	0	***	0	***
8-3	-/M	121	22.74	101.3	108	112	0	***	0	***
5-8	M/M	122	19.76	96.49	100	111.8	0	***	0	***
8-5	M/M	118	24.12	88.34	94	106.6	0	***	2.32×10^{-13}	***

The mean, median, and maximal lifespan values are reported for each genotype as well as P-values for the log-rank test of the null hypothesis of identical survival functions between wild-type (+/+; 6-7) or the reverse cross wild-type (+/+; 7-6) and *p53* mutant flies are denoted by superscript *a* and *b*, respectively.

⊗ Indicates exclusion of an outlier vial.

Table S9. Summary of the effect of *p53* deletion on life span when flies were subject to ionizing radiation or a 100% oxygen environment

Stress experiments Male											
M-F	**Gr**	**N**	**± SD**	**Mean life span**		**Med life span**		**Max life span**		**P-val**	**Sig**
				Mean	**CI %Δ**	**Med**	**CI %Δ**	**Max**	**CI %Δ**		
Standard conditions											
6-7	+/+	129	17.12	79.81	NA	82	NA	98	NA	NA	NA
2-3	-/-	117	13.14	75.56	–9.12 - –1.15	78	–7.64 - –1.03	88	–14.36 – 7.09	7.84×10^{-6}	**
3-7	-/+	124	15.96	79.81	–4.18 - 4.43	82	–5.30 - 4.00	98	–5.52 – 3.24	0.73	---
Ionizing radiation											
6-7	+/+	274	5.78	40.82	NA	42	NA	46	NA	NA	NA
2-3	-/-	273	5.43	33.12	–20.68 - –17.06	34	–25.54 - –19.05	38	–22.65 - – 12.41	0	***
3-7	-/+	273	6.15	42.39	1.80 - 6.00	42	–7.48 - 0.00	47.6	–1.24 – 11.02	2.02×10^{-7}	**
100% O2											
6-7	+/+	238	0.56	17.83	NA	18	NA	18	NA	NA	NA
2-3	-/-	232	1.56	15.16	–16.13 - –14.10	16	–11.11 - –11.11	16	–11.11 - –11.11	0	***
3-7	-/+	244	1.05	17.16	–4.38 - –3.05	18	NaN - NaN	18	NaN-NaN	4.44×10^{-16}	***

Stress experiments Female											
M-F	**Gr**	**N**	**± SD**	**Mean life span**		**Med life span**		**Max life span**		**P-val**	**Sig**
				Mean	**CI %Δ**	**Med**	**CI %Δ**	**Max**	**CI %Δ**		
Standard conditions											
6-7	+/+	126	19.49	82.78	NA	88	NA	96	NA	NA	NA
2-3	-/-	123	13.13	89.17	3.77 – 12.09	90	–2.90 -4.99	100	1.29 - 6.42	9.02×10^{-5}	**
3-7	-/+	123	19.56	88.34	1.60 -11.64	92	–0.21 - 6.87	100	1.21 - 7.20	2.10×10^{-7}	**
Ionizing radiation											
6-7	+/+	280	13.79	48.27	NA	50	NA	60	NA	NA	NA
2-3	-/-	270	9.22	54.38	9.09 – 16.71	56	7.67 – 16.15	62	–3.92 - 4.63	2.98×10^{-4}	**
3-7	-/+	271	17.12	51.17	13.13 – 23.36	62	18.57 – 28.81	72	12.21 - 21.04	0	***
100% O2											
6-7	+/+	238	0.367	17.97	NA	18	NA	18	NA	NA	NA
2-3	-/-	242	1.49	17.22	–5.06 - –3.34	18	NaN - NaN	18	NaN - NaN	1.28×10^{-13}	***
3-7	-/+	233	0.95	17.85	–1.56 - –0.19	18	NaN - NaN	18	NaN - NaN	0.09	---

95% double bootstrap-t confidence intervals for the ratio of the means (or ratio of the percentiles) of the mutant and wild-type samples in each condition were computed as listed. The mean, median, and maximal lifespan values are reported for each genotype as well as the P-values representing the significance of the log-rank test of the null hypothesis that there is no difference in the probability of death between wild-type and *p53* mutant flies.

Table S10. Summary of food (fly culture media) recipes

For One Liter	Old Food	New Food
Water (L)	1	1
Sucrose (g)	0	0
Dextrose (g)	0	105
Molasses (ml)	100	0
Agar (g)	9	8
Yeast (g)	41	26
Cornmeal (g)	100	50
Tegosept (g)	2.5	1.7
95% Ethanol (ml)	22.5	8.6
Propionic Acid (ml)	8	1.9
phosphoric acid	0	0

The W cohort was cultured on "Old food" recipe, as were all flies in experiments in Tower laboratory prior to September 2005. The L cohort and all other experiments presented here were conducted using "New food" recipe.

Research paper

The relative contributions of the p53 and pRb pathways in oncogene-induced melanocyte senescence

Sebastian Haferkamp, Sieu L Tran, Therese M Becker, Lyndee L Scurr, Richard F Kefford and Helen Rizos

Westmead Institute for Cancer Research and Melanoma Institute of Australia, University of Sydney at Westmead Millennium Institute, Westmead Hospital, Westmead NSW 2145, Australia

Running title: *p53 and pRb pathways in melanocyte senescence*
Key words: *Oncogene-induced senescence, melanocytes, p53, pRb, p16^{INK4a}, p21^{Waf1}*
Correspondence: *Helen Rizos, PhD, Westmead Institute for Cancer Research, University of Sydney at Westmead Millennium Institute, Westmead Hospital, Westmead NSW 2145, Australia*
Received: *03/09/09; accepted: 05/15/09; published on line: 05/16/09*
E-mail: *helen_rizos@wmi.usyd.edu.au*
Copyright: *© 2009 Haferkamp et al. This is an open-access article distributed under the terms of the Creative Commons Attribution License, which permits unrestricted use, distribution, and reproduction in any medium, provided the original author and source are credited*

Abstract: Oncogene-induced senescence acts as a barrier against tumour formation and has been implicated as the mechanism preventing the transformation of benign melanocytic lesions that frequently harbour oncogenic B-RAF or N-RAS mutations. In the present study we systematically assessed the relative importance of the tumour suppressor proteins p53, p21^{Waf1}, pRb and p16^{INK4a} in mediating oncogene-induced senescence in human melanocytes. We now show that oncogenic N-RAS induced senescence in melanocytes is associated with DNA damage, a potent DNA damage response and the activation of both the p16^{INK4a}/pRb and p53/p21^{Waf1} tumour suppressor pathways. Surprisingly neither the pharmacological inhibition of the DNA damage response pathway nor silencing of p53 expression had any detectable impact on oncogene-induced senescence in human melanocytes. Our data indicate that the pRb pathway is the dominant effector of senescence in these cells, as its specific inactivation delays the onset of senescence and weakens oncogene-induced proliferative arrest. Furthermore, we show that although both p16^{INK4a} and p21^{Waf1} are upregulated in response to N-RAS^{Q61K}, the activities of these CDK inhibitors are clearly distinct and only the loss of p16^{INK4a} weakens senescence. We propose that the ability of p16^{INK4a} to inhibit the cyclin D-dependent kinases and DNA replication, functions not shared by p21^{Waf1}, contribute to its role in senescence. Thus, in melanocytes with oncogenic signalling only p16^{INK4a} can fully engage the pRb pathway to alter chromatin structure and silence the genes that are required for proliferation.

INTRODUCTION

Fewer than 5% of patients with distant visceral metastases from cutaneous melanoma survive 12 months and there are no effective drug treatments [1]. The early molecular steps in formation of melanoma are therefore the subjects of intense scrutiny. Cutaneous melanoma arises from benign melanocytic lesions (benign naevi) or de novo from melanocytes of the skin [2]. Mutations activating the N-RAS or B-RAF kinase components of the mitogen-activated protein kinase (MAPK) pathway are found in approximately 15% and 60% of human melanomas, respectively [3-5]. Greater than 89% of B-RAF mutations in melanoma alter a single amino acid (V600E and V600K), whereas highly recurrent mutations affecting Gly-12, Ala-18 and Gln-61 account for approximately 12%, 5% and 70% of melanoma-associated N-RAS mutations, respectively [6]. The B-RAF^{V600E} and N-RAS^{Q61K} mutations are also found in up to 80% and 55% of benign naevi, respectively [7, 8] and benign naevi display several markers of senescence, including positive senescence-associated ß-galactosidase (SA-ß-Gal) activity and p16^{INK4a} expression [9, 10]. Although the presence of senescent cells in human benign naevi remains controversial [11], accumulating evidence suggests that

senescence occurs *in vivo* and acts as an effective barrier to tumour formation (Reviewed in [12]). Defining the relationship between oncogene activation, melanocyte senescence and escape from senescence remains an essential step in understanding melanomagenesis. For this reason we have sought to dissect the regulation of senescence in melanocytes.

The senescence program is established and maintained by the p53 and $p16^{INK4a}$/retinoblastoma (pRb) tumour suppressor pathways. p53 engages a formidable proliferative arrest primarily in response to DNA-damage checkpoint signals triggered by telomere dysfunction and activated oncogenes [13-16]. For instance, the stable knockdown of p53-regulators (including ataxia telangiectasia mutated (ATM) and checkpoint-2 (CHK2) kinases) or p53 itself overcame RAS-induced sensecence in BJ human foreskin fibroblasts [15] (Table 1). Similarly, inactivation of the upstream p53 activator, ARF (p19ARF in mouse and p14ARF in human), overcame oncogene-induced senescence in mouse embryo fibroblasts (MEFs) [17, 18], and loss of $p21^{Waf1}$, a CDK inhibitor, activator of pRb and critical downstream target of p53 transactivation, caused cells to bypass telomere-dependent replicative and oncogene-induced senescence in normal human fibroblasts and MEFs, respectively (Table 1) [19-21].

Although inactivation of the p53 pathway can reverse the senescence in some cells, there is an emerging consensus that it fails to do so in cells with an activated $p16^{INK4a}$/pRb pathway [14, 22, 23]. Active, hypophosphorylated pRb interacts with E2F transcription factors and facilitates chromosome condensation at E2F target promoters. The reorganization of chromatin leads to the formation of senescence associated heterochromatin foci (SAHF) and the stable repression of E2F target genes that are involved in the irreversible cell cycle arrest associated with senescence [24]. Each SAHF contains portions of a single condensed chromosome, which is enriched for common markers of heterochromatin, including HP1γ, histone H3 methylated at lysine 9 (H3K9Me) and the non-histone chromatin protein, HMGA2 (reviewed in [25])

$p16^{INK4a}$ is a positive regulator of pRb, via cyclin dependent kinase inhibition, and is crucial in generating SAHF [24]. Not surprisingly, $p16^{INK4a}$ also acts as a tumour suppressor and is frequently inactivated in established human tumours. Inherited inactivating mutations in $p16^{INK4a}$ are associated with melanoma susceptibility in melanoma-dense kindreds [26]. In fact, $p16^{INK4a}$-deficient human melanocytes, derived from melanoma affected individuals, show an extended lifespan and are immortalized by ectopic expression of telomerase reverse transcriptase, whereas normal melanocytes display neither of these features [27, 28]. Furthermore, replicative and oncogene-induced senescence are accompanied by accumulation of $p16^{INK4a}$ in primary human cells [29-31] and ectopically expressed $p16^{INK4a}$ initiates a senescence program characterized by cell cycle arrest, senescence-associated changes in cell morphology, increased SA-ß-Gal activity and the appearance of SAHF [32, 33].

The senescent states induced by the p53 and pRb pathways may be distinct and whether cells engage one or the other pathway appears to reflect the type of stress signal, the tissue and species of origin. The relative contribution of the p53 and $p16^{INK4a}$/pRb pathways in melanocyte senescence remains unclear, and recent data suggest the possibility of p53- and pRb-independent senescence pathways in these cells. For instance, N-RAS induced melanocyte senescence was associated with the activation of the $p16^{INK4a}$/pRb and p53 pathways, but did not require expression of $p16^{INK4a}$ or p14ARF [34]. Similarly, neither p53 nor $p16^{INK4a}$ were required for H-RAS induced senescence in human melanocytes. Instead, H-RAS-driven senescence was mediated by the endoplasmic reticulum-associated unfolded protein response [35]. In another report, senescence induced by $B\text{-}RAF^{V600E}$ or $N\text{-}RAS^{Q61R}$ did not depend on $p16^{INK4a}$ or p53 but could be partially overcome by expression of the oncogenic transcription factor c-MYC [36]. In contrast, p53 was found to be one of 17 genes (also included IGFBP7) required for $BRAF^{V600E}$-mediated senescence of human melanocytes and p53 was also required for the induction of $p16^{INK4a}$ following $B\text{-}RAF^{V600E}$ expression [37] (Table 1).

In this study we systematically assessed the relative importance of the tumour suppressor proteins p53, $p21^{Waf1}$, pRb and $p16^{INK4a}$ in mediating oncogene-induced senescence in human melanocytes. We confirm that $N\text{-}RAS^{Q61K}$ induced senescence in melanocytes is associated with DNA damage, a potent DNA damage response and the activation of both the $p16^{INK4a}$/Rb and p53/$p21^{Waf1}$ tumour suppressor pathways. In melanocytes, the pRb pathway was the dominant effector of senescence, as its specific inactivation delayed the onset of senescence and weakened oncogene-induced proliferative arrest, as shown by the reduced formation of SAHF. Although p53-deficient melanocytes underwent a senescence response that was indistinguishable from that seen in wild-type melanocytes, the p53 pathway did contribute to the senescence program. In particular, the p53 pathway initiated a delayed arrest in pRb-deficient melanocytes, whereas melanocytes lacking both p53 and pRb continued to proliferate in response to oncogenic N-RAS. We also show that, although $p21^{Waf1}$

and $p16^{INK4a}$ [34] are not required for N-RAS induced senescence, both can activate pRb and promote senescence but only $p16^{INK4a}$ triggers chromatin reorganization and the formation of SAHF. These data help to explain the observation that whereas $p16^{INK4a}$ mutations are common in human cancer, $p21^{Waf1}$ mutations occur rarely [38].

Table 1. Requirements of oncogene-induced senescence in human and mouse cells

	Human Cells				**Mouse Cells**
	IMR90 Lung Fibroblasts[1]	*BJ Foreskin Fibroblasts*[1]	*Fibroblasts from melanoma-prone individuals*[2]	*Melanocytes*	*MEFs*
p53-DNA damage response					
1. ATM	Required[16]/Not required[61]	Required [15, 16]	Not studied	Not studied	Not studied
2. Chk2	Not studied	Required [15]	Not studied	Not studied	Not studied
3. p53	Partial[3][62]/ Not required [24, 29, 61, 63]	Required [15, 64]/ Partial[3] [62]	Not studied	Required [37]/ Not required [35, 36]	Required [29]
4. ARF	Not required [65]	Not required [64]	Not required [66]	Not required [34]	Required [18, 67]
5. $p21^{Waf1}$	Not required [63]	Not studied	Not studied	Not required (this work)	Not required [21]
pRb pathway					
1. pRb	Partial[3,4] [24, 62]/ Not Required [61]	Partial[4][62]/ Not required[64]	Not studied	Partial[3,4] (this work)	Not required [45, 68]
2. p107	Not studied	Not studied	Not studied	Not studied	Not required [68]
3. pRb and p107	Not studied	Not studied	Not studied	Not studied	Required [68]
4. p107 and p130	Not studied	Not studied	Not studied	Not studied	Not required [45]
5. pRb, p107 and p130	Not studied	Not studied	Not studied	Not studied	Required [45, 68]
6. $p16^{INK4a}$	Partial[4][24]/ Not required [16]	Partial[3] [15] / Not required [64]	Required[39, 66, 69, 70]/ Not required [71]	Partial[4][34]/ Not required [35, 36]	Required [29]/ Not required [18]
p53 and pRb	Required [61, 62]	Required [62]	Not studied	Required (this work)	Required [29]
p53- and pRb-independent					
1. ER-stress response	Not studied	Not studied	Not studied	Required [35]	Not studied
2. IL-6	Required [72]	Not studied	Not studied	Not studied[6] [72]	Not studied
3. IGFBP7	Not studied	Not studied	Not studied	Required [37]	Not studied
4. C-MYC	Not studied	Not studied	Not studied	Partial[5] [36]	Not studied

Not required, gene expression is dispensable for oncogene-induced cell cycle arrest and senescence

Required, loss of gene expression overcame oncogene-induced cell cycle arrest

[1]IMR90 cells senesce with longer telomeres and have higher basal levels of $p16^{INK4a}$ than BJ cells [64, 73]

[2]Fibroblasts from melanoma prone individuals with germline mutations inactivating $p16^{INK4a}$

[3]Loss of gene expression delayed or reduced oncogene-induced cell cycle arrest or SA-ß-Gal activity

[4]Loss of gene expression reduced oncogene-induced formation of SAHF

[5]Overexpression of gene partially suppresses oncogene-induced SA-ß-Gal activity

[5]IL-6 expression is induced by oncogenic B-RAF in human melanocytes

RESULTS

The response of primary human melanocytes to the oncogenic, melanoma-associated N-RAS^{Q61K} mutant was evaluated by stably transducing N-RAS^{Q61K} into human epidermal melanocytes. Accumulation of N-RAS^{Q61K} was detected three days post-transduction and the impact of N-RAS on melanocyte proliferation was monitored over 15 days. As expected, 15 days post-transduction the majority of N-RAS^{Q61K} transduced melanocytes displayed several markers of oncogene-driven senescence, namely cell flattening, increase in cellular size, significantly reduced Ki67 expression, increased SA-ß-Gal activity and the formation of SAHF (Figure 1A). As expected these foci were enriched for histone H3 methylated at lysine 9 (H3K9Me), a common marker of hetero-chromatin [24] (Figure 1B). In contrast, melanocytes accumulating the co-expressed Copepod GFP (copGFP) did not arrest, showed no evidence of chromatin condensation nor increased SA-ß-Gal activity (Figure 1A).

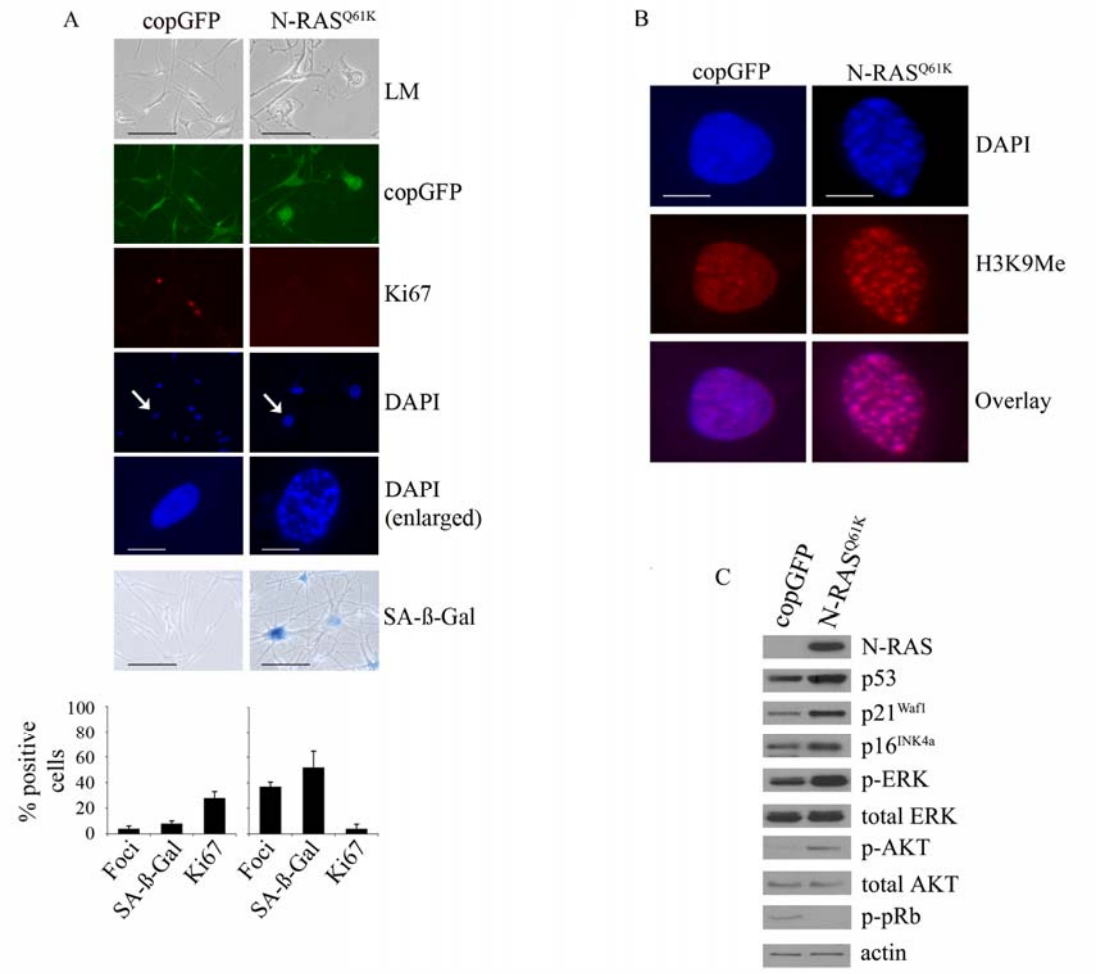

Figure 1. Oncogenic N-RAS^{Q61K} induces proliferative arrest and senescence of human melanocytes. (**A**) Human melanocytes were transduced with lentiviruses expressing N-RAS^{Q61K} or copGFP control. The efficiency of transduction was controlled with the co-expression of copGFP and was consistently above 90%. Cell proliferation (Ki67), chromatin condensation (DAPI), and the appearance of increased SA-ß-Gal activity were analyzed and quantitated 15 days after infection. Percentage of cells positive for the indicated marker is shown in histograms, which correspond to the mean ± s.d. of at least two independent transduction experiments from a total of at least 300 cells. Cells enlarged to show DAPI-stained chromatin foci are indicated with arrows (bar =10 μm). LM, light microscopy (bar=100μm). (**B**) Human epidermal melanocytes infected with lentiviruses expressing N-RAS^{Q61K} or copGFP were stained with DAPI and antibodies to H3K9Me, 15 days post transduction (bar =10 μm). (**C**) Expression of the indicated proteins was determined by western blot analysis 15 days after infection of human epidermal melanocytes with lentiviruses expressing N-RAS^{Q61K} or copGFP control.

N-RAS^{Q61K} induced melanocyte senescence was also associated with activation of the MAPK and AKT pathways, as shown by the increased phosphorylation of ERK (p-ERK), and AKT (p-AKT) at 5, 10 (data not shown) and 15 days post infection (Figure 1C). In addition, expression of oncogenic N-RAS led to p53 induction, increased expression of the p16^{INK4a} and p21^{Waf1} cyclin dependent kinase inhibitors and reduced accumulation of pRb phosphorylated at serine residues -807 and -811 (p-pRb) (Figure 1C). As previously reported, induced p14ARF was not detectable by Western blot analysis [34]. Oncogenic N-RAS also induced a robust DNA damage response in melanocytes that was associated with the accumulation of senescence-associated DNA damage foci, which contain phosphorylated histone H2AX (γ-H2AX) and are not equivalent to SAHF [15] (Figure 2A). Further, there was a marked increase in the phosphorylation of CHK2 on Thr-68 (p-CHK2) and increased p53 phosphorylation on Ser-15 (p-p53), two events associated with DNA damage (Figure 2B).

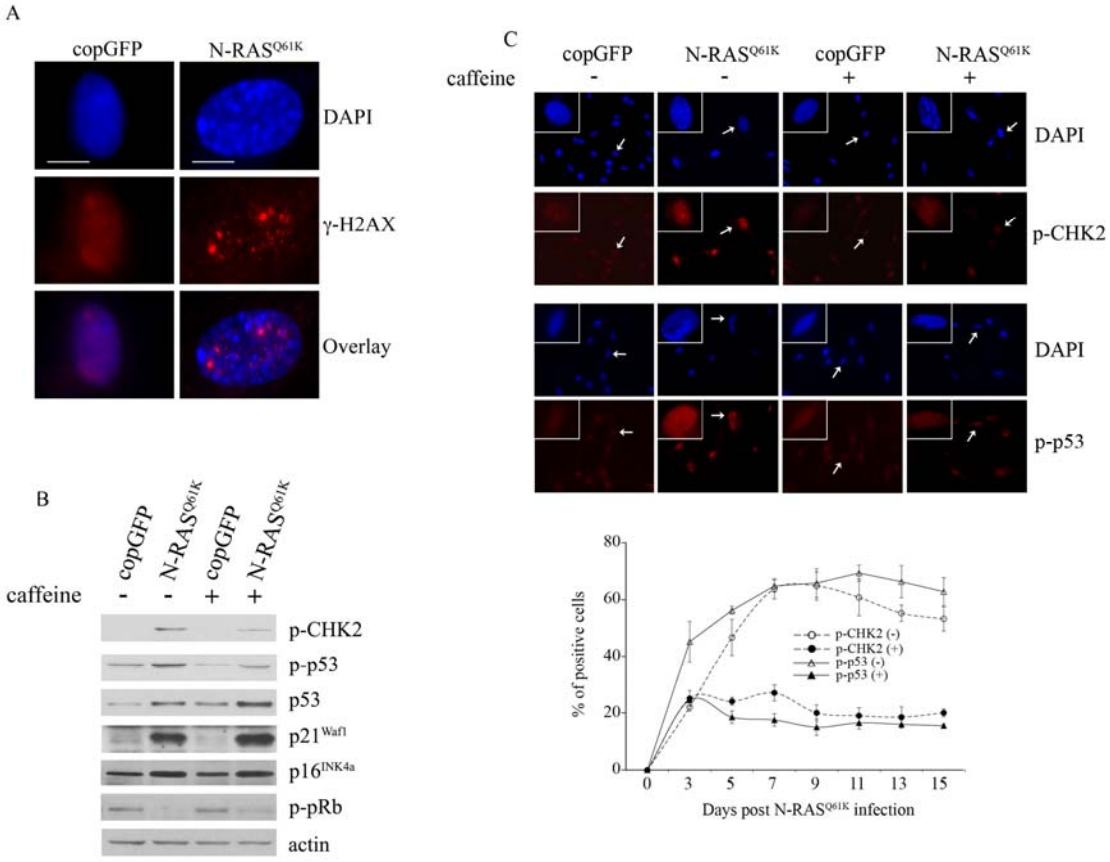

Figure 2. Oncogenic N-RAS^{Q61K} induces DNA damage response in human melanocytes. (**A**) Human epidermal melanocytes infected with lentiviruses expressing N-RAS^{Q61K} or copGFP were stained with DAPI and antibodies to the DNA damage marker γ-H2AX, 15 days post transduction (bar =10 μm). (**B**) Human melanocytes were transduced with lentiviruses expressing N-RAS^{Q61K} or copGFP and cultured for 15 days in the presence (+) or absence (-) of 4mM caffeine. Expression of the indicated proteins was determined by western blot analysis 15 days after infection. (**C**) Melanocytes transduced with lentivirus expressing N-RAS^{Q61K} or copGFP and cultured for 15 days in the presence (+) or absence (-) of 4mM caffeine were stained with DAPI and antibodies against the phosphorylated forms of p53 (p-p53) or CHK2 (p-CHK2) (bar=100μm). Enlarged images of representative cells (marked with arrow) are also shown. The percentage of transduced melanocytes positive for p-p53 and p-CHK2 expression was quantitated from at least two independent transduction experiments from a total of at least 300 cells. The graph corresponds to the mean percentage of transduced cells treated with caffeine (+) or left untreated (-) ± s.d.

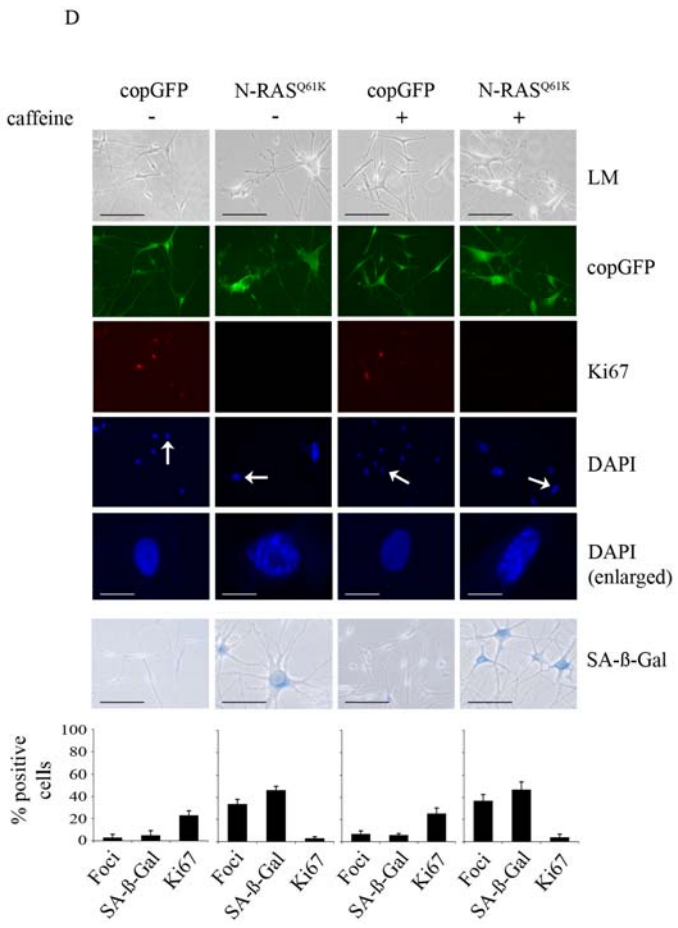

Figure 2. Oncogenic N-RAS^{Q61K} induces DNA damage response in human melanocytes. (D) Human melanocytes were transduced with lentiviruses expressing N-RAS^{Q61K} or copGFP and cultured for 15 days in presence (+) or absence (-) of 4mM caffeine. The efficiency of transduction was controlled with the co-expression of copGFP and was consistently above 90%. Cell proliferation (Ki67), chromatin condensation (DAPI), and the appearance of increased SA-ß-Gal activity were analyzed and quantitated 15 days after infection. Percentage of cells positive for the indicated marker is shown in histograms, which correspond to the mean ± s.d. of at least two independent transduction experiments from a total of at least 300 cells. Cells enlarged to show DAPI-stained chromatin foci are indicated with arrows (bar =10 μm). LM, light microscopy (bar=100μm).

To examine the contribution of the DNA damage response to RAS-induced melanocyte senescence we suppressed ATM and ATR kinase activity with the addition of 4mM caffeine for 15 days. As expected, in the presence of N-RAS^{Q61K}, the addition of caffeine markedly inhibited phosphorylation of the ATM targets CHK2 and p53 (Figures 2B, 2C). Nevertheless, suppression of the DNA damage response had no detectable impact on the N-RAS induced melanocyte senescence program. In particular, melanocytes accumulating N-RAS^{Q61K}, regardless of exposure to caffeine, underwent potent cell cycle arrest (reduced Ki67 staining) that was associated with increased SA-ß-Gal activity an the appearance of SAHF (Figure 2D). In addition, inhibition of the DNA damage checkpoint response did not impact on the N-RAS^{Q61K}-mediated induction of total p53, p21^{Waf1}, p16^{INK4a} and hypophosphorylated pRb (Figure 2B).

Considering that the p53 pathway remained active (increased p53 and p21^{Waf1} expression; see Figure 2B) in N-RAS^{Q61K}-expressing melanocytes with a diminished DNA damage response, we examined whether oncogene-induced senescence of human melanocytes required the p53 protein. To silence p53 expression we utilised lentiviral shRNA vectors that specifically target p53 and to minimise confounding effects of shRNA off-target silencing two independent p53 silencing molecules were generated (Supplementary Figure 1). HEM1455 melanocytes were transduced with these shRNA molecules and three days post-infection the cells were re-transduced with lentiviral vectors expressing N-RAS^{Q61K} or copGFP. In all experiments we also applied a negative control shRNA molecule without homology to any human gene.

The inhibition of p53 expression did not alter the cell cycle arrest induced by oncogenic N-RAS^{Q61K} (15 days after infection only 5% of N-RAS^{Q61K} melanocytes showed positive Ki67 staining regardless of p53 expression and this can be compared to 23% Ki67 positive p53-null melanocytes infected with the copGFP control; Figure 3A). Similarly, cellular senescence was initiated and maintained in the presence or absence of p53 expression; increased SA-ß-Gal activity appeared in 48% of p53-null cells compared to 38% in the p53-positive control cells, 15 days post transduction (Figure 3A) and the two different p53-specific shRNAs exerted similar effects (data not shown). In fact no markers of senescence, including cell morphology, SA-ß-Gal activity, appearance of SAHF or Ki67 incorporation discriminated between p53-intact and p53-null senescent melanocytes. It is important to note, however, that p21^{Waf1} expression was not induced by oncogenic N-RAS in p53-deficient melanocytes (Figure 3B).

In p53-null N-RAS melanocytes the induction of p16^{INK4a} and hypophosphorylation of pRb was maintained (Figure 3B), and it seemed likely that the activation of pRb was dominant and sufficient to establish melanocyte senescence. Certainly silencing expression of both p53 and pRb bypassed N-RAS induced cell cycle arrest and senescence in this cell type

(15 days after infection only 5% of N-RAS^{Q61K} melanocytes showed positive Ki67 staining, compared to 24% of N-RAS^{Q61K} melanocytes lacking both p53 and pRb and 23% of melanocytes expressing only control shRNA/copGFP; Figure 3A). To examine the individual role of pRb, HEM1455 melanocytes were transduced with a pRb-specific shRNA molecule and three days post-infection the cells were re-transduced with lentiviral vectors expressing N-RAS^{Q61K} or copGFP. pRb-null melanocytes responded to oncogenic N-RAS with delayed onset of cell cycle arrest and senescence. In particular, 10 days post infection with oncogenic N-RAS, 16% of pRb-null melanocytes remained positive for the proliferation marker Ki67 compared to only 5% of the pRb-positive melanocytes. Similarly, SA-ß-Gal activity was detected in only 19% of pRb-deficient N-RAS^{Q61K} melanocytes compared to 35% in the pRb-positive N-RAS^{Q61K} cells. Further, the percentage of N-RAS^{Q61K} expressing cells with SAHF was clearly reduced, and remained so in the absence of pRb (Figure 3C).

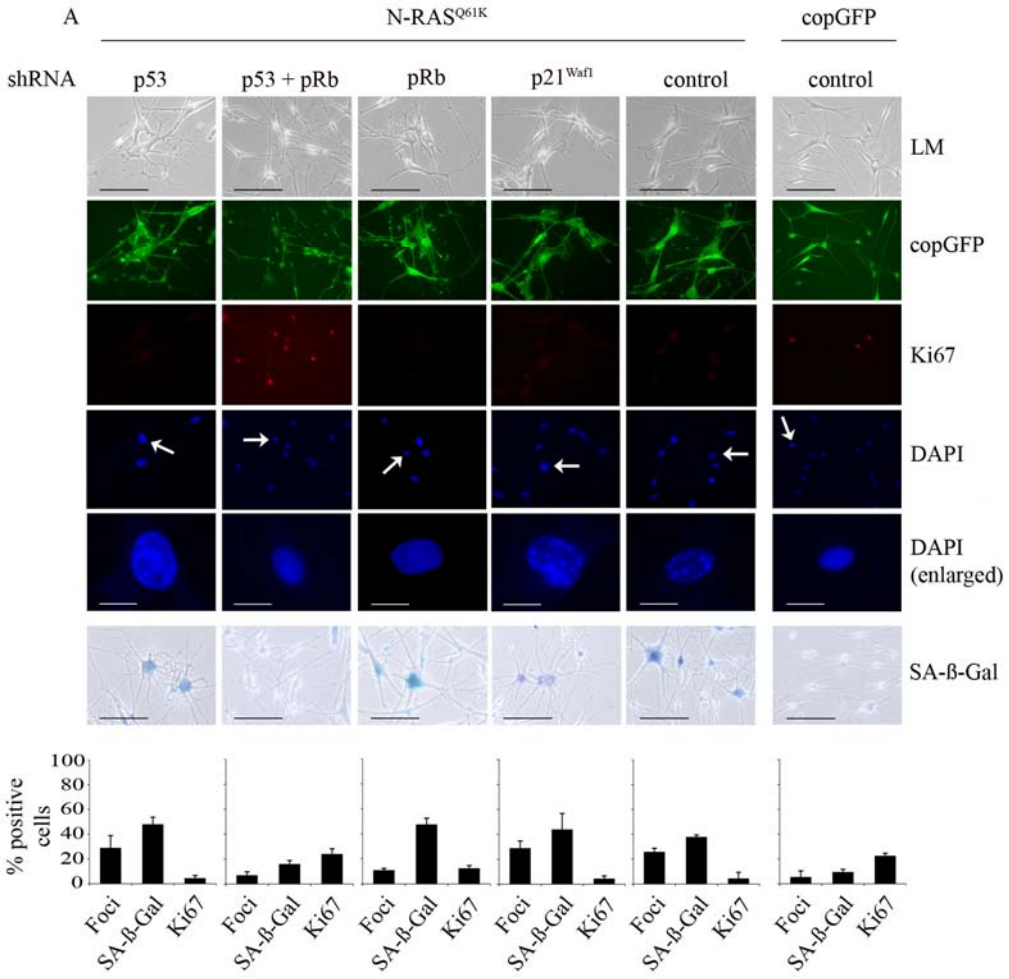

Figure 3. Relative contributions of the p53 and pRb tumour suppressor pathways in N-RAS^{Q61K}-induced melanocyte senescence. (**A**) Melanocytes were transduced with lentiviruses containing the indicated shRNA constructs. Three days post infection the cells were re-transduced with lentiviruses expressing N-RAS^{Q61K} or copGFP, as shown. Representative examples at 15days after infection are shown. Cell proliferation (Ki67), chromatin condensation (DAPI), and the appearance of increased SA-ß-Gal activity were analyzed and quantitated. Percentage of cells positive for each indicated marker are shown in histograms, which correspond to the mean ± s.d. of at least two independent transduction experiments from a total of at least 300 cells. Cells enlarged to show DAPI-stained chromatin foci are indicated with arrows (bar =10 μm). LM, light microscopy (bar=100μm).

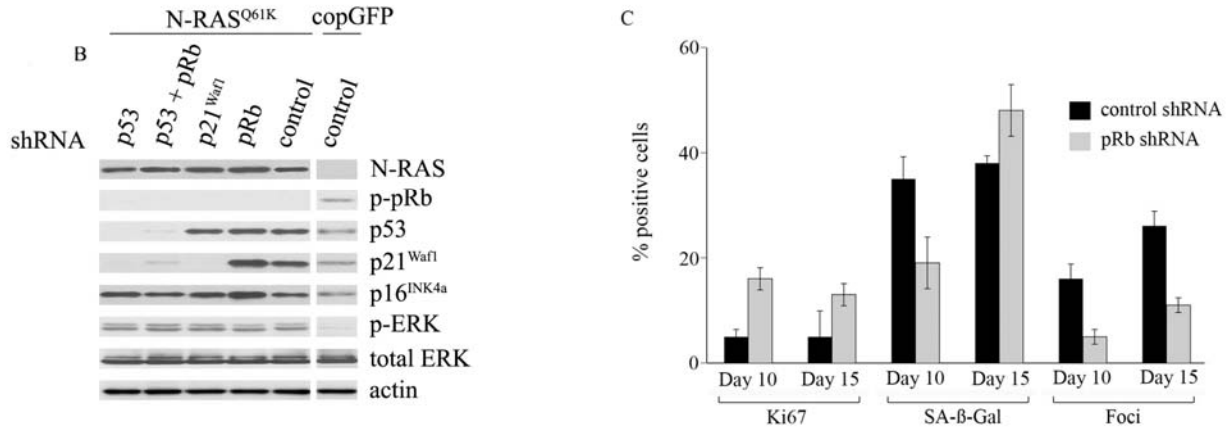

Figure 3. Relative contributions of the p53 and pRb tumour suppressor pathways in N-RAS^{Q61K}-induced melanocyte senescence. (**B**) Expression of the indicated proteins was determined by western blot analysis at 15 days after infection of human epidermal melanocytes with the indicated shRNA constructs and either lentivirus expressing N-RAS^{Q61K} or the copGFP control. (**C**) The impact of pRb-silencing on the N-RAS^{Q61K} induced senescence was determined by quantitating key senescence markers (Ki67 expression, SAHF formation, SA-ß-Gal activity) at 10 and 15 days post N-RAS transduction. Percentage of cells positive for each indicated marker is shown in histograms, which correspond to the mean ± s.d. of at least two independent transduction experiments from a total of at least 300 cells.

These data suggest that the activation of pRb is the dominant effector of oncogene-induced melanocyte senescence, and thus upstream regulators of pRb function may represent critical melanoma tumour suppressors. For instance, loss of the melanoma predisposition gene p16^{INK4a}, detectably weakened the pRb-pathway and the senescence program in melanocytes by inhibiting the pRb-dependent development of SAHF [34]. Considering that the CDK inhibitors p16^{INK4a} and p21^{Waf1} were both potently induced in melanocytes in response to N-RAS^{Q61K} expression (see Figure 1C), we wanted to establish whether the function of p16^{INK4a} in the formation of SAHF was specific to this CDK inhibitor or whether another senescence-associated CDK inhibitor p21^{Waf1} was equivalent in activity. The role of p21^{Waf1} was examined utilising two, highly effective p21^{Waf1}-specific lentiviral shRNA vectors (Supplementary Figure 1). HEM1455 melanocytes were transduced with these shRNA molecules and three days post-infection the cells were re-transduced with lentiviral vectors expressing N-RAS^{Q61K} or copGFP. In all experiments we also applied a negative control shRNA molecule without homology to any human gene.

Depletion of p21^{Waf1} did not detectably alter N-RAS induced cell cycle arrest or senescence in human melanocytes. The p21^{Waf1}-deficient melanocytes responded to oncogenic N-RAS by accumulating hypophosphorylated pRb, p16^{INK4a} and p53 (Figure 3B), they enlarged, acquired increased SA-ß-Gal activity and were negative for the proliferation marker Ki67 (Figure 3A). Unlike pRb-null melanocytes, there was no detectable delay in N-RAS induced arrest and senescence in p21^{Waf1}-deficient melanocytes. Importantly, in the absence of the p21^{Waf1} CDK inhibitor, the formation of SAHF was not altered 10 and 15-post transduction (29% foci in p21^{Waf1}-null, vs 11% foci in pRb-null vs 26% foci in shRNA control cells, 15 days post infection with N-RAS^{Q61K}; Figure 3A). The second p21^{Waf1}-specific shRNA exerted similar effects (data not shown).

To further investigate whether p16^{INK4a} was unique in promoting SAHF formation we developed a transient melanoma model to rapidly assess the functions of the p21^{Waf1} and p16^{INK4a}. The functionally impaired p16^{INK4a}_R24P mutant that is unable to bind and inhibit CDK4 but retains CDK6 inhibitory activity was used as a control [34, 39]. The WMM1175 melanoma cells were transiently transfected with plasmids encoding each of these CDK inhibitors along with a plasmid encoding the enhanced green fluorescent protein (EGFP), which was used as a marker of transfection. The cell cycle proliferation, SAHF formation and SA-ß-Gal activity of transfected WMM1175 cells was then assessed over 5-days. This was enough time to observe

the induction of senescence and protein expression from the transiently transfected plasmids was still detectable. As expected, ectopic expression of wild-type $p16^{INK4a}$ and $p21^{Waf1}$, but not $p16^{INK4a}$_R24P promoted rapid cell cycle arrest (Figure 4A). Similarly, $p16^{INK4a}$ and $p21^{Waf1}$ but not the R24P variant induced cell enlargement, and increased SA-ß-Gal activity by five days post transfection (Figure 4B). The only detectable difference between the two wild type CDK inhibitors was the induction of SAHF; only $p16^{INK4a}$ accumulation led to the appearance of these distinctive foci, which were enriched for H3K9Me (Figure 4C).

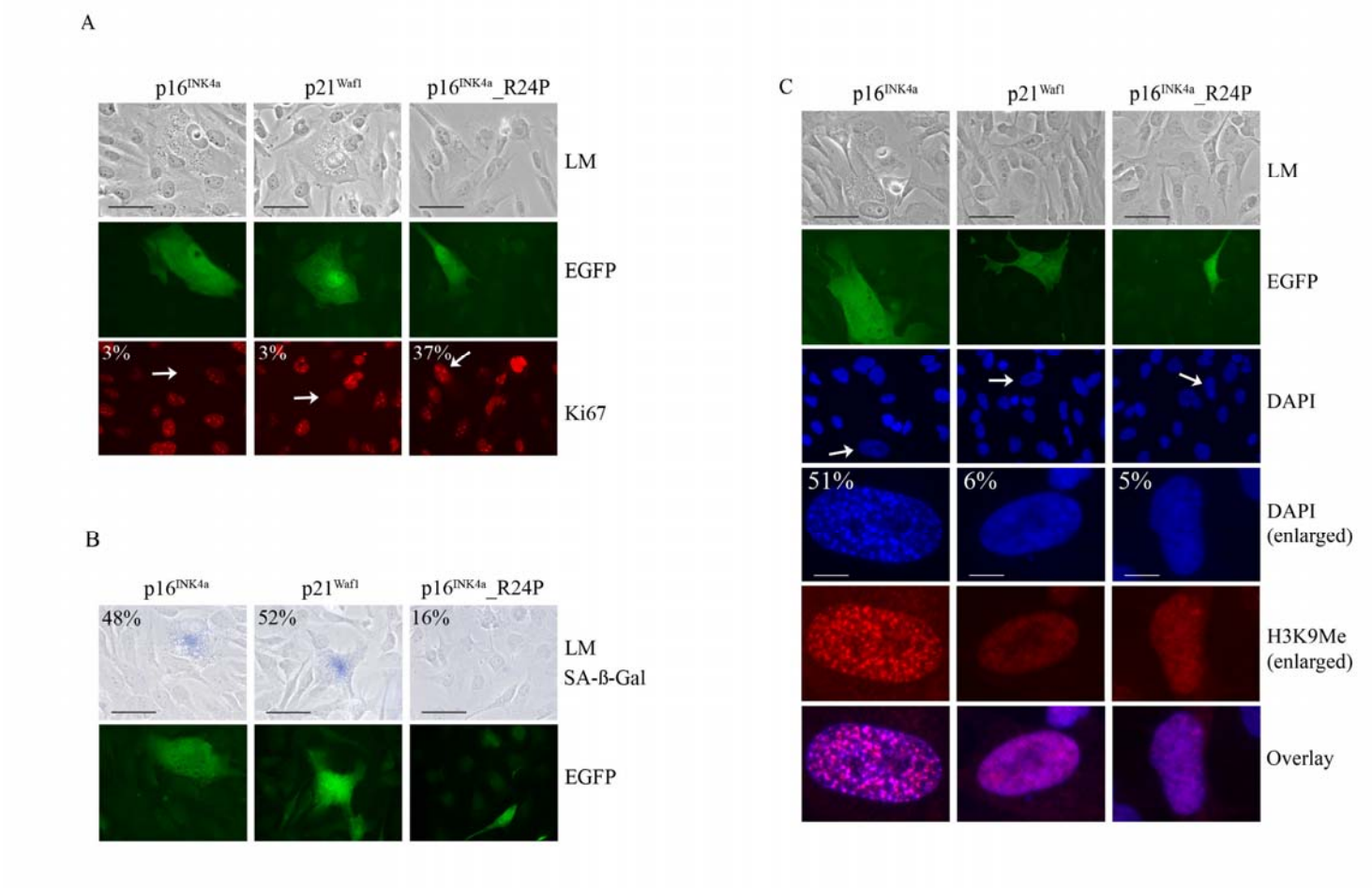

Figure 4. Impact of $p16^{INK4a}$ or $p21^{Waf1}$ expression on the cellular senescence program. WMM1175 melanoma cells were co-transfected with plasmids encoding $p16^{INK4a}$, $p21^{Waf1}$ or the melanoma-associated $p16^{INK4a}$_R24P along with *pCMV-EGFPN1*, which was used as a marker of transfection. Five days post transfection cells were fixed, permeabilized and analyzed. (**A**) Cell proliferation was monitored by Ki67 immunostaining and the percentage of transfected WMM1175 cells with positive Ki67 staining is indicated and was determined from at least two separate transfection experiments and from a total of at least 300 cells. All standard deviations were less than ±5% (bar=100μm). (**B**) Transfected WMM1175 cells were analyzed for SA-β-Gal activity, and the percentage of positive SA-ß-Gal transfected cells is indicated, and was determined as detailed above (bar=100μm). (**C**) The appearance of SAHF was analyzed by immunostaining with antibodies to H3K9Me and co-staining DNA with DAPI. The percentage of transfected cells with detectable foci is indicated, and was determined as detailed above (bar=100μm).

DISCUSSION

The molecular mechanisms that trigger oncogene-induced senescence have been studied extensively, and yet the relative contribution of the $p16^{INK4a}$/pRb and the p53/$p21^{Waf1}$ pathways in initiating and maintaining the senescence program remains poorly understood. In this study, we show that N-RAS^{Q61K} induces senescence in human melanocytes that was associated with markers of DNA damage response, and involved the activation of both the p53 and pRb pathways. Surprisingly neither the pharmacological inhibition of the DNA damage response pathway with caffeine nor silencing of p53 expression had a detectable impact on the N-RAS^{Q61K} induced senescence of human melanocytes. In fact, no markers of senescence, including cell morphology, SA-ß-Gal activity, appearance of SAHF or Ki67 incorporation discriminated between p53-intact and p53-null senescent melanocytes. Interestingly, caffeine diminished the phosphorylation of p53 on Ser-15, but did not reduce the overall levels of p53, or its activity (as measured by $p21^{Waf1}$ induction; Figure 2B) in melanocytes. Several other reports have also shown that inhibition of p53 phosphorylation at Ser-15 did not correlate with diminished p53 activity and this is indicative of p53 stabilization via multiple mechanisms [40, 41]. It is tempting to suggest that the melanoma tumour suppressor p14ARF is the critical activator of p53 in melanocytes. p14ARF stabilizes p53 by binding and inhibiting the p53 specific ubiquitin ligase, mdm2 [42], rather than inducing p53 phosphorylation. We have previously shown however that p14ARF is only weakly induced by oncogenic N-RAS in human melanocytes, and is not required for p53 activation in response to N-RAS [34]. In fact, the ARF tumour suppressor appears to contribute to oncogene-induced senescence only in mouse cells (Table 1).

It is reasonable to assume that in the absence of p53 the activated $p16^{INK4a}$/pRb pathway was sufficient to initiate and maintain senescence, and this appears to be the case in melanocytes. Not only did oncogenic N-RAS potently induce $p16^{INK4a}$ in melanocytes, pRb existed in its active hypophosphorylated form, and silencing of pRb significantly delayed the onset of senescence. Ultimately, the senescence program was activated in pRb-null melanocytes and this required the p53 pathway, as the simultaneous loss of p53 and pRb completely overcame N-RAS induce senescence in melanocytes. This is the first demonstration showing that melanocytes senesce in response to oncogenic signaling by engaging both the p53 and pRb pathways.

It has been suggested that p53, $p21^{Waf1}$ and pRb act in a linear pathway, with p53-induced $p21^{Waf1}$ activating pRb to regulate cell entry into replicative senescence [43]. This model does not adequately account for the fact that pRb-null melanocytes ultimately senescence in response to oncogenic N-RAS. It is possible that the pRb homologues, p107 and p130 participate in oncogene-induced senescence as they can functionally compensate for pRb loss and, like pRb, are activated by $p21^{Waf1}$ and $p16^{INK4a}$ [44]. Certainly, pRb-deficient MEFs senesce in culture, whereas MEFs with targeted deletion of all three pRb family members (pRb, p107 and p130) do not [45]. Furthermore, p53 was capable of inducing senescence in pRb-null prostate cancer cells, but not in p107 and pRb depleted cells [46]. Although such compensation clearly exists, the fact that pRb mutations are common in human cancer, whereas p107 and p130 mutations occur rarely [47], suggests that functional compensation for pRb loss must be context dependent. In the case of melanocytes, pRb (not p107 and p130) is required for normal mouse melanocyte proliferation although arrest in response to growth factor deprivation was associated with the formation of pRb- and p130-transcription repressor complexes in human melanocytes (reviewed in [48]). We are currently exploring whether the response of human melanocytes to oncogenic signalling involves the pRb homologues, p107 and p130 and whether the contribution of p53 to melanocyte senescence is strictly dependent on the pRb family of proteins.

Our data clearly demonstrate that oncogenic N-RAS acts primarily through the pRb pathway in melanocytes. Activation of this pathway involves both $p21^{Waf1}$ and $p16^{INK4a}$, and these were the only CDK inhibitors potently induced by oncogenic N-RAS in melanocytes (data not shown). We confirm that both $p16^{INK4a}$ and $p21^{Waf1}$ can induce senescence, but their activities are clearly distinct. $p16^{INK4a}$ expression promoted the formation of DAPI-stained heterochromatin foci that were enriched for the H3K9Me marker of SAHF. In contrast, ectopic $p21^{Waf1}$ expression had no detectable impact on chromatin structure even though cells were clearly arrested. Similarly, loss of $p16^{INK4a}$ reduced the formation of SAHF in melanocytes [34], whereas loss of $p21^{Waf1}$, either via direct silencing or by silencing p53, had no detectable effect on SAHF formation. Although both $p16^{INK4a}$ and $p21^{Waf1}$ can activate pRb their actions are not equivalent. $p16^{INK4a}$ is a potent inhibitor of the cyclin D-dependent kinases, CDK4 and CDK6, whereas $p21^{Waf1}$ is sequestered by and acts as a positive regulator of these kinases. This pool of tethered $p21^{Waf1}$ is released as $p16^{INK4a}$ accumulates and $p21^{Waf1}$ redistributes to bind and inhibit cyclin E-CDK2 complexes and induce G1 arrest [49]. The ability of $p16^{INK4a}$ to inhibit the cyclin D-dependent kinases also enables it to block the assembly of DNA replication

complexes onto chromatin and thus inhibit DNA replication, a function not shared by $p21^{Waf1}$ [50]. Thus, in melanocytes with oncogenic signalling only $p16^{INK4a}$ can fully engage the pRb pathway to alter chromatin structure and silence the genes that are required for proliferation. Melanocytes undergoing replicative senescence also rely on the $p16^{INK4a}$/pRb axis, as p53 and $p21^{Waf1}$ levels remain low in these arrested melanocytes [27]. We suggest that inhibition of cyclin D-dependent kinases and induction by senescence-causing stimuli necessitate $p16^{INK4a}$ inactivation in human cancers and distinguish this CDK inhibitor as a tumour suppressor.

MATERIALS AND METHODS

Cell culture and transfections. Human WMM1175 melanoma cells (ARF-null, p53-null, pRb+/+; [51]) and U20S osteosarcoma cells were grown in Dulbecco's modified Eagle's medium (DMEM, Gibco BRL, Carlsbad, CA, USA) supplemented with 10% foetal bovine serum and glutamine. Human epidermal melanocytes (HEMs) were obtained from Cell Applications (Cell Applications, San Diego, CA, USA) and grown in HAM's F10 media (Sigma, St. Louis. MO, USA), supplemented with ITS premix (Becton Dickinson, Franklin Lakes, NJ, USA), TPA, IBMX, cholera toxin, 20% fetal bovine serum and glutamine (modified from [52]). All cells were cultured in a 37°C incubator with 5% CO_2. Caffeine (Sigma) was used at 4mM for 15 days.

For *$p16^{INK4a}$*, *$p21^{Waf1}$*, *$p16^{INK4a}$_R24P* transfections, WMM1175 cells (1×10^5) were seeded on coverslips in six-well plates and transfected with 2µg plasmid encoding $p16^{INK4a}$, $p21^{Waf1}$, or $p16^{INK4a}$_R24P and 100ng *pEGFPN1* (Clontech, Mountain View, CA, USA), as a transfection marker, using Lipofectamine 2000 (Invitrogen, Carlsbad, CA, USA).

Lentivirus transductions. Lentiviruses were produced in HEK293T cells using the *pSIH1-H1-copGFP* (Copepod green fluorescent protein) shRNA expression vector or the *pCDH-CMV-MCS-EF1-copGFP* lentiviral vector (Systems Biosciences, Mountain View, CA, USA) encased in viral capsid encoded by three packaging plasmids as described previously [53]. Viruses were concentrated as described previously [54]. Viral titres were determined using 1×10^5 U2OS cells/well in six-well plates, transduced with serial dilutions of the concentrated viral stocks in the presence of Polybrene (8 µg/ml; Sigma). Cells were harvested 48 h post-transduction, analysed by flow cytometry for GFP expression and viral titre calculated. Cells were infecting using an MOI of 5-10 to provide infection efficiency above 90%.

Constructs. The *N-RAS* lentiviral construct and $p16^{INK4a}$ plasmids have been described elsewhere [33, 55]. The $p21^{Waf1}$ cDNA was kindly provided by Dr B. Vogelstein and subcloned into the *pFLAG-CMV5b* mammalian expression vector (Sigma). The p53-directed shRNA sequences correspond to nucleotides 956-974 and 1026-1044 [56, 57] (Genbank accession number NM_000546). The $p21^{Waf1}$-directed shRNA sequences correspond to nucleotides 560-578 and 569-587 (Genebank accession number NM_078467) [58]. The shRNA sequence targeting pRb corresponded to nucleotides 662-680 (Genebank accession number NM_000321.1) [59]. The non-silencing negative control shRNA did not show complete homology to any known human transcript and had the following sequence: 5'-TTAGAGGCGAGCAAGACTA-3'.

Western Blotting. Total cellular proteins were extracted at 4°C using RIPA lysis buffer containing protease inhibitors (Roche, Basel, Switzerland). Proteins (30-50µg) were resolved on 12% SDS-polyacrylamide gels and transferred to Immobilon-P membranes (Millipore, Bedford, MA, USA). Western blots were probed with antibodies against $p16^{INK4a}$ (N20, Santa Cruz, CA, USA), $p21^{Waf1}$ (C-19, Santa Cruz), ß-actin (AC-74, Sigma-Aldrich), p53 (DO-1, Santa Cruz), p-p53 (#9284, Cell Signalling, Danvers, MA, USA), p-ERK (E4, Santa Cruz), ERK (137F5, Cell Signalling), p-AKT (L32A4, Cell Signalling), AKT (11E7, Cell Signalling), c-MYC (A14, Santa Cruz), H3K9Me (Millipore) and phosphorylated p-pRb (#9308, Cell Signalling).

Indirect immunofluorescence. Cultured cells ($3\text{-}4 \times 10^4$) seeded on coverslips in 12-well plates were washed in PBS and fixed in 2% formaldehyde, 0.2% glutaraldehyde, 7.4 mM Na_2HPO_4, 1.47 mM KH_2PO_4, 137 mM NaCl, and 2.68 mM KCl. Cells were then rinsed three times with PBS and SA-ß-Gal activity was detected as previously described [60]. Cells fixed in 3.7% formaldehyde were immunostained for 50 min with primary antibody followed by a 50 min exposure to Alexa Fluor 594-conjugated secondary IgG (Molecular Probes, Carlsbad, CA, USA).

ACKNOWLEDGEMENTS

This work is supported by Program Grant 402761 of the National Health and Medical Research Council of Australia (NHMRC) and an infrastructure grant to Westmead Millennium Institute by the Health Department of NSW through Sydney West Area Health Service. Westmead Institute for Cancer Research is the

recipient of capital grant funding from the Australian Cancer Research Foundation. HR is a Cancer Institute of NSW Fellow and LS is Melanoma Foundation Cameron Melanoma Research Fellow, Melanoma Institute of Australia, University of Sydney. SH is a Cancer Institute of NSW Scholar and is supported by a PhD scholarship provided by the German Academic Exchange Service (DAAD).

CONFLICT OF INTEREST STATEMENT

The authors in this manuscript have no conflict of interest to declare.

REFERENCES

1. Thompson JF, Scolyer RA and Kefford RF. Cutaneous melanoma. Lancet. 2005; 365:687-701.

2. Chin L, Garraway LA, and Fisher DE. Malignant melanoma: genetics and therapeutics in the genomic era. Genes Dev. 2006; 20:2149-2182.

3. Davies H, Bignell GR, Cox C, Stephens P, Edkins S, Clegg S, Teague J, Woffendin H, Garnett MJ, Bottomley W, Davis N, Dicks E, Ewing R, et al. Mutations of the BRAF gene in human cancer. Nature. 2002; 417:949-954.

4. Houben R, Becker JC, Kappel A, Terheyden P, Brocker EB, Goetz R, Rapp UR. Constitutive activation of the Ras-Raf signaling pathway in metastatic melanoma is associated with poor prognosis. J Carcinog. 2004; 3:6.

5. Curtin JA, Fridlyand J, Kageshita T, Patel HN, Busam KJ, Kutzner H, Cho KH, Aiba S, Brocker EB, LeBoit PE, Pinkel D, and Bastian BC. Distinct sets of genetic alterations in melanoma. N Engl J Med. 2005; 353:2135-2147.

6. Hocker T and Tsao H. Ultraviolet radiation and melanoma: a systematic review and analysis of reported sequence variants. Hum Mutat. 2007; 28:578-588.

7. Pollock PM, Harper UL, Hansen KS, Yudt LM, Stark M, Robbins CM, Moses TY, Hostetter G, Wagner U, Kakareka J, Salem G, Pohida T, Heenan P, et al. High frequency of BRAF mutations in nevi. Nat Genet. 2003; 33:19-20.

8. Papp T, Pemsel H, Zimmermann R, Bastrop R, Weiss DG, and Schiffmann D. Mutational analysis of the N-ras, p53, p16INK4a, CDK4, and MC1R genes in human congenital melanocytic naevi. J Med Genet. 1999; 36:610-614.

9. Gray-Schopfer VC, Cheong SC, Chong H, Chow J, Moss T, Abdel-Malek ZA, Marais R, Wynford-Thomas D, and Bennett DC. Cellular senescence in naevi and immortalisation in melanoma: a role for p16? Br J Cancer. 2006; 95:496-505.

10. Michaloglou C, Vredeveld LC, Soengas MS, Denoyelle C, Kuilman T, van der Horst CM, Majoor DM, Shay JW, Mooi WJ, and Peeper DS. BRAFE600-associated senescence-like cell cycle arrest of human naevi. Nature. 2005; 436:720-724.

11. Cotter MA, Florell SR, Leachman SA, and Grossman D. Absence of senescence-associated beta-galactosidase activity in human melanocytic nevi in vivo. J Invest Dermatol. 2007; 127:2469-2471.

12. Prieur and .Peeper DS. Cellular senescence in vivo: a barrier to tumorigenesis. Curr Opin Cell Biol. 2008; 20:150-155.

13. Ramirez RD, Morales CP, Herbert BS, Rohde JM, Passons C, Shay JW, and Wright WE. Putative telomere-independent mechanisms of replicative aging reflect inadequate growth conditions. Genes Dev. 2001; 15:398-403.

14. Herbig U, Jobling WA, Chen BP, Chen DJ, and Sedivy JM. Telomere shortening triggers senescence of human cells through a pathway involving ATM, p53, and p21(CIP1), but not p16(INK4a). Mol Cell. 2004; 14:501-513.

15. Di Micco R, Fumagalli M, Cicalese A, Piccinin S, Gasparini P, Luise C, Schurra C, Garre M, Nuciforo PG, Bensimon A, Maestro R, Pelicci PG, and d'Adda di Fagagna F. Oncogene-induced senescence is a DNA damage response triggered by DNA hyper-replication. Nature. 2006; 444:638-642.

16. Bartkova J, Rezaei N, Liontos M, Karakaidos P, Kletsas D, Issaeva N, Vassiliou LV, Kolettas E, Niforou K, Zoumpourlis VC, Takaoka M, Nakagawa H, Tort F, et al. Oncogene-induced senescence is part of the tumorigenesis barrier imposed by DNA damage checkpoints. Nature. 2006; 444:633-637.

17. Serrano M, Lee H-W, Chin L, Cordon-Cardo C, Beach D, and DePinho RA. Role of the INK4a locus in tumor suppression and cell mortality. Cell. 1996; 85:27-37.

18. Kamijo T, Zindy F, Roussel MF, Quelle DE, Downing JR, Ashmun RA, Grosveld G, and Sherr CJ. Tumor suppression at the mouse INK4a locus mediated by the alternative reading frame product $p19^{ARF}$. Cell. 1997; 91:649-659.

19. Brown JP, Wei W, and Sedivy JM. Bypass of senescence after disruption of p21CIP1/WAF1 gene in normal diploid human fibroblasts. Science. 1997; 277:831-834.

20. Wei W and Sedivy JM. Differentiation between senescence (M1) and crisis (M2) in human fibroblast cultures. Exp Cell Res. 1999; 253:519-522.

21. Pantoja C and Serrano M. Murine fibroblasts lacking p21 undergo senescence and are resistant to transformation by oncogenic Ras. Oncogene. 1999; 18:4974-4982.

22. Sakamoto K et al. Relative mitogenic activities of wild-type and retinoblastoma binding deficient SV40 T antigens in serum-deprived human diploid fibroblasts. Oncogene. 1993; 8:1887-1893.

23. Beausejour CM, Krtolica A, Galimi F, Narita M, Lowe SW, Yaswen P, and Campisi J. Reversal of human cellular senescence: roles of the p53 and p16 pathways. EMBO J. 2003; 22:4212-4222.

24. Narita M, Nunez S, Heard E, Lin AW, Hearn SA, Spector DL, Hannon GJ, and Lowe SW. Rb-mediated heterochromatin formation and silencing of E2F target genes during cellular senescence. Cell. 2003; 113:703-716.

25. Adams PD. Remodeling of chromatin structure in senescent cells and its potential impact on tumor suppression and aging. Gene. 2007; 397:84-93.

26. Goldstein AM, Chan M, Harland M, Gillanders EM, Hayward NK, Avril MF, Azizi E, Bianchi-Scarra G, Bishop DT, Bressac-de Paillerets B, Bruno W, Calista D, Cannon Albright LA, et al. High-risk Melanoma Susceptibility Genes and Pancreatic Cancer,

Neural System Tumors, and Uveal Melanoma across GenoMEL. Cancer Res. 2006; 66:9818-9828.

27. Sviderskaya EV, Gray-Schopfer VC, Hill SP, Smit NP, Evans-Whipp TJ, Bond J, Hill L, Bataille V, Peters G, Kipling D, Wynford-Thomas D, and Bennett DC. p16/Cyclin-Dependent Kinase Inhibitor 2A Deficiency in Human Melanocyte Senescence, Apoptosis, and Immortalization: Possible Implications for Melanoma Progression. J Natl Cancer Inst. 2003; 95:723-732.

28. Bennett DC. Human melanocyte senescence and melanoma susceptibility genes. Oncogene. 2003; 22:3063-3069.

29. Serrano M, Lin AW, McCurrach ME, Beach D, and Lowe SW. Oncogenic ras provokes premature cell senescence associated with accumulation of p53 and p16INK4a. Cell. 1997; 85:593-602.

30. Hara E, Smith R, Parry D, Tahara H, Steven S, and Peters G. Regulation of p16(CDKN2) expression and its implications for cell immortalization and senescence. Mol Cell Biol. 1996; 16:859-867.

31. Alcorta DA, Xiong Y, Phelps D, Hannon G, Beach D, and Barrett JC. Involvement of the cyclin-dependent kinase inhibitor p16 (INK4a) in replicative senescence of normal human fibroblasts. Proc Natl Acad Sci USA. 1996; 93:13742-13747.

32. Dai CY and Enders GH. p16 INK4a can initiate an autonomous senescence program. Oncogene. 2000; 19:1613-1622.

33. Haferkamp S, Becker TM, Scurr LL, Kefford RF, and Rizos H. p16INK4a-induced senescence is disabled by melanoma-associated mutations. Aging Cell. 2008; 7:733-745.

34. Haferkamp S, Scurr LL, Becker TM, Frausto M, Kefford RF, and Rizos H. Oncogene-Induced Senescence Does Not Require the p16(INK4a) or p14ARF Melanoma Tumor Suppressors. J Invest Dermatol. 2009; 12:12.

35. Denoyelle C, Abou-Rjaily G, Bezrookove V, Verhaegen M, Johnson TM, Fullen DR, Pointer JN, Gruber SB, Su LD, Nikiforov MA, Kaufman RJ, Bastian BC, and Soengas MS. Anti-oncogenic role of the endoplasmic reticulum differentially activated by mutations in the MAPK pathway. Nat Cell Biol. 2006; 8:1053-1063.

36. Zhuang D, Mannava S, Grachtchouk V, Tang WH, Patil S, Wawrzyniak JA, Berman AE, Giordano TJ, Prochownik EV, Soengas MS, and Nikiforov MA. C-MYC overexpression is required for continuous suppression of oncogene-induced senescence in melanoma cells. Oncogene. 2008; 27:6623-6634.

37. Wajapeyee N, Serra RW, Zhu X, Mahalingam M, and Green MR. Oncogenic BRAF induces senescence and apoptosis through pathways mediated by the secreted protein IGFBP7. Cell. 2008; 132:363-374.

38. Shiohara M, Koike K, Komiyama A, and Koeffler HP. p21WAF1 mutations and human malignancies. Leuk Lymphoma. 1997; 26:35-41.

39. Jones R, Ruas M, Gregory F, Moulin S, Delia D, Manoukian S, Rowe J, Brookes S, and Peters G. A CDKN2A mutation in familial melanoma that abrogates binding of p16INK4a to CDK4 but not CDK6. Cancer Res. 2007; 67:9134-9141.

40. Berkovich E and Ginsberg D. ATM is a target for positive regulation by E2F-1. Oncogene. 2003; 22:161-167.

41. Ashcroft M, Taya Y, and Vousden KH. Stress signals utilize multiple pathways to stabilize p53. Mol Cell Biol. 2000; 20:3224-3233.

42. Stott FJ, Bates S, James MC, McConnell BB, Starborg M, Brookes S, Palmero I, Ryan K, Hara E, Vousden KH, and Peters G. The alternative product from the human *CDKN2A* locus, $p14^{ARF}$, participates in a regulatory feedback loop with p53 and MDM2. EMBO J. 1998; 17:5001-5014.

43. Wei W, Herbig U, Wei S, Dutriaux A, and Sedivy JM. Loss of retinoblastoma but not p16 function allows bypass of replicative senescence in human fibroblasts. EMBO Rep. 2003; 4:1061-1066.

44. Sage J, Miller AL, Perez-Mancera PA, Wysocki JM, and Jacks T. Acute mutation of retinoblastoma gene function is sufficient for cell cycle re-entry. Nature. 2003; 424:223-228.

45. Sage J, Mulligan GJ, Attardi LD, Miller A, Chen S, Williams B, Theodorou E, and Jacks T. Targeted disruption of the three Rb-related genes leads to loss of G(1) control and immortalization. Genes Dev. 2000; 14:3037-3050.

46. Lehmann BD, Brooks AM, Paine MS, Chappell WH, McCubrey JA, and Terrian DM. Distinct roles for p107 and p130 in Rb-independent cellular senescence. Cell Cycle. 2008; 7:1262-1268.

47. Classon M and Harlow E. The retinoblastoma tumour suppressor in development and cancer. Nat Rev Cancer. 2002; 2:910-917.

48. Halaban R. Rb/E2F: a two-edged sword in the melanocytic system. Cancer Metastasis Rev. 2005; 24:339-356.

49. Sherr CJ and Roberts JM. CDK inhibitors: positive and negative regulators of G1-phase progression. Genes Dev. 1999; 13:1501-1512.

50. Braden WA, Lenihan JM, Lan Z, Luce KS, Zagorski W, Bosco E, Reed MF, Cook JG, and Knudsen E.S. Distinct action of the retinoblastoma pathway on the DNA replication machinery defines specific roles for cyclin-dependent kinase complexes in prereplication complex assembly and S-phase progression. Mol Cell Biol. 2006; 26:7667-7681.

51. Rizos H, Darmanian AP, Indsto JO, Shannon JA, Kefford RF, and Mann GJ. Multiple abnormalities of the p16INK4a-pRb regulatory pathway in cultured melanoma cells. Melanoma Res. 1999; 9:10-9.

52. Halaban R, Ghosh S, Duray P, Kirkwood JM, and Lerner AB. Human melanocytes cultured from nevi and melanomas. J Invest Dermatol. 1986; 87:95-101.

53. Dull T, Zufferey R, Kelly M, Mandel RJ, Nguyen M, Trono D, and Naldini L. A third generation lentivirus vector with a conditional packaging system. Journal of Virology. 1998; 72:8463-8471.

54. Reiser J. Production and concentration of pseudotyped HIV-1-based gene transfer vectors. Gene Ther. 2000; 7:910-913.

55. Rizos H, Darmanian AP, Holland EA, Mann GJ, and Kefford RF. Mutations in the INK4a/ARF melanoma susceptibility locus functionally impair p14ARF. J Biol Chem. 2001; 276:41424-41434.

56. Brummelkamp TR, Bernards R, and Agami R. A system for stable expression of short interfering RNAs in mammalian cells. Science. 2002; 296:550-553.

57. Berns K, Hijmans EM, Mullenders J, Brummelkamp TR, Velds A, Heimerikx M, Kerkhoven RM, Madiredjo M, Nijkamp W, Weigelt B, Agami R, Ge W, Cavet G, et al. A large-scale RNAi screen in human cells identifies new components of the p53 pathway. Nature. 2004; 428:431-437.

58. Zhang Z, Wang H, Li M, Agrawal S, Chen X, and Zhang R. MDM2 is a negative regulator of p21 WAF1/CIP1, independent of p53. J Biol Chem. 2004; 3:3.

59. Bosco EE, Wang Y, Xu H, Zilfou JT, Knudsen KE, Aronow BJ, Lowe SW, and Knudsen ES. The retinoblastoma tumor

suppressor modifies the therapeutic response of breast cancer. J Clin Invest. 2007; 117:218-228.

60. Dimri GP, Lee X, Basile G, Acosta M, Scott G, Roskelley C, Medrano EE, Linskens M, Rubelj I, Pereira-Smith O, Peacocke M, and Campisi J. A biomarker that identifies senescent human cells in culture and in aging skin in vivo. Proc Natl Acad Sci U S A. 1995; 92:9363-9367.

61. Mallette FA, Gaumont-Leclerc MF, and Ferbeyre G. The DNA damage signaling pathway is a critical mediator of oncogene-induced senescence. Genes Dev. 2007; 21:43-48.

62. Courtois-Cox S, Genther Williams SM, Reczek EE, Johnson BW, McGillicuddy LT, Johannessen CM, Hollstein PE, MacCollin M, and Cichowski K. A negative feedback signaling network underlies oncogene-induced senescence. Cancer Cell. 2006; 10:459-472.

63. Zhu J, Woods D, McMahon M, and Bishop JM. Senescence of human fibroblasts induced by oncogenic Raf. Genes Dev. 1998; 12:2997-3007.

64. Voorhoeve PM and Agami R. The tumor-suppressive functions of the human INK4A locus. Cancer Cell. 2003; 4:311-319.

65. Guney I, Wu S, and Sedivy JM. Reduced c-Myc signaling triggers telomere-independent senescence by regulating Bmi-1 and p16(INK4a). Proc Natl Acad Sci U S A. 2006; 103:3645-3650.

66. Drayton S, Rowe J, Jones R, Vatcheva R, Cuthbert-Heavens D, Marshall J, Fried M, and Peters G. Tumor suppressor p16INK4a determines sensitivity of human cells to transformation by cooperating cellular oncogenes. Cancer Cell. 2003; 4:301-310.

67. Palmero I, Pantoja C, and Serrano M. $p19^{ARF}$ links the tumour suppressor p53 to Ras. Nature. 1998; 395:125-126.

68. Peeper DS, Dannenberg JH, Douma S, te Riele H, and Bernards R. Escape from premature senescence is not sufficient for oncogenic transformation by Ras. Nat Cell Biol. 2001; 3:198-203.

69. Brookes S, Rowe J, Ruas M, Llanos S, Clark PA, Lomax M, James MC, Vatcheva R, Bates S, Vousden KH, Parry D, Gruis N, Smit N, et al. INK4a-deficient human diploid fibroblasts are resistant to RAS-induced senescence. EMBO J. 2002; 21:2936-2945.

70. Huot TJ, Rowe J, Harland M, Drayton S, Brookes S, Gooptu C, Purkis P, Fried M, Bataille V, Hara E, Newton-Bishop J, and Peters G. Biallelic mutations in p16(INK4a) confer resistance to Ras- and Ets-induced senescence in human diploid fibroblasts. Mol Cell Biol. 2002; 22:8135-8143.

71. Skinner J, Bounacer A, Bond JA, Haughton MF, deMicco C, and Wynford-Thomas D. Opposing effects of mutant ras onco-protein on human fibroblast and epithelial cell proliferation: implications for models of human tumorigenesis. Oncogene. 2004; 23:5994-5999.

72. Kuilman T, Michaloglou C, Vredeveld LC, Douma S, van Doorn R, Desmet CJ, Aarden LA, Mooi WJ, and Peeper DS. Oncogene-induced senescence relayed by an interleukin-dependent inflammatory network. Cell. 2008; 133:1019-1031.

73. Itahana K, Zou Y, Itahana Y, Martinez JL, Beausejour C, Jacobs JJ, Van Lohuizen M, Band V, Campisi J, and Dimri GP. Control of the replicative life span of human fibroblasts by p16 and the polycomb protein Bmi-1. Mol Cell Biol. 2003; 23:389-401.

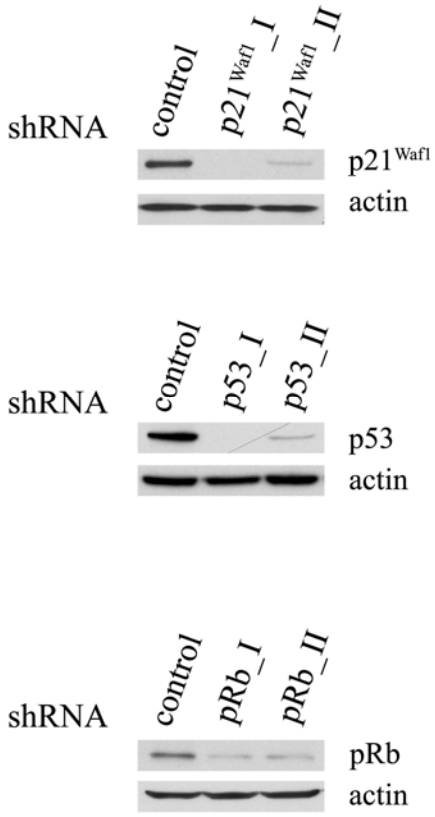

Supplementary Figure 1. Lentiviruses containing the indicated shRNA constructs cloned into the *pSIH-H1-copGFP* vector (System Biosciences) were used to infect the U20S osteosarcoma cells. Approximately three-four days post infection, $p21^{Waf1}$, p53 and pRb protein expression was analysed by western blot as indicated.

Research paper

Alterations in gene expression and sensitivity to genotoxic stress following HdmX or Hdm2 knockdown in human tumor cells harboring wild-type p53

Katherine Heminger[1], Michael Markey, Meldrick Mpagi, and Steven J. Berberich

Wright State University Boonshoft School of Medicine Biochemistry & Molecular Biology Department, Dayton, OH 45435, USA

[1] current address: Procter and Gamble Co., Cincinnati OH 45241, USA

Running title: *HdmX/2 loss inhibits tumor cell proliferation*

Key words: *p53, HdmX, Hdm2, RNAi, gene expression profiling*

Correspondence: *Steven J. Berberich, PhD, Wright State University Boonshoft School of Medicine Biochemistry & Molecular Biology Department, 3640 Colonel Glenn Hwy., Dayton, OH 45435*

Received: *11/18/08; accepted: 01/03/09; published on line: 01/07/09*

E-mail: *steven.berberich@wright.edu*

Copyright: *© 2009 Heminger et al. This is an open-access article distributed under the terms of the Creative Commons Attribution License, which permits unrestricted use, distribution, and reproduction in any medium, provided the original author and source are credited*

Abstract: While half of all human tumors possess p53 mutations, inactivation of wild-type p53 can also occur through a variety of mechanisms that do not involve p53 gene mutation or deletion. Our laboratory has been interested in tumor cells possessing wild-type p53 protein and elevated levels of HdmX and/or Hdm2, two critical negative regulators of p53 function. In this study we utilized RNAi to knockdown HdmX or Hdm2 in MCF7 human breast cancer cells, which harbor wild-type p53 and elevated levels of HdmX and Hdm2 then examined gene expression changes and effects on cell growth. Cell cycle and growth assays confirmed that the loss of either HdmX or Hdm2 led to a significant growth inhibition and G1 cell cycle arrest. Although the removal of overexpressed HdmX/2 appears limited to an anti-proliferative effect in MCF7 cells, the loss of HdmX and/or Hdm2 enhanced cytotoxicity in these same cells exposed to DNA damage. Through the use of Affymetrix GeneChips and subsequent RT-qPCR validations, we uncovered a subset of anti-proliferative p53 target genes activated upon HdmX/2 knockdown. Interestingly, a second set of genes, normally transactivated by E2F1 as cells transverse the G1-S phase boundary, were found repressed in a p21-dependent manner following HdmX/2 knockdown. Taken together, these results provide novel insights into the reactivation of p53 in cells overexpressing HdmX and Hdm2.

INTRODUCTION

Only half of all human tumors contain mutations in the p53 tumor suppressor gene [1], with the other half retaining wild-type p53 but possessing defects in the expression of p53 regulatory proteins and pathways. Under non-stress conditions, p53 protein is maintained at a low basal level by constant ubiquitination and proteasomal degradation [2]. Upon DNA damage or various types of cellular stress, p53 is stabilized and functions as a transcription factor to induce genes involved in cell cycle arrest, apoptosis, and DNA repair [3]. The stringent regulation of p53 involves a complex network of proteins, and is critical for maintaining genomic stability and suppressing tumor formation.

Hdm2 and its structural homologue HdmX represent two essential negative regulators of p53 as demonstrated by their embryonic lethality in knockout mice and subsequent rescue by concurrent elimination of p53 [4]. Hdm2 inactivates p53 function through direct association resulting in an inhibition of transactivation [5] and, through its E3 ligase activity targeting p53, by ubiquitin-mediated proteasome degradation [6, 7]. While HdmX shows conservation in the Hdm2 E3 ligase ring finger domain through which it

can heterodimerize with Hdm2 [8, 9], HdmX lacks the ability to ubiquitinate p53 in vivo [10, 11] and thus can only antagonize p53 transactivation [12]. The heterodimerization of Hdm2 and HdmX also plays a critical role in the response to DNA damage enabling Hdm2 to promote the ubiquitination and rapid proteasomal degradation of HdmX, thereby facilitating the tumor suppressor activity of p53 [13-15]. Thus, the interactions between p53, Hdm2 and HdmX are critical for complete regulation of p53 [4].

The overexpression of either Hdm2 or HdmX can inhibit the activity of p53 and directly contribute to tumor formation. It is not surprising that either one or both proteins are found overexpressed in many human tumors and tumor cell lines which harbor wild-type p53 [16]. Diverse approaches to activate the wild-type p53 in these tumors include the use of small molecule antagonists like Nutlin to inhibit the Hdm2-p53 interaction [17-19], and the use of antisense oligonucleotides, antibodies, and small interfering RNAs directed at Hdm2 or HdmX [20-23]. Recent findings suggest that Hdm2 and HdmX are specific independent therapeutic targets for activating wild-type p53 and that anti-cancer approaches that target both Hdm2 and HdmX should be considered as a means of treatment for tumors [16, 18, 24].

This study undertook an examination of gene expression alterations and the biological effects resulting from RNAi silencing of HdmX and Hdm2 in a breast cancer cell line overexpressing both proteins. Unlike previous studies examining only the biological effect of either HdmX or Hdm2 loss, this study focuses on a cell line where both proteins are overexpressed and further compliments those previous studies with a systematic examination of gene expression changes following loss of HdmX or Hdm2. Interestingly, only p53 target genes primarily associated with cell cycle arrest were induced. More striking was the repression of a large group of E2F-regulated genes upon HdmX/2 knockdown. Using siRNA approaches targeting p21, we were able to show that these E2F-regulated genes were repressed through p53 activation of p21. Furthermore, cell proliferation and colony formation assays confirmed that loss of HdmX or Hdm2 inhibited tumor cell growth and could sensitize these cells to treatment with doxorubicin. Taken together, these results suggest that in cells where both Hdm2 and HdmX are overexpressed, removal of one leads to an anti-proliferative effect in tumor cells harboring wild-type p53 and induction of p53 cell cycle arrest genes that negatively feedback onto the E2F pathway.

RESULTS

RNAi knockdown of Hdm2 and HdmX in MCF7 cells

Given that HdmX and Hdm2 are overexpressed in approximately 17% of human tumors [16] the majority of which possess wild-type p53, this study set out to examine how loss of Hdm2/X affected gene expression and tumor cell growth. MCF7, which possess wild-type p53 [25] and elevated levels of both HdmX and Hdm2 (Figure 1A) was the tumor cell line used in these studies. To inactivate HdmX and Hdm2 we employed siRNA targeting each gene as described in the materials and methods.

Before performing the Affymetrix GeneChip experiments we developed a triple transfection protocol that led to over 90% of the MCF7 cells taking up the siRNA (data not shown). Next, the effectiveness of the knockdown was assessed using RT-qPCR (data not shown) and Western blotting. Following the triple transfection protocol HdmX and p53 protein levels were undetectable with Hdm2 showing a greater than 80% reduction in protein expression (Figure 1B). As expected, the loss of either HdmX or Hdm2 led to an increase in the levels of p21. This p21 increase is p53-dependent since no increase in p21 protein levels was detected upon concurrent knockdown of HdmX and p53. While it has been suggested that Hdm2 controls the levels of p53 in non-stressed cells [26, 27], in our hands MCF7 cells showed only a slight increase in p53 protein levels following the combined loss of HdmX and Hdm2. The inability of Hdm2 knockdown to result in an increase in p53 protein could be the result of MCF7 cells harboring an elevated level of HdmX. Consistent with this suggestion, the treatment of MCF7 cells with Nutlin leads to increased p53 protein levels through loss of Hdm2 binding to p53 and concurrent Hdm2 mediated degradation of HdmX [28].

Loss of Hdm2 and HdmX triggers inhibition of cell growth

Other groups have reported that in cells where wild-type p53 is kept in check by overexpression of HdmX or Hdm2, their inhibition can trigger alterations in cell growth [29] and in some conditions apoptosis [30]. To assess the growth properties of RNAi knockdown of p53 regulators Hdm2 and HdmX, siRNA-transfected MCF7 cells were plated at low density in 6 well plates and allowed to grow for an additional 10 days. While transfection of siCon or sip53 resulted in only minimal changes in cell growth (Figure 2B), knockdown of either

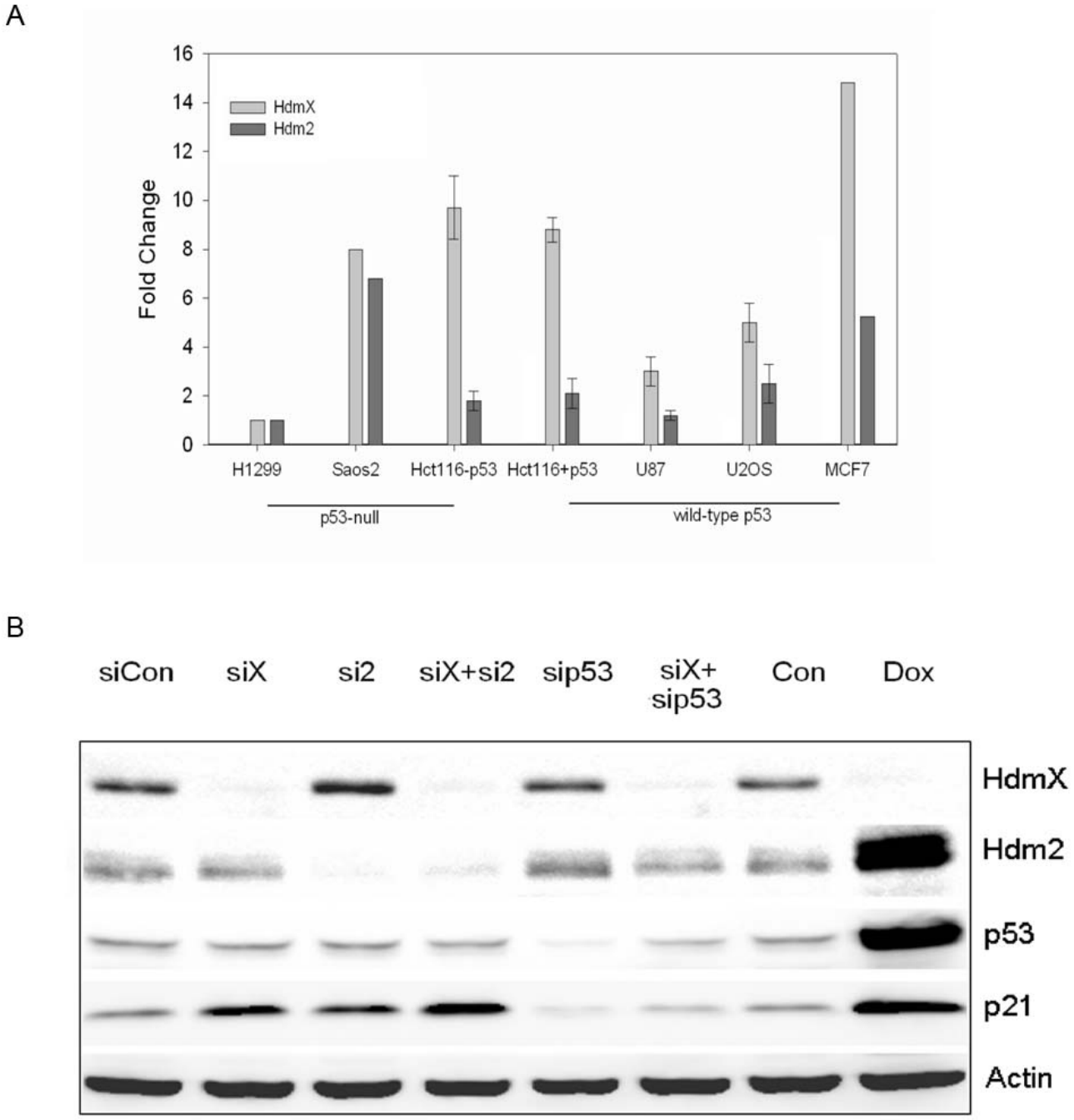

Figure 1. (**A**) RT-PCR analysis of *hdmX* and *hdm2* gene expression in various human cell lines. The endogenous levels of *hdmX* and *hdm2* were determined relative to H1299 cells. All samples were normalized to GAPDH. (**B**) RNAi knockdown of HdmX or Hdm2 triggers p53-dependent p21 induction. Western blot analysis of indicated proteins from the various siRNA or doxorubicin (Dox) treated MCF7 cells. Knockdowns of the indicated proteins were greater than 80%. Protein extracts were made 24 hours after the last siRNA transfection or treatment with 5 μg/ml doxorubicin.

HdmX or Hdm2, alone or in combination led to significantly fewer colonies (Figure 2A) and suppressed cell growth when compared to siCon (Figure 2B). This decrease in colony formation correlated with an increase in G1 arrest and not apoptosis (i.e. sub-G1) as determined by flow cytometry (data not shown).

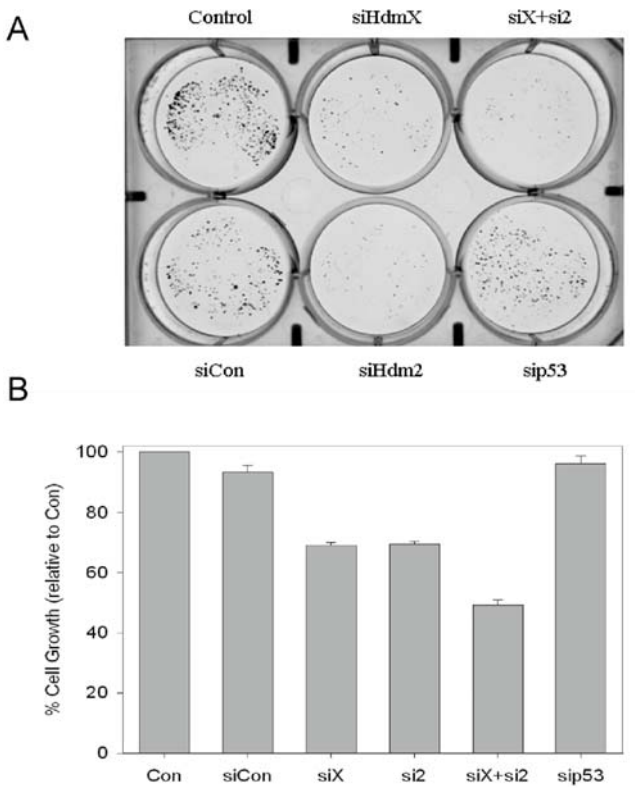

Figure 2. Loss of HdmX and/or Hdm2 inhibits MCF7 colony formation. (**A**) Following siRNA transfections, MCF7 cells were seeded at 500 cells/well in 6-well plates. The cells were allowed to grow for ten days then the colonies were stained with crystal violet. Significantly fewer colonies were present following knockdown of HdmX and/or Hdm2. The cells transfected with sip53 or a non-targeting control (siCon) showed minimal effects on colony formation relative to non-transfected control (Con/Control). (**B**) The percent cell growth relative to untransfected control was determined by extracting the stain in 10% acetic acid and quantifying the stain by reading absorbance at 590 nm.

Loss of HdmX or Hdm2 sensitizes MCF7 cells to DNA damage

Several recent studies using Nutlin and various DNA damaging agents reported that blocking Mdm2:p53 association led to increased chemosensitivity to DNA damaging agents [31, 32]. To examine whether knockdown of HdmX and Hdm2 can also elicit increased cytotoxicity to DNA damage, MCF7 cells were transfected with the indicated siRNA leading to alterations of gene expression (Figure 3B). Cells were then treated with varying doses of doxorubicin and cell viability assessed. siRNAs targeting HdmX or Hdm2 increased doxorubicin cytotoxicity, while removing both HdmX and Hdm2 led to the greatest level of chemosensitivity (Figure 3A). Enhanced chemosensitivity was also observed in cisplatin treatment of siHdmX or siHdm2 MCF7 cells (data not shown).

Gene expression profiles of MCF7 cells lacking HdmX or Hdm2

Having established an effective knockdown approach with effects on cell growth and increased sensitivity to DNA damage, we performed an Affymetrix GeneChip experiment to assess how loss of HdmX or Hdm2 affected global gene expression in MCF7 cells. Each RNAi transfection was performed in three separate biological replicates. The data analysis was carried out using GeneSpring GX software. Given the similarity of biological function uncovered in the previous experiments we focused our informatics on genes commonly altered following RNAi treatment with siHdmX or siHdm2. In summary, .cel files were normalized using GCRMA, genes filtered by ANOVA and fold change, and genes significantly altered by both siHdmX and siHdm2 but not siHdmX + sip53 identified (see materials and methods for detailed approach). From this approach we uncovered 394 gene alterations common to knockdown of both siHdmX and siHdm2 (Table 1).

p53 activation following loss of HdmX or Hdm2 triggers growth repressive genes

The initial examination of the 394 genes focused on those genes (n=222) that were increased following siHdmX or siHdm2 treatment relative to siCon. Thirteen genes were identified that were known p53-regulated genes (Figure 4). As expected these genes increased with siHdmX or siHdm2 treatment but had expression levels comparable or lower than siCon when treated with siHdmX+sip53 or sip53. Interestingly, with the exception of Fas, this list of p53 target genes consisted predominately of genes encoding proteins involved in cell cycle arrest or DNA repair. Consistent with a model whereby p53 proapoptotic target genes require p53 that is phosphorylated at serine 46 by HIPK2 [33-35], we observed no detectable phosphorylation at serines 6, 15, 20, 46, or 392 following the RNAi transfection protocol employed in these studies (data not shown).

To confirm these results, we performed RT-qPCR using TaqMan primers targeting five known p53 target genes, three of which were identified in our analysis. p21, BTG2 and ACTA2 are p53 target genes that are associated with cell cycle arrest or growth inhibition [36-38], while Hdm2 is a negative regulator of p53 and Noxa a pro-apoptotic factor not observed in our list of

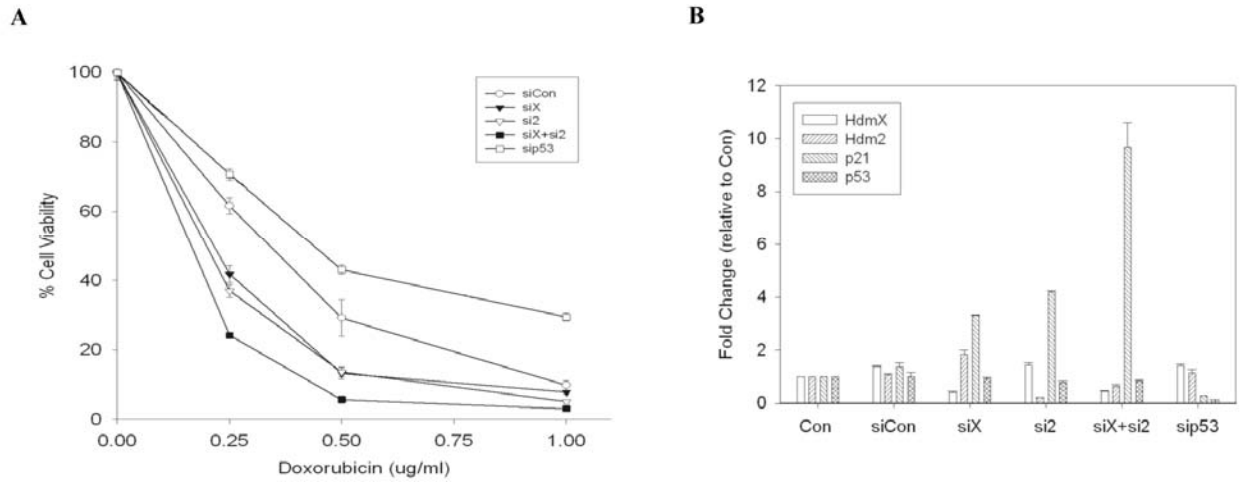

Figure 3. Knockdown of HdmX enhances doxorubicin-induced cytotoxicity. (**A**) Percent cell viability relative to untransfected untreated control cells. MCF7 cells were treated with doxorubicin (0.25-1.0 μg/mL) for 48 hours and cell viability was determined by absorbance at 590 nm. The loss of HdmX and/or Hdm2 showed an enhanced cytotoxicity relative to control cells. (**B**) RT-qPCR analysis of hdmX, hdm2, p21 and p53 gene expression in the indicated siRNA transfected MCF7 cells. The hdmX, hdm2, and p53 transcripts were effectively knocked down by siRNA prior to drug treatment.

altered genes [39]. MCF7 cells were either mock transfected (Mock), transfected with siRNA that does not target any human gene (siCon) or transfected with siRNA to HdmX or Hdm2 either alone or in combination. The results in Figure 5 demonstrate that relative to siCon, knockdown of HdmX led to significant increases in hdm2, p21, BTG2 and ACTA2 gene expression. No significant change in gene expression was observed with Noxa, which is consistent with our GeneChip results. With the obvious exception of hdm2, siRNA-targeting Hdm2 led to similar alterations in gene expression (Figure 5). Finally, when both HdmX and Hdm2 were eliminated, the levels of the cell cycle arrest genes p21, BTG2 and ACTA2 increased either synergistically or additively while levels of Noxa remained unchanged. These results validate our GeneChip data that p53-target genes were induced upon HdmX or Hdm2 knockdown and that several of these genes encode proteins involved in the cell cycle arrest.

p53 upregulation of p21 leads to global repression of E2F regulated genes

After searching for genes that were directly upregulated by p53 we next evaluated those genes that were repressed (N=172) following HdmX and Hdm2 knockdown (Figure 7). Within the list of downregulated genes were a set of genes that encode proteins involved in G1-S phase transition, the majority of which were known E2F1 regulated genes. It is concomitant decrease in both CCNA2 and E2F1 (Figure 7). In contrast, loss of Hdm2/X and p21 completely abrogated CCNA2 and E2F1 repression consistent with p53 activation inactivating E2F1 transactivation via p21 induction.

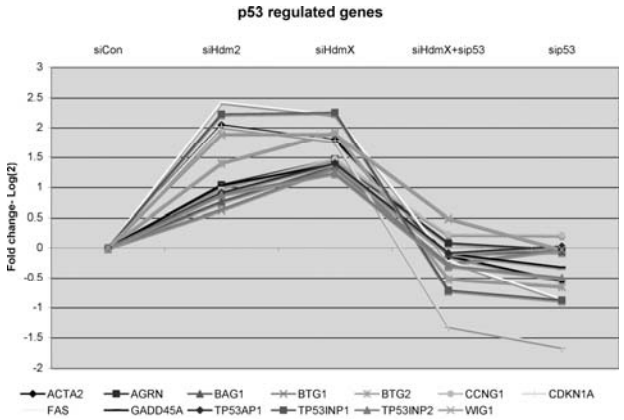

Figure 4. GeneChip expression of 13 known p53-regulated genes that were induced by knockdown of either siHdmX or siHdm2. Y-axis represents the average fold change (log_2) for each of the genes in the indicated siRNA transfections relative to siCon (X-axis, conditions labeled at the top of the chart).

DISCUSSION

As an essential tumor suppressor it is no surprise that human tumors demonstrate a diverse array of genetic mechanisms to inactivate p53 function. Central to this present study are tumors where one or both of the negative regulators of p53, Hdm2 and HdmX, are overexpressed leading to loss of p53 activity. Previous studies have focused on Hdm2 overexpression, where a small molecule inhibitor Nutlin 3 has proven to activate wild-type p53 in cell lines with elevated Hdm2, triggering apoptosis when combined with genotoxic agents that do not function as anti-mitotics [44]. Unfortunately, Nutlins have not proven as effective in tumors where HdmX is overexpressed [18, 45-47], suggesting the need for additional approaches aimed at blocking the HdmX:p53 association particularly given the recent observation of HdmX overexpression in retinoblastoma [48].

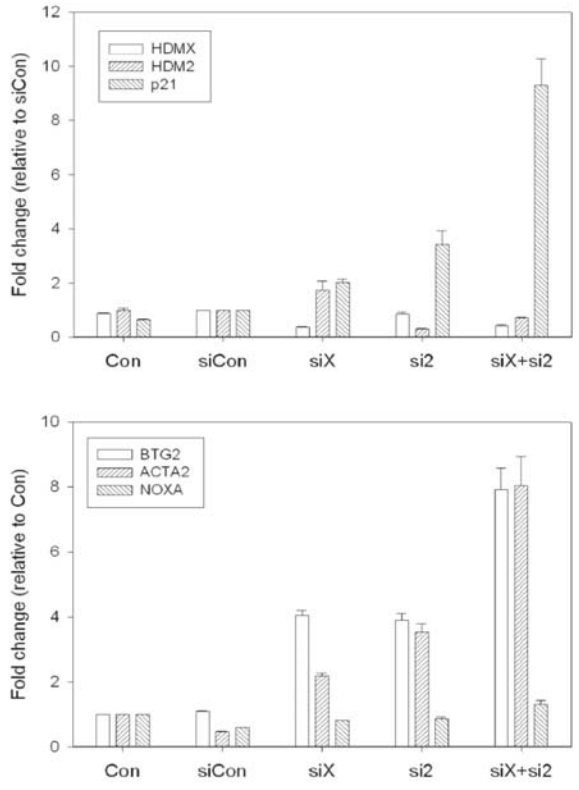

Figure 5. RT-qPCR validation of siRNA knockdown in MCF7 cells. (**A**) The hdmX, hdm2, and p21 mRNA expression relative to siCon (non-targeting siRNA) is shown. The p21 transcript is induced following loss of HdmX or Hdm2, and synergistically induced following loss of both HdmX and Hdm2. (**B**) BTG2, ACTA2, and NOXA mRNA expression relative to untransfected control (Con). The p53 target genes, BTG2 and ACTA2, are induced by loss of HdmX and/or Hdm2, while the expression of the proapoptotic gene, NOXA, is not altered.

Here we have employed RNAi approaches and DNA microarrays to better understand the activation of p53 in cells overexpressing Hdm2 and HdmX. In MCF7 cells a growth arrest with no detectable apoptosis was observed following knockdown of either Hdm2 or HdmX (Figure 2 and data not shown). While loss of either HdmX or Hdm2 was sufficient to trigger an anti-proliferative effect, the combined loss of both HdmX and Hdm2 resulted in a more significant growth inhibition.

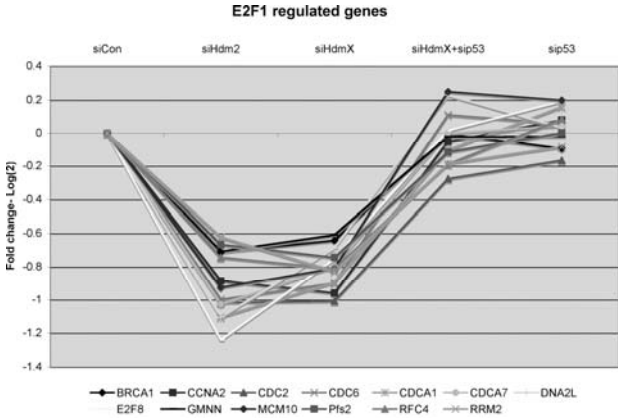

Figure 6. GeneChip expression of 13 reported E2F1-regulated genes that were repressed by knockdown of either siHdmX or siHdm2. Y-axis represents the average fold change (log_2) for each of the genes in the indicated siRNA transfections relative to siCon (X-axis, conditions labeled at the top of the chart).

Even though this RNAi approach appears to activate p53 without triggering its phosphorylation (data not shown), the loss of either HdmX or Hdm2 did effectively sensitize the cells to doxorubicin with the loss of both Hdm2 and HdmX being most sensitive to DNA damage (Figure 3). Surprisingly our results showed only a modest elevation of endogenous p53 levels following loss of HdmX and Hdm2 (Figure 1). This result maybe unique to MCF7 cells which harbor elevated Hdm2 and HdmX, in contrast to most tumor cell lines with wild-type p53 that possessed only elevated Hdm2 (Figure 1A). Consistent with the need for only one negative regulator to be elevated 65% of retinoblastoma tumors overexpress HdmX and possess wild-type p53 [48]. Based on our previous HdmX overexpression studies [10] we would predict that the overexpression of HdmX might inhibit Hdm2 degradation of p53 in MCF7 cells and thus could explain why modulating Hdm2 levels in MCF7 cells has no dramatic effect on p53 levels.

The DNA microarray experiment directly tested whether HdmX or Hdm2 knockdown triggered an increase in p53-regulated genes. While 394 genes were

significantly altered by either HdmX or Hdm2 knockdown (Table 1), only a small group was previously identified p53 targets (Figure 4). A few of the remaining genes induced by HdmX or Hdm2 loss are likely novel p53 regulated genes (S. Berberich, personal communication) but most probably represent downstream effects of the cell cycle arrest induced by p53. Within the 13 identified p53 target genes it is noteworthy that only one apoptotic gene (Fas) was found activated by loss of either HdmX or Hdm2. Upon careful examination of 16 known p53 pro-apoptotic genes we found that several of them were repressed following p53 knockdown, suggesting that their failure to be induced by loss of HdmX or Hdm2 was not a cell-type specific phenotype. Rather, we propose that the non-genotoxic release of p53 from Hdm2 of HdmX results in a preferential activation of growth arrest target genes, like p21 (Figure 5). This model is consistent with recent work suggesting that p53 promoter selection is dependent on its phosphorylation [49].

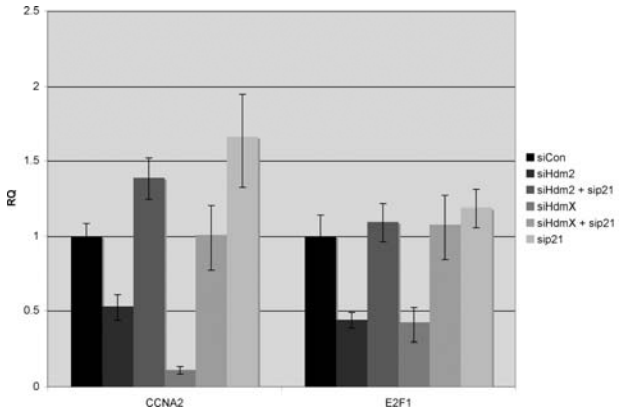

Figure 7. Repression of E2F1-regulated genes by Hdm2 or HdmX knockdown is blocked by concurrent knockdown of p21. MCF7 cells were transfected with the indicated siRNA combinations. Twenty-four hours later, RNA was isolated and subjected to RT-qPCR to quantify expression of CCNA2, p21 and E2F1 after normalization to GAPDH. Expression levels (Y-axis) were relative to siCon and reported as RQ values. Error bars represent the 95% confidence interval of the relative expression.

Another interesting finding within the microarray data was a subgroup of genes that were repressed upon HdmX and Hdm2 knockdown and could be classified as known E2F-regulated genes. Other groups have noted that p53 activation of p21 could lead to the repression of TERT [42] or Chk2 [41], known E2F-target genes, and another group recently reported similar findings using microarray assays [50].

While this report focused on genes commonly regulated by HdmX and Hdm2, it is worth mentioning that within genes uniquely regulated by either HdmX or Hdm2 we did not observe any additional p53 regulated genes (M. Markey, personal communication). The common biological effects of HdmX or Hdm2-loss and significant overlap of gene expression patterns are in contrast to recent in vivo studies where the knockout of Mdm2 or MdmX in adult mouse tissues lead to non-overlapping roles in regards to regulating p53 activity [51]. We believe these findings point to either differences in cell culture verses tissue studies or more likely represent a significant departure in the roles that Hdm2 and HdmX play when expressed at physiological levels compared to the elevated levels in tumor cells.

Finally these studies demonstrate that non-genotoxic activation of p53 by knockdown of its inhibitors Hdm2 and HdmX leads to the induction of genes involved in cell-cycle arrest, as well as repression of genes along the E2F/Rb pathway that promote cell cycle entry. These alterations in gene expression resulted in a decreased population of proliferative cells without necessarily increasing apoptosis. A non-genotoxic activation of p53 is one possible mechanism for the reduction in cellular proliferation observed during aging. This further underscores the critical importance of tumor suppressor activation in senescence and organismal aging.

MATERIALS AND METHODS

Cell lines, antibodies, siRNA and chemotherapeutic agents. The human breast tumor cell line MCF7 was grown in Dulbecco's modified Eagle medium (DMEM) supplemented with 10% bovine growth serum (BGS), and 10 μg/ml gentamicin unless otherwise indicated. HdmX polyclonal antibody (Bethyl Laboratories, Inc.), p21 polyclonal antibody C-19 (Santa Cruz Biotechnology, Inc.), p53 monoclonal antibody Ab-6 (Oncogene), Hdm2 monoclonal antibody SMP-14 (Santa Cruz Biotechnology, Inc.) and beta-actin monoclonal antibody (Sigma, Inc.) were used as indicated. A phosphorylation-specific p53 polyclonal antibody kit (Cell Signaling Technology, Inc.) was utilized per manufacturer's protocol. Horseradish peroxidase (HRP)-conjugated anti-mouse or anti-rabbit secondary antibodies (Promega) were used with Super Signal substrate (Pierce) for chemiluminescence detection of proteins. siGENOME duplex RNA targeting mRNA from hdmX, hdm2, or p53, and a non-targeting control siRNA were obtained from Dharmacon Research, Inc. and siRNA transfection was performed using Oligofectamine or Lipofectamine 2000 (Invitrogen) as described below. Doxorubicin hydro-

chloride (Tocris Bioscience) was prepared as a 5 mg/ml stock solution in water.

siRNA transfection. Cells were seeded at 200,000 cells per well in 6-well plates (for RNA isolation), or at 700,000 cells per 6-cm dish (for protein extraction) in antibiotic free DMEM containing 1% BGS in a small volume. Cells were reverse transfected with 100 nM siRNA (Dharmacon Research, Inc.) at time of seeding using Lipofectamine 2000 (Invitrogen). After a five hour incubation, the media was removed and cells were refed with DMEM containing 10% BGS. Twenty hours later, the cells were transfected again with 100 nM siRNA in a small volume of serum free media using Oligofectamine (Invitrogen). After a four-hour incubation, an equal volume of DMEM containing 20% BGS was added to each well or dish without removing the transfection mixture. Total RNA was isolated 24 hours post siRNA transfection and protein was extracted at 48 hours post siRNA unless otherwise indicated.

Analysis of Affymetrix GeneChips. The Affymetrix HG-U133 plus 2.0 GeneChips containing probe sets detecting over 54,000 transcripts were used in this study and each transfection condition was performed in triplicate. GeneChip cel files were imported into GeneSpring GX and preprocessed by GCRMA. Measurements less than 0.01 were then set to 0.01, and each chip was normalized to the 50th percentile of the measurements taken from that chip. Extra background correction was never applied. Each gene was normalized to the median of the measurements for that gene, and then to the median of that gene's expression in the siCon condition.

Initially all genes were filtered in GeneSpring GX first by Welch ANOVA to find expression changes based on siRNA treatment, using a p-value cut off of 0.05 and the Benjamini and Hochberg False Discovery Rate as a multiple testing correction. The cross-gene error model was active and based on replicates. From this list, genes were removed which varied between the mock and siCon treatments by 1.5 fold with a p-value < 0.05. Next, lists of genes with expression changes of 1.5 fold and a p-value < 0.05 were then made for siHdm2 versus siCon and siHdmX versus siCon. We then eliminated all but the union between these two lists. One gene that was repressed in the siHdm2 condition but upregulated in the siHdmX condition (encoding hypothetical protein MGC5370) was manually removed. Finally, genes that were not changed 1.5 fold with a p-value of <0.05 between the siHdmX and siHdmX + sip53 conditions were removed leaving a total of 394 selected genes.

Quantitative RT-pPCR. Cells were lysed directly in the culture dish and total RNA was isolated using the RNeasy kit (Qiagen) according to manufacturer's protocol. The RNA was quantified by spectrophotometer reading at 260 nm, and 1 µg RNA was reverse transcribed with random hexamers to create cDNA using the TaqMan Reverse transcription kit (Applied Biosystems). Quantitative PCR was performed in a 96-well micro titer plate format on an ABI Prism 7900HT sequence detection system using 1 µl cDNA, TaqMan Universal PCR master mix and Assay-on-Demand Gene Expression products (Applied Biosystems) specific for genes of interest. Each cDNA sample was analyzed in triplicate and fold change relative to control was calculated based on a PCR efficiency of two and normalized to GAPDH (endogenous control) RNA levels. Average fold change and standard deviation were obtained from 2-3 biological replicate samples per treatment assayed in triplicate.

Western blot analysis. Frozen cells were lysed in an aqueous extraction buffer composed of 120 mM NaCl, 50 mM Tris-HCl (pH 8.0), 5 mM EGTA, 1 mM EDTA, 5 mM NaPPi, 10 mM NaF, 30 mM para-nitrophenylphosphate, 1 mM Benzamidine, 0.1% NP-40 (Ipegal Ca-630), 0.2 mM PMSF, and 1% protease inhibitor cocktail (Sigma), and soluble protein was recovered by centrifugation. Protein concentration was determined using Bradford reagent (Bio-Rad), and proteins were resolved on a sodium dodecyl sulfate-10% polyacrylamide gel followed by transfer of proteins to a polyvinylidene difluoride membrane (Millipore) using a Transblot system (Bio-Rad). Immunoblotting was performed as previously described [52] using appropriate primary antibodies at 1:1000-1:10,000 dilution and secondary antibodies (goat anti-mouse or goat anti-rabbit HRP-conjugated, Promega) at 1:5000-1:10,000 dilution. Blots were exposed to chemiluminescent reagent (Pierce) and protein was visualized on a FUJIFILM LAS-3000 image reader.

Colony formation and cell viability assays. Twenty-four hours after the second siRNA transfection, the cells were trypsinized, counted and seeded at 500 cells per well in 6-well plates for the colony formation assay. The cells were allowed to grow for ten days, and then the colonies were fixed and stained in 1% crystal violet in 70% methanol. The cell viability assays were performed in 96-well plates using either CellQuanti-Blue™ Reagent (BioAssay Systems) according to manufacturer's protocol or by staining the cells with crystal violet, extracting the stain in 10% acetic acid, and then reading absorbance at 590 nm. Again, cells were trypsinized after the second siRNA transfection, counted and seeded at 20,000 cells per well. Cell

viability was determined at various time points post-seeding or following treatment with chemotherapeutic agents for the times indicated.

ACKNOWLEDGEMENTS

This work was funded by the National Cancer Institute (CA66430 to SJB). The Biomedical Sciences Ph.D. program and NIH supported KAH. MM was supported by NIH and the Center for Genomics Research. DNA microarray facilities and bioinfomatic programs were provided by the Center for Genomics Research.

CONFLICT OF INTERESTS STATEMENT

The authors of this manuscript have no conflict of interests to declare.

REFERENCES

1. Hollstein M, Rice K, Greenblatt MS, Soussi T, Fuchs R, Sorlie T, Hovig E, Smith-Sorensen B, Montesano R, and Harris CC. Database of p53 gene somatic mutations in human tumors and cell lines. Nucleic Acids Res. 1994; 22:3551-3555.

2. Kubbutat MH and Vousden KH. Keeping an old friend under control: regulation of p53 stability. Mol Med Today. 1998; 4:250-256.

3. Vousden KH and Lu X. Live or let die: the cell's response to p53. Nat Rev Cancer. 2002; 2:594-604.

4. Marine JC and Jochemsen AG. Mdmx and Mdm2: brothers in arms? Cell Cycle. 2004; 3:900-904.

5. Oliner JD, Peitenol JA, Thiagalingam S, Gyuris J, Kinzler KW, and Vogelstein B. Oncoprotein MDM2 conceals the activation domain of tumour suppressor p53. Nature. 1993; 362:857-860.

6. Haupt Y, Maya R, and Oren M. Mdm2 promotes the rapid degradation of p53. Nature. 1997; 387:296.

7. Kubbutat MHG, Jones SN, and Vousden KH. Regulation of p53 stability by Mdm2. Nature. 1997; 387:299-303.

8. Sharp DA, Kratowicz SA, Sank MJ, and George DL. Stabilization of the MDM2 Oncoprotein by Interaction with the Structurally Related MDMX Protein. J Biol Chem. 1999; 274:38189-38196.

9. Tanimura S, Ohtsuka S, Mitsui K, Shirouzu K, Yoshimura A, and Ohtsubo M. MDM2 interacts with MDMX through their RING finger domains. FEBS Lett. 1999; 447:5-9.

10. Jackson MW and Berberich SJ. MdmX protects p53 from Mdm2-mediated degradation. Mol. Cell. Biol. 2000; 20:1001-1007.

11. Stad R, Little NA, Xirodimas DP, Frenk R, van der Eb AJ, Lane DP, Saville MK, and Jochemsen AG. Mdmx stabilizes p53 and Mdm2 via two distinct mechanisms. EMBO Rep. 2001; 2:1029-1034.

12. Shvarts A, Steegenga W, van Laar RNT, Dekker P, Bazuine M, van Ham R, van der Houven van Oordt W, Hateboer G, van der Eb A, and Jochemsen A. MDMX: a novel p53-binding protein with some functional properties of MDM2. The EMBO Journal. 1996; 15:5349-5357.

13. de Graaf P, Little NA, Ramos YF , Meulmeester E, Letteboer SJ, and Jochemsen AG. Hdmx protein stability is regulated by the ubiquitin ligase activity of Mdm2. J Biol Chem. 2003; 278:38315-38324.

14. Kawai H, Wiederschain D, Kitao H, Stuart J, Tsai KK, and Yuan ZM. DNA damage-induced MDMX degradation is mediated by MDM2. J Biol Chem. 2003; 278:45946-45953.

15. Pan Y and J. Chen J. MDM2 promotes ubiquitination and degradation of MDMX. Mol Cell Biol. 2003; 23:5113-5121.

16. Toledo F and Wahl GM Regulating the p53 pathway: in vitro hypotheses, in vivo veritas. Nat Rev Cancer. 2006; 6:909-923.

17. Kojima K, Konopleva M, Samudio IJ, Shikami M, Cabreira-Hansen M, McQueen T, Ruvolo V, Tsao T, Zeng Z, Vassilev LT, Andreeff M. MDM2 antagonists induce p53-dependent apoptosis in AML: implications for leukemia therapy. Blood. 2005; 106:3150-3159.

18. Patton JT, Mayo LD, Singhi AD, Gudkov AV, Stark GR, and Jackson MW, Levels of HdmX expression dictate the sensitivity of normal and transformed cells to Nutlin-3. Cancer Res. 2006; 66:3169-3176.

19. Vassilev, LT. Small-Molecule Antagonists of p53-MDM2 Binding: Research Tools and Potential Therapeutics. Cell Cycle. 2004; 3:419-421.

20. Chene P. Inhibiting the p53-MDM2 interaction: an important target for cancer therapy. Nat Rev Cancer. 2003; 3:102-109.

21. Linares LK and Scheffner M. The ubiquitin-protein ligase activity of Hdm2 is inhibited by nucleic acids. FEBS Lett. 2003; 554:73-76.

22. Yu Y, Sun P, Sun LC, Liu GY, Chen GH, Shang LH, Wu HB, Hu J, Li Y, Mao YL, Sui GJ, and Sun XW. Downregulation of MDM2 expression by RNAi inhibits LoVo human colorectal adenocarcinoma cells growth and the treatment of LoVo cells with mdm2siRNA3 enhances the sensitivity to cisplatin. Biochem Biophys Res Commun. 2006; 339:71-78.

23. Zhang R, Wang H, and Agrawal S. Novel antisense anti-MDM2 mixed-backbone oligonucleotides: proof of principle, in vitro and in vivo activities, and mechanisms. Curr Cancer Drug Targets. 2005; 5:43-49.

24. Hu B, Gilkes DM, and Chen J. Efficient p53 activation and apoptosis by simultaneous disruption of binding to MDM2 and MDMX. Cancer Res. 2007; 67:8810-8817.

25. Ramos YF, Stad R, Attema J, Peltenburg LT, van der Eb AJ, and Jochemsen AG. Aberrant expression of HDMX proteins in tumor cells correlates with wild-type p53. Cancer Res. 2001; 61:1839-1842.

26. Fuchs SY, Adler V, Buschmann T, Wu X, and Ronai Z. Mdm2 association with p53 targets its ubiquitination. Oncogene. 1998; 17:2543-2547.

27. Little NA and Jochemsen AG. Hdmx and Mdm2 can repress transcription activation by p53 but not by p63. Oncogene. 2001; 20:4576-4580.

28. Xia M, Knezevic D, Tovar C, Huang B, Heimbrook DC, and Vassilev LT. Elevated MDM2 boosts the apoptotic activity of p53-MDM2 binding inhibitors by facilitating MDMX degradation. Cell Cycle. 2008; 7:1604-1612.

29. Efeyan A, Ortega-Molina A, Velasco-Miguel S, Herranz D, Vassilev LT, and Serrano M. Induction of p53-dependent senescence by the MDM2 antagonist nutlin-3a in mouse cells of fibroblast origin. Cancer Res. 2007; 67:7350-7357.

30. Vassilev LT, Vu BT, Graves B, Carvajal D, Podlaski F, Filipovic Z, Kong N, Kammlott U, Lukacs C, Klein C, Fotouhi N, and Liu EA.

In vivo activation of the p53 pathway by small-molecule antagonists of MDM2. Science. 2004; 303:844-848.

31. Barbieri E, Mehta P, Chen Z, Zhang L, Slack A, Berg S, and Shohet JM. MDM2 inhibition sensitizes neuroblastoma to chemotherapy-induced apoptotic cell death. Mol Cancer Ther. 2006; 5:2358-2365.

32. Coll-Mulet L, Iglesias-Serret D, Santidrian AF, Cosialls AM, de Frias M, Castano E, Campas C, Barragan M, de Sevilla AF, Domingo A, Vassilev LT, Pons G, and Gil J. MDM2 antagonists activate p53 and synergize with genotoxic drugs in B-cell chronic lymphocytic leukemia cells. Blood. 2006; 107:4109-4114.

33. D'Orazi G, Cecchinelli B, Bruno T, Manni I, Higashimoto Y, Saito S, Gostissa M, Coen S, Marchetti A, Del Sal G, Piaggio G, Fanciulli M, Appella E, and Soddu S. Homeodomain-interacting protein kinase-2 phosphorylates p53 at Ser 46 and mediates apoptosis. Nat Cell Biol. 2002; 4:11-19.

34. Hofmann TG, Moller A, Sirma H, Zentgraf H, Taya Y, Droge W, Will H, and Schmitz ML. Regulation of p53 activity by its interaction with homeodomain-interacting protein kinase-2. Nat Cell Biol. 2002; 4:1-10.

35. Oda K, Arakawa H, Tanaka T, Matsuda K, Tanikawa C, Mori T, Nishimori H, Tamai K, Tokino T, Nakamura Y, and Taya Y. p53AIP1, a potential mediator of p53-dependent apoptosis, and its regulation by Ser-46-phosphorylated p53. Cell. 2000; 102:849-862.

36. el-Deiry, WS. Regulation of p53 downstream genes [In Process Citation]. Semin Cancer Biol. 1998; 8:345-357.

37. Cui XS and Donehower LA. Differential gene expression in mouse mammary adenocarcinomas in the presence and absence of wild type p53. Oncogene. 2000; 19:5988-5996.

38. Boiko AD, Porteous S, Razorenova OV, Krivokrysenko VI, Williams BR, and Gudkov AV. A systematic search for downstream mediators of tumor suppressor function of p53 reveals a major role of BTG2 in suppression of Ras-induced transformation. Genes Dev. 2006; 20:236-252.

39. Oda E, Ohki R, Murasawa H, Nemoto J, Shibue T, Yamashita T, Tokino T, Taniguchi T, and Tanaka N. Noxa, a BH3-only member of the bcl-2 family and candidate mediator of p53-induced apoptosis [In Process Citation]. Science. 2000; 288:1053-1058.

40. Boulaire J, Fotedar A, and Fotedar R. The functions of the cdk-cyclin kinase inhibitor p21WAF1. Pathol Biol (Paris). 2000; 48:190-202.

41. Gottifredi V, Karni-Schmidt O, Shieh SS, and Prives C. p53 down-regulates CHK1 through p21 and the retinoblastoma protein. Mol Cell Biol. 2001; 21:1066-1076.

42. Shats I, Milyavsky M, Tang X, Stambolsky P, Erez N, Brosh R, Kogan I, Braunstein I, Tzukerman M, Ginsberg D, and Rotter V. p53-dependent down-regulation of telomerase is mediated by p21waf1. J Biol Chem. 2004; 279:50976-50985.

43. Chen KY. Transcription factors and the down-regulation of G1/S boundary genes in human diploid fibroblasts during senescence. Front Biosci. 1997; 2:d417-426.

44. Carvajal D, Tovar C, Yang H, Vu BT, Heimbrook DC, and Vassilev LT. Activation of p53 by MDM2 antagonists can protect proliferating cells from mitotic inhibitors. Cancer Res. 2005; 65:1918-1924.

45. Hu B, Gilkes DM, Farooqi B, Sebti SM, and Chen J. MDMX overexpression prevents P53 activation by the MDM2 inhibitor nutlin. J Biol Chem. 2006.

46. Kranz D and Dobbelstein M. Nongenotoxic p53 activation protects cells against S-phase-specific chemotherapy. Cancer Res. 2006; 66:10274-10280.

47. Wade M, Wong ET, Tang M, Vassilev LT and Wahl GM. Hdmx modulates the outcome of p53 activation in human tumor *cells.* J Biol Chem. 2006.

48. Laurie NA, SDonovan SL, Shih CS, Zhang J, Mills N, Fuller C, Teunisse A, Lam S, Ramos Y, Mohan A, Johnson D, Wilson M, et al. Inactivation of the p53 pathway in retinoblastoma. Nature. 2006; 444:61-66.

49. Mayo LD, Seo YR, Jackson MW, Smith ML, Rivera Guzman J, Korgaonkar CK, and Donner DB. Phosphorylation of human p53 at serine 46 determines promoter selection and whether apoptosis is attenuated or amplified. J Biol Chem. 2005; 280:25953-25959.

50. Scian MJ, Carchman EH, Mohanraj L, Stagliano KE, Anderson MA, Deb D, Crane BM, Kiyono T, Windle B, Deb SP, and Deb S. Wild-type p53 and p73 negatively regulate expression of proliferation related genes. Oncogene. 2008; 27:2583-2593.

51. Francoz S, Froment P, Bogaerts S, De Clercq S, Maetens M, Doumont G, Bellefroid E, and Marine JC. Mdm4 and Mdm2 cooperate to inhibit p53 activity in proliferating and quiescent cells in vivo. Proc Natl Acad Sci U S A. 2006; 103:3232-3237.

52. Berberich SJ, Litteral V, Mayo LD, Tabesh D, and Morris D. mdm-2 gene amplification in 3T3-L1 preadipocytes. Differentiation. 1999; 64:205-212.

Table 1: Genes deregulated by HdmX and Hdm2 in MCF7 cells.

AffyID	Fold Change vs. siCon siHdmX	siHdm2	Gene Symbol	Description
212354_at	5.673	2.914	SULF1	sulfatase 1
205916_at	5.6	2.427	S100A7	S100 calcium binding protein A7 (psoriasin 1)
211163_s_at	5.167	6.472	TNFRSF10C	tumor necrosis factor receptor superfamily, member 10c, decoy without an intracellular domain
206222_at	4.986	7.782	TNFRSF10C	tumor necrosis factor receptor superfamily, member 10c, decoy without an intracellular domain
208180_s_at	4.603	4.544	HIST1H4H	histone 1, H4h
206488_s_at	4.424	3.301	CD36	CD36 antigen (collagen type I receptor, thrombospondin receptor)
237737_at	4.4	4.846	LOC375010 ;	hypothetical LOC375010 ; hypothetical LOC401131
232035_at	4.209	4.263	HIST1H4H	histone 1, H4h
216252_x_at	3.97	5.55	FAS	Fas (TNF receptor superfamily, member 6)
213110_s_at	3.929	3.082	COL4A5	collagen, type IV, alpha 5 (Alport syndrome)
209555_s_at	3.927	3.001	CD36	CD36 antigen (collagen type I receptor, thrombospondin receptor)
229331_at	3.756	4.49	SPATA18	spermatogenesis associated 18 homolog (rat)
228766_at	3.703	1.865	CD36	CD36 antigen (collagen type I receptor, thrombospondin receptor)
208083_s_at	3.664	3.871	ITGB6	integrin, beta 6
212097_at	3.631	1.804	CAV1	caveolin 1, caveolae protein, 22kDa
204781_s_at	3.627	5.375	FAS	Fas (TNF receptor superfamily, member 6)
202917_s_at	3.61	1.752	S100A8	S100 calcium binding protein A8 (calgranulin A)
225912_at	3.59	4.665	TP53INP1	tumor protein p53 inducible nuclear protein 1
215856_at	3.493	2.626	CD33L3	CD33 antigen-like 3
215719_x_at	3.479	5.572	FAS	Fas (TNF receptor superfamily, member 6)
226535_at	3.47	3.972	ITGB6	integrin, beta 6
212344_at	3.331	2.234	SULF1	sulfatase 1
202833_s_at	3.198	1.717	SERPINA1	serpin peptidase inhibitor, clade A (alpha-1 antiproteinase, antitrypsin), member 1
209504_s_at	3.138	3.235	PLEKHB1	pleckstrin homology domain containing, family B (evectins) member 1
218692_at	3.104	2.476	FLJ20366	hypothetical protein FLJ20366
208096_s_at	3.103	1.783	COL21A1	collagen, type XXI, alpha 1 ; collagen, type XXI, alpha 1
204780_s_at	3.049	4.444	FAS	Fas (TNF receptor superfamily, member 6)
208683_at	3.027	2.795	CAPN2	calpain 2, (m/II) large subunit
219628_at	2.982	3.714	WIG1	p53 target zinc finger protein
211429_s_at	2.976	1.724	SERPINA1	serpin peptidase inhibitor, clade A (alpha-1 antiproteinase, antitrypsin), member 1
1554062_at	2.871	3.334	XG	Xg blood group (pseudoautosomal boundary-divided on the X chromosome)
207695_s_at	2.847	1.969	IGSF1	immunoglobulin superfamily, member 1
212298_at	2.819	2.164	NRP1	neuropilin 1
201236_s_at	2.8	2.654	BTG2	BTG family, member 2
207392_x_at	2.795	1.882	UGT2B15	UDP glucuronosyltransferase 2 family, polypeptide B15
215125_s_at	2.784	1.964	UGT1A10 ; U	UDP glucuronosyltransferase 1 family, polypeptide A10
210387_at	2.776	2.855	HIST1H2BG	histone 1, H2bg

Table 1: Genes deregulated by HdmX and Hdm2 in MCF7 cells.

AffyID	Fold Change vs. siCon siHdmX	siHdm2	Gene Symbol	Description
208596_s_at	2.739	2.215	UGT1A10 ; U	UDP glucuronosyltransferase 1 family, polypeptide A10
208084_at	2.687	3.504	ITGB6	integrin, beta 6
242444_at	2.665	2.379	C1QTNF6	C1q and tumor necrosis factor related protein 6
212998_x_at	2.65	2.139	HLA-DQB1	major histocompatibility complex, class II, DQ beta 1 ; major histocompatibility complex, class II, DQ beta 1
202743_at	2.648	2.41	PIK3R3	phosphoinositide-3-kinase, regulatory subunit 3 (p55, gamma)
202688_at	2.635	2.027	TNFSF10	tumor necrosis factor (ligand) superfamily, member 10 ; tumor necrosis factor (ligand) superfamily, member 10
205306_x_at	2.633	3.434	KMO	kynurenine 3-monooxygenase (kynurenine 3-hydroxylase)
212347_x_at	2.62	2.552	MXD4	MAX dimerization protein 4
211161_s_at	2.581	1.685	COL3A1	collagen, type III, alpha 1 (Ehlers-Danlos syndrome type IV, autosomal dominant)
227863_at	2.577	2.524	CTSD	cathepsin D (lysosomal aspartyl peptidase)
220999_s_at	2.573	3.036	CYFIP2	cytoplasmic FMR1 interacting protein 2 ; cytoplasmic FMR1 interacting protein 2
1559116_s_at	2.559	1.995	AD-020	Chromosome 1 open reading frame 119
222150_s_at	2.555	2.22	LOC54103	hypothetical protein LOC54103
206280_at	2.533	1.924	CDH18	cadherin 18, type 2
228315_at	2.528	3.249		CDNA FLJ31683 fis, clone NT2RI2005353
1557779_at	2.523	2.226		Homo sapiens, clone IMAGE:4400004, mRNA
200974_at	2.52	4.108	ACTA2	actin, alpha 2, smooth muscle, aorta
221756_at	2.511	2.171	MGC17330	HGFL gene ; HGFL gene
202180_s_at	2.505	2.634	MVP	major vault protein
221218_s_at	2.484	2.759	TPK1	thiamin pyrophosphokinase 1
219049_at	2.479	1.767	ChGn	chondroitin beta1,4 N-acetylgalactosaminyltransferase
227020_at	2.448	2.095	YPEL2	yippee-like 2 (Drosophila)
225207_at	2.441	2.274	PDK4	pyruvate dehydrogenase kinase, isoenzyme 4
215779_s_at	2.439	2.315	HIST1H2BG	histone 1, H2bg
210778_s_at	2.432	1.917	MXD4	MAX dimerization protein 4
202284_s_at	2.428	4.05	CDKN1A	cyclin-dependent kinase inhibitor 1A (p21, Cip1)
211580_s_at	2.405	1.801	PIK3R3	phosphoinositide-3-kinase, regulatory subunit 3 (p55, gamma)
213261_at	2.388	1.842	LBA1	lupus brain antigen 1
215785_s_at	2.388	3.311	CYFIP2	cytoplasmic FMR1 interacting protein 2
210218_s_at	2.381	2.055	SP100	nuclear antigen Sp100
215465_at	2.375	2.541	ABCA12	ATP-binding cassette, sub-family A (ABC1), member 12
203058_s_at	2.365	2.382	PAPSS2	3'-phosphoadenosine 5'-phosphosulfate synthase 2
200984_s_at	2.35	2.369	CD59	CD59 antigen p18-20 (antigen identified by monoclonal antibodies 16.3A5, EJ16, EJ30, EL32 and G344)
225613_at	2.346	2.243	MAST4	microtubule associated serine/threonine kinase family member 4

Table 1: Genes deregulated by HdmX and Hdm2 in MCF7 cells.

AffyID	Fold Change vs. siCon siHdmX	siHdm2	Gene Symbol	Description
212463_at	2.34	2.5	CD59	CD59 antigen p18-20 (antigen identified by monoclonal antibodies 16.3A5, EJ16, EJ30, EL32 and G344)
204846_at	2.338	2.398	CP	ceruloplasmin (ferroxidase)
236835_at	2.336	1.973	FUT8	fucosyltransferase 8 (alpha (1,6) fucosyltransferase)
236278_at	2.333	2.228		
214616_at	2.322	2.008	HIST1H3E	histone 1, H3e
209737_at	2.31	2.216	MAGI2	membrane associated guanylate kinase, WW and PDZ domain containing 2
203060_s_at	2.304	2.3	PAPSS2	3'-phosphoadenosine 5'-phosphosulfate synthase 2
1552632_a_at	2.303	1.894	KIAA1001	Arylsulfatase G
209460_at	2.302	2.261	ABAT	4-aminobutyrate aminotransferase
207664_at	2.264	1.981	ADAM2	ADAM metallopeptidase domain 2 (fertilin beta)
200696_s_at	2.249	2.239	GSN	gelsolin (amyloidosis, Finnish type)
238439_at	2.24	2.4	ANKRD22	ankyrin repeat domain 22
223315_at	2.237	2.067	NTN4	netrin 4
224847_at	2.237	2.597	CDK6	cyclin-dependent kinase 6
242093_at	2.234	1.698		
223686_at	2.208	3.069	TPK1	thiamin pyrophosphokinase 1
210484_s_at	2.204	3.38	TNFRSF10C	tumor necrosis factor receptor superfamily, member 10c, decoy without an intracellular domain ; hypothetical protein MGC31957
201852_x_at	2.203	1.924	COL3A1	collagen, type III, alpha 1 (Ehlers-Danlos syndrome type IV, autosomal dominant)
1564573_at	2.193	2.13	LOC402778	similar to RIKEN cDNA 6330512M04 gene (mouse)
213744_at	2.192	1.528	ATRNL1	attractin-like 1
229553_at	2.192	1.863	PGM2L1	phosphoglucomutase 2-like 1
223600_s_at	2.191	2.291	KIAA1683	KIAA1683
209160_at	2.185	2.108	AKR1C3	aldo-keto reductase family 1, member C3 (3-alpha hydroxysteroid dehydrogenase, type II)
211138_s_at	2.18	2.362	KMO	kynurenine 3-monooxygenase (kynurenine 3-hydroxylase)
228390_at	2.179	1.883		CDNA clone IMAGE:5259272
206463_s_at	2.172	2.849	DHRS2	dehydrogenase/reductase (SDR family) member 2
212346_s_at	2.169	2.327	MXD4	MAX dimerization protein 4
1555756_a_at	2.164	1.907	CLEC7A	C-type lectin domain family 7, member A
214455_at	2.15	1.773	HIST1H2BC	histone 1, H2bc
228151_at	2.148	1.989		Transcribed locus
1559322_at	2.145	2.587	PTP4A1	Protein tyrosine phosphatase type IVA, member 1
203543_s_at	2.127	1.708	KLF9	Kruppel-like factor 9
205776_at	2.124	1.96	FMO5	flavin containing monooxygenase 5
206110_at	2.122	2.096	HIST1H3H	histone 1, H3h
40016_g_at	2.119	2.19	MAST4	microtubule associated serine/threonine kinase family member 4
205059_s_at	2.114	2.441	IDUA	iduronidase, alpha-L-
202963_at	2.113	2.189	RFX5	regulatory factor X, 5 (influences HLA class II expression)
213664_at	2.105	2.326	SLC1A1	solute carrier family 1 (neuronal/epithelial high affinity glutamate transporter, system Xag), member 1
218280_x_at	2.101	2.187	HIST2H2AA	histone 2, H2aa

Table 1: Genes deregulated by HdmX and Hdm2 in MCF7 cells.

AffyID	Fold Change vs. siCon siHdmX	siHdm2	Gene Symbol	Description
214696_at	2.1	2.282	MGC14376	hypothetical protein MGC14376
225725_at	2.091	2.788		CDNA FLJ31683 fis, clone NT2RI2005353
224848_at	2.075	2.117	CDK6	cyclin-dependent kinase 6
202964_s_at	2.071	2.222	RFX5	regulatory factor X, 5 (influences HLA class II expression)
238935_at	2.07	2.278	RPS27L	Ribosomal protein S27-like
1568629_s_at	2.055	2.066	PIK3R2	phosphoinositide-3-kinase, regulatory subunit 2 (p85 beta)
223201_s_at	2.055	1.808	RP13-360B22	hypothetical protein FLJ22679
218346_s_at	2.037	2.688	SESN1	sestrin 1
202291_s_at	2.026	1.539	MGP	matrix Gla protein
203887_s_at	2.013	1.968	THBD	thrombomodulin
230093_at	2.008	1.981	TSGA2	testis specific A2 homolog (mouse)
219099_at	2.002	2.401	C12orf5	chromosome 12 open reading frame 5
229441_at	1.996	1.589	PRSS23	Protease, serine, 23
215076_s_at	1.988	1.606	COL3A1	collagen, type III, alpha 1 (Ehlers-Danlos syndrome type IV, autosomal dominant)
202073_at	1.973	2.071	OPTN	optineurin
202357_s_at	1.968	1.822	BF	B-factor, properdin
227221_at	1.966	3		CDNA FLJ31683 fis, clone NT2RI2005353
205110_s_at	1.957	1.806	FGF13	fibroblast growth factor 13
203888_at	1.953	1.979	THBD	thrombomodulin
203571_s_at	1.941	1.905	C10orf116	chromosome 10 open reading frame 116
223878_at	1.935	1.539	INPP4B	inositol polyphosphate-4-phosphatase, type II, 105kDa
223179_at	1.934	2.243	YPEL3	yippee-like 3 (Drosophila)
205174_s_at	1.916	1.606	QPCT	glutaminyl-peptide cyclotransferase (glutaminyl cyclase)
218113_at	1.908	1.569	TMEM2	transmembrane protein 2
235534_at	1.908	2.274		Homo sapiens, clone IMAGE:5723825, mRNA
200983_x_at	1.903	2.087	CD59	CD59 antigen p18-20 (antigen identified by monoclonal antibodies 16.3A5, EJ16, EJ30, EL32 and G344)
211864_s_at	1.885	2.053	FER1L3	fer-1-like 3, myoferlin (C. elegans)
206482_at	1.884	1.66	PTK6	PTK6 protein tyrosine kinase 6
223434_at	1.883	1.588	GBP3	guanylate binding protein 3
223196_s_at	1.877	2.476	SESN2	sestrin 2
1553033_at	1.868	1.821	SYTL5	synaptotagmin-like 5
226771_at	1.856	2.23	ATP8B2	ATPase, Class I, type 8B, member 2
201798_s_at	1.855	1.889	FER1L3	fer-1-like 3, myoferlin (C. elegans)
227134_at	1.854	2.659	SYTL1	synaptotagmin-like 1
202708_s_at	1.846	1.881	HIST2H2BE	histone 2, H2be
229566_at	1.845	1.815	LOC440449	hypothetical gene supported by AF086204
205326_at	1.823	1.651	RAMP3	receptor (calcitonin) activity modifying protein 3
238673_at	1.82	1.691		Transcribed locus
222450_at	1.818	1.724	TMEPAI	transmembrane, prostate androgen induced RNA
225927_at	1.81	1.514	MAP3K1	mitogen-activated protein kinase kinase kinase 1
213142_x_at	1.804	1.742	LOC54103	hypothetical protein LOC54103
1556308_at	1.803	2.048	FLJ33674	hypothetical protein FLJ33674
225822_at	1.803	2.181	MGC17299	hypothetical protein MGC17299
208796_s_at	1.8	1.994	CCNG1	cyclin G1

Table 1: Genes deregulated by HdmX and Hdm2 in MCF7 cells.

AffyID	Fold Change vs. siCon siHdmX	siHdm2	Gene Symbol	Description
226403_at	1.795	1.785	TMC4	transmembrane channel-like 4
209333_at	1.794	1.599	ULK1	unc-51-like kinase 1 (C. elegans)
226864_at	1.794	1.541	PKIA	Protein kinase (cAMP-dependent, catalytic) inhibitor alpha
203059_s_at	1.787	2.03	PAPSS2	3'-phosphoadenosine 5'-phosphosulfate synthase 2
214290_s_at	1.773	1.898	HIST2H2AA	histone 2, H2aa
205726_at	1.766	1.86	DIAPH2	diaphanous homolog 2 (Drosophila)
219410_at	1.753	1.508	TMEM45A	transmembrane protein 45A
37996_s_at	1.752	1.871	DMPK	dystrophia myotonica-protein kinase
200766_at	1.744	1.73	CTSD	cathepsin D (lysosomal aspartyl peptidase)
232306_at	1.742	1.779	CDH26	cadherin-like 26
217419_x_at	1.732	1.94	AGRN	agrin
219561_at	1.723	1.849	COPZ2	coatomer protein complex, subunit zeta 2
216264_s_at	1.718	1.998	LAMB2	laminin, beta 2 (laminin S)
212120_at	1.712	1.606	RHOQ	Ras homolog gene family, member Q
212285_s_at	1.711	2.049	AGRN	agrin
218007_s_at	1.707	1.645	RPS27L	ribosomal protein S27-like
230780_at	1.707	1.809		CDNA FLJ31839 fis, clone NT2RP7000086
207655_s_at	1.7	2.051	BLNK	B-cell linker
231406_at	1.7	1.665	LOC401394	hypothetical LOC401394 ; hypothetical LOC402578
204462_s_at	1.699	1.527	SLC16A2	solute carrier family 16 (monocarboxylic acid transporters), member 2
214481_at	1.699	1.542	HIST1H2AM	Histone 1, H2am
231766_s_at	1.693	1.786	COL12A1	collagen, type XII, alpha 1
219687_at	1.692	1.503	HHAT	hedgehog acyltransferase
202376_at	1.69	1.527	SERPINA3	serpin peptidase inhibitor, clade A (alpha-1 antiproteinase, antitrypsin), member 3
204954_s_at	1.689	2.736	DYRK1B	dual-specificity tyrosine-(Y)-phosphorylation regulated kinase 1B
208792_s_at	1.677	1.825	CLU	clusterin (complement lysis inhibitor, SP-40,40, sulfated glycoprotein 2, testosterone-repressed prostate message 2, apolipoprotein J)
217529_at	1.676	1.979	LOC401394	hypothetical LOC401394 ; hypothetical LOC402578
218471_s_at	1.673	1.821	BBS1	Bardet-Biedl syndrome 1
203767_s_at	1.664	1.758	STS	steroid sulfatase (microsomal), arylsulfatase C, isozyme S
208791_at	1.663	2.024	CLU	clusterin (complement lysis inhibitor, SP-40,40, sulfated glycoprotein 2, testosterone-repressed prostate message 2, apolipoprotein J)
201648_at	1.654	1.684	JAK1	Janus kinase 1 (a protein tyrosine kinase)
209917_s_at	1.646	1.874	TP53AP1	TP53 activated protein 1
212450_at	1.645	1.534	KIAA0256	KIAA0256 gene product
222043_at	1.636	1.867	CLU	clusterin (complement lysis inhibitor, SP-40,40, sulfated glycoprotein 2, testosterone-repressed prostate message 2, apolipoprotein J)
204546_at	1.625	2.033	KIAA0513	KIAA0513
236668_at	1.621	1.853		CDNA clone IMAGE:5312086
209623_at	1.618	1.859	MCCC2	methylcrotonoyl-Coenzyme A carboxylase 2 (beta)

Table 1: Genes deregulated by HdmX and Hdm2 in MCF7 cells.

AffyID	Fold Change vs. siCon siHdmX	siHdm2	Gene Symbol	Description
209360_s_at	1.616	1.583	RUNX1	runt-related transcription factor 1 (acute myeloid leukemia 1; aml1 oncogene)
220613_s_at	1.614	1.616	SYTL2	synaptotagmin-like 2
217767_at	1.613	1.596	C3	complement component 3
209166_s_at	1.611	1.58	MAN2B1	mannosidase, alpha, class 2B, member 1
207813_s_at	1.61	3.021	FDXR	ferredoxin reductase
217783_s_at	1.609	1.626	YPEL5	yippee-like 5 (Drosophila)
201116_s_at	1.608	1.764	CPE	carboxypeptidase E
209739_s_at	1.6	1.817	PNPLA4	patatin-like phospholipase domain containing 4
219529_at	1.59	1.596	CLIC3	chloride intracellular channel 3
223195_s_at	1.59	2.022	SESN2	sestrin 2
203725_at	1.589	2.034	GADD45A	growth arrest and DNA-damage-inducible, alpha
209216_at	1.583	1.712	WDR45	WD repeat domain 45
234644_x_at	1.582	1.738		CDNA: FLJ22426 fis, clone HRC08780
214542_x_at	1.581	1.637	HIST1H2AI	histone 1, H2ai
210886_x_at	1.577	1.681	TP53AP1	TP53 activated protein 1
201939_at	1.575	1.54	PLK2	polo-like kinase 2 (Drosophila)
208890_s_at	1.568	1.97	PLXNB2	plexin B2
211979_at	1.561	1.549	GPR107	G protein-coupled receptor 107
210241_s_at	1.557	1.585	TP53AP1	TP53 activated protein 1
210930_s_at	1.557	1.629	ERBB2	v-erb-b2 erythroblastic leukemia viral oncogene homolog 2, neuro/glioblastoma derived oncogene homolog (avian)
218706_s_at	1.557	1.533	NS3TP2	HCV NS3-transactivated protein 2
202387_at	1.545	1.691	BAG1	BCL2-associated athanogene ; BCL2-associated athanogene
225968_at	1.545	1.679	PRICKLE2	prickle-like 2 (Drosophila)
200920_s_at	1.54	1.545	BTG1	B-cell translocation gene 1, anti-proliferative
216080_s_at	1.539	1.537	FADS3	fatty acid desaturase 3
39248_at	1.537	1.845	AQP3	aquaporin 3
217270_s_at	1.535	1.844	DYRK1B	dual-specificity tyrosine-(Y)-phosphorylation regulated kinase 1B
214433_s_at	1.534	1.634	SELENBP1	selenium binding protein 1 ; selenium binding protein 1
210224_at	1.524	1.575	MR1	major histocompatibility complex, class I-related
224836_at	1.512	1.833	TP53INP2	tumor protein p53 inducible nuclear protein 2
212890_at	1.511	1.874	MGC15523	hypothetical protein MGC15523
214086_s_at	0.666	0.605	PARP2	poly (ADP-ribose) polymerase family, member 2
213346_at	0.665	0.616	LOC93081	hypothetical protein BC015148
228559_at	0.665	0.657		CDNA clone IMAGE:6043059
227337_at	0.663	0.544	ANKRD37	ankyrin repeat domain 37
235425_at	0.663	0.554	SGOL2	shugoshin-like 2 (S. pombe)
204435_at	0.661	0.587	NUPL1	nucleoporin like 1
201890_at	0.66	0.636	RRM2	ribonucleotide reductase M2 polypeptide
220840_s_at	0.66	0.588	C1orf112	chromosome 1 open reading frame 112
222843_at	0.658	0.543	FIGNL1	fidgetin-like 1
204240_s_at	0.657	0.631	SMC2L1	SMC2 structural maintenance of chromosomes 2-like 1 (yeast)
228273_at	0.657	0.612	FLJ11029	Hypothetical protein FLJ11029
203625_x_at	0.656	0.579	SKP2	S-phase kinase-associated protein 2 (p45)
218350_s_at	0.656	0.613	GMNN	geminin, DNA replication inhibitor

Table 1: Genes deregulated by HdmX and Hdm2 in MCF7 cells.

AffyID	Fold Change vs. siCon siHdmX	siHdm2	Gene Symbol	Description
219502_at	0.656	0.492	NEIL3	nei endonuclease VIII-like 3 (E. coli)
209608_s_at	0.655	0.664	ACAT2	acetyl-Coenzyme A acetyltransferase 2 (acetoacetyl Coenzyme A thiolase)
203213_at	0.653	0.543	CDC2	Cell division cycle 2, G1 to S and G2 to M
227787_s_at	0.653	0.636	THRAP6	thyroid hormone receptor associated protein 6
219555_s_at	0.65	0.621	BM039	uncharacterized bone marrow protein BM039
203302_at	0.646	0.569	DCK	deoxycytidine kinase
222608_s_at	0.646	0.54	ANLN	anillin, actin binding protein (scraps homolog, Drosophila)
222740_at	0.646	0.473	ATAD2	ATPase family, AAA domain containing 2
216228_s_at	0.645	0.554	WDHD1	WD repeat and HMG-box DNA binding protein 1
222848_at	0.645	0.464	FKSG14	leucine zipper protein FKSG14
220865_s_at	0.644	0.641	TPRT	trans-prenyltransferase
205394_at	0.642	0.541	CHEK1	CHK1 checkpoint homolog (S. pombe)
223256_at	0.642	0.568	KIAA1333	KIAA1333
229442_at	0.642	0.618	C18orf54	chromosome 18 open reading frame 54
204531_s_at	0.641	0.61	BRCA1	breast cancer 1, early onset
209754_s_at	0.641	0.59	TMPO	thymopoietin
211767_at	0.641	0.613	SLD5	SLD5 homolog ; SLD5 homolog
223255_at	0.641	0.554	KIAA1333	KIAA1333
225300_at	0.641	0.639	C15orf23	chromosome 15 open reading frame 23
229886_at	0.641	0.627	FLJ32363	FLJ32363 protein
209709_s_at	0.638	0.638	HMMR	hyaluronan-mediated motility receptor (RHAMM)
218755_at	0.638	0.596	KIF20A	kinesin family member 20A
1568596_a_at	0.637	0.657	TROAP	trophinin associated protein (tastin)
219531_at	0.637	0.653	Cep72	centrosomal protein 72 kDa
227545_at	0.637	0.626	BARD1	BRCA1 associated RING domain 1
234944_s_at	0.637	0.597	FAM54A	family with sequence similarity 54, member A
238075_at	0.637	0.601	CHEK1	CHK1 checkpoint homolog (S. pombe)
204962_s_at	0.636	0.666	CENPA	centromere protein A, 17kDa
222039_at	0.636	0.582	LOC146909	hypothetical protein LOC146909
202705_at	0.635	0.651	CCNB2	cyclin B2
229610_at	0.635	0.603	FLJ40629	hypothetical protein FLJ40629
219650_at	0.634	0.605	FLJ20105	FLJ20105 protein
201663_s_at	0.633	0.618	SMC4L1	SMC4 structural maintenance of chromosomes 4-like 1 (yeast)
218883_s_at	0.633	0.641	MLF1IP	MLF1 interacting protein
209715_at	0.632	0.621	CBX5	chromobox homolog 5 (HP1 alpha homolog, Drosophila)
220239_at	0.629	0.626	KLHL7	kelch-like 7 (Drosophila)
209680_s_at	0.628	0.531	KIFC1	kinesin family member C1
218768_at	0.627	0.61	NUP107	nucleoporin 107kDa
38158_at	0.627	0.661	ESPL1	extra spindle poles like 1 (S. cerevisiae)
204127_at	0.626	0.6	RFC3	replication factor C (activator 1) 3, 38kDa
209714_s_at	0.625	0.629	CDKN3	cyclin-dependent kinase inhibitor 3 (CDK2-associated dual specificity phosphatase)
235545_at	0.625	0.556	DEPDC1	DEP domain containing 1
208955_at	0.624	0.604	DUT	dUTP pyrophosphatase
201896_s_at	0.623	0.65	PSRC1	proline/serine-rich coiled-coil 1
212621_at	0.622	0.623	KIAA0286	KIAA0286 protein
213647_at	0.622	0.465	DNA2L	DNA2 DNA replication helicase 2-like (yeast)

Table 1: Genes deregulated by HdmX and Hdm2 in MCF7 cells.

AffyID	Fold Change vs. siCon siHdmX	siHdm2	Gene Symbol	Description
204822_at	0.62	0.523	TTK	TTK protein kinase
204825_at	0.62	0.606	MELK	maternal embryonic leucine zipper kinase
215773_x_at	0.62	0.664	PARP2	poly (ADP-ribose) polymerase family, member 2
204162_at	0.619	0.573	KNTC2	kinetochore associated 2
205393_s_at	0.619	0.561	CHEK1	CHK1 checkpoint homolog (S. pombe)
221685_s_at	0.619	0.555	FLJ20364	hypothetical protein FLJ20364
227928_at	0.619	0.523	FLJ20641	hypothetical protein FLJ20641
228069_at	0.619	0.575	FAM54A	family with sequence similarity 54, member A
230165_at	0.619	0.548	SGOL2	shugoshin-like 2 (S. pombe)
218585_s_at	0.618	0.555	DTL	denticleless homolog (Drosophila)
218355_at	0.616	0.638	KIF4A	kinesin family member 4A
223307_at	0.616	0.63	CDCA3	cell division cycle associated 3
218039_at	0.615	0.612	NUSAP1	nucleolar and spindle associated protein 1
204033_at	0.614	0.628	TRIP13	thyroid hormone receptor interactor 13
225687_at	0.613	0.621	C20orf129	chromosome 20 open reading frame 129
226308_at	0.61	0.633	NY-SAR-48	sarcoma antigen NY-SAR-48
204752_x_at	0.608	0.618	PARP2	poly (ADP-ribose) polymerase family, member 2
206653_at	0.608	0.473	POLR3G	Polymerase (RNA) III (DNA directed) polypeptide G (32kD)
210983_s_at	0.608	0.666	MCM7	MCM7 minichromosome maintenance deficient 7 (S. cerevisiae)
218782_s_at	0.608	0.5	ATAD2	ATPase family, AAA domain containing 2
219258_at	0.608	0.527	FLJ20516	timeless-interacting protein
208795_s_at	0.607	0.634	MCM7	MCM7 minichromosome maintenance deficient 7 (S. cerevisiae)
220060_s_at	0.607	0.506	FLJ20641	hypothetical protein FLJ20641
221436_s_at	0.607	0.623	CDCA3	cell division cycle associated 3 ; cell division cycle associated 3
223542_at	0.607	0.512	ANKRD32	ankyrin repeat domain 32
1553244_at	0.604	0.592	FANCB	Fanconi anemia, complementation group B
219004_s_at	0.604	0.627	C21orf45	chromosome 21 open reading frame 45
221591_s_at	0.603	0.647	FAM64A	family with sequence similarity 64, member A
203805_s_at	0.602	0.59	FANCA	Fanconi anemia, complementation group A ; Fanconi anemia, complementation group A
219978_s_at	0.601	0.579	NUSAP1	nucleolar and spindle associated protein 1
221879_at	0.601	0.596	CALML4	calmodulin-like 4
203755_at	0.6	0.577	BUB1B	BUB1 budding uninhibited by benzimidazoles 1 homolog beta (yeast)
203764_at	0.6	0.567	DLG7	discs, large homolog 7 (Drosophila)
204887_s_at	0.6	0.59	PLK4	polo-like kinase 4 (Drosophila)
206550_s_at	0.6	0.61	NUP155	nucleoporin 155kDa
227211_at	0.6	0.577	PHF19	PHD finger protein 19
205053_at	0.599	0.638	PRIM1	primase, polypeptide 1, 49kDa
64408_s_at	0.598	0.515	CALML4	calmodulin-like 4
221521_s_at	0.597	0.63	Pfs2	DNA replication complex GINS protein PSF2
222962_s_at	0.595	0.496	MCM10	MCM10 minichromosome maintenance deficient 10 (S. cerevisiae)
205519_at	0.594	0.533	WDR76	WD repeat domain 76
219990_at	0.594	0.423	E2F8	E2F transcription factor 8
213226_at	0.592	0.485	CCNA2	Cyclin A2
219703_at	0.592	0.44	MNS1	meiosis-specific nuclear structural 1

Table 1: Genes deregulated by HdmX and Hdm2 in MCF7 cells.

AffyID	Fold Change vs. siCon siHdmX	siHdm2	Gene Symbol	Description
242584_at	0.589	0.516	FLJ13305	hypothetical protein FLJ13305
1552619_a_at	0.587	0.48	ANLN	anillin, actin binding protein (scraps homolog, Drosophila)
204603_at	0.583	0.503	EXO1	exonuclease 1
223570_at	0.583	0.502	MCM10	MCM10 minichromosome maintenance deficient 10 (S. cerevisiae)
204492_at	0.582	0.628	ARHGAP11A	Rho GTPase activating protein 11A
214240_at	0.582	0.643	GAL	galanin
219306_at	0.582	0.56	KIF15	kinesin family member 15
203145_at	0.581	0.645	SPAG5	sperm associated antigen 5
203968_s_at	0.581	0.561	CDC6	CDC6 cell division cycle 6 homolog (S. cerevisiae)
230847_at	0.58	0.521	WRNIP1	Werner helicase interacting protein 1
221520_s_at	0.578	0.662	CDCA8	cell division cycle associated 8
219294_at	0.577	0.509	C6orf139	chromosome 6 open reading frame 139
1552921_a_at	0.575	0.56	FIGNL1	fidgetin-like 1
224428_s_at	0.575	0.491	CDCA7	cell division cycle associated 7 ; cell division cycle associated 7
218663_at	0.573	0.579	HCAP-G	chromosome condensation protein G
1553984_s_at	0.572	0.643	DTYMK	deoxythymidylate kinase (thymidylate kinase)
220651_s_at	0.571	0.527	MCM10	MCM10 minichromosome maintenance deficient 10 (S. cerevisiae)
236641_at	0.571	0.48	KIF14	kinesin family member 14
204023_at	0.57	0.598	RFC4	replication factor C (activator 1) 4, 37kDa
205024_s_at	0.568	0.584	RAD51	RAD51 homolog (RecA homolog, E. coli) (S. cerevisiae)
218662_s_at	0.566	0.516	HCAP-G	chromosome condensation protein G
222958_s_at	0.566	0.473	DEPDC1	DEP domain containing 1
242787_at	0.565	0.526		
1554768_a_at	0.564	0.522	MAD2L1	MAD2 mitotic arrest deficient-like 1 (yeast)
204641_at	0.564	0.521	NEK2	NIMA (never in mitosis gene a)-related kinase 2
209773_s_at	0.564	0.65	RRM2	ribonucleotide reductase M2 polypeptide
223229_at	0.564	0.605	UBE2T	ubiquitin-conjugating enzyme E2T (putative)
201897_s_at	0.563	0.602	CKS1B	CDC28 protein kinase regulatory subunit 1B
214804_at	0.563	0.582	FSHPRH1	FSH primary response (LRPR1 homolog, rat) 1
225834_at	0.562	0.489	FAM72A	family with sequence similarity 72, member A
202954_at	0.56	0.641	UBE2C	ubiquitin-conjugating enzyme E2C
205909_at	0.557	0.55	POLE2	polymerase (DNA directed), epsilon 2 (p59 subunit)
205967_at	0.553	0.556	HIST1H4C	histone 1, H4c
212949_at	0.551	0.558	BRRN1	barren homolog (Drosophila)
1553528_a_at	0.548	0.438	TAF5	TAF5 RNA polymerase II, TATA box binding protein (TBP)-associated factor, 100kDa
207891_s_at	0.548	0.582	TREX2 ; UIP	three prime repair exonuclease 2 ; 26S proteasome-associated UCH interacting protein 1
219494_at	0.547	0.562	RAD54B	RAD54 homolog B (S. cerevisiae)
209891_at	0.546	0.504	SPBC25	spindle pole body component 25 homolog (S. cerevisiae)
205733_at	0.545	0.521	BLM	Bloom syndrome
227165_at	0.545	0.517	C13orf3	chromosome 13 open reading frame 3
210416_s_at	0.544	0.572	CHEK2	CHK2 checkpoint homolog (S. pombe)
215509_s_at	0.544	0.493	BUB1	BUB1 budding uninhibited by benzimidazoles 1 homolog (yeast)

Table 1: Genes deregulated by HdmX and Hdm2 in MCF7 cells.

AffyID	Fold Change vs. siCon siHdmX	siHdm2	Gene Symbol	Description
37577_at	0.544	0.538	ARHGAP19	Rho GTPase activating protein 19
212619_at	0.542	0.501	KIAA0286	KIAA0286 protein
211080_s_at	0.541	0.524	NEK2	NIMA (never in mitosis gene a)-related kinase 2 ; NIMA (never in mitosis gene a)-related kinase 2
204128_s_at	0.54	0.562	RFC3	replication factor C (activator 1) 3, 38kDa
204126_s_at	0.539	0.606	CDC45L	CDC45 cell division cycle 45-like (S. cerevisiae)
223381_at	0.538	0.465	CDCA1	cell division cycle associated 1
203967_at	0.536	0.501	CDC6	CDC6 cell division cycle 6 homolog (S. cerevisiae)
220295_x_at	0.535	0.444	DEPDC1	DEP domain containing 1
242939_at	0.535	0.595	TFDP1	transcription factor Dp-1
222680_s_at	0.533	0.532	DTL	denticleless homolog (Drosophila)
232278_s_at	0.53	0.495	DEPDC1	DEP domain containing 1
204728_s_at	0.529	0.501	WDHD1	WD repeat and HMG-box DNA binding protein 1
210053_at	0.529	0.461	TAF5	TAF5 RNA polymerase II, TATA box binding protein (TBP)-associated factor, 100kDa
206632_s_at	0.522	0.526	APOBEC3B	apolipoprotein B mRNA editing enzyme, catalytic polypeptide-like 3B
202779_s_at	0.517	0.642	UBE2S	ubiquitin-conjugating enzyme E2S
209464_at	0.517	0.566	AURKB	aurora kinase B
203418_at	0.514	0.541	CCNA2	cyclin A2
223700_at	0.514	0.504	GAJ	GAJ protein
203214_x_at	0.507	0.505	CDC2	cell division cycle 2, G1 to S and G2 to M
218726_at	0.507	0.527	DKFZp762E1	hypothetical protein DKFZp762E1312
230021_at	0.501	0.575	MGC45866	leucine-rich repeat kinase 1
209408_at	0.498	0.564	KIF2C	kinesin family member 2C
211519_s_at	0.498	0.537	KIF2C	kinesin family member 2C
210559_s_at	0.497	0.494	CDC2	cell division cycle 2, G1 to S and G2 to M
219000_s_at	0.49	0.519	DCC1	defective in sister chromatid cohesion homolog 1 (S. cerevisiae)
239002_at	0.488	0.416	ASPM	asp (abnormal spindle)-like, microcephaly associated (Drosophila)
210334_x_at	0.483	0.544	BIRC5	baculoviral IAP repeat-containing 5 (survivin)